FEDERAL UNIVERSITY OF MINAS GERAIS (UFMG)
SCHOOL OF ENGINEERING
DEPARTMENT OF STRUCTURAL ENGINEERING
GRADUATE PROGRAM IN STRUCTURAL ENGINEERING (PROPEES)

Pâmela Daniela Nogueira Reges

DAMAGE MODELS FOR THE MICROMORPHIC CONTINUUM

Belo Horizonte, **14th May, 2021**

Pâmela Daniela Nogueira Reges

DAMAGE MODELS FOR THE MICROMORPHIC CONTINUUM

Final Version

Thesis submitted to the Graduate Program in Structural Engineering (PROPEES) of the School of Engineering at the Federal University of Minas Gerais (UFMG), in partial fulfillment of the requirements for the degree of "Master in Science of Structural Engineering".

Supervisor: Prof. Dr. Roque Luiz da Silva Pitangueira

Co-Supervisor: Prof. Dr. Leandro Lopes da Silva

Belo Horizonte, 14th May, 2021

Reges, Pâmela Daniela Nogueira.
R333d Damage models for the micromorphic continuum [recurso eletrônico] / Pâmela Daniela Nogueira Reges. - 2021.
1 recurso online (xxvi, 215 f. : il., color.) : pdf.

Orientador: Roque Luiz da Silva Pitangueira.
Coorientador: Leandro Lopes da Silva.

Dissertação (mestrado) - Universidade Federal de Minas Gerais, Escola de Engenharia.

Apêndices: f. 149-215.

Bibliografia: f. 142-148.
Exigências do sistema: Adobe Acrobat Reader.

1. Engenharia de estruturas - Teses. 2. Mecânica do dano continuo - Teses. I. Pitangueira, Roque Luiz da Silva. II. Silva, Leandro Lopes da. III. Universidade Federal de Minas Gerais. Escola de Engenharia. IV. Título.

CDU: 624(043)

Ficha catalográfica elaborada pela bibliotecária Roseli Alves de Oliveira CRB/6 2121
Biblioteca Prof. Mário Werneck, Escola de Engenharia da UFMG

UNIVERSIDADE FEDERAL DE MINAS GERAIS

PROGRAMA DE PÓS-GRADUAÇÃO EM ENGENHARIA DE ESTRUTURAS

ATA DA DEFESA DE DISSERTAÇÃO DE MESTRADO EM ENGENHARIA DE ESTRUTURAS Nº: 382 DA ALUNA PAMELA DANIELA NOGUEIRA.

Às **09:00** horas do dia **14** do mês de **maio** de **2021**, reuniu-se, totalmente por videoconferência para atender aos novos protocolos de distanciamento social adotados pelo Governo Federal e pela Prefeitura de Belo Horizonte, que integram medidas para combater o avanço da pandemia de Covid-19, provocada pelo novo coronavírus, a Comissão Examinadora indicada pelo Colegiado do Programa em **24 de abril de 2021**, para julgar a defesa da Dissertação de Mestrado intitulada **"Damage Models for the Micromorphic Continuum**, cuja aprovação é um dos requisitos para a obtenção do Grau de MESTRE EM ENGENHARIA DE ESTRUTURAS na área de Estruturas.

Abrindo a sessão, o Presidente da Comissão, **Prof. Dr. Roque Luiz da Silva Pitangueira**, após dar a conhecer aos presentes o teor das Normas Regulamentares passou a palavra à candidata para apresentação de seu trabalho. Seguiu-se a argüição pelos examinadores, com a respectiva defesa da candidata. Logo após, a Comissão se reuniu, sem a presença da candidata e do público, para julgamento e expedição do resultado final. Foram atribuídas as seguintes indicações:

Prof. Dr. Roque Luiz da Silva Pitangueira - DEES - UFMG (Orientador)
Prof. Dr. Leandro Lopes da Silva - DEES - UFMG (Coorientador)
Prof. Dr. Samuel Silva Penna - DEES - UFMG
Prof. Dr. Lapo Gori - DEES - UFMG
Prof. Dr. Eduardo Nobre Lages - UFAL

Pelas indicações acima, a candidata foi considerada APROVADA, conforme pareceres em anexo.

O resultado final foi comunicado publicamente à candidata pelo Presidente da Comissão. Nada mais havendo a tratar, o Presidente encerrou a reunião e lavrou a presente ATA, que será assinada por todos os membros participantes da Comissão Examinadora.

Belo Horizonte, 14 de maio de 2021.

Observações:

1. A aprovação da candidata na defesa da Dissertação de Mestrado não significa que a mesma tenha cumprido todos os requisitos necessários para obtenção do Grau de Mestre em Engenharia de Estruturas;
2. Este documento não terá validade sem a assinatura do Coordenador do Programa de Pós-Graduação.

Documento assinado eletronicamente por **Eduardo Nobre Lages**, **Usuário Externo**, em 14/05/2021, às 13:25, conforme horário oficial de Brasília, com fundamento no art. 5º do Decreto nº 10.543, de 13 de novembro de 2020.

Documento assinado eletronicamente por **Roque Luiz da Silva Pitangueira**, **Professor do Magistério Superior**, em 14/05/2021, às 13:25, conforme horário oficial de Brasília, com fundamento no art. 5º do Decreto nº 10.543, de 13 de novembro de 2020.

Documento assinado eletronicamente por **Samuel Silva Penna**, **Professor do Magistério Superior**, em 14/05/2021, às 13:26, conforme horário oficial de Brasília, com fundamento no art. 5º do Decreto nº 10.543, de 13 de novembro de 2020.

Documento assinado eletronicamente por **Leandro Lopes da Silva**, **Professor do Magistério Superior**, em 14/05/2021, às 13:26, conforme horário oficial de Brasília, com fundamento no art. 5º do Decreto nº 10.543, de 13 de novembro de 2020.

Documento assinado eletronicamente por **Lapo Gori**, **Professor do Magistério Superior**, em 14/05/2021, às 13:27, conforme horário oficial de Brasília, com fundamento no art. 5º do Decreto nº 10.543, de 13 de novembro de 2020.

A autenticidade deste documento pode ser conferida no site https://sei.ufmg.br/sei/controlador_externo.php?acao=documento_conferir&id_orgao_acesso_externo=0, informando o código verificador **0701471** e o código CRC **16E24D62**.

Referência: Processo nº 23072.222176/2021-13 SEI nº 0701471

Aos meus pais e ao Jônatas.

Acknowledgements

A Deus, por sua infinita bondade e misericórdia.

À minha família, por todo apoio e incentivo.

Ao Jônatas, por toda paciência e carinho, sempre trazendo leveza aos meus dias.

Ao Roque, pela orientação, pela confiança e por sempre acreditar.

Ao Leandro, pela coorientação, pela paciência, pela disponibilidade e pelas risadas.

Aos demais professores do Departamento de Engenharia de Estruturas da UFMG que contribuíram em minha formação.

Aos colegas de curso pelos papos, pelos almoços e pelos cafezinhos.

À CAPES e ao CNPq, pelo apoio financeiro.

in whom are hidden all the treasures of wisdom and knowledge

Colossians 2:3

Resumo

Numerosos materiais, embora pareçam macroscopicamente homogêneos, geralmente apresentam uma microestrutura heterogênea que influencia diretamente o comportamento estrutural. A abordagem fenomenológica adotada na mecânica do contínuo clássica não contabiliza individualmente essa influência, especialmente nos casos em que a estrutura em análise é pequena em comparação com sua microestrutura. Dentro do quadro da mecânica do contínuo, as chamadas teorias de contínuos generalizados são particularmente adequadas para lidar com as questões acima incorporando o comportamento microestrutural em sua formulação. A teoria micromórfica está incluída nesta classe geral de contínuos generalizados e, mais especificamente, no grupo que incorpora graus adicionais de liberdade às partículas materiais. Outro aspecto dos contínuos generalizados é sua capacidade de lidar com a questão da localização em materiais parcialmente frágeis modelados com modelos de degradação elástica como resultado de seu caráter não-local. A fim de permitir a representação de meios parcialmente frágeis com a teoria do contínuo micromórfico, este trabalho formula modelos de dano escalar-isotrópico para um contínuo micromórfico na estrutura de modelos constitutivos do sistema INSANE, inicialmente concebido para o contínuo clássico e depois expandido para o contínuo micropolar. A fim de representar meios heterogêneos, o algoritmo *take-and-place* para a geração da microestrutura heterogênea associado a uma estratégia de homogeneização para a representação de meios heterogêneos é proposto. As implementações computacionais são baseadas em um formato tensorial de uma formulação unificada de modelos constitutivos propondo uma representação tensorial compacta para o contínuo micromórfico e uma técnica de homogeneização para obter as relações constitutivas micromórficas. Foram realizadas simulaçẽs para atestar os modelos constitutivos implementados, bem como para estudar a influência no comportamento material e estrutural da introdução da heterogeneidade. Os resultados obtidos verificam as hipóteses propostas e as implementações realizadas,

fornecendo uma base para a análise não linear de meios micromórficos homogêneos e não homogêneos e possibilitando possíveis pesquisas futuras sobre o tema.

Palavras-Chave: Contínuo micromórfico; Mecânica do dano contínuo; modelos constitutivos de degradação elástica; meios heterogêneos; materiais parcialmente frágeis; sistema INSANE.

Abstract

Numerous materials, although they appear macroscopically homogeneous, usually presents a heterogeneous microstructure that directly influences the structural behavior. The phenomenological approach pursued in the classical continuum mechanics does not individually accounts for this influence, specially in cases where the structure or the specimen under analysis is small compared to its microstructure. Within the framework of continuum mechanics, so-called generalized continuum theories are particularly suited to deal with the above issues incorporating the microstructural behavior on the formulation. The micromorphic theory is included in this general class of generalized continua and, more specifically, in the group that incorporates additional degrees of freedom to the material particles. Another aspect of generalized continua is its ability to address the issue of localization in quasi-brittle material modeled as elastic-degrading media as a result of its non-local character. In order to allow the representation of quasi-brittle media with the micromorphic continuum theory, this work formulates scalar-isotropic damage models for a micromorphic continuum in the constitutive models framework of the INSANE system, initially conceived for classic media and later expanded for the micropolar continuum. In order to represent heterogeneous media, the take-and-place algorithm for the microstructure generation associated to a homogenization strategy is proposed. The computational implementations are based on a tensorial format of a unified constitutive models formulation applying a compact tensorial representation for the micromorphic continuum, and a homogenization technique to obtain the micromorphic constitutive relations. Simulations were conducted in order to attest the implemented constitutive models as well as for studying the influence on the material and structural behavior of the heterogeneity introduction. The obtained results verify the proposed hypotheses and the conducted implementations, providing the basis for non-linear analysis of homogeneous and inhomogeneous micromorphic media and allowing possible further research on the topic.

Keywords: Micromorphic continuum theory; Continuum damage mechanics; Elastic-degrading constitutive models; Heterogeneous media; Quasi-brittle materials; INSANE system.

List of Figures

List of abbreviations and acronyms

CAPES	Coordenação de Aperfeiçoamento de Pessoal de Nível Superior
CNPq	Conselho Nacional de Desenvolvimento Científico e Tecnológico
INSANE	INteractive Structural ANalysis Environment
CDM	Continuum Damage Models
RVE	Representative Volume Element
FEM	Finite Element Method
PF	particle fraction
DF	distribution fraction

List of symbols

n	unit vector normal to a plane
D	damage variable
E	Young's modulus (classical continuum)
E_{ijkl}	stiffness tensor (classical continuum)
C_{ijkl}	compliance tensor (classical continuum)
σ_{ij}	stress tensor (classical continuum)
ε_{ij}	strain tensor (classical continuum)
$\dot{E}_{ijkl}$	stiffness rate tensor (classical continuum)
$\dot{C}_{ijkl}$	compliance rate tensor (classical continuum)
$\dot{\sigma}_{ij}$	stress rate tensor (classical continuum)
$\dot{\varepsilon}_{ij}$	strain rate tensor (classical continuum)
$\dot{\varepsilon}_{ij}^{S}$	elastic part of the stress rate tensor (classical continuum)
$\dot{\varepsilon}_{ij}^{d}$	degrading part of the stress rate tensor (classical continuum)
$\dot{\lambda}_m$	inelastic multipliers
$\boldsymbol{F}$	loading function
$\boldsymbol{p}$	vector of internal variables
$\boldsymbol{m}$	directions of degradation (stress-based formulation)
$\boldsymbol{n}$	directions of the loading functions (stress-based formulation)

$\boldsymbol{H}$	Hardening-Softening modulus (stress-based formulation)
E^t_{ijkl}	tangential stiffness tensor (classical continuum)
$\boldsymbol{\bar{m}}$	directions of degradation (strain-based formulation)
$\boldsymbol{\bar{n}}$	directions of the loading functions (strain-based formulation)
M_{mijkl}	degradation rule (compliance-based formulation)
$\mathcal{D}_*$	set of damage variables (compliance-based formulation)
$\mathcal{M}_{m*}$	damage rule (compliance-based formulation)
$\bar{\mathcal{D}}_*$	set of damage variables (stiffness-based formulation)
$\bar{\mathcal{M}}_{m*}$	damage rule (stiffness-based formulation)
ε_{eq}	equivalent strain (classical continuum)
$K(D)$	history variable
ψ^0	internal energy
P	material particle
B_0	continuous body in the material configuration
B_t	continuous body in the spatial configuration
$\boldsymbol{\chi}$	microdeformation tensor
$\boldsymbol{R}$	microrotation tensor
$\boldsymbol{U}$	right stretch tensor
$\boldsymbol{V}$	left stretch tensor
$\boldsymbol{\Xi}$	position vector for the microcontinuum in the material configuration
$\boldsymbol{\xi}$	position vector for the microcontinuum in the spatial configuration
$\boldsymbol{\mathfrak{X}}$	inverse microdeformation gradient tensor
$\mathfrak{C}_{KL}$	deformation tensor

$\mathcal{C}_{KL}$	microdeformation tensor
Γ_{KLM}	wryness tensor
ϵ_{kl}	linear strain tensor (micromorphic theory)
e_{kl}	linear strain tensor (micromorphic theory)
γ_{klm}	linear strain tensor (micromorphic theory)
u_l	displacement vector
ϕ_{kl}	micromotion gradient tensor
A_{klmn}	constitutive tensor (micromorphic theory)
B_{klmn}	constitutive tensor (micromorphic theory)
E_{klmn}	constitutive tensor (micromorphic theory)
C_{klmnpq}	constitutive tensor (micromorphic theory)
F_{klmnp}	constitutive tensor (micromorphic theory)
G_{klmnp}	constitutive tensor (micromorphic theory)
t_{kl}	stress tensor
s_{kl}	micro-stress average
m_{klm}	stress moments tensor
$\mathcal{E}_{\beta\nu\delta\psi}$	generalized constitutive relation
$\Sigma_{\beta\nu}$	generalized stress operator
$\Gamma_{\delta\psi}$	generalized strain operator
Γ_{eq}	generalized equivalent strain

Table of contents

Chapter 1

Introduction

The modeling of damage and fracture in structures is and has always been an important topic in the field of computational mechanics. As a consequence, there is a growing demand for reliable material models which are capable of representing all the phenomena involved in material failure. Concerning *quasi-brittle* materials, a proper characterization of their behavior is of great importance taking into account the large number of materials that falls into this category, e.g., concrete, rocks, coarse-grained ceramics, and most fiber-reinforced materials.

As defined by Lemaitre and Desmorat (2005), a material "is considered quasi-brittle when a dissipation prior to cracking exists with no or negligible permanent strains" (p. 321). This macroscopic behavior of quasi-brittle materials is mainly due to its characteristics at the *micro* scales[1] and to defects that may exist at such scales, such as grain and phase boundaries, inclusions, voids, and nucleation and growth of microcracks. These features are closely related to the *heterogeneity* at the micro scale. Figures 1.1 and 1.2 illustrate the heterogeneous microscopic structure of concrete, wherein the features in the micro scale can be identified.

[1] In this study, the micro scale is considered as the observation level at a scale of around 10^{-3} m where individual aggregate particles in the concrete are distinguished. However, other authors may refer to this scale as the *meso scale* (see, e.g., Van Mier (1995); Krajcinovic and Lemaitre (1987)).

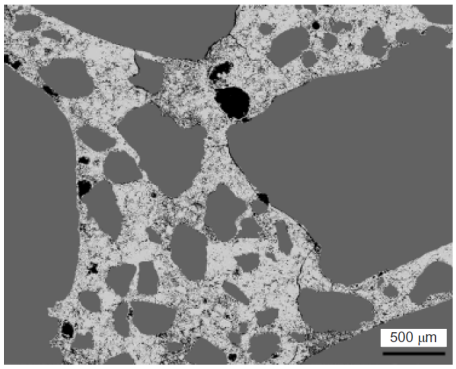

Figure 1.1: Image of concrete at 70% aggregate volume (Wong et al., 2009)

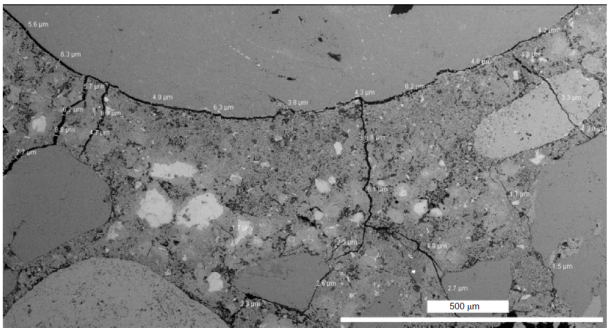

Figure 1.2: Low-magnification image showing the microcracks on the microstructure of concrete (Wong et al., 2009)

Therefore, the degradation of a quasi-brittle material is a complex phenomenon strongly correlated to the heterogeneous character of its microstructure. Hence, a detailed modeling of each individual process involved in failure proves to be complicated and often not necessary, especially if only their overall impact in the material behavior is of interest. For this reason, the discipline of *Continuum Damage Models* (CDM) emerged, accounting for degrading effects in an average sense by incorporating *damage* variables into a standard continuum mechanics description. In other words, applying this approach, a quasi-brittle medium is considered at the macro scale as a continuum body throughout the loading process. One advantage of CDM models is the modeling of crack initiation and propagation at the level of the constitutive formulation, facilitating its implementation into standard non-linear finite element codes.

In spite of the advantages, finite element computations based on continuum damage models may suffer from a number of issues, e.g., strong mesh dependence. These problems emerge from the *softening* behavior of such models, which is a

characteristic of quasi-brittle materials. This softening phase is characterized by a reduction in the load-carrying capacity of the material when a certain deformation threshold is reached, leading to the concentration of the degrading phenomena in a certain part of the body, process that called *strain localization*.

To overcome these shortcomings related to the problem of strain localization, several methodologies were developed. Among the most efficient approaches are those that introduce at the formulation level an *internal material length* based on the *non-local* character of plasticity and damage. A valid alternative is represented by the *micromorphic continuum* (Mindlin, 1964; Eringen and Şuhubi, 1964; Şuhubi and Eringen, 1964), a generalized continuum theory in which the internal length is related to an additional field that enriches the continuum kinematics with effects connected to the microstructure of the material.

Considering the numerical modeling of heterogeneous materials, various concepts have been developed regarding multiple scales. The theoretical concept of homogenization primarily builds on the contributions of Hill (1963) and most homogenization techniques have in common a procedure for determining the macroscopic overall characteristics of a heterogeneous material (Hirschberger, 2008).

Taking into account the topics previously presented, this work proposes a formulation for scalar-isotropic damage models specifically designed for the micromorphic continuum implemented in the unified constitutive models framework of the software *INSANE* (*INteractive Structural ANalysis Environment*)[2]. For the numerical modeling of heterogeneous materials, the homogenization technique proposed by Silva (2019) is applied to a heterogeneous microcontinuum, where the macroscopic micromorphic constitutive relations are obtained through the solution of boundary value problems at the micro scale according to the classical continuum theory.

The implementations were based on the tensorial format of a unified constitutive models formulation that allows to implement different constitutive models independently of the particular numerical method adopted for the problem solution.

[2]More information about the system and the studies developed on it are presented in Chapter 5.

1.1 Objectives

1.1.1 General Objective

This work aimed to expand a unified formulation for elastic degradation based on the micromorphic continuum, analogous to the existent ones based on the classical and micropolar continua. Similar to the work of Gori (2018), peculiar efforts were devoted to the extension and implementation of scalar-isotropic damage models for the micromorphic theory. Furthermore, this work presents a multi-scale homogenization technique to incorporate into the micromorphic theory the consideration of a heterogeneous micro scale based on Silva (2019).

1.1.2 Specific Objectives

This study sought to achieve the following specific objectives:

1. Conduct a study of generalized continua in the literature focusing on the micromorphic theory;
2. Study the formulation and implementation in the INSANE system of the unified framework for elastic degradation for the classical and micropolar continua;
3. Carry out a study of scalar-isotropic damage models with focus on models applied to generalized continua;
4. Expand the implementation of the unified framework to the micromorphic case in the INSANE system;
5. Adapt the homogenization technique proposed by Silva (2019) to incorporate heterogeneities at the micro scale;
6. Conduct a series of simulations in order to verify the implementations made.

1.2 Outline

This work is divided into eight chapters and one appendix. After this introduction (Chapter 1), Chapter 2 presents some aspects related to the modeling of quasi-brittle media. Basic concepts on the physics of quasi-brittle materials are presented as well as on the analysis of such materials through continuum damage

models, with focus on a unified framework for constitutive models. Chapter 2 also briefly discusses the modeling of heterogeneous media.

Chapter 3 deals more specifically with the micromorphic continuum theory and its formulation aspects, containing a brief summary of generalized continuum mechanics. It also presents an extension to micromorphic media of a unified formulation for elastic degradation, where a tensorial formulation and scalar-isotropic damage models are proposed.

The homogenization technique employed in this work is presented in Chapter 4 and also its extension for the homogenization of heterogeneous media. The computational implementations performed are detailed in Chapter 5 with a brief overview of the INSANE system.

Chapter 6 illustrates the application of the damage models proposed for the micromorphic continuum for the case of homogeneous media and also compares the results here obtained with the formulation proposed by Silva (2019) that considers damage at the micro scale.

For the case of heterogeneous media, Chapter 7 presents a study of the parameters required for the analysis and a non-linear problem characterized by induced localization. Finally, Chapter 8 concludes this work and the complete results for the study introduced in Chapter 7 are presented in Appendix A.

Chapter 2

Modeling of quasi-brittle and heterogeneous media

2.1 Basic concepts

For the appropriate representation and modeling of a given media, the characterization of its mechanical behavior is essential as the structural response is directly defined by the material performance under stress. According to this response, at a *macro scale*, a material may be classified in *ductile*, *brittle*, and *quasi-brittle*.

Materials that are classified as ductile are those that under a uniaxial tensile state are capable of sustaining large amounts of plastic deformation and, upon unloading, follow a path parallel to the initial elastic phase and present a permanent deformation, i.e., a *residual strain*. Ductile materials generally have their static strength limited by yielding, where a small increase in stress usually cause a relatively large additional deformation, as seen in Figure 2.1(a).

Those materials that fracture without much plastic deformation and without any dissipation prior to cracking (sudden failure) behave in a brittle manner (Figure 2.1(b)). For the case of a quasi-brittle material, there is a dissipation prior to cracking but no or negligible permanent strains (Lemaitre and Desmorat, 2005). A brittle-material presents a linear and a non-linear phase and, upon unloading, follows a path with a smaller slope compared to the initial elastic one (Figure 2.1(c)).

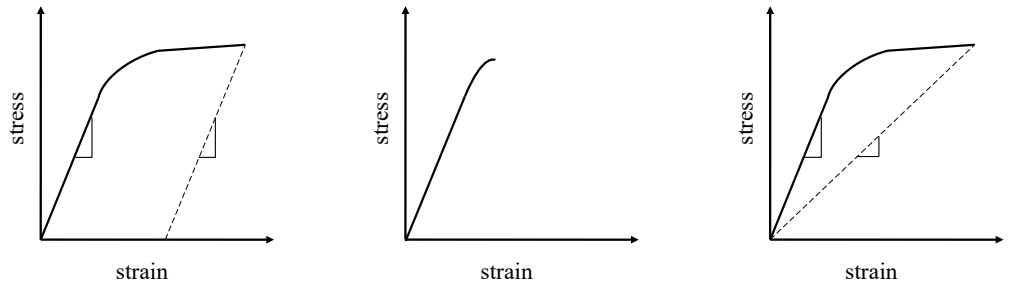

(a) Ductile material (b) Brittle material (c) Quasi-brittle material

Figure 2.1: Material behavior: classification

The behavior of a material and its classification under the described categories is strongly influenced by its characteristics at the *atomic* and *micro scales*.

On the atomic scale a solid represents an ensemble of atoms and molecules chains where the properties of a material are determined by the bonding between these discrete particles. At this level of observation, defects such as atomic vacancies and dislocations can be observed. On a micro scale the solid is heterogeneous and the features of its microstructure (e.g., grains and fibers) as well as defects (e.g., microcracks), pores, and slips, are clearly recognizable. On the macro scale, mentioned before, the solid is idealized as a continuous body and only defects such as macrocracks and shear bands can be identified (Krajcinovic and Sumarac, 1987; Van Mier, 1995; Krajcinovic, 1996). These three levels of observations and modeling are illustrated in Figure 2.2 (Van Mier, 1995).

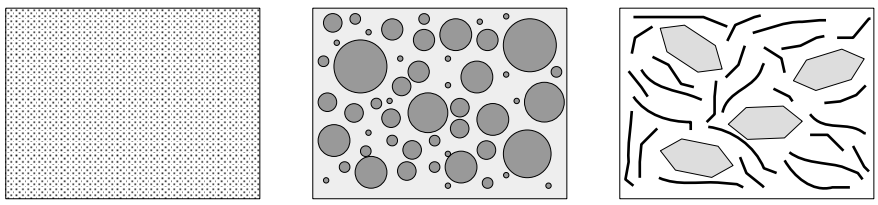

Figure 2.2: Material structure: macro, micro, and atomic scales

For the case of quasi-brittle materials, focus of this study, the deformation process is dominated by the formation of microcracks that nucleate randomly over large parts of the material without necessarily forming a macrocrack. This behavior is due to

the *heterogeneity* observed at the micro scale of materials as concrete, rocks, and coarse-grained ceramics. For the specific case of concrete, the heterogeneity induced by aggregates seems to be responsible for most of the short-term inelastic behavior of concrete (Shah and Slate, 1965).

The choice of the scale for modeling is directly correlated to the choice of analytical models and their structure. The preference for continuum models dealing with homogeneous media is justified by their relative simple mathematical structure and computational efficiency. However, the range for the application of such theories is limited to solids that contain a large number of heterogeneities (e.g., defects and grains) that directly influence the macroscopic behavior.

In view of the behavior of quasi-brittle materials here discussed, in the following sections the modeling aspects of such media will be examined in view of a continuum damage approach as well as its common issues.

2.2 Continuum damage models

As seen in the previous section, materials when loaded deform and this deformation may be elastic or inelastic. After a certain deformation rupture occurs, being either ductile, brittle or quasi-brittle. This deformation is influenced by the material composition as well as by temperature and rate of loading. A complete comprehension of the deformation behavior of a certain material would require a deep understanding of its atomic structure in addition to great computational capacity. To work around this issue, *constitutive equations* based on micromechanical or statistical considerations are used to describe the deformational process modeling the solid as a *continuum*.

After a certain load, the structure of a given material may begin to deteriorate with the formation of cracks weakening the solid and reducing its load carrying capacity. By nature, these defects are discrete entities and an accurate analysis of their influence would have to consider this disturbances of the material continuum.

Based on the same idea used for the formulation of constitutive equations, Kachanov (1958) introduced the basis for the *continuum damage theories* where the medium is modeled at the macro scale as a continuum body and the collective effect of damage is described by field variables denominated *damage variables*. Therefore, a discrete process is modeled by a continuous variable and computational simplicity is gained with loss of accuracy in modeling the deterioration.

In the words of Hult (1987)

> Continuum damage mechanics (CDM) has evolved as a mean to analyse the effect of material deterioration in solids under mechanical or thermal load. Whereas fracture mechanics deals with the influence of macroscopic cracks, CDM deals with the collective effect of distributed cracklike defects. The aim of CDM is to describe the influence of such material damage on stiffness and strength of loaded structures.
>
> A characteristic feature of CDM is the introduction into the constitutive equations of one or more, scalar or tensorial, field quantities as measures of the degradation of the material. (p. 1)

The hypotheses of a continuum body is based on the definition of a representative volume element (RVE). The RVE is structurally entirely typical of the whole mixture on average (Hill, 1963) and allows, in the transition from microscopic to macroscopic variables, the averaging of certain tensor fields over the system (Hill, 1967). In other words, as define by Nemat-Nasser and Hori (1993), the RVE for a material point of a continuum mass is a material volume which is statistically representative of the infinitesimal material neighborhood of that material point.

Figure 2.3 illustrates a continuum and identifies a material point P. When the material point is magnified it may have its own complex microstructure composed by grains, voids, cracks, and other heterogeneities. To be representative, the RVE must include a considerable number of these microheterogenities in order to represent the local properties by their mean values through continuous variables (Nemat-Nasser and Hori, 1993). According to Lemaitre (1987), roughly speaking:

- $0.1 \times 0.1 \times 0.1$ mm for metals;
- $1 \times 1 \times 1$ mm for polymers and composites;
- $10 \times 10 \times 10$ mm for wood;
- $100 \times 100 \times 100$ mm for concrete.

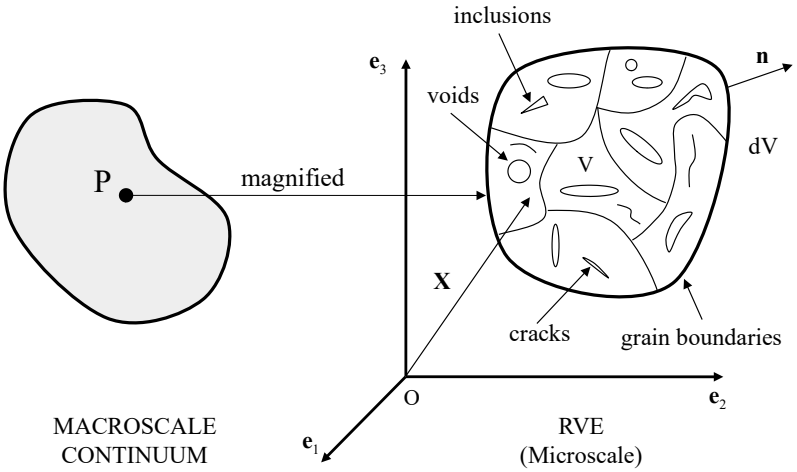

Figure 2.3: RVE as a material point with a possible microstructure (Nemat-Nasser and Hori, 1993)

2.2.1 Continuum damage modeling: concepts

As previously mentioned, damage variables quantifies the material deterioration in terms of continuous field variables. Physically, the damage variable is "defined by the surface density of microcracks and intersections of microvoids lying on a plane cutting the RVE of cross section δS" (Lemaitre and Desmorat (2005), p. 3). Hence, this density, for a plane with normal $\vec{n}$, is defined as

$$D(\vec{n}) = \frac{\delta S_D}{\delta S} \tag{2.1}$$

where δS_D is the area of the defects (microcracks and voids) contained in δS, as depicted in Figure 2.4. The damage variable $D(\vec{n})$ goes from 0 for an undamaged material to 1 where the material is completely damaged.

For a *scalar-isotropic* damage model, the variable $D(\vec{n})$ does not depend on the normal and the intrinsic variable is a scalar (Kachanov, 1958; Lemaitre and Desmorat, 2005):

$$D = \frac{\delta S_D}{\delta S} \tag{2.2}$$

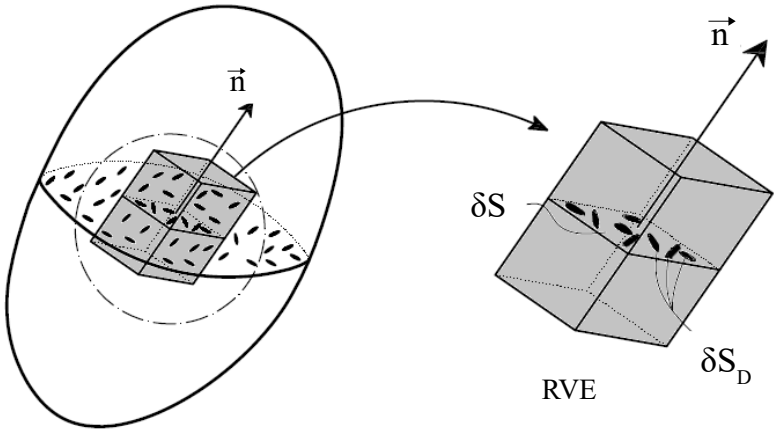

Figure 2.4: Damage representation (Penna, 2011)

The progressive material degradation may be represented by the deterioration of its elastic properties. In this case, for a uniaxial state, the original Young's modulus is progressively degraded passing from an initial value E^0 to E^S that represents the modulus for the damaged material and evolves during the loading process (Figure 2.5):

$$D = 1 - \frac{E^S}{E^0} \tag{2.3}$$

or

$$E^S = (1 - D)E^0 \tag{2.4}$$

For a more general case, the process is represented by the degradation of the constitutive operator E^0_{ijkl} and the relation between the initial and current secant stiffness can be defined as

$$E^S_{ijkl} = (1 - D)E^0_{ijkl} \tag{2.5}$$

Such model is called an isotropic model since the damage variable impacts the whole initial constitutive operator E^0_{ijkl} and, therefore, does not compromise a possible isotropy of the tensor.

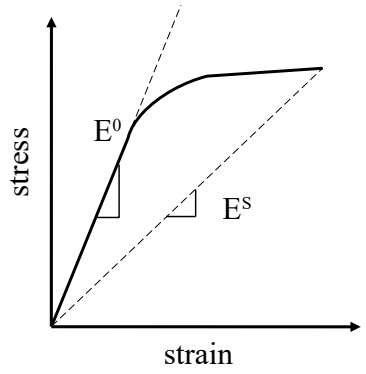

Figure 2.5: Elastic degradation

For cases wherein the hypotheses of a scalar damage variable is not sufficient to account for the damage dependence on the considered direction, tensorial damage variables may be used (e.g., vector, and second and fourth order tensors) (see Krajcinovic and Lemaitre (1987); Krajcinovic (1996); Lemaitre and Desmorat (2005)). For brevity, this topic will not be covered in this work as it focus on scalar-isotropic damage models to represent the degradation of micromorphic media (Section 3.3).

2.2.2 Unified framework for constitutive models

In this work, the modeling of the elastic degradation for micromorphic continua is based on the unified framework for constitutive modeling presented in the work of Penna (2011). This framework is able to enclose a large amount of constitutive models (e.g., elasto-plastic, isotropic, orthotropic, and anisotropic elastic-degrading) based on multiple loading functions.

A particularity of the system is the use of a *tensorial* format instead of a *vectorial-matricial* one. The vectorial-matricial format strongly depends both on the analysis model of the problem (i.e., three-dimensional, plane-stress, etc.) and on the numerical method. When a implementation is based on the tensorial format instead, such dependency is reduced, and the generality and possibility of expansion of a code is greatly increased. In this case, an operation, such as the introduction of a new constitutive method, requires modifications related solely to the constitutive model that can be introduced in the code with a syntax as close as possible to their original mathematical representation (Gori et al., 2017*a*).

The theoretical basis for a unified formulation for constitutive models has been

developed in the last years by a number of authors (see, e.g., de Borst (1987); Carol et al. (1994); de Borst and Gutiérrez (1999); Armero and Oller (2000*a*,*b*); Carol et al. (2001*a*,*b*)). The unified framework here presented (Penna, 2011) proposed an expansion based on the work of Carol et al. (1994). In the following, a brief summary of its formulation is provided.

In a geometrically linear context, an elastic-degrading medium is characterized by *total* stress-strain relations

$$\sigma_{ij} = E_{ijkl}\varepsilon_{kl} \qquad \text{and} \qquad \varepsilon_{ij} = C_{ijkl}\sigma_{kl} \tag{2.6a,b}$$

where E_{ijkl} and C_{ijkl} are the components of the fourth-order stiffness and compliance tensors, inverse of each other (i.e., $C^{-1}_{ijkl} = E_{ijkl}$ and $E^{-1}_{ijkl} = C_{ijkl}$). The equations presented correspond to the assumption of an *unloading-reloading* process where the stiffness remains equal to the current secant one, i.e., a full unload leads to no permanent strains. It should also be emphasized that this formulation refers to the classical continuum theory, then the tensors σ_{ij} and ε_{ij} are the stress and strain tensors of a classical continuum. The time derivatives of (2.6) are

$$\dot{\sigma}_{ij} = E_{ijkl}\dot{\varepsilon}_{kl} + \dot{E}_{ijkl}\varepsilon_{kl} \qquad \text{and} \qquad \dot{\varepsilon}_{ij} = C_{ijkl}\dot{\sigma}_{kl} + \dot{C}_{ijkl}\sigma_{kl} \tag{2.7a}$$

Considering a *stress-based* approach, the strain rate $\dot{\varepsilon}_{ij}$ is decomposed in one part related to the current secant stiffness $\dot{\varepsilon}^S_{ij}$ and other to the stiffness degradation $\dot{\varepsilon}^d_{ij}$ ($\dot{\varepsilon}_{ij} = \dot{\varepsilon}^S_{ij} + \dot{\varepsilon}^d_{ij}$), as seen in Figure 2.6.

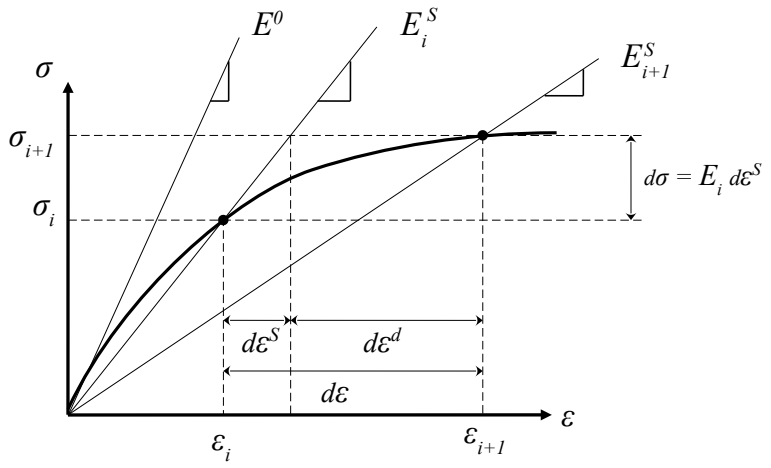

Figure 2.6: Elastic degradation: additive decomposition of the strain rate

Based on the incremental process, the following equation can be written

$$\dot{\sigma}_{ij} = E_{ijkl}(\dot{\varepsilon}_{kl} - \dot{\varepsilon}^d_{kl}) \tag{2.8}$$

with

$$\dot{\varepsilon}^d_{kl} = \dot{\lambda}_m m_{mkl} \tag{2.9}$$

where $\dot{\lambda}_m$ are the *inelastic multipliers*, defining the degrading process magnitude, and m_{mkl} are the *directions of degradation*. The different phases of the loading process are described by a loading function that can be expressed as $F[\boldsymbol{\sigma}, \boldsymbol{p}]$, where $\boldsymbol{p}$ is a vector of internal variables that control the deformation process. The linearized form of the consistency condition can be written

$$\dot{F}_n = \left.\frac{\partial F_n}{\partial \sigma_{ij}}\right|_p \dot{\sigma}_{ij} + \left.\frac{\partial F_n}{\partial p_q}\right|_\sigma \dot{p}_q = 0 \tag{2.10}$$

Assuming that the parameters p_q are functions of the degrading strains ε^d_{kl} (i.e., $\dot{p}_q = \frac{\partial p_q}{\partial \varepsilon^d_{kl}} \dot{\varepsilon}^d_{kl}$), (2.10) can be rewritten as

$$n_{nij}\dot{\sigma}_{ij} - H_{nm}\dot{\lambda}_m = 0 \tag{2.11}$$

with

$$n_{nij} = \left.\frac{\partial F_n}{\partial \sigma_{ij}}\right|_p \tag{2.12}$$

and

$$H_{nm} = -\left.\frac{\partial F_n}{\partial \lambda_m}\right|_\sigma = -\left.\frac{\partial F_n}{\partial p_q}\right|_\sigma \frac{\partial p_q}{\partial \varepsilon^d_{kl}} m_{mkl} \tag{2.13}$$

In these expressions, $\boldsymbol{m}$ indicates the directions of degradation, $\boldsymbol{n}$ the directions of the loading functions, and $\boldsymbol{H}$ the Hardening-Softening modulus. Once the "directions" $\boldsymbol{n}$ and $\boldsymbol{m}$ are established, the combination of (2.8), (2.9) and (2.11) leads to the format of the inelastic multiplier:

$$\dot{\lambda}_m = \frac{n_{nij} E_{ijkl} \dot{\varepsilon}_{kl}}{H_{nm} + n_{nij} E_{ijkl} m_{mkl}} \tag{2.14}$$

By introducing (2.14) into (2.9) and (2.8), the tangential stiffness tensor can be obtained:

$$\dot{\sigma}_{ij} = E^t{}_{ijkl} \dot{\varepsilon}_{kl} \tag{2.15}$$

where

$$E^t_{ijkl} = E_{ijkl} - \frac{E_{ijab} m_{mab} n_{ncd} E_{cdkl}}{H_{nm} + n_{npq} E_{pqrs} m_{mrs}} \tag{2.16}$$

Similarly, for a *strain-based* formulation, the stress rate is decomposed ($\dot{\sigma}_{kl} = \dot{\sigma}^S_{kl} + \dot{\sigma}^d_{kl}$) and the loading function is expressed as a function of strains and the internal variables $F_n(\boldsymbol{\varepsilon}, \bar{\boldsymbol{p}})$, where $\bar{\boldsymbol{p}}$ is the set of internal variables defined in the strain domain. Hence,

$$\dot{\varepsilon}_{ij} = C_{ijkl}(\dot{\sigma}_{kl} - \dot{\sigma}^d_{kl}) \tag{2.17}$$

with

$$\dot{\sigma}^d_{kl} = \dot{\lambda}_m \bar{m}_{mkl} \tag{2.18}$$

where, as in the stress-based formulation, $\dot{\lambda}_m$ are the inelastic multipliers and $\bar{m}_{mkl}$ the directions of degradation.

Following an analogous procedure to the previous case, the tangential stiffness can be obtained

$$\dot{\sigma}_{ij} = E^t_{ijkl}\dot{\varepsilon}_{kl} \tag{2.19}$$

with

$$E^t_{ijkl} = E_{ijkl} + \frac{1}{\bar{H}_{nm}}\bar{m}_{mij}\bar{n}_{nkl} \tag{2.20}$$

$$\bar{n}_{nij} = \left.\frac{\partial F_n}{\partial \varepsilon_{ij}}\right|_{\bar{p}} \tag{2.21}$$

and

$$\bar{H}_{nm} = -\left.\frac{\partial F_n}{\partial \lambda_m}\right|_{\varepsilon} = -\left.\frac{\partial F_n}{\partial \bar{p}_q}\right|_{\varepsilon}\frac{\partial \bar{p}_q}{\partial \varepsilon^d_{kl}}\bar{m}_{mkl} \tag{2.22}$$

The stress- and strain-based formulations here presented may be considered as equivalent dual formulations. The loading functions have in general different expressions in terms of strain or stress, but both give the same value when evaluated for a stress state or for it corresponding strain state. Under these conditions, the tensorial gradient components of stress- and strain-based formulations can be related to each other:

$$n_{nij} = C_{ijkl}\bar{n}_{nkl} \quad \text{or} \quad \bar{n}_{nij} = E_{ijkl}n_{nkl} \tag{2.23a,b}$$

$$m_{mij} = -C_{ijkl}\bar{m}_{mkl} \quad \text{or} \quad \bar{m}_{mij} = -E_{ijkl}m_{mkl} \tag{2.24a,b}$$

$$\bar{H}_{nm} = H_{nm} + n_{nij}E_{ijkl}m_{mkl} \quad \text{or} \quad H_{nm} = \bar{H}_{nm} + \bar{n}_{nij}C_{ijkl}\bar{m}_{mkl} \tag{2.25a,b}$$

2.2.2.1 Generalized degradation rule

Similarities can be noticed comparing the formulation here presented with that of plasticity models[1]. However, important differences should be noted. Elastic-degrading models adopt variable secant stiffness and compliance. Therefore, the functions and parameters usually defined in plasticity (expressions for F, hardening-softening laws and flow rule) are not sufficient to define the evolution of the degradation model. To address this aspect, the degrading strain rate ($\dot{\varepsilon}^d_{kl}$) should be formulated as a function of the stiffness or the compliance rate. Comparing equations (2.7a) and (2.8), it can be obtained

$$E_{ijkl}\dot{\varepsilon}^d_{kl} = -\dot{E}_{ijkl}\varepsilon_{kl} \tag{2.26}$$

By definition, $\boldsymbol{E} : \boldsymbol{C} = \boldsymbol{I}_4$. This equation may be differentiated as $\dot{\boldsymbol{C}} : \boldsymbol{E} + \boldsymbol{C} : \dot{\boldsymbol{E}} = 0$, and multiplied by $\boldsymbol{E}$ on the left or $\boldsymbol{C}$ on the right, yielding the relations between the stiffness and compliance changes

$$\dot{E}_{ijkl} = -E_{ijpq}\dot{C}_{pqrs}E_{rskl} \tag{2.27a}$$

or

$$\dot{C}_{ijkl} = -C_{ijpq}\dot{E}_{pqrs}C_{rskl} \tag{2.27b}$$

Equation (2.27a) can now be introduced in the right-hand side of (2.26), both sides can be multiplied by C_{pqij}, and, using (2.6a), the following expression can be obtained:

$$\dot{\varepsilon}^d_{ij} = \dot{C}_{ijkl}\sigma_{kl} \tag{2.28}$$

This equation indicates a relationship between the increment of secant compliance and the increment of degrading strain. Now, it is convenient to define a "generalized flow rule" or *degrading rule* for the secant compliance

$$\dot{C}_{ijkl} = \dot{\lambda}_m M_{mijkl} \tag{2.29}$$

[1]In this work, the formulation of plasticity models is not presented. For further reference, see Chapter 2 of Penna (2011).

where $\dot{\lambda}_m$ defines the magnitude and M_{mijkl} the direction of the rate of change of C_{ijkl}. By replacing (2.29) and (2.9) in (2.28), and eliminating the multipliers from both sides, one obtains

$$m_{mij} = M_{mijkl}\sigma_{kl} \tag{2.30}$$

Summarizing, the constitutive description of elastic degradation becomes complete after definition of $\boldsymbol{F}$, the hardening-softening law $\boldsymbol{H}$ and the degradation rule $\boldsymbol{M}$. The final expression for the tangent stiffness tensor is obtained by direct substitution of (2.30) into (2.16)

$$E^t_{ijkl} = E_{ijkl} - \frac{E_{ijab}M_{mabxy}\sigma_{xy}n_{ncd}E_{cdkl}}{H_{nm} + n_{npq}E_{pqrs}M_{mrsuv}\sigma_{uv}} \tag{2.31}$$

The evolution of the secant compliance can be rewritten combining equations (2.14) and (2.30), and applying it to (2.29):

$$\dot{C}_{ijkl} = M_{mijkl}\frac{n_{nab}E_{abcd}\dot{\varepsilon}_{cd}}{H_{nm} + n_{npq}E_{pqrs}M_{mrsuv}\sigma_{uv}} \tag{2.32}$$

Similarly, the evolution of the secant stiffness may be obtained as

$$\dot{E}_{ijkl} = \bar{M}_{mijkl}\frac{\bar{n}_{ncd}C_{cdkl}\dot{\sigma}_{kl}}{\bar{H}_{nm}} + \bar{n}_{npq}C_{pqrs}\bar{M}_{mrsuv}\varepsilon_{uv} \tag{2.33}$$

with

$$\dot{E}_{ijkl} = \dot{\lambda}_m\bar{M}_{mijkl} \tag{2.34}$$

2.2.2.2 Damage variables in elastic degrading models

In the previous sections, the stiffness degradation was defined by the evolution of the secant compliance and stiffness tensors through loading functions and degrading rules. That is the most general way of approaching the problem, but usually not the most simple, because it requires the definition of the evolution of each material

parameter. If the media is characterized by an orthotropic behavior, for example, there are 21 independent components of C_{ijkl} and E_{ijkl}.

It is reasonable to assume that exists a much more reduced set of parameters able to characterize the state of degradation or *damage* achieved by the material at any state of loading. This reduced set of descriptors is called the *set of damage variables*, and is designated by the symbol $\mathcal{D}_*$. The symbol "*" represents the set of indexes, which depends on the problem nature, e.g., $\mathcal{D}$ is a scalar, $\mathcal{D}_i$ is a vector, and $\mathcal{D}_{ij}$ is a second-order tensor.

Compliance-based formulation

In stress-based formulations, the degradation process is modeled by means of some rules that describe the progressive increase of the secant compliance tensor C_{ijkl}. With the introduction of a set of damage variables $\mathcal{D}_*$ that fully characterize the state of degradation, the secant compliance tensor may be written as

$$C^S_{ijkl} = C_{ijkl}(C^0_{pqrs}, \mathcal{D}_*) \tag{2.35}$$

where C^0_{pqrs} is the initial compliance. Differentiating (2.35):

$$\dot{C}^S_{ijkl} = \frac{\partial C^S_{ijkl}}{\partial \mathcal{D}_*}\dot{\mathcal{D}}_* \tag{2.36}$$

A flow rule for damage can now be written as

$$\dot{\mathcal{D}}_* = \dot{\lambda}_m \mathcal{M}_{m*} \tag{2.37}$$

in which, similar to the flow rules previously defined, $\dot{\lambda}_m$ is a *damage multiplier* defining the magnitude, and $\mathcal{M}_{m*}$ defines the direction of the rate of change of the damage variables ($\mathcal{M}_{m*}$ has the same character and dimensions of $\mathcal{D}_*$). By substituting (2.29) and (2.37) in (2.36), one obtains

$$M_{mijkl} = \frac{\partial C^S_{ijkl}}{\partial \mathcal{D}_*}\mathcal{M}_{m*} \tag{2.38}$$

Since the partial derivatives are known functions, (2.38) means that once the damage rule $\mathcal{M}_{m*}$ is established, the compliance rule M_{mijkl} follows automatically.

Stiffness-based formulation

Similarly as presented for the compliance-based formulation, a set of damage variables $\bar{\mathcal{D}}_*$ that fully characterize the state of degradation is introduced. In this case, the process is described by the progressive reduction of the secant stiffness tensor E_{ijkl}, that can be written as

$$E^S_{ijkl} = E_{ijkl}(E^0_{pqrs}, \dot{\bar{\mathcal{D}}}_*) \tag{2.39}$$

and

$$\dot{E}^S_{ijkl} = \frac{\partial E^S_{ijkl}}{\partial \bar{\mathcal{D}}_*} \dot{\bar{\mathcal{D}}}_* \tag{2.40}$$

Again, a damage rule $\bar{\mathcal{M}}_{m*}$ is assumed for $\bar{\mathcal{D}}_*$ and is related to the stiffness rule $\bar{M}_{mijkl}$

$$\dot{\bar{\mathcal{D}}}_* = \dot{\lambda}_m \bar{\mathcal{M}}_{m*} \quad \text{and} \quad \bar{M}_{mijkl} = \frac{\partial E^S_{ijkl}}{\partial \bar{\mathcal{D}}_*} \bar{\mathcal{M}}_{m*} \tag{2.41a,b}$$

2.2.2.3 Scalar-isotropic damage models in the unified framework

The unified theory here presented can encompass many of the continuum damage models proposed in the recent literature. In this section, standard scalar-isotropic damage models (as defined by de Borst and Gutiérrez (1999)) will be presented in the context of the unified framework in order to generalize common definitions and identify the gradients of the unified theory.

As previously addressed, for scalar-isotropic damage models the degrading process is characterized by a single scalar damage variable that impacts the whole initial constitutive tensor (Eq. 2.5). Hence, the total stress-strain relation is defined as

$$\sigma_{ij} = (1 - D) E^0_{ijkl} \varepsilon_{kl} \tag{2.42}$$

where D is the scalar damage variable ($\bar{\mathcal{D}}_* = D$). The loading function can be written as

$$F(\varepsilon_{ij}, D) = \varepsilon_{eq}(\varepsilon_{ij}) - K(D) \tag{2.43}$$

in which $\varepsilon_{eq}(\varepsilon_{ij})$ can be defined as an *equivalent strain* and $K(D)$ is a *history variable*, which has the same nature as $\varepsilon_{eq}(\varepsilon_{ij})$ and is written as a function of the damage, being representative of the highest level of deformation reached during loading.

Based on (2.42), the same relation can be applied to define the relation between initial and current secant stiffness

$$E^S_{ijkl} = (1 - D)E^0_{ijkl} \tag{2.44}$$

After differentiation of (2.44), one obtains

$$\dot{E}^S_{ijkl} = -\dot{D}E^0_{ijkl} \tag{2.45}$$

Comparing (2.45) with (2.40) and (2.41a), one can identify

$$\frac{\partial E^S_{ijkl}}{\partial D} = -E^0_{ijkl}; \quad \bar{\mathcal{M}} = 1; \quad \dot{\lambda} = \dot{D} \tag{2.46a,b,c}$$

From the definition of the loading function, the gradient and the hardening-softening law can be obtained

$$\bar{n}_{kl} = \frac{\partial F}{\partial \tilde{\varepsilon}} \quad \text{and} \quad \bar{H} = \frac{\partial K(D)}{\partial D} \tag{2.47a,b}$$

where the term $\frac{\partial K(D)}{\partial D}$ requires an explicit function of the history variable in terms of damage. Usually, only an evolution law for damage in terms of the strain measurement is available such as the following exponential law

$$D(\varepsilon_{eq}) = 1 - \frac{K_0}{\varepsilon_{eq}}\left(1 - \alpha + \alpha e^{-\beta(\varepsilon_{eq} - K_0)}\right) \tag{2.48}$$

where K_0 is the threshold for the equivalent strain, and α and β define the maximum allowed damage level and the damage evolution intensity, respectively. The influence of each of the parameters in the damage evolution are illustrated in Figure 2.7 by graphs relating the equivalent strain ε_{eq} and the damage variable D.

Figure 2.7(a) illustrates the effect of the parameter K_0 where, as K_0 increases, the equivalent strain limit from which damage occurs also increases. On the other hand, the parameter β (Figure 2.7(b)) controls the velocity with which the material achieves a completely damaged state. Therefore, with the decrease of β, the longer it takes for the damage to reach $D = 1$. Lastly, α sets the limit for the damage level, thus, with its increase, the closer the damage may get to the maximum damage allowed $D = 1$ (Figure 2.7(c)).

The classic damage models of *Mazars-Lemaitre* (Mazars and Lemaitre, 1985), *Simo-Ju* (Simo and Ju, 1987), *Ju* (Ju, 1989), and *Marigo* (Marigo, 1985; Lemaitre and Desmorat, 2005) are defined by the different definitions for the equivalent strain as presented

$$\varepsilon_{eq} = \begin{cases} \sqrt{\varepsilon_{ij}\varepsilon_{ij}} & \text{(Mazars-Lemaitre)} \\ \sqrt{2\psi^0} & \text{(Simo-Ju)} \\ \psi^0 & \text{(Ju)} \\ \sqrt{2\psi^0/E} & \text{(Marigo)} \end{cases} \tag{2.49}$$

in which $2\psi^0 = \varepsilon_{ij} E^0_{ijkl} \varepsilon_{kl}$ is the internal energy and E is the initial Young's modulus.

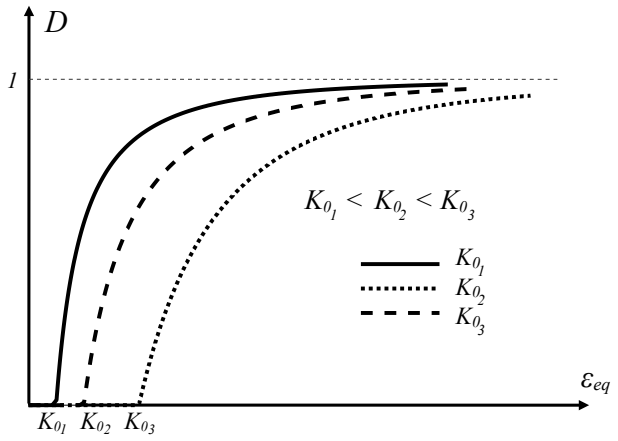

(a) K_0

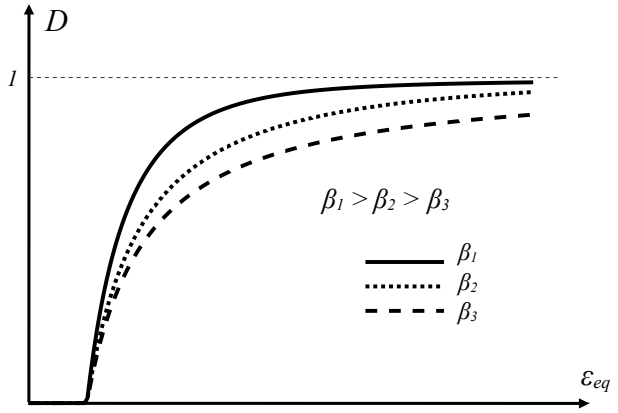

(b) β

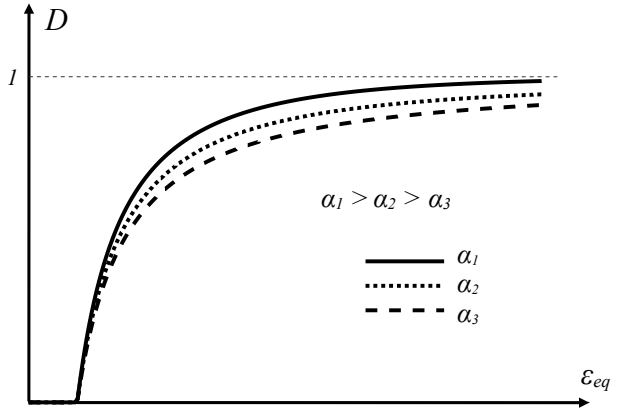

(c) α

Figure 2.7: Exponential law: parameters

2.3 Modeling of heterogeneous media

As discussed in Section 2.1 the behavior of quasi-brittle materials is directly related to its heterogeneous structure. To account for the effects provoked by the heterogeneity, the material may be modeled considering the different materials that compose it, introducing, in the analysis, parameters related to the microstructure. Such models, called *mesoscopic* models, have proven to be a reliable approach for studying the influence of the concrete composition on the macroscopic properties (Wang et al., 1999) and have as working hypothesis the direct simulation of the random structure of inhomogeneous materials.

Bažant et al. (1990) present a model for composite materials where the microstructure is generated by a random method and each particle is assumed to be elastic and have only axial deformations, behaving as a truss element. Therefore, the material is simulated using a truss model where each element links the centers of adjacent circular particles generated. The interparticle contact layers of the matrix are described by a softening stress-strain relation.

A framework model was used by Schorn and Rode (1991) in order to simulate crack propagation in concrete for three-dimensional models where the different properties of aggregate, interface and matrix were considered. Schlangen and van Mier (1992), for simulating fracture in concrete, employ a triangular lattice model where the spatial randomness of inhomogeneities are considered using two approaches. First, the lattice model is projected on a grain structure randomly generated and different material properties are assigned to the respective bar elements (matrix, bond-zone or interface, and aggregates). Secondly, a distribution of bar strength or stiffness is specified, for example a normal distribution, and each element is associated to a material according to the defined distribution.

Bažant et al. (1990), Schorn and Rode (1991), and Schlangen and van Mier (1992) all proposed models that the constituents of the microstructure are modeled using one-dimensional elements associated to a non-linear law to describe each material behavior under tension. Another possibility developed by Wittmann and co-workers (Wittmann et al., 1985; Roelfstra et al., 1985) is the modeling of mortar and aggregates as continua using plane elements. In this process, the particles are generated according to a specified particle size distribution and, following, a finite elements mesh able to represent the generated particles (Figure 2.8) is constructed and the properties for the different phases are associated to the respective elements.

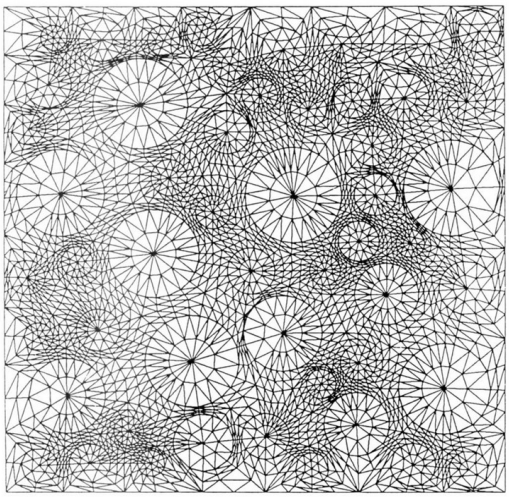

Figure 2.8: Finite element mesh proposed by Wittmann et al. (1985) to analyze concrete built up of about 8000 finite elements representing rounded aggregates, interface and mortar matrix

For micro scale analyzes of concrete, the generation of a random aggregate structure is necessary where shape, size, and distribution of coarse aggregates is representative of real concrete from a statistical point of view. Generating this random structure consists of an assembly of randomly distributed aggregate particles and the mortar matrix in the space between particles (Wang et al., 1999).

Bažant et al. (1990), Schlangen and van Mier (1992) and Wittmann et al. (1985) simulated size and spatial distributions of aggregate particles by the random sampling principle of Monte Carlo's where samples of particles are taken from a source that follows a given grading curve and placed one by one into the analysis domain with no overlapping with particles already placed. This process tries to achieve a spatial distribution as macroscopically homogeneous as possible and is commonly called the *take-and-place* method.

The take-and-place algorithm can be classified as a *stochastic-heuristic* process considering its intrinsic randomness (each new simulation is a different problem even with same input parameters) and the trial-error process to verify whether a particle can be placed or not, evaluating if there is no overlapping and if all particles are completely inside the domain and limiting distances ("particle-to-particle" and "particle-to-boundary") (Monteiro et al., 2017).

The *take-process* and the *place-process* are performed concurrently as each generated particle is immediately placed in the concrete[2]. This process begins with

[2]For a more detailed discussion of the take-and-place method and its steps, the reader may refer

the largest size particles and goes on until all particles in that size range has been placed, considering that this is generally the easiest manner to arrange particles into the concrete (Wang et al., 1999).

The total amount of coarse aggregates to be included in the process is defined by the *volumetric ratio*, calculated dividing the weight of coarse aggregates per volume of concrete by the density of the aggregate. This ratio, herein called *particle fraction* (PF) varies between 40% and 50% for most concrete (Wang et al., 1999). The sizes for the aggregates are set as the width of the particle to conform with the definition used in sieving analysis, instead of providing an average diameter. Generally, the particle size distribution is expressed in terms of cumulative percentage passing through a series of sizes of sieve openings. One commonly used continuous distribution is given by Fuller, which can be described by the following equation (Wriggers and Moftah, 2006)

$$P(d) = 100 \left(\frac{d}{d_{max}} \right)^n \tag{2.50}$$

where $P(d)$ is the cumulative percentage passing a sieve with size d, d_{max} is the maximum size of aggregate particles, and n is the exponent of the equation ($n = 0.45 - 0.70$ according to Wriggers and Moftah (2006)).

In order to guarantee that all aggregate particles are coated with a minimum thickness of mortar film, a *distribution factor* (DF) is defined, where an offset on the radius of the particle is set, enlarging the aggregate size prior to checking the existence of overlapping.

Another aspect of the microstructure generator is the definition of the shape of the particles, which is closely related to the aggregate type. Generally, grave aggregates have a round shape while crushed rock aggregates present an angular shape (Wang et al., 1999). For simulating both shapes, the aggregates can be modeled as circular or polygonal/irregular particles, wherein, for the second option, the particle characteristic dimension is taken as an average radius. For the case of polygonal aggregates, the generation is based on an average circumference circumscribed to a regular polygon with PS sides to which an angular deviation Δ_α and radial deviation Δ_R are applied.

To illustrate the capacity of the microstructure generator, Monteiro et al. (2017) presented some distribution examples for a 10 cm $\times$ 20 cm section considering typical

to Wang et al. (1999) and Wriggers and Moftah (2006).

particle fractions of concrete mixtures. For the aggregate size distribution, a Fuller curve was used associated to the sieve sizes specified by ABNT NBR 7211 (2005) (25.0 mm to 4.75 mm). Figures 2.9(a) and 2.9(b) show the generated structure for circular particles and Figures 2.9(c) and 2.9(d) for polygonal particles obtained by Monteiro et al. (2017).

2.3.1 Micromechanics considerations

As extensively discussed, concrete is a composite material with a number of inhomogeneities. Determining the macroscopic mechanical behavior based on the microscopic deformation is of great interest. A method for obtaining such relation may be referred to as *homogenization*, in which the heterogeneous material is replaced by an *equivalent* homogeneous continuum considering a statistically representative sample of material, the RVE (see Section 2.2)[3].

A numerical method that has proven to be efficient is the FEM [4], whereby the effective responses can be obtained by volumetrically averaging the internal fields over an RVE of the heterogeneous material (Wriggers and Moftah, 2006). This principle was applied in this work in order to obtain an equivalent microcontinuum for a micromorphic media based on a heterogeneous RVE wherein the particles where generated by the take-and-place method. More details on this procedure will be given in Chapter 4.

[3]For a review of classical analytical micromechanics models proposed to estimate the effective properties of heterogeneous media, the reader may refer to Christensen (1990).

[4]In this field, other numerical methods have been developed to account for the spatially variable microstructure of heterogeneous materials as the finite-volume theory (Cavalcante et al., 2006*a*,*b*), which, as FEM models, also involves the discretization of all the constituent phases, as well as approaches based on Fast Fourier Transform (FFT) (Lages and Cavalcanti Marques, 2022).

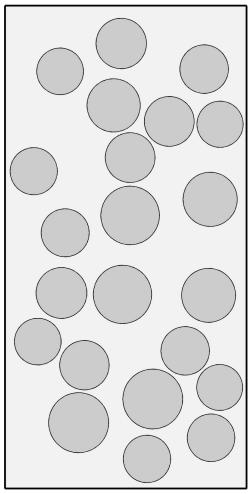

(a) $PF = 40\%$;
$DF = 0.1$;
sieves $25 - 19$ mm

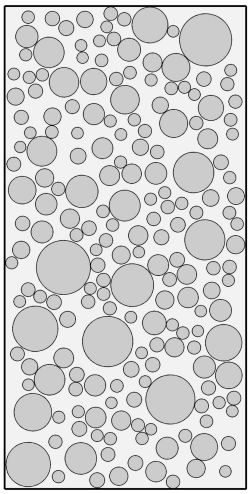

(b) $PF = 50\%$;
$DF = 0.02$;
sieves $25 - 4.75$ mm

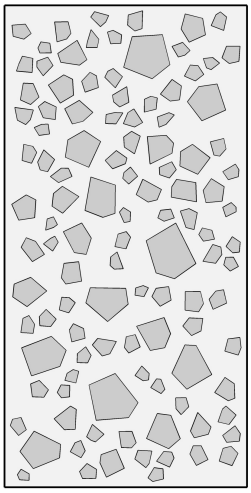

(c) $PF = 30\%$;
$DF = 0.03$; $PS = 5$;
$\Delta_R = 0.7$;
$\Delta_\alpha = 0.05$;
sieves$25 - 6.3$ mm

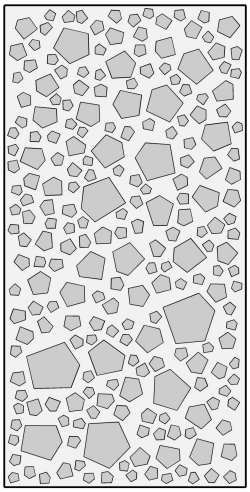

(d) $PF = 40\%$;
$DF = 0.02$; $PS = 5$;
$\Delta_R = 0.5$;
$\Delta_\alpha = 0.01$;
sieves$25 - 4.75$ mm

Figure 2.9: Random aggregate structures generated: circular and polygonal particles (Monteiro et al., 2017)

Chapter 3

Micromorphic Media

3.1 Generalized Continua

In the study of material behavior based on the classical continuum mechanics every point in the material is occupied by a small element of the solid, called *material particle*. These particles can be idealized as mathematical points as its dimensions are small compared to all characteristics lengths, but are nevertheless large compared to atomic dimensions (Mal and Singh, 1991). In this context, the medium kinematics is described by the translational degrees of freedom of the material particles and by the consequent measures of deformation.

The idea here presented of *classical continuum mechanics* is based on the paradigm constructed with the combinations of ideas from Leonard Euler (1707-1783), Joseph L. Lagrange (1736-1813), and Augustin L. Cauchy (1789-1857), and the divergence theory proposed by George Green (1793-1841) (Maugin, 2017). According to Maugin (2014), the notion of stress in a general continuum was initially proposed in a magisterial paper by Cauchy in 1822, but published only in 1828 (Cauchy, 1828). In his work, Cauchy generalized Euler's notion of pressure in the notion of *stress tensor*.

When dealing with composite inhomogeneous materials in the classical continuum the constitutive equations are developed using the concept of material particle associated to the idea of a representative volume element (RVE), as discussed in Section 2.2 (Hashin, 1983; Kröner, 1977; Willis, 1981).

In the classical continuum, the kinematics and statics descriptions of the medium consider only average macroscopic characteristics, disregarding the microstructure constituents behavior. In the analysis of usual structures in the engineering field the hypotheses of the classical continuum are sufficient. However, in situations wherein

the RVE concept does not represent satisfactorily all the phenomena related to the influence of the substructure or the structural dimensions are small comparatively to the microstructure, theories that incorporate information on the material microstructure are required.

In this context, *generalized continuum mechanics* were developed. In the work of Voigt (1887) and Cosserat and Cosserat (1909) begins the generalization of standard continuum mechanics of Cauchy through the expansion of its basic working hypotheses. These generalizations involve additional degrees of freedom (*higher order continua*) or/and higher order gradients of the displacement fields (*higher grade continua*) (Germain, 1973*a*,*b*; Forest, 1998; Hirschberger, 2008).

Remark 3.1.1. *Kinematics of deformation*

The motion of the material particle P in a continuously deforming body B (Fig. 3.1) can be expressed by a mapping from the material configuration B_0 to the spatial configuration B_t developed in a Taylor series expansion as follows:

$$d\boldsymbol{x} = \nabla_{\boldsymbol{X}}\, \boldsymbol{x}(\boldsymbol{X},t) \cdot d\boldsymbol{X} + \frac{1}{2}\nabla_{\boldsymbol{X}}[\nabla_{\boldsymbol{X}}\, \boldsymbol{x}(\boldsymbol{X},t)] : [d\boldsymbol{X} \otimes d\boldsymbol{X}] + \mathcal{O}(d\boldsymbol{X}^3) \qquad (3.1)$$

Therein $\boldsymbol{F} = \nabla_{\boldsymbol{X}}\, \boldsymbol{x}(\boldsymbol{X},t)$ is a linear map, its gradient $\nabla_{\boldsymbol{X}}[\nabla_{\boldsymbol{X}}\, \boldsymbol{x}(\boldsymbol{X},t)]$ represents the quadratic term, while $\mathcal{O}(d\boldsymbol{X}^3)$ corresponds to the terms of cubic or higher grade.

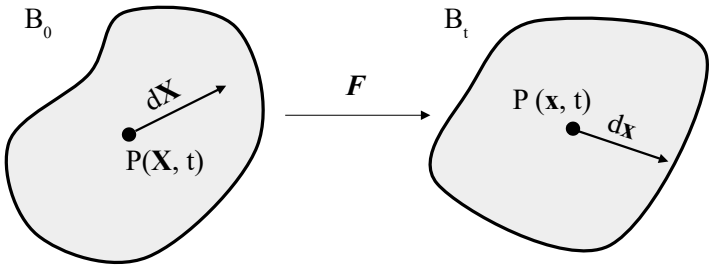

Figure 3.1: Kinematics of deformation

In the classical continuum, only the linear term is considered in the deformation map (3.1) and, consequently, the vicinity of the material particle P stays unconsidered (*local* continuum theory):

$$d\boldsymbol{x} = \nabla_{\boldsymbol{X}}\, \boldsymbol{x}(\boldsymbol{X}, t) \cdot d\boldsymbol{X} \tag{3.2}$$

When the quadratic term (second-order gradient theory), as a special case of the second gradient of strain theory of Mindlin (Mindlin, 1965), or even higher grade terms are considered in the non-linear deformation mapping (3.1) a higher grade continua is obtained. They are appropriated to the analysis of cases wherein only the linear term is not sufficient to describe the media behavior as, with high order terms, size effect can be take into account (Hirschberger, 2008). The classical continuum can be considered a special case of a higher grade continuum with grade one.

On the other hand, higher order continua are characterized by additional degrees of freedom per material point instead of considering higher gradients of deformation. From a microcoscopic point of view, each material point in the macrocontinuum is a continuum of small extent, being its kinematics described by a linear deformation map as in (3.2) (Germain, 1973*b*). Embedded in each point is assumed to be a *micro-continuum*, whose kinematics defines the additional degrees of freedom (Germain, 1973*b*; Mindlin, 1964; Hirschberger, 2008). The micromorphic continuum, due to the characteristics of its formulation, which will be approached in the next sections, is able to capture size-effects and its particularly suited to account for materials possessing a significant microstructure.

In the works of Germain (1973*b*) and Eringen (1966) higher order continua are denominated *micromorphic continua* of order n. The practicality of continua of order $n > 1$ is highly questionable, considering that the first order theory is complicated enough for genuine physical applications. Moreover, considering the physical conditions for which the theory is valid, the microcontinuum presents small dimensions compared to the size of the macrocontinuum. Hence, if the continuum undergoes small deformation, the second and higher terms considered in the kinematics description may be neglected similar to neglecting higher order displacements gradients in the deformation of an elastic solid (Eringen, 1966).

For the first order theory of the micromorphic continuum, the kinematics of each material particle is described by the mapping ($\boldsymbol{\Xi} \xrightarrow{\boldsymbol{X},t} \boldsymbol{\xi}$) of its attached vector $\boldsymbol{\Xi}$, located at the centroid of the particle,

$$\boldsymbol{\xi} = \boldsymbol{\chi}(\boldsymbol{X}, t)\, \Xi_K \tag{3.3}$$

in which

$$\boldsymbol{\chi}_K(\boldsymbol{X}, t) = \left.\frac{\partial \boldsymbol{\xi}}{\partial \Xi_K}\right|_{\Xi=0} \tag{3.4}$$

As exposed in Eringen (1999), the second order tensor $\boldsymbol{\chi}$ is called *microdeformation* tensor (alternatively, *deformable directors*) and represents three deformable directors related to the degrees of freedom arising from microdeformations of the physical particle. Thus, the micromorphic continuum is none other than a classical continuum endowed with nine additional degrees of freedom, being six related to the *micro deformations* and three to the *micro rotations*. The kinematics of a point can be illustrated with the deformable director triad as shown in Figure 3.2. A more detailed explanation of the micromorphic theory for a small-strain framework as developed by Eringen (1999) is presented in Section 3.2.

Remark 3.1.2. *Microcontinuum theories (Eringen, 1999; Hirschberger, 2008)*

According to the polar decomposition theorem, a matrix may be decomposed as product of an orthogonal matrix and a symmetric matrix (Mal and Singh, 1991; Eringen, 1980). Hence, the tensor $\boldsymbol{\chi}$ can be written as

$$\boldsymbol{\chi} = \boldsymbol{R}\boldsymbol{U} = \boldsymbol{V}\boldsymbol{R} \tag{3.5}$$

where $\boldsymbol{R}$ represents the *micro rotation tensor* related to rigid rotations, and $\boldsymbol{U}$ and $\boldsymbol{V}$ are called *right* and *left stretch tensors* for micro deformations.

Therefore, in a micromorphic continuum the particle may experience stretching/compression and rotation comprised in the tensor $\boldsymbol{\chi}$ (Figure 3.2). Several sub-theories can be derived from the general case applying constraints to the deformation of the microcontinuum, i.e., to the micro-deformation tensor $\boldsymbol{\chi}$. The micromorphic theory and its sub-theories are grouped under the name *microcontinuum theories*, being this classification and the corresponding continuum frameworks well elaborated by Eringen (1999).

For instance, considering that the *micropolar continuum* (or *Cosserat continuum*) (Cosserat and Cosserat, 1909; Eringen, 1999) may only experience rotation, it can be obtained by assuming $\boldsymbol{\chi} = \boldsymbol{R}$, as illustrated in Figure 3.3 with the rigid director triad. If a scalar variable χ, besides the rotation $\boldsymbol{R}$, is incorporated to account for isotropic extension, i.e., $\boldsymbol{\chi} = \chi\boldsymbol{R}$, the *microstretch*

continuum (Eringen, 1999) is obtained, as depicted in Figure 3.4. For the case in which only the stretch tensor $\boldsymbol{U}$ is considered and the rotation is neglected ($\boldsymbol{\chi} = \boldsymbol{U}$), as seen in Figure 3.5, the *microstrain continuum*, proposed by Forest and Sievert (2006), may be derived.

Lastly, if both stretch and rotation are restrained, the classical continuum is obtained, where the hypotheses of unalterable particles is considered. As seen in Figure 3.6, for this case, $\boldsymbol{\chi} = \boldsymbol{I}$, in which $\boldsymbol{I}$ is the second order identity tensor.

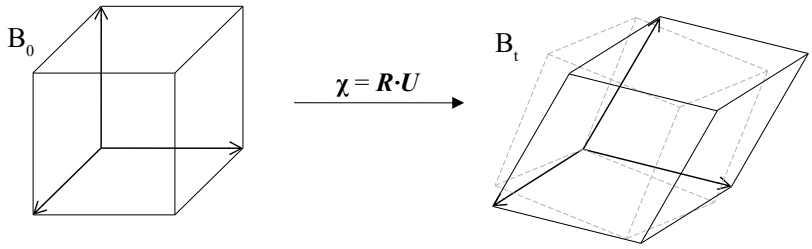

Figure 3.2: Micromorphic micro deformation: deformable director triad

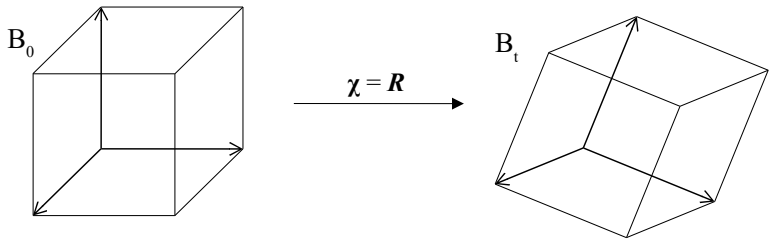

Figure 3.3: Micropolar micro deformation: rigid director triad

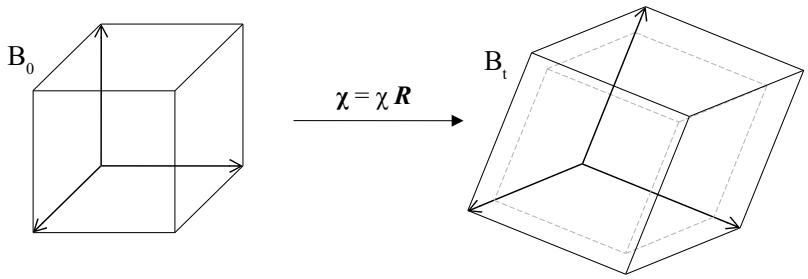

Figure 3.4: Microstretch micro deformation: extensible director triad

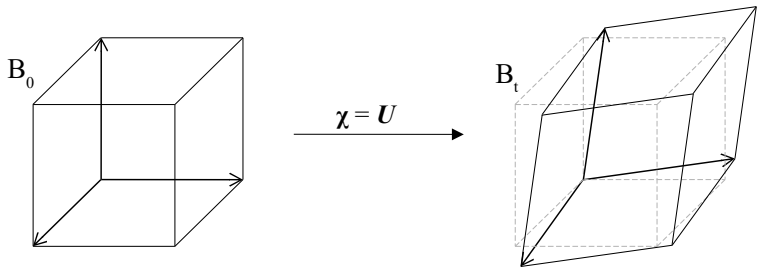

Figure 3.5: Microstrain micro deformation: stretchable director triad excluding rotation

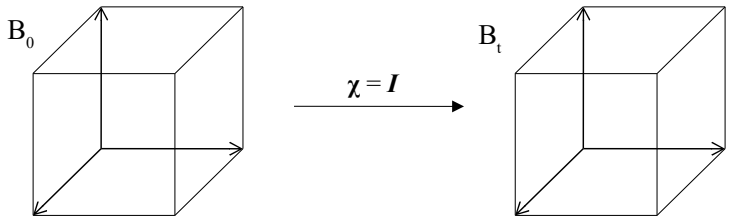

Figure 3.6: Classical micro deformation: no director triad

3.2 Micromorphic Continuum Theory

As aforementioned, in the micromorphic continuum, additional degrees of freedom are considered at each material point or, as defined by Eringen (1999), “A

microcontinuum is a continuous collection of deformable point particles." (p. 3)

In order to represent the intrinsic deformation of a point, each deformable particle is replaced with a geometrical point P and some vectors attached to P that are related to the orientations and deformations of its material points. In addition, the vectors assigned to P also represent the additional degrees of freedom of each particle. A particle P is defined by its position vector $\boldsymbol{X}$ $(X_K, K = 1, 2, 3)$ in the reference state B and vectors attached to P, representing the inner structure of P by $\boldsymbol{\Xi}_\alpha, \alpha = 1, 2, \ldots, N$. Both $\boldsymbol{X}$ and $\boldsymbol{\Xi}_\alpha$ have their own motions

$$\boldsymbol{X} \overset{t}{\longrightarrow} \boldsymbol{x}, \qquad \boldsymbol{\Xi}_\alpha \overset{\boldsymbol{X},t}{\longrightarrow} \boldsymbol{\xi}_\alpha, \qquad \alpha = 1, 2, \ldots, N. \tag{3.6}$$

Such a medium may be called microcontinuum of *grade N*. As pointed out by Eringen (1999), there were not in his time a general theory of this magnitude. This work is only concerned with the case of grade 1 ($\alpha = 1$).

3.2.1 Kinematics of Deformation

A material point $P(\boldsymbol{X}, \boldsymbol{\Xi}) \in B$ is characterized by its centroid C and vector $\boldsymbol{\Xi}$ attached to C. The point C is identified by its rectangular coordinates X_K $(K = 1, 2, 3)$ and the vector $\boldsymbol{\Xi}$ by its components Ξ_K $(K = 1, 2, 3)$. Under solicitation, motion accompanied by deformation of the solid occurs and the point $P(\boldsymbol{X}, \boldsymbol{\Xi})$ is carried to $p(\boldsymbol{x}, \boldsymbol{\xi}, t)$ in a spatial frame of reference b, so that, $X_K \longrightarrow x_k, \Xi_K \longrightarrow \xi_k (K = 1, 2, 3; k = 1, 2, 3)$ (Figure 3.7).

From a physical (and practical) point of view, a visual benefit will result if the vectors $\boldsymbol{\Xi}$ and $\boldsymbol{\xi}$ are considered to be the positions of the material points – contained in the particle P – relative to the particle centroid C in the *material* (undeformed state) and *spatial* (deformed state) configurations (Figure 3.7).

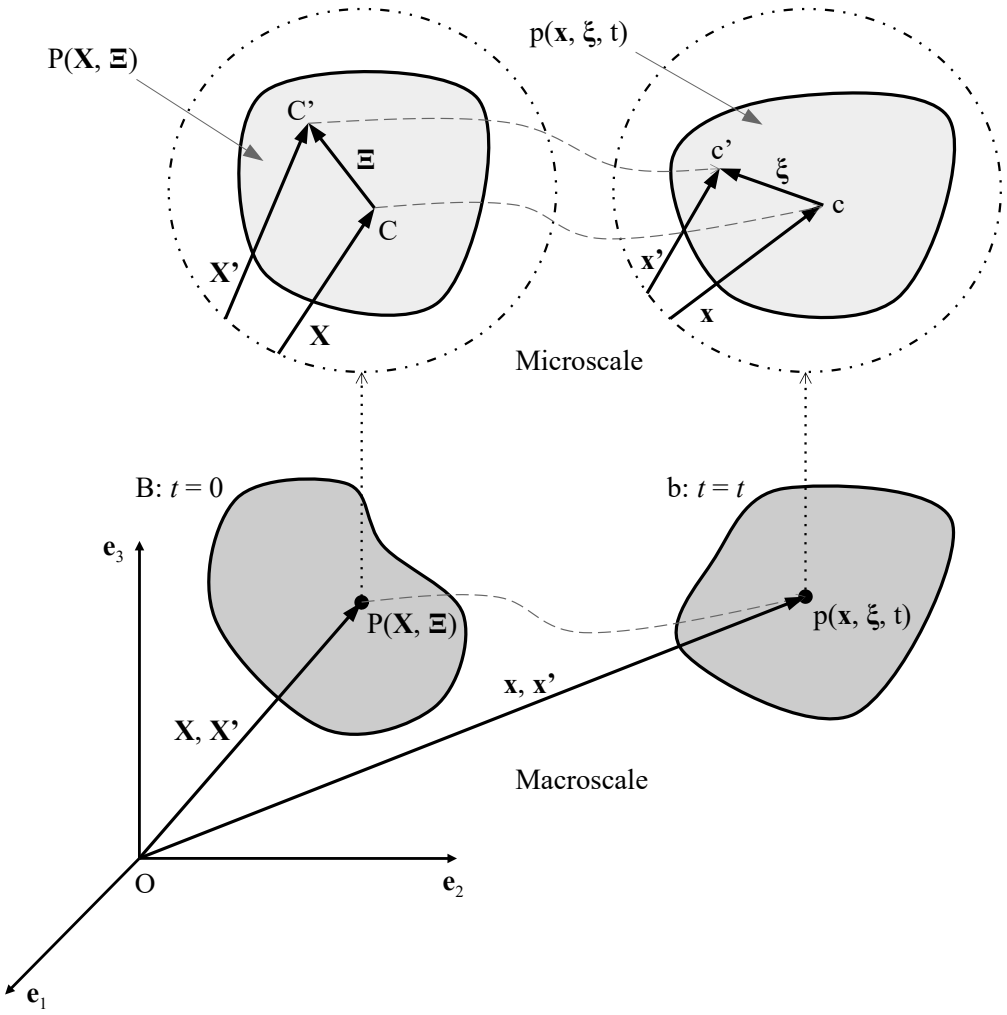

Figure 3.7: Micromorphic continuum kinematics (Silva, 2019)

As aforesaid, $\boldsymbol{\Xi}$ and $\boldsymbol{\xi}$ have their own motions, expressed by

$$\boldsymbol{X} \longrightarrow \boldsymbol{x} = \boldsymbol{x}(\boldsymbol{X}, t) \quad \text{or} \quad x_k = x_k(X_K, t) \tag{3.7}$$

$$\boldsymbol{\Xi} \longrightarrow \boldsymbol{\xi} = \boldsymbol{\xi}(\boldsymbol{X}, \boldsymbol{\Xi}, t) \quad \text{or} \quad \xi_k = \xi_k(X_K, \Xi_K, t) \tag{3.8}$$

The mapping (3.7) is called *macromotion* (or simply, the motion) and (3.8) the *micromotion*.

Considering that the material particles are of very small size (infinitesimally small) as compared to macroscopic scales of the body, a linear approximation in $\boldsymbol{\Xi}$ may be used and the micromotion (3.8) can be approximated by

$$\boldsymbol{\xi} = \boldsymbol{\chi}_K(\boldsymbol{X}, t)\Xi_K \quad \text{or} \quad \xi_k = \chi_{kK}(\boldsymbol{X}, t)\Xi_K \tag{3.9}$$

where $\boldsymbol{\chi}$ is the microdeformation gradient (alternatively, deformable directors) presented in Section 3.1 and defined as

$$\boldsymbol{\chi}_K(\boldsymbol{X}, t) = \left.\frac{\partial \boldsymbol{\xi}}{\partial \Xi_K}\right|_{\boldsymbol{\Xi}=\mathbf{0}} \tag{3.10}$$

Note that $\boldsymbol{\Xi} = 0$ is taken to be the centroid of P in the particle local system.

The motion of the material point $C' \in P$ with coordinates X'_K $(K = 1, 2, 3)$ is, thus, completely described by the macro-micromotion composition

$$\boldsymbol{x}' = \boldsymbol{x}(\boldsymbol{X}, t) + \boldsymbol{\xi}(\boldsymbol{X}, \boldsymbol{\Xi}, t) \tag{3.11}$$

Then, from (3.9),

$$\boldsymbol{x}' = \boldsymbol{x}(\boldsymbol{X}, t) + \boldsymbol{\chi}_K(\boldsymbol{X}, t)\Xi_K \tag{3.12}$$

Note that, by (3.9), $\boldsymbol{\xi}(\boldsymbol{X}, \boldsymbol{\Xi}, t)|_{\boldsymbol{\Xi}=\mathbf{0}} = 0$, i.e., the motion of the centroid of P is, by definition, entirely described in the macro-scale.

Definition 3.2.1. *Micromorphic Continuum* (Eringen, 1999)

A material body is called a micromorphic continuum of grade one (or simply micromorphic continuum) if its motions are described by (3.7) and (3.8) which possess continuous partial derivatives with respect to X_K and t, and they are invertible uniquely, i.e.,

$$X_K = X_K(\boldsymbol{x}, t), \qquad K = 1, 2, 3, \tag{3.13}$$

$$\Xi_K = \mathfrak{X}_{Kk}(\boldsymbol{x}, t)\xi_k, \qquad K = 1, 2, 3, \quad k = 1, 2, 3. \tag{3.14}$$

where $\mathfrak{X}$ is the *inverse microdeformation gradient* tensor.

A material point in the body is now considered to possesses three deformable directors ($\mathfrak{X}_k \longrightarrow \boldsymbol{\chi}_K$), as illustrated in Figure 3.8, which represent the degrees of freedom arising from microdeformations of the physical particle.

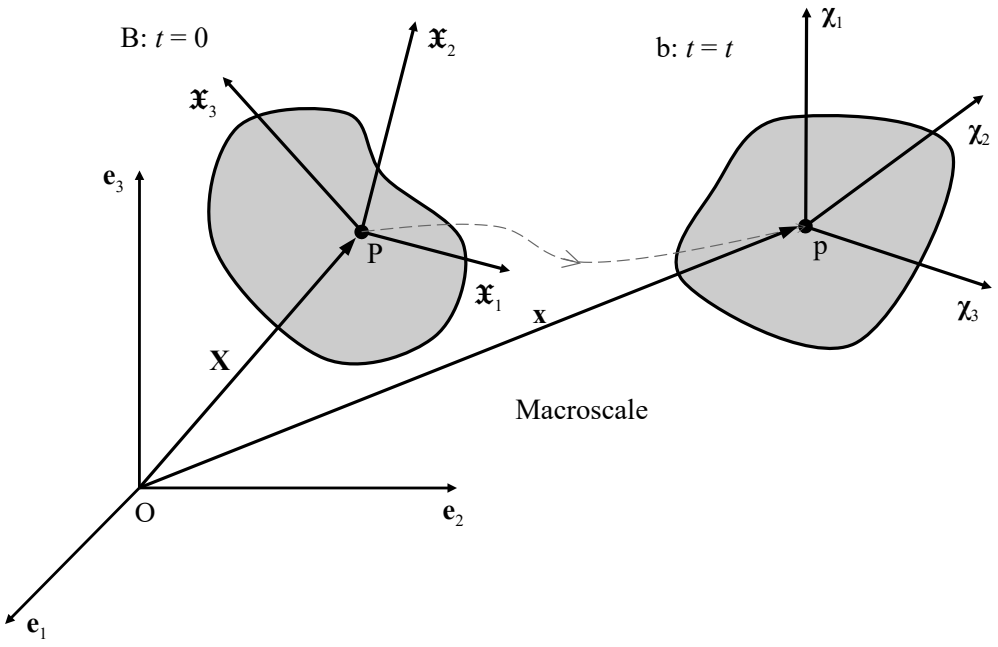

Figure 3.8: Deformable directors

3.2.2 Linear Elasticity

Based on the kinematics of deformation presented here briefly, Eringen and Şuhubi (1964) and Şuhubi and Eringen (1964) constructed several sets of strain tensors. One such set of strain measures is given by

$$\mathfrak{C}_{KL} = x_{k,K}\mathfrak{X}_{Lk}, \qquad \mathcal{C}_{KL} = \chi_{kK}\chi_{kL} = \mathcal{C}_{LK}, \qquad \Gamma_{KLM} = \mathfrak{X}_{Kk}\chi_{kL,M} \tag{3.15}$$

where $\mathfrak{C}_{KL}$ is called the *deformation tensor*, $\mathcal{C}_{KL}$ the *microdeformation tensor*, and Γ_{KLM} the *wryness tensor*.

In a linear approximation, the strain tensors (Eq. 3.15) can be rewritten as

$$\mathfrak{C}_{KL}-\delta_{KL} \approx \epsilon_{kl}\delta_{kK}\delta_{lL}, \quad \mathcal{C}_{KL}-\delta_{KL} \approx 2e_{kl}\delta_{kK}\delta_{lL}, \quad \Gamma_{KLM} = \gamma_{klm}\delta_{kK}\delta_{lL}\delta_{mM} \tag{3.16}$$

in which ϵ_{kl}, e_{kl}, and γ_{klm} are the linear strain tensors defined by

$$\epsilon_{kl} = u_{l,k} - \phi_{lk}, \qquad 2e_{kl} = \phi_{kl} + \phi_{lk}, \qquad \gamma_{klm} = \phi_{kl,m} \tag{3.17}$$

where u_l is the *displacement vector* related to the particle centroid and $\phi_{kl} = \chi_{kl}-\delta_{kl}$ is the *micromotion gradient tensor*.

Disregarding temperature variations the *free energy density* ψ is, then, approximated by

$$\begin{aligned}\psi \approx \psi^0 + \frac{1}{2}A_{klmn}\epsilon_{kl}\epsilon_{mn} + \frac{1}{2}B_{klmn}e_{kl}e_{mn} + \frac{1}{2}C_{klmnpq}\gamma_{klm}\gamma_{npq} + E_{klmn}\epsilon_{kl}e_{mn} + \\ + F_{klmnp}\epsilon_{kl}\gamma_{mnp} + G_{klmnp}e_{kl}\gamma_{mnp}\end{aligned} \tag{3.18}$$

where ψ^0 is the initial internal energy density; $U_0 = \psi - \psi_0$ is the strain energy density; and $A_{klmn}, B_{klmn}, C_{klmnpq}, E_{klmn}, F_{klmnp}$ and G_{klmnp} are the constitutive moduli.

From these, Eringen (1999) observed the following symmetry regulations:

$$\begin{aligned} A_{klmn} = A_{mnkl}, \quad B_{klmn} = B_{mnkl} = B_{lkmn} = B_{nmkl}, \\ C_{klmnpq} = C_{npqklm}, \quad E_{klmn} = E_{klnm}, \quad G_{klmnp} = G_{lkmnp} \end{aligned} \tag{3.19}$$

From (3.18), the linear constitutive equations of micromorphic solids can be obtained:

$$t_{kl} \approx \frac{\partial \Sigma}{\partial \epsilon_{kl}} = A_{klmn}\epsilon_{mn} + E_{klmn}e_{mn} + F_{klmnp}\gamma_{mnp} \tag{3.20}$$

$$s_{kl} \approx \frac{\partial \Sigma}{\partial e_{kl}} = E_{mnkl}\epsilon_{mn} + B_{klmn}e_{mn} + G_{klmnp}\gamma_{mnp} \tag{3.21}$$

$$m_{klm} \approx \frac{\partial \Sigma}{\partial \gamma_{lmk}} = F_{nplmk}\epsilon_{np} + G_{nplmk}e_{np} + C_{lmknpq}\gamma_{npq} \tag{3.22}$$

where t_{kl} is the *stress tensor*, s_{kl} is a symmetric stress tensor named *micro-stress average* Eringen and Şuhubi (1964), and m_{klm} is the *stress moments tensor* or, as defined in Eringen and Şuhubi (1964), the *first stress moments* and represented by the symbol λ^{klm}.

For an isotropic linear elastic micromorphic solid the constitutive equations (3.20), (3.21) and (3.22) can be simplified applying the appropriated symmetries and the constitutive moduli may be constructed by the product of the Kronecker delta δ_{kl}, i.e.,

$$
\begin{aligned}
A_{klmn} &= \lambda\delta_{kl}\delta_{mn} + (\mu+\kappa)\delta_{km}\delta_{ln} + \mu\delta_{kn}\delta_{lm},\\
E_{klmn} &= (\lambda+\nu)\delta_{kl}\delta_{mn} + (\mu+\sigma)(\delta_{km}\delta_{ln} + \delta_{kn}\delta_{lm})\\
F_{klmnp} &= 0,\\
B_{klmn} &= (\lambda+2\nu+\tau)\delta_{kl}\delta_{mn} + (\mu+2\sigma+\eta)(\delta_{km}\delta_{ln} + \delta_{kn}\delta_{lm}),\\
G_{klmnpq} &= 0,\\
C_{klmnpq} &= \tau_1(\delta_{kl}\delta_{mn}\delta_{pq} + \delta_{kq}\delta_{lm}\delta_{np}) + \tau_2(\delta_{kl}\delta_{mp}\delta_{nq} + \delta_{km}\delta_{lq}\delta_{np}) +\\
&\quad + \tau_3\delta_{kl}\delta_{mq}\delta_{np} + \tau_4\delta_{kn}\delta_{lm}\delta_{pq} + \tau_5(\delta_{km}\delta_{ln}\delta_{pq} + \delta_{kp}\delta_{lm}\delta_{nq}) +\\
&\quad + \tau_6\delta_{km}\delta_{lp}\delta_{nq} + \tau_7\delta_{kn}\delta_{lp}\delta_{mq} + \tau_8(\delta_{kp}\delta_{lq}\delta_{mn} + \delta_{kq}\delta_{ln}\delta_{mp}) +\\
&\quad + \tau_9\delta_{kn}\delta_{lq}\delta_{mp} + \tau_{10}\delta_{kp}\delta_{ln}\delta_{mq} + \tau_{11}\delta_{kq}\delta_{lp}\delta_{mn}
\end{aligned}
\tag{3.23}
$$

wherein λ, μ, κ, ν, τ, η and $\tau_1 \ldots \tau_{11}$ are 18 elastic parameters.

Hence, (3.20), (3.21) and (3.22) may be rewritten disregarding the constitutive moduli of odd order:

$$t_{kl} = A_{klmn}\epsilon_{mn} + E_{klmn}e_{mn} \tag{3.24}$$

$$s_{kl} = E_{mnkl}\epsilon_{mn} + B_{klmn}e_{mn} \tag{3.25}$$

$$m_{klm} = C_{lmknpq}\gamma_{npq} \tag{3.26}$$

Nevertheless, the micromorphic continuum presents two main drawbacks: the definition of the additional constitutive equations and the determination of the high number of constitutive parameters. For the case of a linear isotropic micromorphic

material there are 18 elastic parameters, as seen in (3.23), in contrast to the two Lamé parameters of a classical isotropic continuum. To overcome these limitations, this work is based in the multiscale formulation proposed by Silva (2019) in order to obtain the macroscopic micromorphic constitutive relations, techique discussed in more details in Chapter 4.

3.3 A Unified Formulation for Elastic Degradation in Micromorphic Continua

In the preceding chapter (Section 2.2.2) a unified formulation for constitutive models has been presented, a framework able to represent a number of multidissipative elasto-plastic and elastic-degrading models with a tensorial formalism. Based on the advantages presented by this unified formulation, an extension of this concept to constitutive models for the micropolar continuum theory was proposed in the work of Gori (2018) resulting in a theoretical and computational framework able to model problems where the localization phenomena is an issue with scalar-isotropic damage models (Gori et al., 2017*b*). In order to address the problem of consistency (or compatibility) between the formulation proposed by Gori (2018) and the existing analogous formulation for classical media previously discussed, a *compact tensorial representation* was proposed by Gori et al. (2017*c*) based on the work of Eremeyev (2005).

Following, the foundation for a unified formulation for the elastic degradation based on the micromorphic continuum is presented, where peculiar efforts were devoted to the extension and implementation of scalar-isotropic damage models for the micromorphic theory similar to the work of Gori (2018). A tensorial compact formulation is also proposed for the micromorphic continuum, which enabled the computational implementation of the proposed models into the existing framework for classical continuum implemented by Penna (2011).

3.3.1 Elastic degradation in micromorphic media

Similar to a classical media, in a geometrically-linear context, a micromorphic elastic-degrading medium is characterized by total stress-strain relations

$$t_{kl} = A_{klmn}\epsilon_{mn} + E_{klmn}e_{mn} \tag{3.27}$$

$$s_{kl} = E_{mnkl}\epsilon_{mn} + B_{klmn}e_{mn} \tag{3.28}$$

$$m_{klm} = C_{lmknpq}\gamma_{npq} \tag{3.29}$$

wherein $A_{klmn}, B_{klmn}, C_{klmnpq}$, and E_{klmn} are the constitutive moduli; t_{kl} , s_{kl}, and m_{klm} are the stress measures; ϵ_{mn}, e_{mn} and γ_{npq} the strain measures, as presented in Section 3.2.2.

Considering the general equations of the classical formulation, there is only a single total stress-strain relation $\sigma_{ij} = E_{ijkl}\varepsilon_{kl}$ (Eq. 2.6a) where E_{ijkl} represents the components of the fourth-order stiffness tensor, while a micromorphic formulation is represented by three total stress-strain relations. To approach this consistency problem a compact tensorial formulation is proposed, in which the micromorphic total stress-strain expressions may be condensed in a single *generalized secant relation*, adopting the same formalism as Gori et al. (2017*c*):

$$\Sigma_{\beta\nu} = \mathcal{E}^{S}_{\beta\nu\delta\psi}\Gamma_{\delta\psi}, \text{ for } \beta, \nu, \delta, \psi = 1, 2, ...9 \tag{3.30}$$

where the *generalized stress operator* $\Sigma_{\beta\nu}$ and the *generalized strain operator* $\Gamma_{\delta\psi}$ represent second-order tensors with dimension nine, as defined

$$\Sigma_{\beta\nu} = \begin{pmatrix} t_{\beta\nu} & \underline{0} & \underline{0} \\ \underline{0} & s_{(\beta-3)(\nu-3)} & \underline{0} \\ m_{1\beta\nu} & m_{2(\beta-3)(\nu-3)} & m_{3(\beta-6)(\nu-6)} \end{pmatrix} \tag{3.31}$$

$$\Gamma_{\delta\psi} = \begin{pmatrix} \epsilon_{\delta\psi} & \underline{0} & \underline{0} \\ \underline{0} & e_{(\delta-3)(\psi-3)} & \underline{0} \\ \gamma_{1\delta\psi} & \gamma_{2(\delta-3)(\psi-3)} & \gamma_{3(\delta-6)(\psi-6)} \end{pmatrix} \tag{3.32}$$

The *generalized secant operator* $\mathcal{E}^{S}{}_{\beta\nu\delta\psi}$ gathers the four constitutive operators of the micromorphic theory for isotropic linear elastic solids, i.e., $A_{klmn}, B_{klmn}, C_{klmnpq}$, and E_{klmn}, in a fourth-order tensor with dimension nine, as follows:

$$\mathcal{E}^{S}{}_{\beta\nu\delta\psi} = \left(\begin{array}{ccc|ccc|ccc} A_{\beta\nu11} & A_{\beta\nu12} & A_{\beta\nu13} & 0 & 0 & 0 & 0 & 0 & 0 \\ A_{\beta\nu21} & A_{\beta\nu22} & A_{\beta\nu23} & 0 & 0 & 0 & 0 & 0 & 0 \\ A_{\beta\nu31} & A_{\beta\nu32} & A_{\beta\nu33} & 0 & 0 & 0 & 0 & 0 & 0 \\ \hline 0 & 0 & 0 & E_{\beta\nu11} & E_{\beta\nu12} & E_{\beta\nu13} & 0 & 0 & 0 \\ 0 & 0 & 0 & E_{\beta\nu21} & E_{\beta\nu22} & E_{\beta\nu23} & 0 & 0 & 0 \\ 0 & 0 & 0 & E_{\beta\nu31} & E_{\beta\nu32} & E_{\beta\nu33} & 0 & 0 & 0 \\ \hline 0 & 0 & 0 & 0 & 0 & 0 & 0 & 0 & 0 \\ 0 & 0 & 0 & 0 & 0 & 0 & 0 & 0 & 0 \\ 0 & 0 & 0 & 0 & 0 & 0 & 0 & 0 & 0 \end{array}\right), \text{ for } \beta, \nu = 1, 2, 3 \tag{3.33}$$

$$\mathcal{E}^{S}{}_{\beta\nu\delta\psi} = \left(\begin{array}{ccc|ccc|ccc} E_{11(\beta-3)(\nu-3)} & E_{12(\beta-3)(\nu-3)} & E_{13(\beta-3)(\nu-3)} & 0 & 0 & 0 & 0 & 0 & 0 \\ E_{21(\beta-3)(\nu-3)} & E_{22(\beta-3)(\nu-3)} & E_{23(\beta-3)(\nu-3)} & 0 & 0 & 0 & 0 & 0 & 0 \\ E_{31(\beta-3)(\nu-3)} & E_{32(\beta-3)(\nu-3)} & E_{33(\beta-3)(\nu-3)} & 0 & 0 & 0 & 0 & 0 & 0 \\ \hline 0 & 0 & 0 & B_{(\beta-3)(\nu-3)11} & B_{(\beta-3)(\nu-3)12} & B_{(\beta-3)(\nu-3)13} & 0 & 0 & 0 \\ 0 & 0 & 0 & B_{(\beta-3)(\nu-3)21} & B_{(\beta-3)(\nu-3)22} & B_{(\beta-3)(\nu-3)23} & 0 & 0 & 0 \\ 0 & 0 & 0 & B_{(\beta-3)(\nu-3)31} & B_{(\beta-3)(\nu-3)32} & B_{(\beta-3)(\nu-3)33} & 0 & 0 & 0 \\ \hline 0 & 0 & 0 & 0 & 0 & 0 & 0 & 0 & 0 \\ 0 & 0 & 0 & 0 & 0 & 0 & 0 & 0 & 0 \\ 0 & 0 & 0 & 0 & 0 & 0 & 0 & 0 & 0 \end{array}\right), \text{ for } \beta, \nu = 4, 5, 6 \tag{3.34}$$

$$\mathcal{E}^{S}{}_{\beta\nu\delta\psi} = \left(\begin{array}{ccc|ccc|ccc} 0 & 0 & 0 & 0 & 0 & 0 & 0 & 0 & 0 \\ 0 & 0 & 0 & 0 & 0 & 0 & 0 & 0 & 0 \\ 0 & 0 & 0 & 0 & 0 & 0 & 0 & 0 & 0 \\ \hline 0 & 0 & 0 & 0 & 0 & 0 & 0 & 0 & 0 \\ 0 & 0 & 0 & 0 & 0 & 0 & 0 & 0 & 0 \\ 0 & 0 & 0 & 0 & 0 & 0 & 0 & 0 & 0 \\ \hline C_{(\beta-6)\nu 1111} & C_{(\beta-6)\nu 1112} & C_{(\beta-6)\nu 1113} & C_{(\beta-6)\nu 1211} & C_{(\beta-6)\nu 1212} & C_{(\beta-6)\nu 1213} & C_{(\beta-6)\nu 1311} & C_{(\beta-6)\nu 1312} & C_{(\beta-6)\nu 1313} \\ C_{(\beta-6)\nu 1121} & C_{(\beta-6)\nu 1122} & C_{(\beta-6)\nu 1123} & C_{(\beta-6)\nu 1221} & C_{(\beta-6)\nu 1222} & C_{(\beta-6)\nu 1223} & C_{(\beta-6)\nu 1321} & C_{(\beta-6)\nu 1322} & C_{(\beta-6)\nu 1323} \\ C_{(\beta-6)\nu 1131} & C_{(\beta-6)\nu 1132} & C_{(\beta-6)\nu 1133} & C_{(\beta-6)\nu 1231} & C_{(\beta-6)\nu 1232} & C_{(\beta-6)\nu 1233} & C_{(\beta-6)\nu 1331} & C_{(\beta-6)\nu 1332} & C_{(\beta-6)\nu 1333} \end{array}\right) \quad \text{for } \beta = 7,8,9 \text{ and } \nu = 1,2,3 \tag{3.35}$$

$$\mathcal{E}^{S}{}_{\beta\nu\delta\psi} = \left(\begin{array}{ccc|ccc|ccc} 0 & 0 & 0 & 0 & 0 & 0 & 0 & 0 & 0 \\ 0 & 0 & 0 & 0 & 0 & 0 & 0 & 0 & 0 \\ 0 & 0 & 0 & 0 & 0 & 0 & 0 & 0 & 0 \\ \hline 0 & 0 & 0 & 0 & 0 & 0 & 0 & 0 & 0 \\ 0 & 0 & 0 & 0 & 0 & 0 & 0 & 0 & 0 \\ 0 & 0 & 0 & 0 & 0 & 0 & 0 & 0 & 0 \\ \hline C_{(\beta-6)(\nu-3)2111} & C_{(\beta-6)(\nu-3)2112} & C_{(\beta-6)(\nu-3)2113} & C_{(\beta-6)(\nu-3)2211} & C_{(\beta-6)(\nu-3)2212} & C_{(\beta-6)(\nu-3)2213} & C_{(\beta-6)(\nu-3)2311} & C_{(\beta-6)(\nu-3)2312} & C_{(\beta-6)(\nu-3)2313} \\ C_{(\beta-6)(\nu-3)2121} & C_{(\beta-6)(\nu-3)2122} & C_{(\beta-6)(\nu-3)2123} & C_{(\beta-6)(\nu-3)2221} & C_{(\beta-6)(\nu-3)2222} & C_{(\beta-6)(\nu-3)2223} & C_{(\beta-6)(\nu-3)2321} & C_{(\beta-6)(\nu-3)2322} & C_{(\beta-6)(\nu-3)2323} \\ C_{(\beta-6)(\nu-3)2131} & C_{(\beta-6)(\nu-3)2132} & C_{(\beta-6)(\nu-3)2133} & C_{(\beta-6)(\nu-3)2231} & C_{(\beta-6)(\nu-3)2232} & C_{(\beta-6)(\nu-3)2233} & C_{(\beta-6)(\nu-3)2331} & C_{(\beta-6)(\nu-3)2332} & C_{(\beta-6)(\nu-3)2333} \end{array}\right) \tag{3.36}$$

for $\beta = 7,8,9$ and $\nu = 4,5,6$

$$\mathcal{E}^{S}{}_{\beta\nu\delta\psi} = \left(\begin{array}{ccc|ccc|ccc} 0 & 0 & 0 & 0 & 0 & 0 & 0 & 0 & 0 \\ 0 & 0 & 0 & 0 & 0 & 0 & 0 & 0 & 0 \\ 0 & 0 & 0 & 0 & 0 & 0 & 0 & 0 & 0 \\ \hline 0 & 0 & 0 & 0 & 0 & 0 & 0 & 0 & 0 \\ 0 & 0 & 0 & 0 & 0 & 0 & 0 & 0 & 0 \\ 0 & 0 & 0 & 0 & 0 & 0 & 0 & 0 & 0 \\ \hline C_{(\beta-6)(\nu-6)3111} & C_{(\beta-6)(\nu-6)3112} & C_{(\beta-6)(\nu-6)3113} & C_{(\beta-6)(\nu-6)3211} & C_{(\beta-6)(\nu-6)3212} & C_{(\beta-6)(\nu-6)3213} & C_{(\beta-6)(\nu-6)3311} & C_{(\beta-6)(\nu-6)3312} & C_{(\beta-6)(\nu-6)3313} \\ C_{(\beta-6)(\nu-6)3121} & C_{(\beta-6)(\nu-6)3122} & C_{(\beta-6)(\nu-6)3123} & C_{(\beta-6)(\nu-6)3221} & C_{(\beta-6)(\nu-6)3222} & C_{(\beta-6)(\nu-6)3223} & C_{(\beta-6)(\nu-6)3321} & C_{(\beta-6)(\nu-6)3322} & C_{(\beta-6)(\nu-6)3323} \\ C_{(\beta-6)(\nu-6)3131} & C_{(\beta-6)(\nu-6)3132} & C_{(\beta-6)(\nu-6)3133} & C_{(\beta-6)(\nu-6)3231} & C_{(\beta-6)(\nu-6)3232} & C_{(\beta-6)(\nu-6)3233} & C_{(\beta-6)(\nu-6)3331} & C_{(\beta-6)(\nu-6)3332} & C_{(\beta-6)(\nu-6)3333} \end{array}\right), \text{ for } \beta, \nu = 7,8,9 \tag{3.37}$$

With the introduction of the generalized secant operator, (3.30) is formally identical to the one for the classical continuum (Eq. 2.6a), except for the tensor dimension. Hence, the compatibility problem between both formulations is addressed enabling the extension of elastic-degrading models to the micromorphic theory within the same computational framework of classical models (implementation details discussed in Chapter 5).

3.3.2 Scalar isotropic damage models

As detailed in Section 2.2.1, for scalar-isotropic damage models the degrading process is characterized by a single scalar damage. Extending this principle to micromorphic media and applying the generalized tensorial formulation presented in the last section, the resulting generalized constitutive operator can be expressed as

$$\mathcal{E}^{S}{}_{\beta\nu\delta\psi}(\mathcal{E}^{0}{}_{\beta\nu\delta\psi}, D) = (1 - D)\mathcal{E}^{0}{}_{\beta\nu\delta\psi} \tag{3.38}$$

where $\mathcal{E}^{0}{}_{\beta\nu\delta\psi}$ represents the initial elastic operator and D the damage variable, which varies from 0 for undamaged material to 1 for completely damaged material. Differentiating (3.38)

$$\dot{\mathcal{E}}^{S}_{\beta\nu\delta\psi} = \frac{\partial \mathcal{E}^{S}{}_{\beta\nu\delta\psi}}{\partial D}\dot{D} = \frac{\partial \mathcal{E}^{S}{}_{\beta\nu\delta\psi}}{\partial D}\dot{\lambda}\bar{\mathcal{M}} \tag{3.39}$$

For a scalar-isotropic model

$$\dot{\mathcal{E}}^{S}_{\beta\nu\delta\psi} = -\dot{D}\mathcal{E}^{0}{}_{\beta\nu\delta\psi} \tag{3.40}$$

Comparing (3.39) and (3.40) the following terms can be identified

$$\frac{\partial \mathcal{E}^{S}{}_{\beta\nu\delta\psi}}{\partial D} = -\mathcal{E}^{0}{}_{\beta\nu\delta\psi}; \quad \bar{\mathcal{M}} = 1; \quad \dot{\lambda} = \dot{D} \tag{3.41a}$$

$$\bar{M}_{\beta\nu\delta\psi} = \frac{\partial \mathcal{E}^{S}{}_{\beta\nu\delta\psi}}{\partial D}\,\bar{\mathcal{M}} = -\mathcal{E}^{0}{}_{\beta\nu\delta\psi} \tag{3.41b}$$

Hence, the directions of degradation can be represented by

$$\bar{m}_{\beta\nu} = \bar{M}_{\beta\nu\delta\psi}\Gamma_{\delta\psi} = -\mathcal{E}^0{}_{\beta\nu\delta\psi}\Gamma_{\delta\psi} = -\Sigma^0{}_{\beta\nu} \tag{3.42}$$

Considering the following loading function

$$F(\Gamma_{eq}, D) = \Gamma_{eq}(\epsilon_{mn}, e_{mn}, \gamma_{npq}) - K(D) \tag{3.43}$$

with Γ_{eq} defined as the *generalized equivalent strain*, the gradient and the hardening-softening law can be obtained

$$\bar{n}_{\delta\psi} = \frac{\partial F}{\partial \Gamma_{eq}} = \frac{\partial \Gamma_{eq}}{\partial \Gamma_{\delta\psi}} \quad \text{and} \quad \bar{H} = \frac{\partial K(D)}{\partial D} = \left(\frac{\partial D(\Gamma_{eq})}{\partial \Gamma_{eq}}\right)^{-1} \tag{3.44a,b}$$

where $D(\Gamma_{eq})$ is a damage law that describes the evolution of the damage variable. The tangent stiffness presented for the classical continuum (Eq. 2.19) can now be rewritten

$$\dot{\Sigma}_{\beta\nu} = \mathcal{E}^t{}_{\beta\nu\delta\psi}\dot{\Gamma}_{\delta\psi} \tag{3.45}$$

with

$$\mathcal{E}^t{}_{\beta\nu\delta\psi} = (1-D)\mathcal{E}^0{}_{\beta\nu\delta\psi} - \left(\frac{\partial D(\Gamma_{eq})}{\partial \Gamma_{eq}}\right)\Sigma^0{}_{\beta\nu}\frac{\partial \Gamma_{eq}}{\partial \Gamma_{\delta\psi}} \tag{3.46}$$

Applying the general formulation proposed, different damage models for the micromorphic continuum can be obtained when specific equivalent strain measures are defined. In the next sections the scalar-isotropic damage models proposed are presented as well as their application in Chapter 6.

3.3.2.1 Mazars-Lemaitre micromorphic model

This model is an extension to the micromorphic continuum of the classical model proposed by Mazars and Lemaitre (1985), which adopts the concept of effective stress that relates to the usual stress by a scalar damage variable as proposed by Kachanov (1958). Hence, the loading function is defined as (3.43) with the following equivalent strain

$$\Gamma_{eq} = \sqrt{\Gamma_{\delta\psi}\Gamma_{\delta\psi}} = \sqrt{\epsilon_{mn}\epsilon_{mn} + e_{mn}e_{mn} + \gamma_{npq}\gamma_{npq}} \tag{3.47}$$

The gradient is then defined

$$\bar{n}_{\delta\psi} = \begin{pmatrix} \frac{\epsilon_{\delta\psi}}{\Gamma_{eq}} & \underline{0} & \underline{0} \\ \underline{0} & \frac{e_{(\delta-3)(\psi-3)}}{\Gamma_{eq}} & \underline{0} \\ \frac{\gamma_{1\delta\psi}}{\Gamma_{eq}} & \frac{\gamma_{2(\delta-3)(\psi-3)}}{\Gamma_{eq}} & \frac{\gamma_{3(\delta-6)(\psi-6)}}{\Gamma_{eq}} \end{pmatrix} \tag{3.48}$$

3.3.2.2 Simo-Ju micromorphic model

Simo and Ju (1987) developed an isotropic damage model within two possible frameworks, either strain or stress based, considering a free energy potential to define the damage variable. Considering the strain based formulation, the equivalent strain associated to a micromorphic model can be defined as

$$\Gamma_{eq} = \sqrt{2\psi^0} \tag{3.49}$$

with

$$\begin{aligned} \psi^0 &= \frac{1}{2}\mathcal{E}^0{}_{\beta\nu\delta\psi}\Gamma_{\beta\nu}\Gamma_{\delta\psi} \\ &= \frac{1}{2}A^0{}_{klmn}\epsilon_{kl}\epsilon_{mn} + \frac{1}{2}B^0{}_{klmn}e_{kl}e_{mn} + \frac{1}{2}C^0{}_{klmnpq}\gamma_{klm}\gamma_{npq} + E^0{}_{klmn}\epsilon_{kl}e_{mn} \end{aligned} \tag{3.50}$$

Based on the loading function, the gradient is obtained:

$$\bar{n}_{\delta\psi} = \frac{\mathcal{E}^0{}_{\beta\nu\delta\psi}\Gamma_{\beta\nu}}{\Gamma_{eq}} \tag{3.51}$$

3.3.2.3 Ju micromorphic model

This model is an extension of the classical formulation of Ju (1989) where the author, reconsidering the Simo-Ju model (Simo and Ju, 1987), proposed a formulation based on the free energy of Helmholtz. For the micromorphic continuum

$$\Gamma_{eq} = \psi^0 \tag{3.52}$$

where the free energy is defined as (3.50). Then, it follows

$$\bar{n}_{\delta\psi} = \mathcal{E}^0{}_{\beta\nu\delta\psi}\Gamma_{\beta\nu} = \Sigma^0{}_{\delta\psi} \tag{3.53}$$

3.3.2.4 Marigo micromorphic model

The model proposed by Marigo (1985), based on strain energy, is here extended to the micromorphic continuum where the following equivalent strain is written

$$\Gamma_{eq} = \sqrt{\frac{2\psi^0}{E}} \tag{3.54}$$

with ψ^0 as defined in (3.50) and E being the material Young's modulus used to construct an equivalent micromorphic continuum through the homogenization technique presented in Chapter 4. As previously discussed, for the micromorphic continuum, there are 18 elastic parameters where there is no equivalence between one of the parameters and the Young's modulus of a classical continuum. Hence, in this work the Marigo model is only applied associated to the homogenization technique, where E is clearly defined. The gradient can be obtained as

$$\bar{n}_{\delta\psi} = \frac{\mathcal{E}^0{}_{\beta\nu\delta\psi}\Gamma_{\beta\nu}}{E\Gamma_{eq}} = \frac{\Sigma^0}{E\Gamma_{eq}} \tag{3.55}$$

Chapter 4

Homogenization of a Classical continuum towards a micromorphic continuum

The analytical and discrete formulations of the micromorphic theory are well established in the literature, however the identification of the corresponding constitutive laws and the determination of the high number of constitutive parameters limit its practical application. As an alternative to circumvent these limitations, the micromorphic homogenization strategy proposed by Silva (2019) and based on Hütter (2017) is here employed, which consists in a multiscale formulation for the construction of macroscopic micromorphic constitutive relations in terms of homogenized microscopic quantities obtained from the solution of boundary value problems at the microscale according to the classical continuum theory. This strategy begins with models of the classical continuum on the microscale, without making any constitutive assumptions on the macroscale. Consequently, the necessary material parameters are those of the classical theory.

For this formulation, the graphical representation of a micromorphic continuum should be retrieved, as seen in Figure 4.1, where the domain V is divided into small but finite volumes $\Delta V(\boldsymbol{X})$.

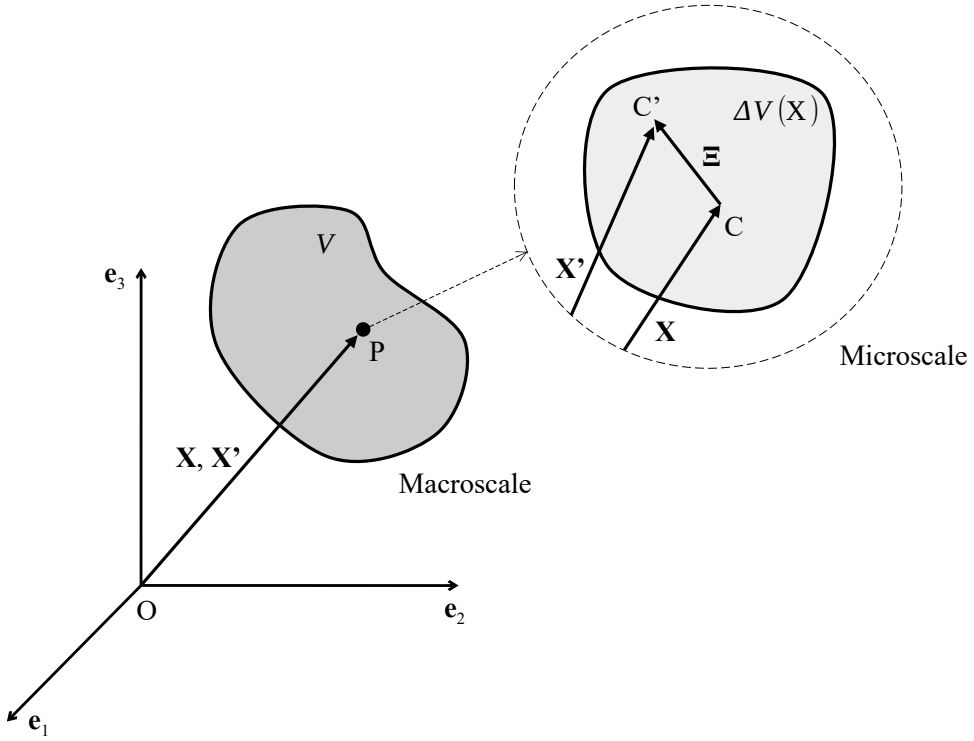

Figure 4.1: Micromorphic continuum (Hütter, 2017; Silva, 2019)

Briefly, for the construction of the constitutive moduli, the material particles are subjected to Cauchy stress states resulting from elementary states of strain, which consist of the successive application of component by component of macroscopic micromorphic strain with unit value, while the others components are kept as zero. To obtain the Cauchy stress states σ_{ij} at the microscale, (4.1) and (4.2) are employed, which approximates the microscale stress based on a micromorphic stress state at the macroscale:

$$u^{,}_{l,k} = \left(K_{pk} + J^{-1}_{\alpha p}\delta_{\alpha kmn}\Xi_m\Xi_n\right)\bar{\epsilon}_{pl} + \bar{\phi}_{lk} + H^{-1}_{mkin}\,\Xi_m\bar{\gamma}_{lin} \quad \therefore \tag{4.1}$$

$$\sigma_{ij} = D_{ijkl}\left[\left(K_{pk} + J^{-1}_{\alpha p}\delta_{\alpha kmn}\Xi_m\Xi_n\right)\bar{\epsilon}_{pl} + \bar{\phi}_{lk} + H^{-1}_{mkin}\,\Xi_m\bar{\gamma}_{lin}\right] \tag{4.2}$$

where K_{pk}, $J_{\alpha p}$ and H_{mkin} are geometric parameters; $\delta_{\alpha kmn}$ is a fourth order Kronecker delta; Ξ_m is a position vector (see Figure 4.1); $\bar{\epsilon}_{pl}$, $\bar{\phi}_{lk}$ and $\bar{\gamma}_{lin}$ are the micromorphic strains obtained by homogenization (where $2e_{kl} = \phi_{kl} + \phi_{lk}$ as defined in (3.17)); D_{ijkl} is the classical constitutive module ($\sigma_{ij} = D_{ijkl}\varepsilon_{kl} = D_{ijkl}u^{,}_{l,k}$).

Based on this approximation, the micromorphic stress tensors at the macroscale are obtained by homogenization applying (4.3), (4.4) and (4.5):

$$\bar{t}_{kl} = \frac{1}{\Delta V(\boldsymbol{X})} \int_{\partial \Delta V(\boldsymbol{X})} \Xi_k \sigma_{il} n_i ds_{(\boldsymbol{X}')} \tag{4.3}$$

$$\bar{m}_{klm} = \frac{1}{\Delta V(\boldsymbol{X})} \int_{\partial \Delta V(\boldsymbol{X})} \Xi_k \sigma_{il} \Xi_m n_i ds_{(\boldsymbol{X}')} \tag{4.4}$$

$$\bar{s}_{kl} = \frac{1}{\Delta V(\boldsymbol{X})} \int_{\Delta V(\boldsymbol{X})} \sigma_{kl} \, dv_{(\boldsymbol{X}')} \tag{4.5}$$

in which $\boldsymbol{n}$ is an unitary vector normal to $\partial \Delta V$. Then, rewriting the constitutive equations (3.24) to (3.26)

$$\bar{t}_{kl} = \bar{A}_{klmn} \bar{\epsilon}_{mn} + \bar{E}_{klmn} \bar{\phi}_{mn} \tag{4.6}$$

$$\bar{s}_{kl} = \bar{E}_{mnkl} \bar{\epsilon}_{mn} + \bar{B}_{klmn} \bar{\phi}_{mn} \tag{4.7}$$

$$\bar{m}_{klm} = \bar{C}_{lmknpq} \bar{\gamma}_{npq} \tag{4.8}$$

the components of macroscopic micromorphic stress are determined, which, as a result of elementary states of strain, consist of the terms of macroscopic micromorphic constitutive relations.

In this work, this formulation is applied so the initial elastic tensor $\mathcal{E}^0{}_{\beta\nu\delta\psi}$ is obtained only for the first step of the first iteration of a non-linear analysis and the micromorphic scalar-isotropic damage models presented in Section 3.3.2 may be employed without the definition of the 18 elastic parameters of the micromorphic theory [1]. For the subsequent iterations and steps, the initial constitutive relations are degraded through the investigation of the degraded state of the material based on the specified damage model. In the next section, the association of the homogenization formulation here presented with a heterogeneous microcontinuum at the micro scale is discussed.

[1] Both possibilities of simulating micromorphic media using the homogenization technique or entering the elastic parameters were implemented.

4.1 Homogenization of heterogeneous media

As previously discussed, in the micromorphic theory the domain V is divided into small but finite elements $\Delta V(\boldsymbol{X})$, here called microcontinuum. In order to incorporate the particle heterogeneity, a square microcontinuum is then considered as heterogeneous with a microscale model generated by the take-and-place algorithm described in Section 2.3. Then a finite elements mesh is associated to the generated structure, where material properties for the aggregates are set to each element whose position coincides with a particle and the remained elements are set as having mortar matrix properties, as illustrated in Figure 4.2. The material properties at the micro scale are defined as for a linear elastic classical medium, as only the parameters for the micro scale are necessary for the homogenization process.

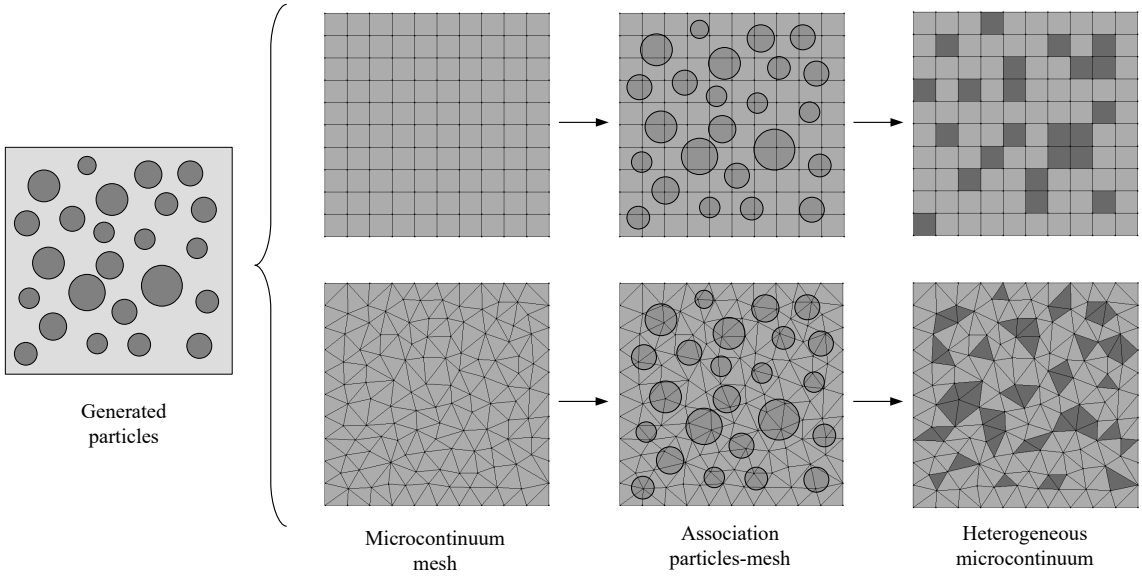

Figure 4.2: Construction of the heterogeneous microcontinuum based on the particles generated by the take-and-place process

For the micro scale mesh, triangular and quadrilateral elements can be used for the microcontinuum discretization (Figure 4.2). The mesh and the microcontinuum size should be defined based on the associated microstructure as, a sample, to be statistically representative, ought to be large compared to the scales of the microstructure, but small compared to the entire body (Wriggers and Moftah, 2006) (Figure 4.3).

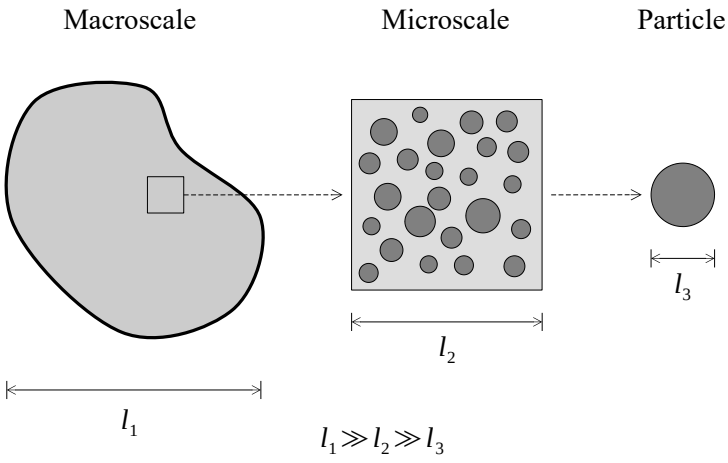

Figure 4.3: Size requirements

After the microstructure generation and the mesh definition, a heterogenous microcontinuum or RVE is associated to each integration point of the model under analysis. Then, the homogenization technique described in the previous section is processed for each element that composes the RVE where (4.3), (4.4) and (4.5) are rewritten as a sum over n that represents the number of elements per microcontinuum:

$$\bar{t}_{kl} = \frac{1}{\Delta V\,(\boldsymbol{X})} \sum_{1}^{n} \int_{\partial \Delta V'(\boldsymbol{X})} \Xi_k \sigma'_{il} n'_i ds'^{(\boldsymbol{X}')} \tag{4.9}$$

$$\bar{m}_{klm} = \frac{1}{\Delta V\,(\boldsymbol{X})} \sum_{1}^{n} \int_{\partial \Delta V'(\boldsymbol{X})} \Xi_k \sigma'_{il} \Xi_m n'_i ds'^{(\boldsymbol{X}')} \tag{4.10}$$

$$\bar{s}_{kl} = \frac{1}{\Delta V\,(\boldsymbol{X})} \sum_{1}^{n} \int_{\Delta V'(\boldsymbol{X})} \sigma'_{kl}\, dv'^{(\boldsymbol{X}')} \tag{4.11}$$

where $\partial \Delta V'$, $\Delta V'$ and σ'_{il} represents the contour, the volume and the stress for each element in the microcontinuum respectively, and n'_i the normal to $\partial \Delta V'$.

Hence, the macro scale micromorphic constitutive equations are obtained for an equivalent micromorphic homogeneous material. As previously discussed, this approach is only used to obtain the initial elastic tensor $\mathcal{E}^0{}_{\beta\nu\delta\psi}$, which is degraded according to the specified damage model. This process is illustrated in Figure 4.4 and its implementation details are discussed in Chapter 5.

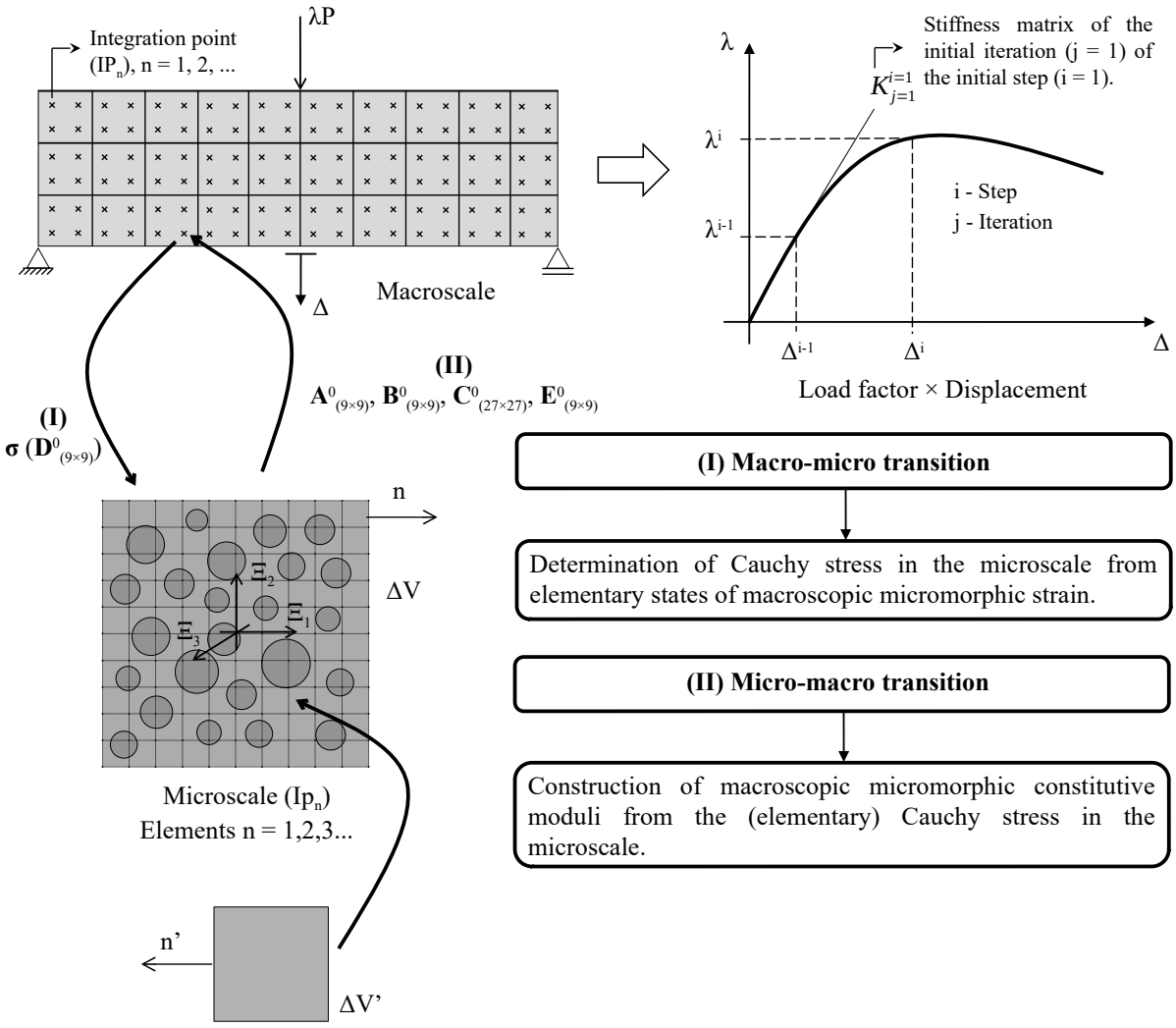

Figure 4.4: Homogenization strategy for a heterogeneous microcontinuum

Chapter 5

Computational implementation

The generalized tensorial format and the micromorphic scalar-isotropic damage models presented in Sections 3.3.1 and 3.3.2 as well as the homogenization strategy described in Chapter 4 were implemented in the INSANE system (INteractive Structural ANalysis Environment), an open-source software developed at the Structural Engineering Department of the Federal University of Minas Gerais. Developed for computational mechanics, this software is basically composed by a set of three interactive graphical applications that enables pre-processing, processing and post-processing, being the second its numerical core, responsible for the analysis of discrete models. Its abstractness and generality enable the simultaneous collaboration of different researchers, responsible for the current state of the system, as well as facilitates its expansion[1]. Penna (2011), who implemented the constitutive framework for the classical continuum briefly discussed in Section 2.2.2, Silva (2019), responsible for the micromorphic homogenization strategy described in Chapter 4, and Monteiro et al. (2017), who dealt with the implementation of the take-and-place algorithm (Section 2.3), are the works most related to this study. Following, the important aspects related to the implementations here proposed are presented with the aid of *UML diagrams* (Unified Modeling Language), where the color code depicted in Figure 5.1 is used.

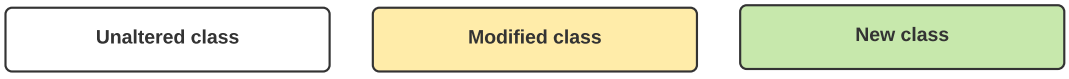

Figure 5.1: UML color code

[1]The reader may refer to the project website (`https://www.insane.dees.ufmg.br/`) where all the publications related to its development are available for consultation.

5.1 Constitutive models framework

In the INSANE system, for the non-linear analysis of a discrete model the following system of equations must be solved:

$$[K]\{X\} = \{R\} \tag{5.1}$$

where $[K]$ is the global stiffness matrix, $\{X\}$ the nodal displacements vector, and $\{R\}$ the nodal forces vector. For a non-linear analysis, $[K] = [K](\{X\})$ and the system is solved through an incremental-iterative process. Hence, (5.1) may be rewritten for the iteration n and step k

$$[K^t]^k_{n-1}\{\Delta X\}^k_n = \Delta\lambda^k_n\{P\} + \{Q\}^k_{n-1} \tag{5.2}$$

in which $[K^t]$ is the tangent stiffness matrix, $\{\Delta X\}$ the vector of incremental displacements, $\Delta\lambda$ an incremental load factor, $\{P\}$ the vector of the nodal reference loads, and $\{Q\}$ the residual forces vector ($\{Q\}^k_{n-1} = \lambda^k_{n-1}\{P\} - \{F\}^k_{n-1}$, where $\{F\}$ is the vector of nodal forces equivalent to the internal stresses).

For the FEM, the matrix $[K^t]$ and the vector $\{F\}$ are assembled with the contribution of each finite element based on

$$[K^t]_{el} = \int_{V_{el}} [B]^T[E]^t[B]dV_{el} \tag{5.3}$$

$$\{F\}_{el} = \int_{V_{el}} [B]^T\{\sigma\}dV_{el} \tag{5.4}$$

where $\{\sigma\}$ is the stress in each element and $[B]$ the matrix that correlates strains and displacements.

In this process, the constitutive models framework is responsible for obtaining the constitutive operator (initial, secant or tangent) and the vector of internal stresses. As initially implemented for a classical media (see, e.g., Penna (2011)), the abstract class `ConstitutiveModel` enclosures the methods able to calculate the constitutive operators and the internal stresses when all the information related to the model is defined. The main activities of the class are represented in the methods `mountC()` (initial operator), `mountCs()` (secant operator), `mountCt()` (tangent operator), and

`mountDualInternalVariableVector()`, where the variables are calculated for each integration point.

For this work, the class `UnifiedConstitutiveModel` and its inherited class `UCMSingleLoadingFunction` are of particularly importance. The class `UnifiedConstitutiveModel` extends the methods `mountC()`, `mountCs()` and `mountDualInternalVariableVector()` of the class `ConstitutiveModel`, while the second extends the method `mountCt()`. The class `UnifiedConstitutiveModel` possesses an instance of the class `UnifiedConstitutiveModelFilter`, the superclass of a family of classes called *filters*, where each filter represents a specific constitutive model. The process of how to assemble the constitutive operators are defined in the class `UCMSingleLoadingFunction` and the parameters that allow this process are provided by the class `UnifiedConstitutiveModelFilter`. This class, as illustrated in Figure 5.2, possesses the methods responsible for defining the loading function and its gradient (`getLoadingFunctionPotential()` and `getHardeningSofteningPotential()`), the directions of degradation (`getInelasticPotential()`) and the secant constitutive operator (`getSecantTensor()`).

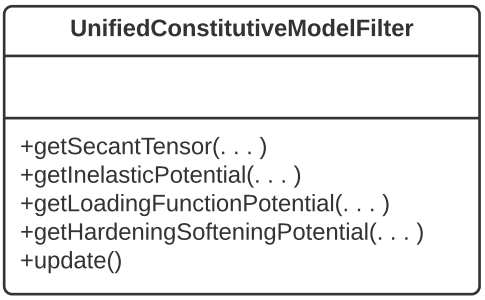

Figure 5.2: Class `UnifiedConstitutiveModelFilter`

As this framework for constitutive models has a tensorial formalism (see Section 2.2.2), it acquires great modularity and expandability, where the introduction of new constitutive models does not requires changes in the existing framework. Applying the compact tensorial formulation presented in Section 3.3.1, this framework can also be made independent of the adopted continuum model, as concluded Gori (2018) for the micromorpolar continuum model. Hence, for calculating the tangent constitutive operator, no changes were required in the class `UCMSingleLoadingFunction` as the expressions for a classical continuum and a micromorphic one are formally identical, differing only in the dimension of the involved tensors. The constitutive models proposed for a micromorphic media can, then, be introduced using the inherited

classes of `UnifiedConstitutiveModelFilter`.

The isotropic models presented in Section 3.3.2 are illustrated in Figure 5.3 within the partial structure of the filters classes:

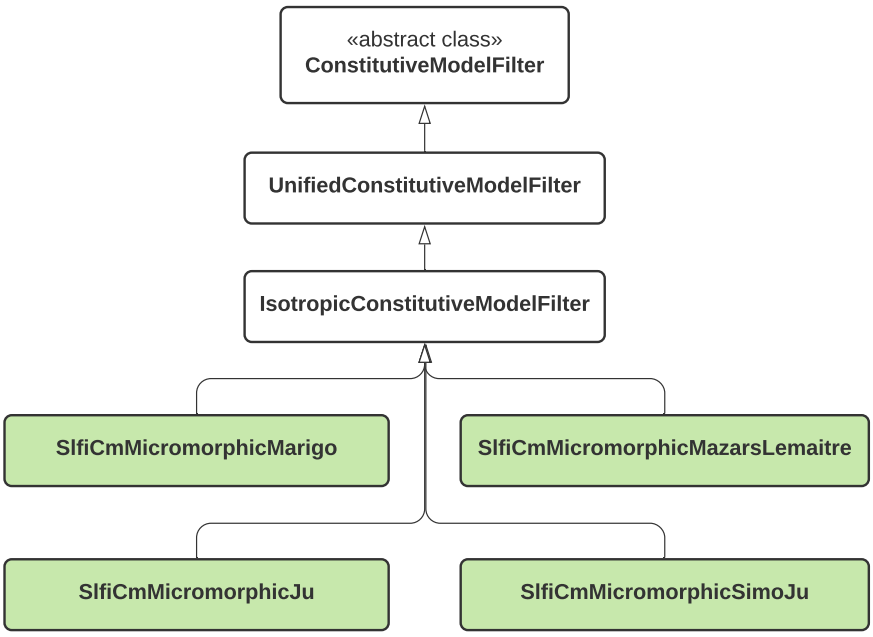

Figure 5.3: Structure of the filter classes with the inclusion of the micromorphic filters

5.2 Mesostructure generator

For the consideration of a heterogeneous microcontinuum, the package `mesostructure` was created in the project `model.mesh` responsible for the construction of meshes for discrete models. The classes enclosured in this package are depicted in Figure 5.4.

The classes `HeterogeneitySetuper`, `NonConformMeshMultiphaseElementTreatTypeSetuper`, `Particle`, `SphericalParticle`, `IrregularParticle`, `MesoModelTags`, and `ParticleDataManager` are existing classes implemented in previous works developed at the INSANE system. In this work, the relocation of this classes was made with the consequential changes due to this relocation.

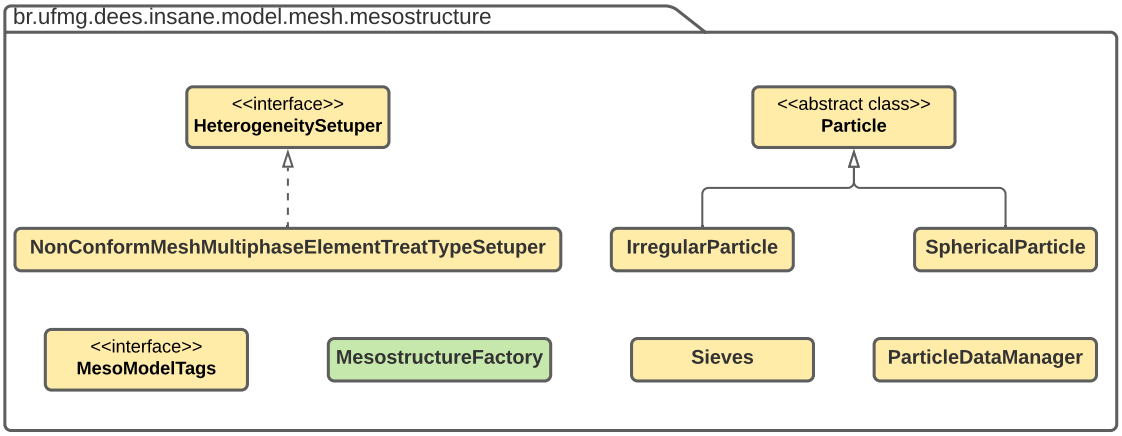

Figure 5.4: Structure of `mesostructure` package

The implemented class `MesostructureFactory` controls the creation of the microstructure of a heterogeneous material and contains the object `ParticleDataManager`, which generates the particle distribution through the take-and-place algorithm, and the method `generateMesostructure` that constructs the discretization of the microcontinuum based on parameters such as the RVE and element sizes, and the element type. For this work, the hypotheses of a square microcontinuum is adopted. The method `generateMesostructure` also initiates the `ParticleDataManager` providing information on the particle distribution (e.g., sieves sizes (class `Sieves`), particle type (class `Particle`), distribution factor, and particle fraction) and sets the distribution of particles generated using the interface `HeterogeneitySetuper` and its inherited class `NonConformMeshMultiphaseElementTreatTypeSetuper` into the *data structure*, which contains the microcontinuum discretization.

In order to store the information related to the heterogeneous microstructure as well as the microcontinuum data structure, the classes `GranularMaterial` and `HomogenizedMaterial` were created extending the abstract superclass `Material`, responsible for representing different material objects in the system, as illustrated in Figure 5.5. The class `HomogenizedMaterial` correlates the macro scale material, which defines the damage law for the macro scale, and the micro scale granular material.

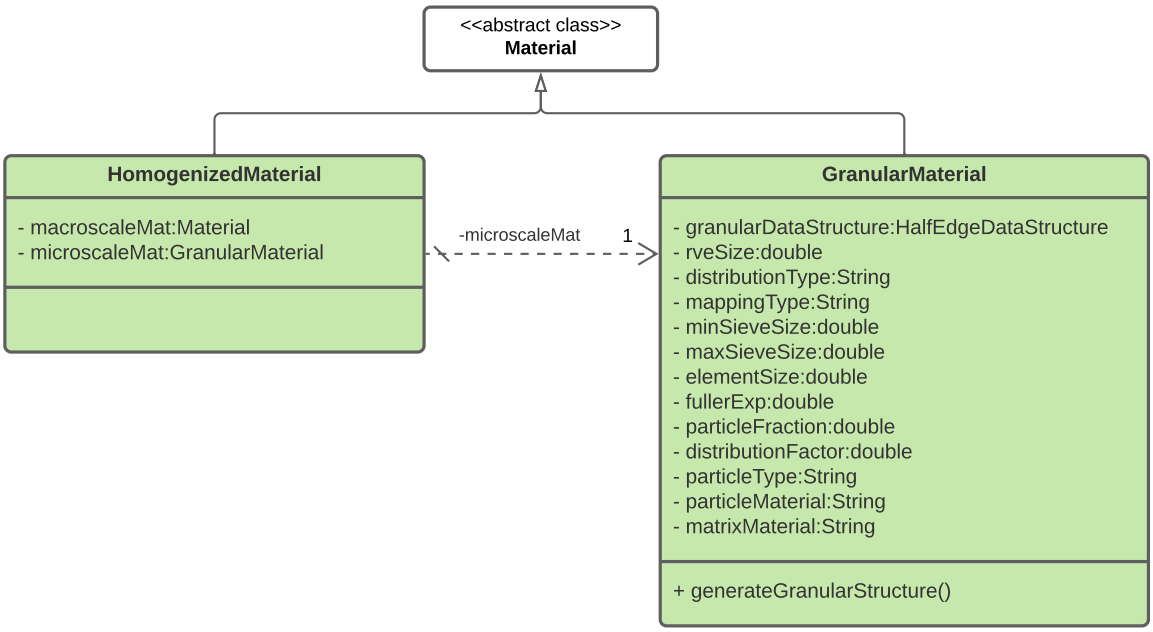

Figure 5.5: Structure of the classes created for the representation of a heterogeneous material

For the homogenization process, the class `GranularSquareMicrocontinuum` was created extending the class `Microcontinuum`, which, in turn, extends the class `Degeneration`, as seen in Figure 5.6. The abstract class `Degeneration` represents the degeneration of a certain solid model into a point where the integration point itself with its coordinates and weigh is represented by the object `Representation`. Numerous classes extend `Degeneration` for different degenerations with specific parameters. The class `PrescribedDegeneration` is one of those, which represents a cross-section whose properties are defined by the user, such as area, thickness, and moment of inertia.

The `Degeneration` is responsible for returning the contribution of each integration point for the assembly of the constitutive operators (`mountC()`, `mountCs()`, and `mountCt()`) referring to its `Representation`, which stores the constitutive model to which is associated.

Therefore, to introduce the homogenization strategy for a micromorphic media, a different `Degeneration`, named `Microcontinuum`, was required in order to extend the methods `mountC()`, `mountCs()`, and `mountCt()` for the specific case where this operators are calculated through the process briefly described in Chapter 4. For

a homogeneous microcontinuum, the classes `CubicMicrocontinuum` (for solid models) and `SquareMicrocontinuum` (for plane models) are responsible for this task and were implemented in Silva (2019). Following the same procedure, in this work, the class `GranularSquareMicrocontinuum` was created to represent a plane square microcontinuum with a heterogenous microstructure in which the operations in Section 4.1 are carried out and each column of the constitutive module is obtained and returned to `Microcontinuum` that assembles the constitutive operators.

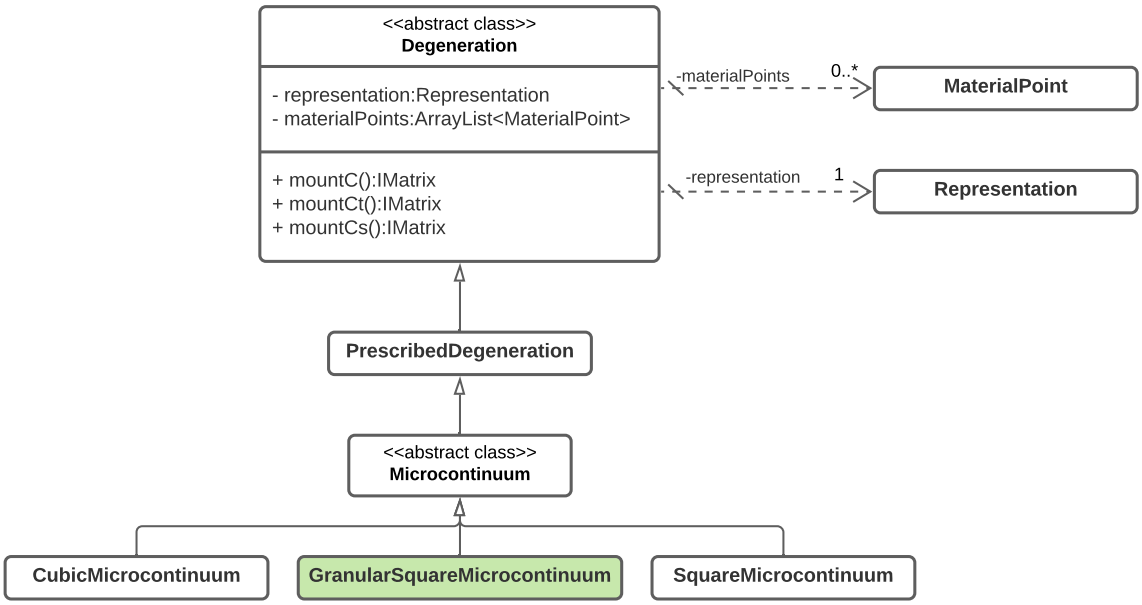

Figure 5.6: Structure of the classes responsible for the homogenization strategy

Chapter 6

Application of the proposed scalar-isotropic damage models

In this chapter, in order to illustrate the application of the scalar-isotropic damage models proposed for the micromorphic continuum, different examples are here presented. First, all scalar-isotropic damage models proposed are presented with a uniaxial stress state example. Following, a problem where the numerical strain localization problem occurs is modeled to illustrate the regularization capacity of the micromorphic continuum. After, a shear band formation under compression loads and an infinitive shear layer problem are modeled where the localization phenomenon is induced by a weakened zone and the results are compared to analysis where the damage is considered at the micro scale.

6.1 Implemented constitutive models: uniaxial stress state

The implemented constitutive models discussed in Section 3.3.2 are here illustrated considering the model in Figure 6.1: a square panel in a plane-stress state with unitary thickness composed of one plane element and loaded in the x direction. This example is well suited for the presentation of the implemented models due to its simplicity, where all models present a similar behavior.

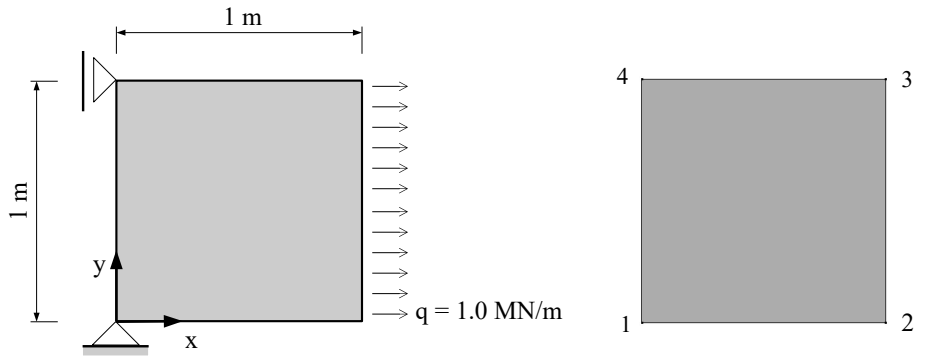

(a) Geometry (b) Mesh

Figure 6.1: Uniaxial stress state

For obtaining the initial elastic tensor necessary for isotropic damage models, the homogenization strategy (Chapter 4) was applied with a square homogeneous microcontinuum of dimension 0.05 m. The equivalent isotropic homogeneous material is characterized by a Young's modulus of 20000 MPa and a Poisson's ratio of 0.2. The appropriated parameters for each constitutive model were adopted considering an exponential damage law described by (6.1) and equivalent to the classical law presented in (2.48):

$$D(\Gamma_{eq}) = 1 - \frac{K_0}{\Gamma_{eq}} \left(1 - \alpha + \alpha e^{-\beta(\Gamma_{eq} - K_0)}\right) \tag{6.1}$$

in which K_0 is the threshold for the equivalent strain, and α and β define the maximum damage level allowed and the damage evolution intensity, respectively. The equivalent strain measures for each model here employed were detailed in Subsection 3.3.2 Hence, it follows:

Mazars-Lemaitre micromorphic model: $\alpha = 0.999$, $\beta = 2000.0$, $K_0 = 0.0001049$;
Simo-Ju micromorphic model: $\alpha = 0.999$, $\beta = 30.0$, $K_0 = 0.0148$;
Ju micromorphic model: $\alpha = 0.999$, $\beta = 15.0$, $K_0 = 0.00011$;
Marigo micromorphic model: $\alpha = 0.999$, $\beta = 4000.0$, $K_0 = 0.0001049$.

The parameters presented for each model vary as the conceptual differences between the models preclude the exact correspondence between the parameters even for the same damage law and were determined in order to obtain a similar behavior. The loading process is driven by the *displacement control method* assuming an increment of 5×10^{-6} m for the horizontal displacement of the loaded face in order

to better describe the peak load behavior, and a tolerance for the convergence of 10^{-4} in load. The results for the analysis are presented in Figure 6.2 wherein the relation between the horizontal displacement for node 2 (Figure 6.1(b)) and the load factor is given. Consistent results for all the models are obtained, attesting that the implemented models for the micromorphic continuum are working properly.

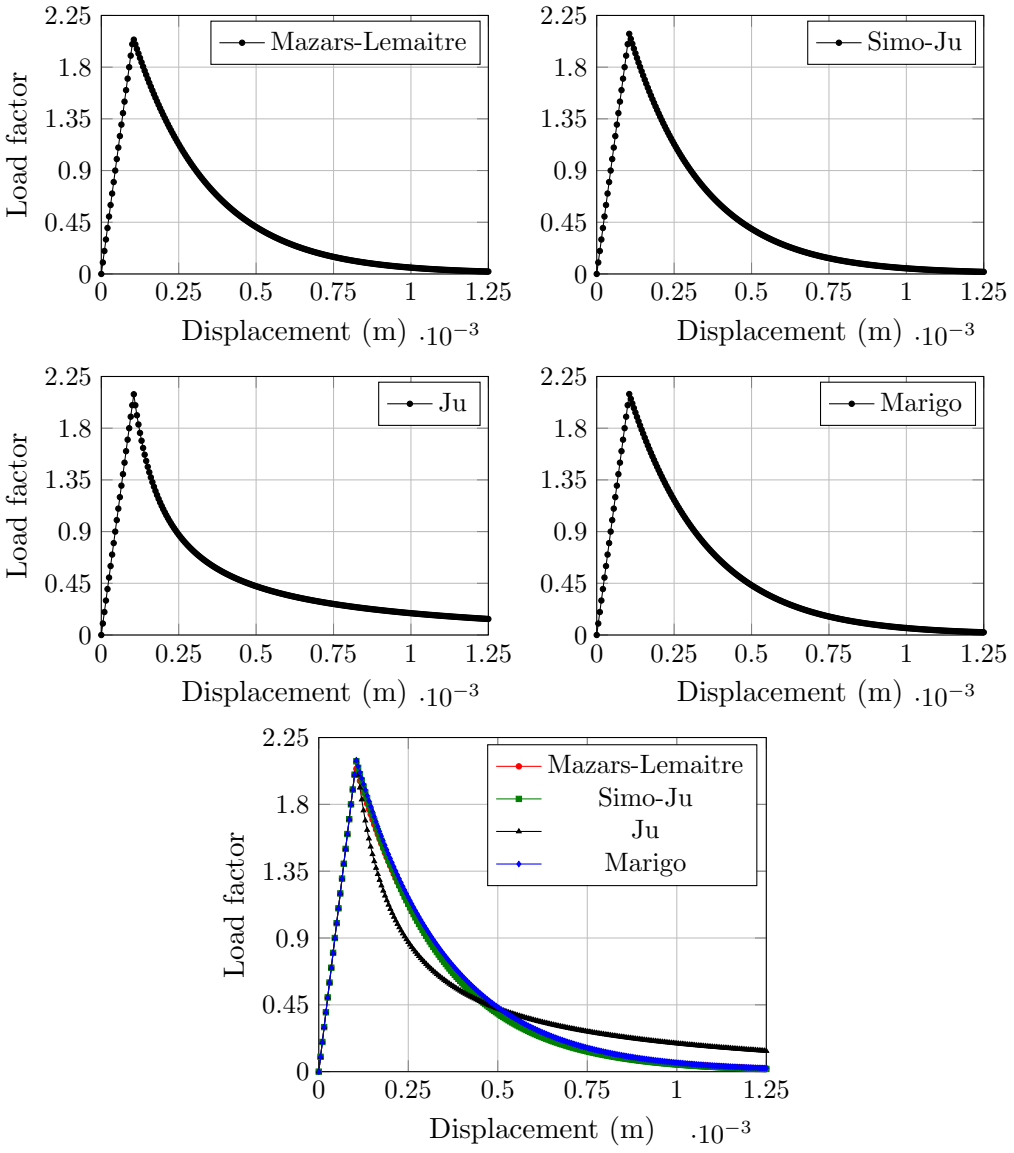

Figure 6.2: Uniaxial stress state: load factor versus horizontal displacement

6.2 Uniaxial stress state: numerical strain localization problem

Quasi-brittle materials are characterized by a softening behavior, where the load-carrying capacity is reduced after a certain strain is reached. In discrete models, the representation of this behavior may lead to mesh-dependent solutions where strains tend to concentrate in an infinitesimal region, compromising the analysis. This phenomenon, named *numerical localization*, originates from an approximation error associated to small differences at the integration points in the model variables, what triggers a solution distinct from the expected one as a small part of the mesh controls the material behavior in the softening phase. Figure 6.3 illustrates this phenomenon using a uniaxial stress state problem in which, for each mesh discretization, a different equilibrium path is obtained due to the localization of strains in a certain part of the mesh where they should be uniform. If these strains concentrate in the highlighted regions in Figure 6.3, the behavior for these regions is described by the descending branch of the stress (σ) $\times$ strain (ε) curve, while the remaining parts of the mesh undergo unloading. This process leads to different responses for each mesh, as the ratio between the loaded zones and the unloaded zones is distinct.

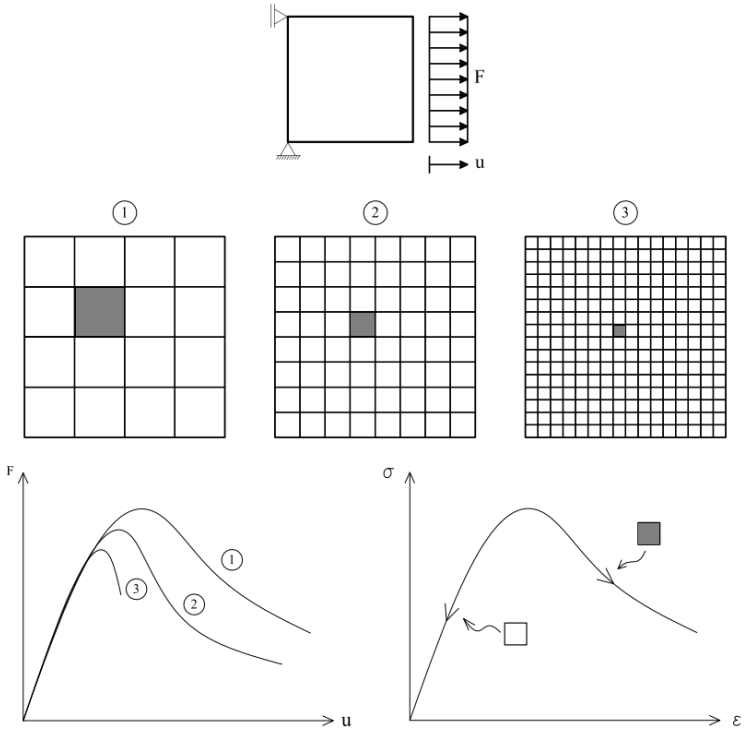

Figure 6.3: Numerical localization phenomenon (Fuina, 2009)

This phenomenon is related to the local character of classical continuum. Hence, the micromorphic continuum, due to its non-local character and its consequent regularization capacity, may present a solution to deal with this problem. Therefore, in this section, a uniaxial stress state problem, similar to the previous example, is simulated to illustrate the capacity of the micromorphic media to provide consistent results regardless of the adopted mesh. The model geometry is depicted in Figure 6.4(a). A square homogeneous and isotropic microcontinuum of dimension 0.05 mm was adopted with Young's modulus E = 20000 N/mm^2 and Poisson's ratio $\nu = 0.30$. The Marigo damage model (Eq. (2.49) for the classical continuum and Eq. (3.54) for the micromorphic continuum) was employed associated to an exponential damage law (Eq. (2.48) and Eq. (6.1)) with $\alpha = 0.999$, $\beta = 500$, and $K_0 = 5 \times 10^{-5}$, leading to the constitutive behavior shown in Figure 6.4(b).

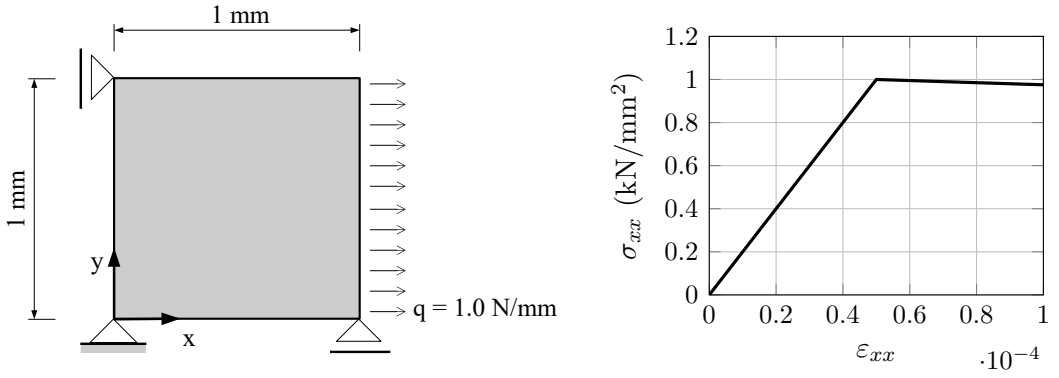

(a) Geometry

(b) Constitutive behavior

Figure 6.4: Numerical localization: uniaxial stress state model

In this example, three meshes were considered, as seen in Figure 6.5, composed by 36, 156 and 616 triangular linear elements with average side size of 0.25 mm, 0.125 mm and 0.0625 mm, respectively.

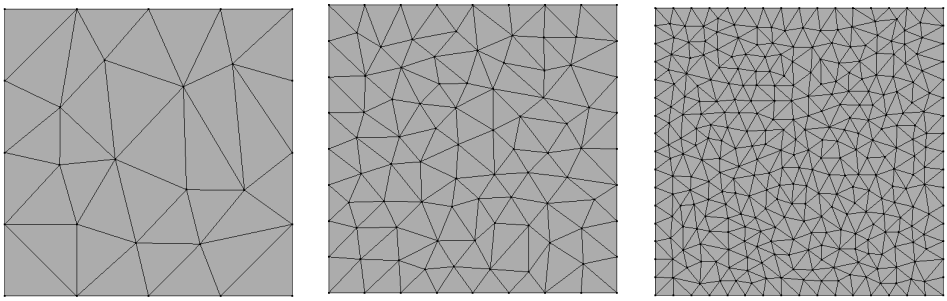

(a) Mesh 1 (b) Mesh 2 (c) Mesh 3

Figure 6.5: Numerical localization: meshes

For the non-linear analysis, the *generalized displacement control method* was adopted with an initial load factor of 5×10^{-3} and a tolerance for convergence of 10^{-4} in displacement. The simulations here presented considered the tangent approximation of the constitutive operator. The results for the classical continuum are presented in Figure 6.6 in terms of the horizontal displacement of the loaded face versus the load factor. For the coarsest mesh the exhibited result reproduces the constitutive behavior depicted in Figure 6.4(b). For the second mesh, there is a deviation from the expected behavior and, the most refine mesh, presents an instability as soon as damage initiates due to numerical localization.

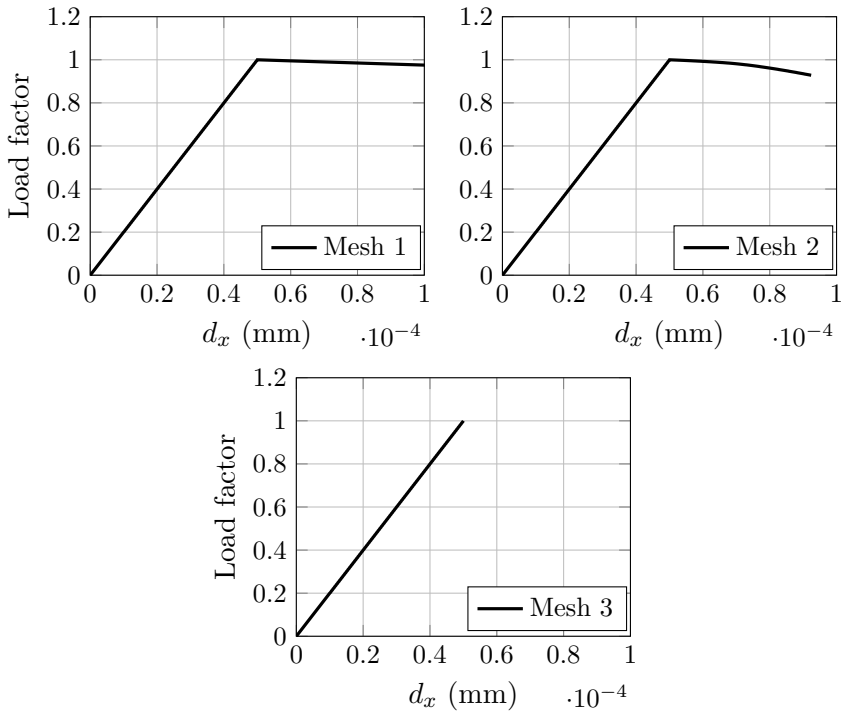

Figure 6.6: Numerical localization: equilibrium paths for the classical continuum

The micromorphic continuum, as it can be seen in the obtained equilibrium paths illustrated in Figure 6.7, was able to replicate the predicted constitutive behavior with all three meshes.

For the second mesh, which presented a divergent solution for a classical continuum, the numerical localization affects the distribution of the state variables, as illustrated in Figure 6.8, which depicts the values for the scalar damage for the last step of the analysis in the classical continuum and in the micromorphic continuum. As it can be noted, the damage tends to concentrate in a part of the square panel for the classical continuum and in others parts tends to zero. This same behavior is not seen for the micromorphic continuum, where the damage remains constant throughout the analysis.

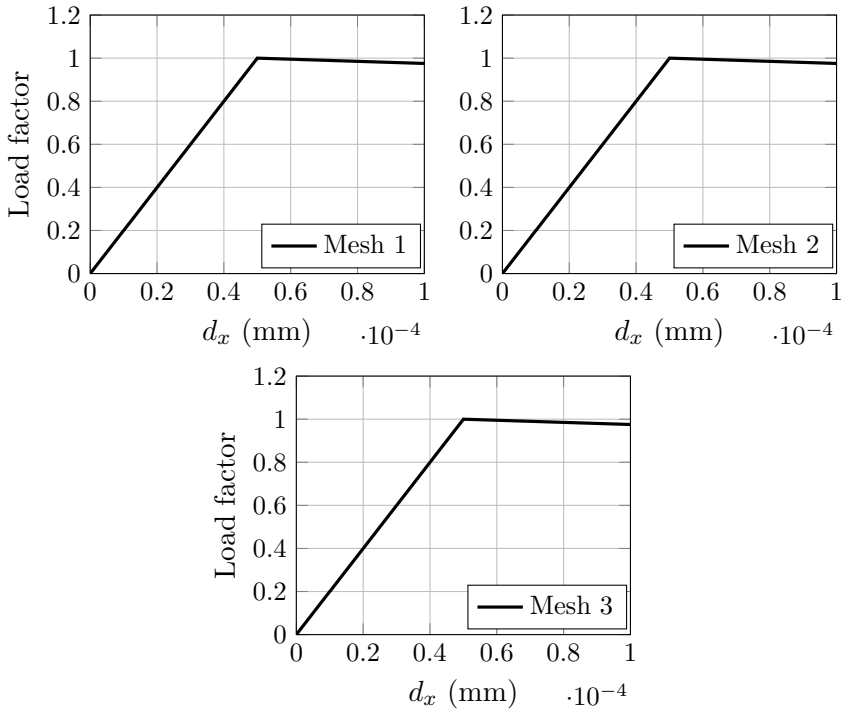

Figure 6.7: Numerical localization: equilibrium paths for the micromorphic continuum

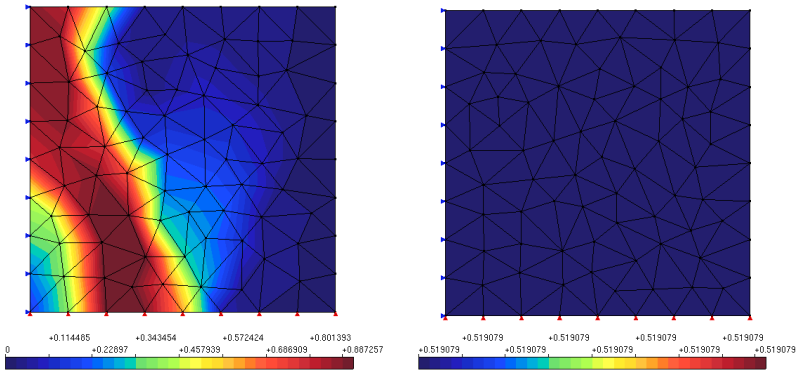

(a) Classical continuum (b) Micromorphic continuum

Figure 6.8: Numerical localization: damage

Another option for non-linear analysis of micromorphic media was proposed by Silva (2019), where, by means of the homogenization strategy described in Chapter 4, the damage is evaluated at the micro scale, which is described by a classical continuum. Hence, considering the damage at the micro scale, does no require the definition of specific damage models for the micromorphic continuum and the classical models can be used.

In order to compare the approaches, the same problem depicted in Figure 6.4, which was previously modeled with the consideration of damage at the macro scale, was simulated considering the damage at the micro scale with identical parameters. The results for the horizontal displacement of the loaded face versus the load factor are presented in Figure 6.9 and they converge with the ones obtained for the damage considered at the macro scale. Therefore, both strategies are able to solve the localization phenomenon due to the non-local nature of the micromorphic continuum, however the processing time greatly increased when the damage was evaluated at the micro scale as the homogenization is done for each step of the analysis. For the simulations here presented, the processing time for damage at the micro scale is, in average, 10 times greater than for the damage at the macro scale.

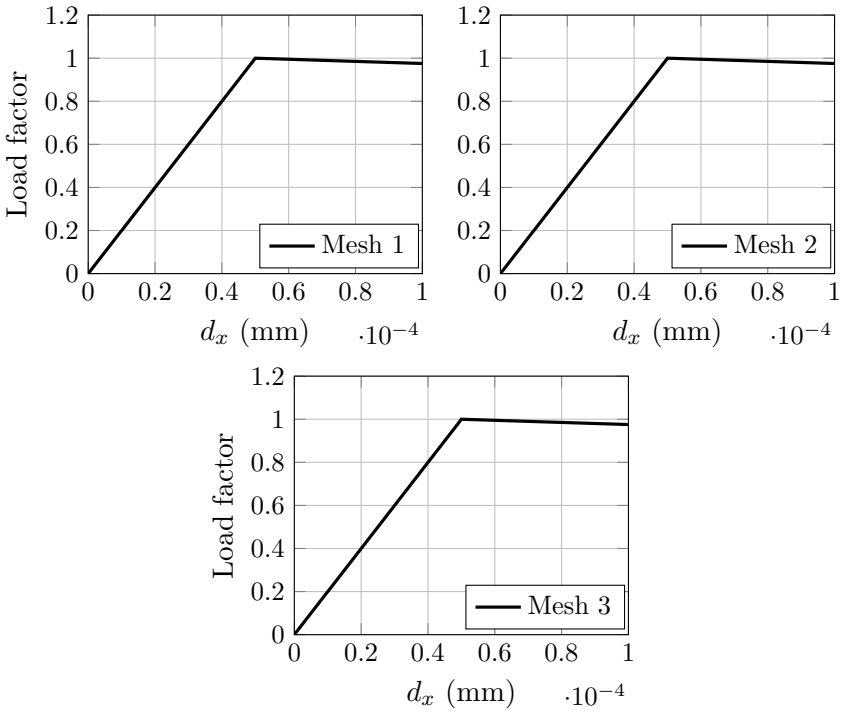

Figure 6.9: Numerical localization: equilibrium paths for the micromorphic continuum with damage in the micro scale

6.3 Shear band

Shear band formation under compression loads was investigated by numerous researches as it may configures a bifurcation problem where the localization phenomenon can occur. For the specific case of studies considering generalized continua theories, Mühlhaus and Vardoulakis (1987), de Borst (1990, 1991, 1993), de Borst and Sluys (1991), Sluys (1992), Steinmann (1994, 1995), Ristinmaa and Vecchi (1996), Lages (1997), and Fuina (2009) can be cited.

A compression test where the formation of the shear band occurs is simulated in order to demonstrate the capacity of the micromorphic continuum to represent the strain localization with no mesh dependency. Figure 6.10 illustrates the adopted model analyzed under plain strain conditions with dimensions 60 mm by 120 mm subjected to a compression load q. As it simulates a compression test where all the points in the loaded face present the same displacement, the strategy *master-slave* available in the INSANE system was employed. In this strategy, a node is selected as the master and the other nodes are assigned as slaves, conditioning their

displacement to that of the master node.

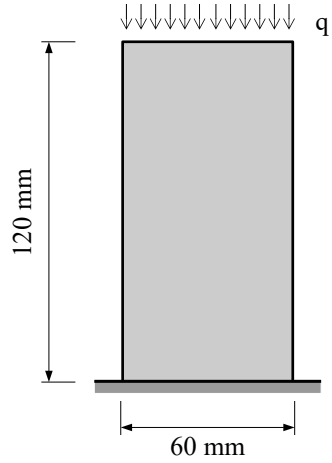

Figure 6.10: Shear band: geometry

A square homogeneous microcontinuum with dimension 1.25 mm was used associated to a Young's modulus $E = 12000$ MPa and a Poisson's ratio $\nu = 0.35$. The Mazars-Lemaitre damage model (Eq. (2.49) for the classical continuum and Eq. (3.47) for the micromorphic continuum) is employed with a linear damage law defined, for the classical continuum, as

$$D(\varepsilon_{eq}) = \frac{K_f}{K_f - K_0}\left(1 - \frac{K_0}{\varepsilon_{eq}}\right) \tag{6.2}$$

or, rewritten for the micromorphic continuum, as

$$D(\Gamma_{eq}) = \frac{K_f}{K_f - K_0}\left(1 - \frac{K_0}{\Gamma_{eq}}\right) \tag{6.3}$$

where, similar to the exponential law, K_0 and K_f are threshold values for the equivalent strain. To simulate an elastoplastic behavior, the following parameters were adopted: $K_0 = 0.0017$ and $K_f = 0.325$. This study was conducted for the three meshes depicted in Figure 6.11 composed of quadrilateral elements with nine nodes and nine integration points. To induce the localization phenomenon a less resistant region was introduced, as highlighted in Figure 6.11, adopting $K_0 = 0.0016$ for the respective elements, which implies an approximated 5% reduction in the stress corresponding to the elastic limit.

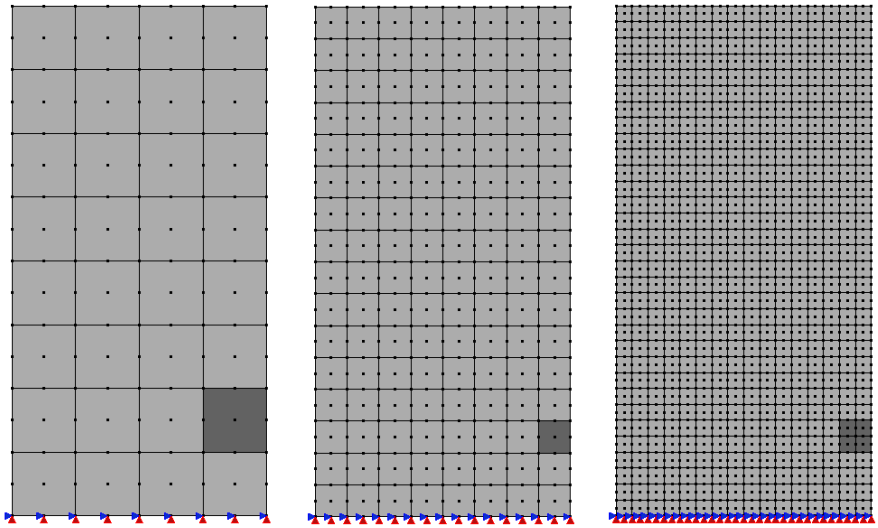

(a) Mesh 1: 32 elements (b) Mesh 2: 128 elements (c) Mesh 3: 512 elements

Figure 6.11: Shear band: meshes

For the loading process, the generalized displacement control method was employed with an initial load factor of 0.02 and a tolerance for convergence of 10^{-4} in load. For the classical continuum, Figure 6.12 illustrates the obtained curves for the load factor versus the vertical displacement of the loaded face for the three meshes. With the mesh refinement, the results diverge from the expected one, pointing to the mesh dependency of the classical model.

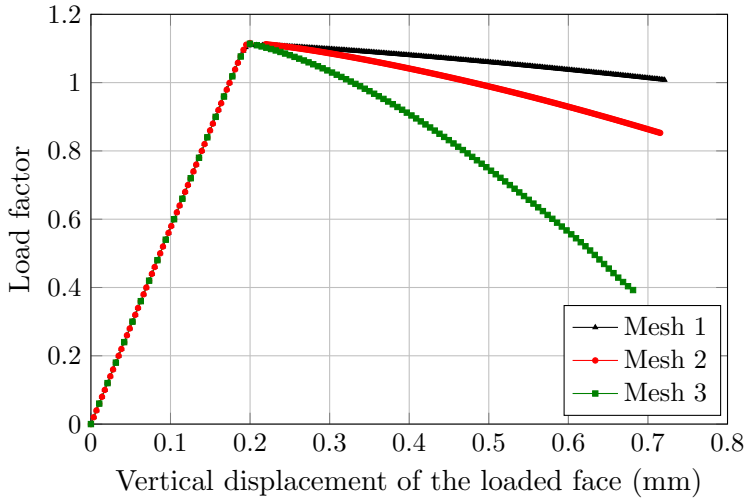

Figure 6.12: Shear band: load factor versus vertical displacement (classical continuum)

Such mesh dependency is not perceived in the results for the micromorphic media,

presented in Figure 6.13.

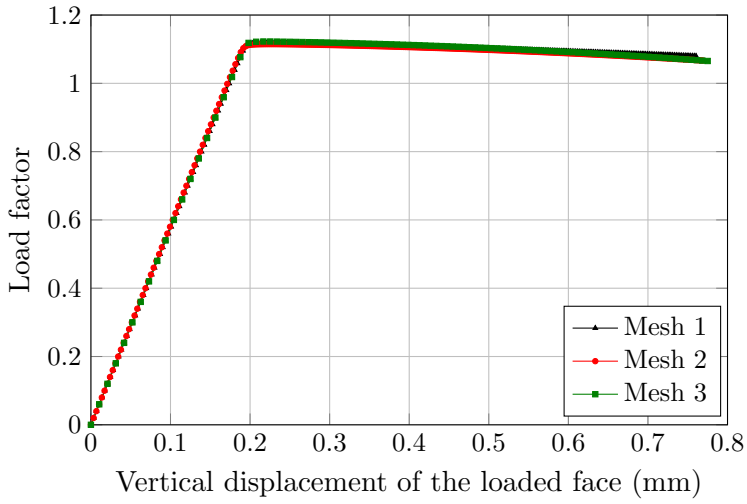

Figure 6.13: Shear band: load factor versus vertical displacement (micromorphic continuum)

The divergence in the results obtained for the classical continuum and the micromorphic continuum is due to the localization phenomenon that, with the mesh refinement, tends to concentrate in an infinitesimal region for a classical media. This localization is noted in the shear band presented for the three meshes in Figure 6.14 for the last step of the nonlinear process. For the micromorphic continuum, the localization phenomenon is well described with no mesh dependency, as seen in Figure 6.15.

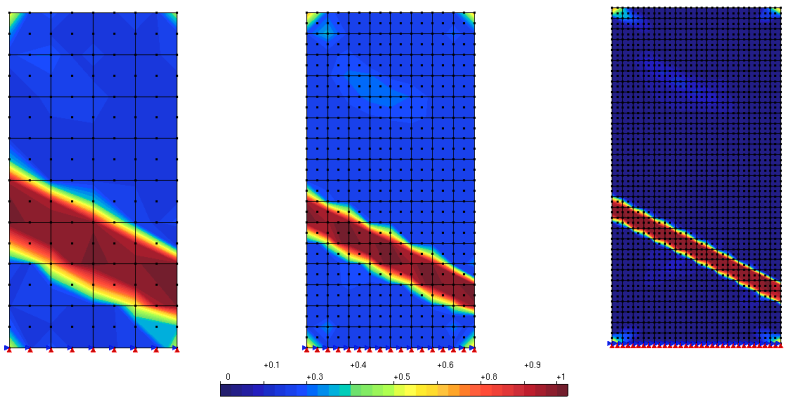

(a) Mesh 1 (b) Mesh 2 (c) Mesh 3

Figure 6.14: Shear band: damage (classical continuum)

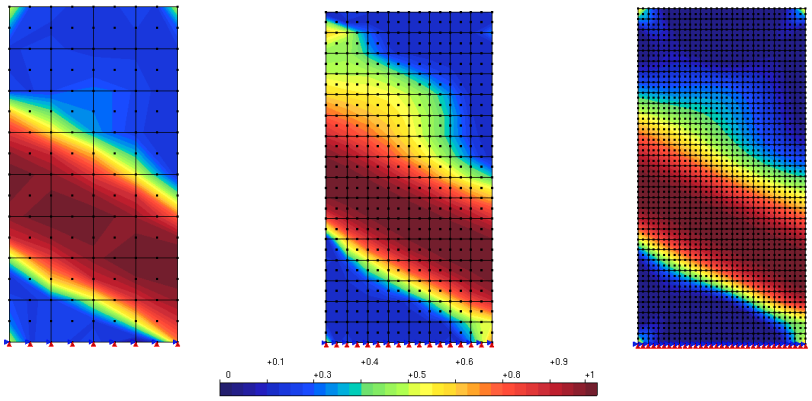

(a) Mesh 1 (b) Mesh 2 (c) Mesh 3

Figure 6.15: Shear band: damage (micromorphic continuum)

As discussed in the previous example, for a non-linear analysis with the micromorphic continuum the damage can be computed at the micro scale instead of at the macro scale, as proposed in this work. In order to compare both strategies, the same model with the same parameters was simulated considering damage at the micro scale. The equilibrium path and the shear band obtained are presented in Figures 6.16 and 6.17, and the results converge with the ones obtained for the *macro-damage* with a description of the localization phenomenon with no mesh dependency. As mentioned, the most prominent difference between both techniques resides in the computational time, that tends to be greater for the *micro-damage* consideration.

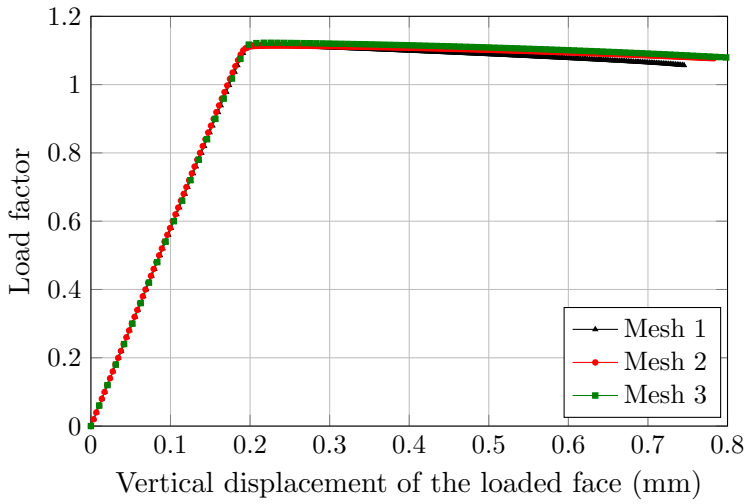

Figure 6.16: Shear band: load factor versus vertical displacement (micromorphic continuum with *micro-damage*)

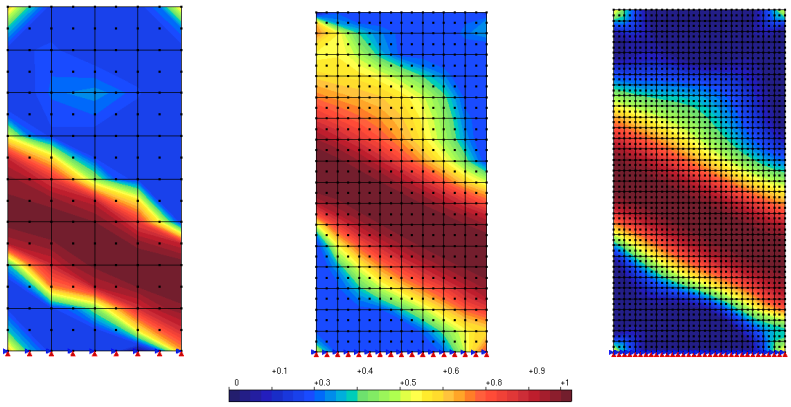

(a) Mesh 1 (b) Mesh 2 (c) Mesh 3

Figure 6.17: Shear band: damage (micromorphic continuum with *micro-damage*)

In order to study the influence on the structural behavior of the relation between the size of the considered microcontinuum and the size of the macroscale problem, the model illustrated in Figure 6.10 was modeled with the increased proportional dimensions presented in Figure 6.18. As the previous analysis, a microcontinuum of 1.25 mm was employed with the same material parameters: Mazars-Lemaitre damage model associated to a linear damage law; $E = 12000$ MPa; $\nu = 0.35$; $K_0 = 0.0017$ and $K_0 = 0.0016$ for the weakened elements (see Figure 6.11); $K_f = 0.325$. Similarly, the analysis was conducted with all three meshes shown in Figure 6.11.

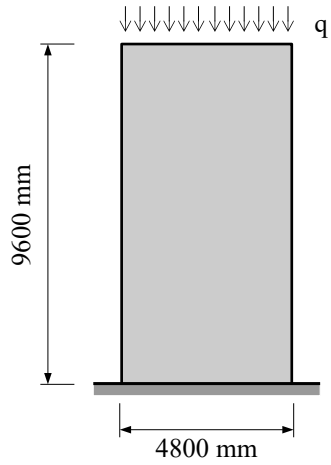

Figure 6.18: Shear band with increased dimensions: geometry

For the non-linear process, the generalized displacement control method was also employed with an initial load factor of 0.05 and a tolerance for convergence of 10^{-4}

in load. The equilibrium paths obtained for the analysis with the classical continuum and with the micromorphic continuum considering macro-damage and micro-damage are illustrated in Figures 6.19, 6.20, and 6.21, respectively. The equilibrium paths obtained for the classical continuum again demonstrates the occurrence of the localization phenomenon, what led to mesh-dependent results. However, for the case of the micromorphic continuum considering damage at the macro-scale and at the micro-scale, the results were not completely mesh-independent, i.e., the micromorphic theory was not able to fully solve the numerical localization. As for the processing time, for the most refined mesh the analysis considering micro-damage was around six times higher than the one for the macro-damage analysis.

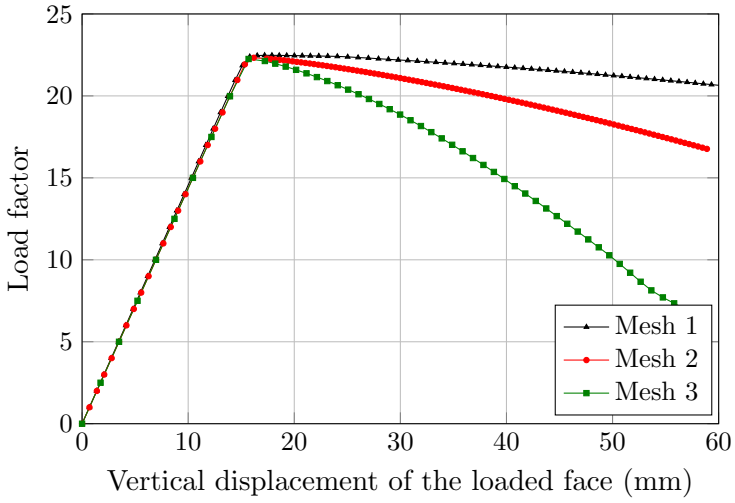

Figure 6.19: Shear band with increased dimensions: load factor versus vertical displacement (classical continuum)

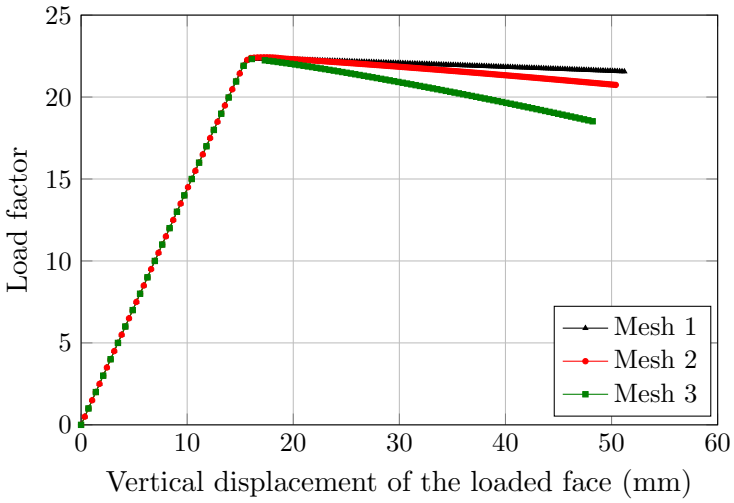

Figure 6.20: Shear band with increased dimensions: load factor versus vertical displacement (micromorphic continuum with macro-damage)

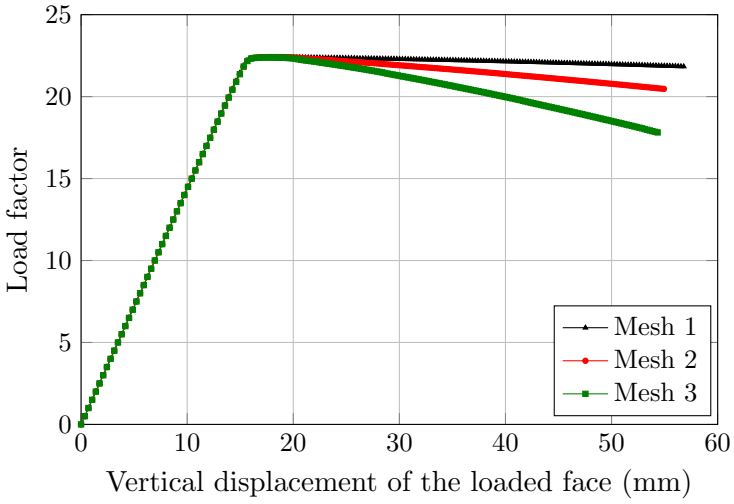

Figure 6.21: Shear band with increased dimensions: load factor versus vertical displacement (micromorphic continuum with micro-damage)

Following, the same analysis was carried out for a square homogeneous microcontinuum of size 100 mm in order to accommodate heterogeneity at the micro scale with aggregates varying from 19 mm to 9.5 mm, characterizing a possible concrete mixture. This study was conducted to analyze the impact of the microcontinuum increase for a homogeneous micro scale, i.e., with no influence of the heterogeneous material. The results for this analysis are illustrated in Figure 6.22 for the macro-damage consideration and in Figure 6.23 for the micro-damage.

With the increase in the microcontinuum dimension, the micromorphic theory is able to provide mesh-independent results when damage is considered at the macro scale. However, for the micro-damage consideration, the analysis for the more refined meshes (mesh 2 and 3) presented numerical instability and it was not able to fully described the loading process. Similarly to the previous analysis, for the most refined mesh when micro-damage is considered the processing time was around nine times higher than the one for the macro-damage analysis.

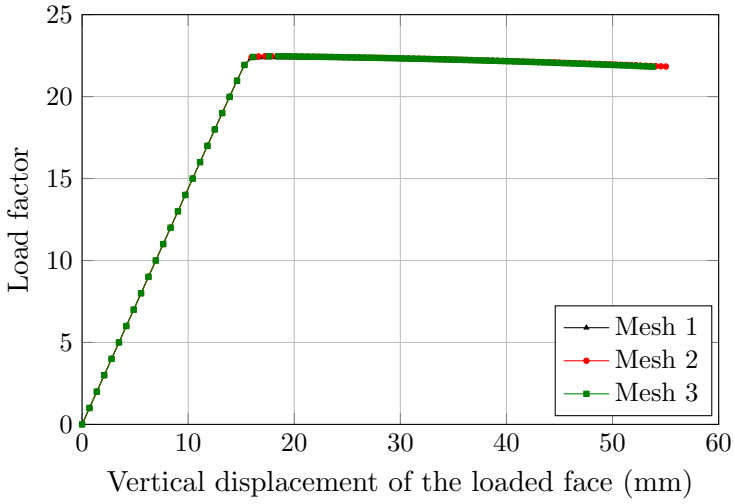

Figure 6.22: Shear band with increased dimensions: load factor versus vertical displacement (micromorphic continuum with macro-damage and microcontinuum with dimension of 100 mm)

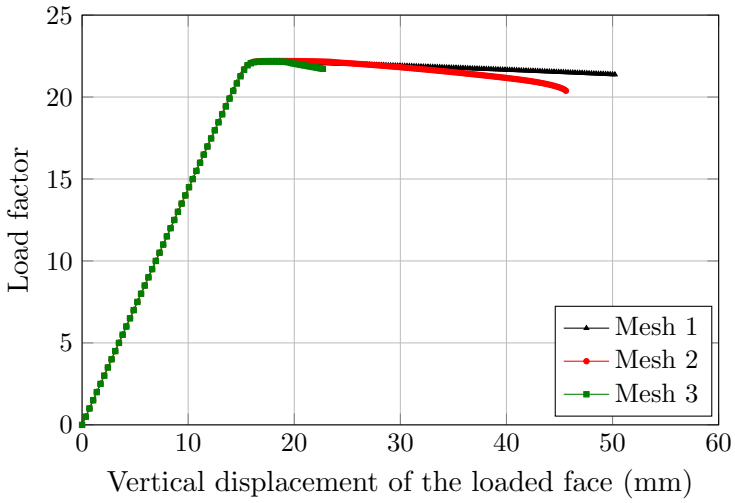

Figure 6.23: Shear band with increased dimensions: load factor versus vertical displacement (micromorphic continuum with micro-damage and microcontinuum with dimension of 100 mm)

Considering the results obtained for the three analysis conducted, it may be concluded that, for the case where the structural dimensions are comparable to the ones of the micro scale, the additional parameters introduced by the micromorphic theory are significant and its non-local character is able to regularize the localization phenomenon and solve the mesh-dependency problem. When there is a reduction in the size of the microcontinuum and the structural dimensions are not more comparable to those of the microstructure, the micromorphic theory tends to the same behavior as that of the classical theory and the induced localization process occurs, leading to mesh-dependent results.

For the last analysis, where the microcontinuum size is also increased and structural and microstructural dimensions are again comparable, the considerable size of the microcontinuum may not observe the hypotheses involved in the formulation of the micromorphic theory as well as of the homogenization technique, where the material particles are considered as small, leading to numerical instability when the damage is considered at the micro scale. However, for the macro-damage consideration, in this case, no such instability is noted and the micromorphic continuum is able to represent the structural behavior with no mesh-dependency, dealing with the induced localization phenomenon. It is important to note that these are preliminary conclusions and further studies should be carried out to verify their veracity.

6.4 Infinite shear layer

The infinite shear layer problem was employed for a number of authors to explore the regularization capacity of generalized continua specially for elasto-plastic models with strain softening (see, e.g., de Borst (1990, 1991, 1993), de Borst and Sluys (1991), Lages (1997), Fuina (2009), Gori (2018), and Hütter (2019)).

The problem, as illustrated in Figure 6.24(a), consists of a layer with an infinite dimension in the horizontal direction and height H under a shear load. Considering the symmetry condition due to the infinite extension assumption, this problem may be modeled as a thin strip with width w assuming no vertical displacement. In this section, the layer presents H = 100 mm and w = 2 mm (Figure 6.24(b)) being analyzed under a plane strain state with unitary thickness.

A square homogeneous microcontinuum was adopted with size 1 mm, Young's modulus $E = 30000$ MPa and Poisson's ratio $\nu = 0.2$. The Marigo damage model is employed with an exponential damage law (Eq. (2.48) and Eq. (6.1)) with the parameters as follows: $\alpha = 0.950$, $\beta = 750$, and $K_0 = 1 \times 10^{-5}$.

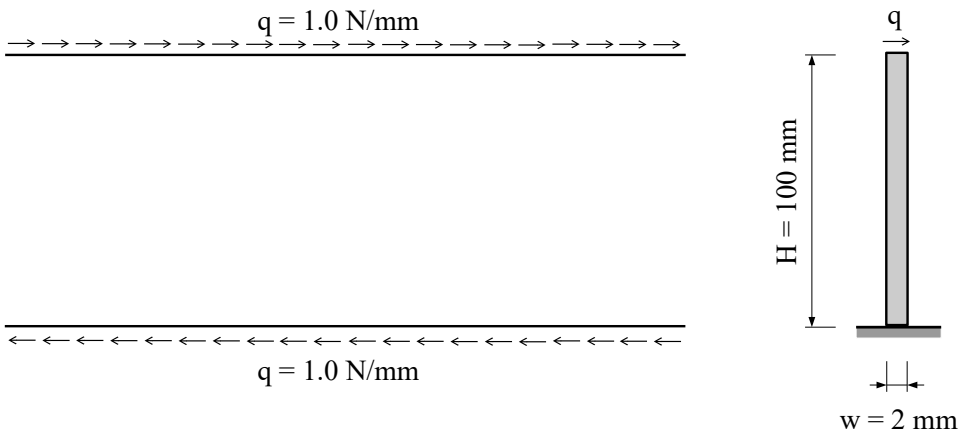

(a) Geometry (b) Model

Figure 6.24: Infinite shear layer: geometry and model

Four meshes, as illustrated in Figure 6.25, composed of 5, 10, 20, and 40 quadrilateral elements with four nodes are considered in this study and four integration points. The bottom of the layer is constrained in both directions and each point of the layer is restrained in order to prevent displacement in the vertical direction.

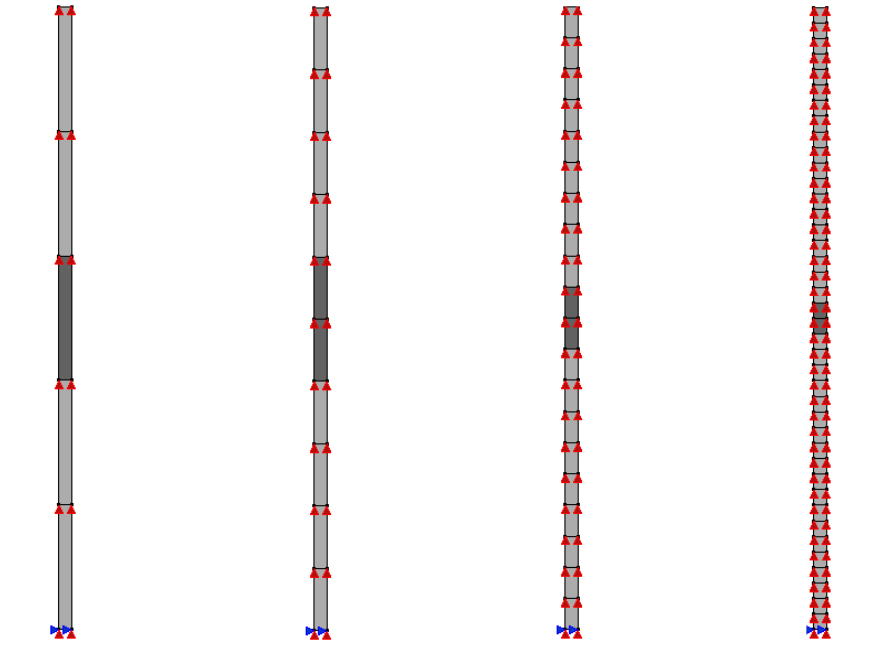

(a) Mesh 1 (b) Mesh 2 (c) Mesh 3 (d) Mesh 4

Figure 6.25: Infinite shear layer: meshes

To induce the localization phenomenon, a weakened region is introduced, located at the center of the strip, as highlighted in Figure 6.25. For the elements in this region, $K_0 = 0.95 \times 10^{-5}$ was adopted. The extension of this weakened region was chosen accordingly with the considered discretization. For mesh 1 (Figure 6.27(a)) this zone enclosures the central element, while, for the other meshes (Figures 6.27(b), 6.27(c), and 6.27(d)), it occupies the two middle elements. Hence, meshes 1 and 2 present the same height for the weakened zone, and meshes 3 and 4 a reduced height.

The loading process is driven by the displacement control method assuming an increment of 10^{-5} for the horizontal displacement of the top of the layer and tolerance for convergence in load of 10^{-4}.

The equilibrium paths obtained for the classical continuum are displayed in Figure 6.26 and the mesh-dependency is clearly noticed. For meshes 1 and 2, which present a weakened zone with same height, the equilibrium paths coincide, while for the more refined meshes (meshes 3 and 4) a stronger softening in the post-peak branch is perceived. The influence of the weakened zone height is also noted in the damaged and deformed configurations presented in Figure 6.27 for the last step of the loading process. It can be observed that, as the degradation process is initiated, the damage was confined to the weakened elements, and this zone did not expand during the loading process. Observing the deformed configuration, it is noticeable

that the deformations tend to concentrate in the weakened zone, while the remaining elements exhibited rigid displacements. These results converge with other studies, as de Borst (1991), Gori (2018), and Silva (2019).

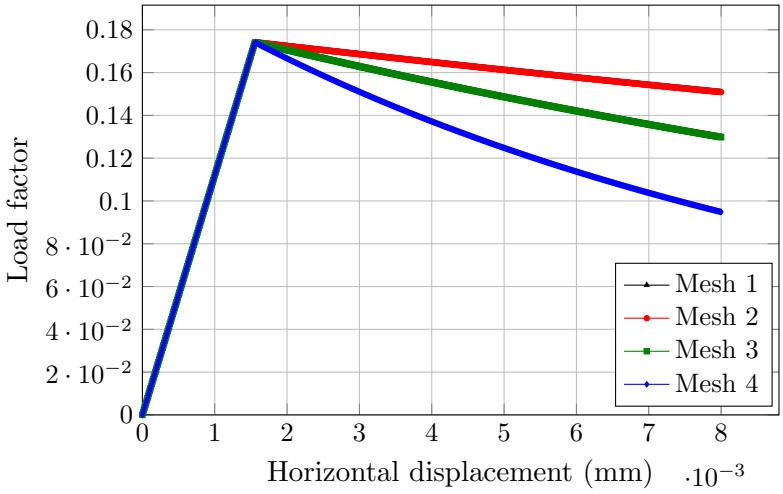

Figure 6.26: Infinite shear layer: load factor versus horizontal displacement (classical continuum)

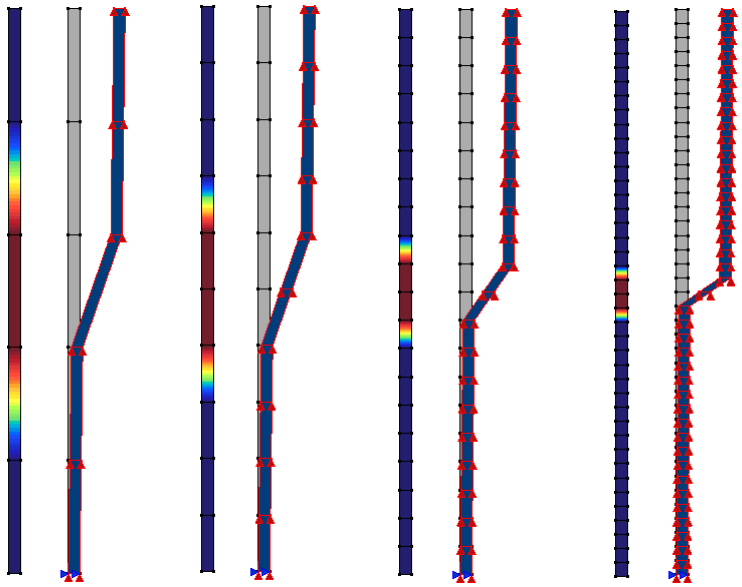

(a) Mesh 1 (b) Mesh 2 (c) Mesh 3 (d) Mesh 4

Figure 6.27: Infinite shear layer: damage and deformed configurations (classical continuum)

For the micromorphic continuum with damage considered at the macro-scale, the

results are presented in Figure 6.28 where the strong mesh-dependency noted for the classical continuum is not perceived. This behavior is also noticeable in the damaged and deformed configurations illustrated in Figure 6.29 due to the regularization capacity of the micromorphic continuum, as discussed in the previous examples.

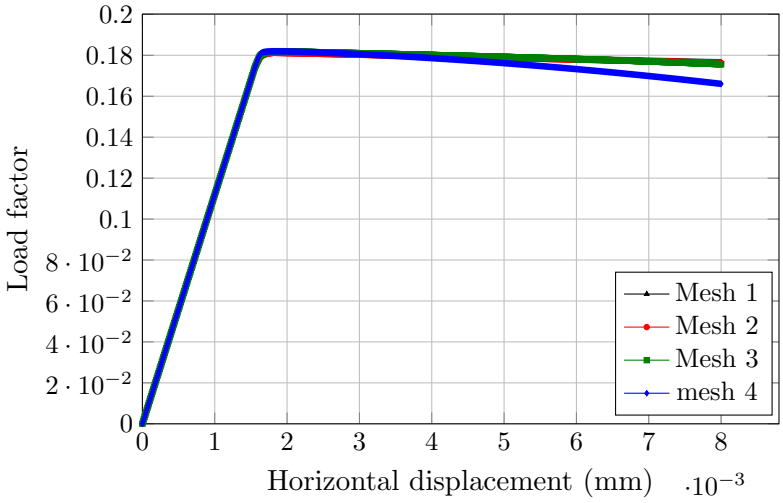

Figure 6.28: Infinite shear layer: load factor versus horizontal displacement (micromorphic continuum with macro-damage)

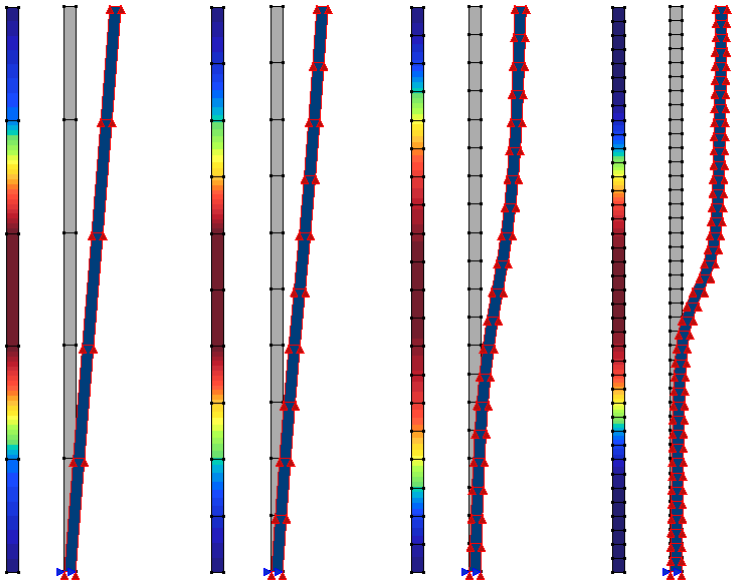

(a) Mesh 1 (b) Mesh 2 (c) Mesh 3 (d) Mesh 4

Figure 6.29: Infinite shear layer: damage and deformed configurations (micromorphic continuum with macro-damage)

Adopting damage at the micro scale, the behavior is similar to the one observed for the macro-damage consideration, as illustrated in Figures 6.30 and 6.31. However, the analysis with macro-damage presented a more significant softening behavior for the more refined mesh at the end of the post-peak branch, where the damaged zone reduces in length (see Figures 6.29(d) and 6.31(d)). This behavior may be due to the influence of the microcontinuum size, however more studies are required for proving this hypotheses.

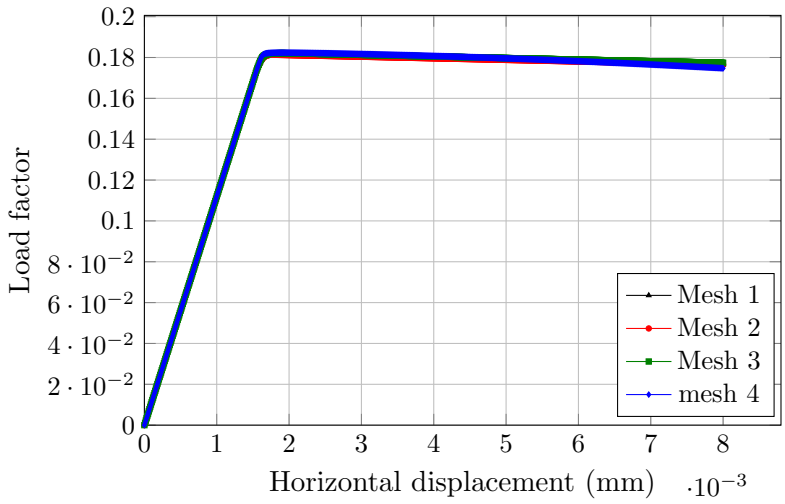

Figure 6.30: Infinite shear layer: load factor versus horizontal displacement (micromorphic continuum with micro-damage)

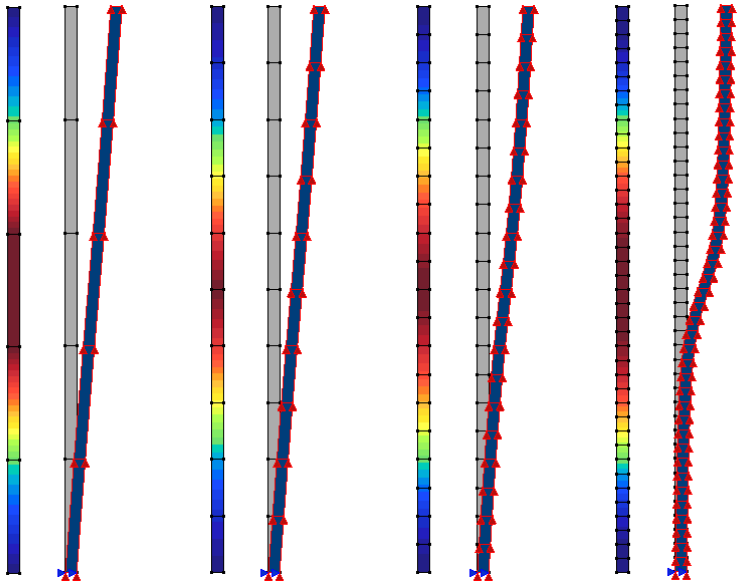

(a) Mesh 1 (b) Mesh 2 (c) Mesh 3 (d) Mesh 4

Figure 6.31: Infinite shear layer: damage and deformed configurations (micromorphic continuum with micro-damage)

Chapter 7

Non-linear analysis of heterogeneous media

In the previous chapter (Chapter 6) examples for the application of the scalar-isotropic models proposed in this work were presented for the case of a homogeneous microcontinuum in order to validate the equivalent strains proposed as well as the implementation of the respective constitutive models. In this chapter, the focus is the analysis of a heterogeneous microcontinuum with a microstructure generated by the take-and-place algorithm and an equivalent homogeneous material obtained by means of the homogenization strategy.

7.1 Study of the homogenization technique

In order to model non-linear problems with the micromorphic theory associated to a heterogenous microcontinuum, an initial study of the proposed homogenization strategy was conducted in order to evaluate the influence on the constitutive relations of the type and size of the elements that compose the mesh for the microcontinuum as well as the impact of the microcontinuum size. The results for both the analysis (*mesh study* and *microcontinuum size and distribution study*) are presented in the following sections.

7.1.1 Mesh study

To evaluate the impact on the homogenized constitutive operator of the type and size of the element that composes the microcontinuum discretization, the meshes illustrated in Figure 7.1 for quadrilateral elements and in Figure 7.2 for triangular elements were studied. A square heterogeneous microcontinuum of size 50 mm was

considered for all the meshes and, for the microstructure, the following parameters: maximum sieve size $d_{max} = 19$ mm; minimum sieve size $d_{min} = 9.5$ mm; continuous particle distribution; spherical particles; particle fraction PF = 30%; distribution factor DF = 0.2; $n = 0.5$ for the Fuller's distribution (Eq. 2.50); Young's modulus for the aggregates $E_{particle} = 300$ GPa; Poisson's ratio for the aggregates $\nu_{particle} = 0.2$; Young's modulus for the matrix $E_{matrix} = 30$ GPa; Poisson's ratio for the matrix $\nu_{matrix} = 0.2$.

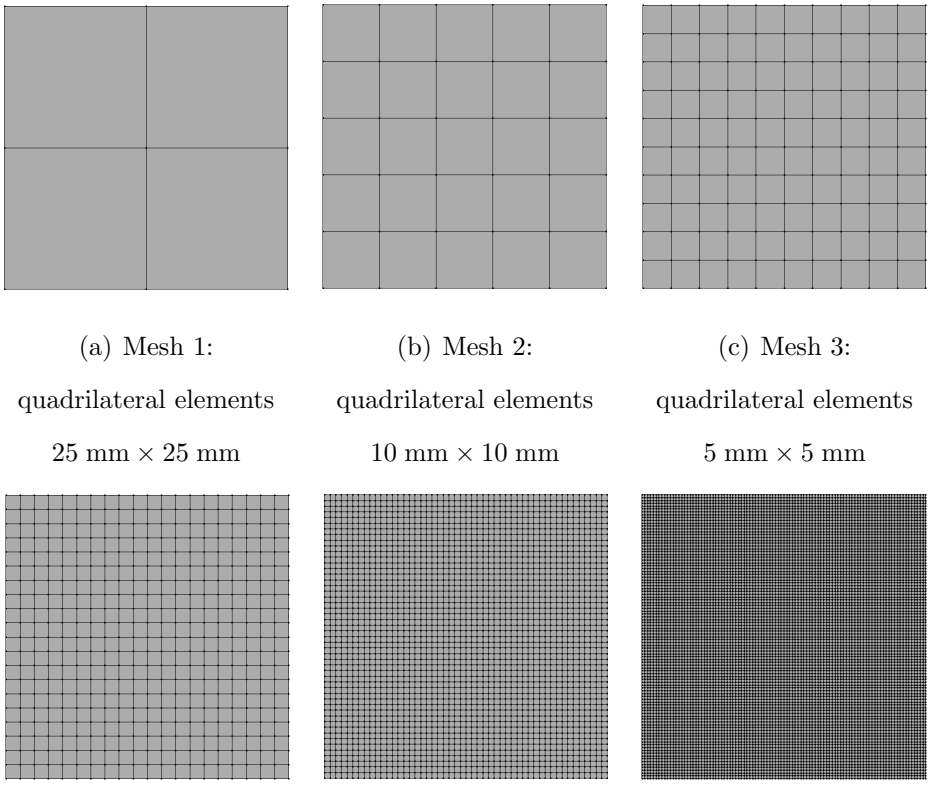

(a) Mesh 1: quadrilateral elements 25 mm × 25 mm

(b) Mesh 2: quadrilateral elements 10 mm × 10 mm

(c) Mesh 3: quadrilateral elements 5 mm × 5 mm

(d) Mesh 4: quadrilateral elements 2.5 mm × 2.5 mm

(e) Mesh 5: quadrilateral elements 1 mm × 1 mm

(f) Mesh 6: quadrilateral elements 0.5 mm × 0.5 mm

Figure 7.1: Mesh study: quadrilateral microcontinuum meshes

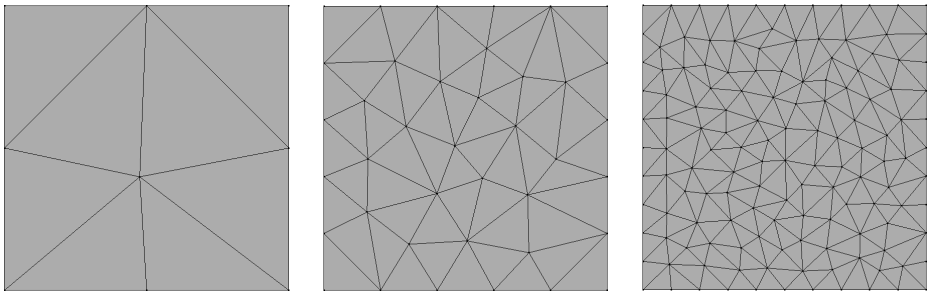

(a) Mesh 1: triangular elements with average size 25 mm

(b) Mesh 2: triangular elements with average size 10 mm

(c) Mesh 3: triangular elements with average size 5 mm

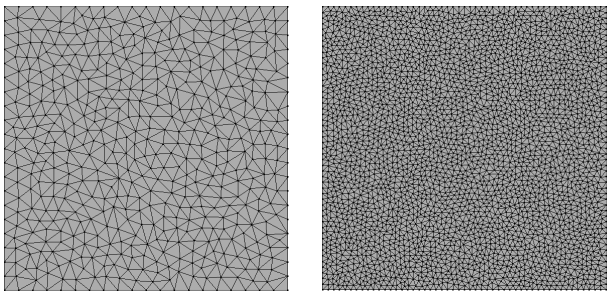

(d) Mesh 4: triangular elements with average size 2.5 mm

(e) Mesh 5: triangular elements with average size 1 mm

Figure 7.2: Mesh study: triangular microcontinuum meshes

Due to the randomness of the take-and-place algorithm, different particle distributions can be obtained for the same input parameters, as seen in Figure 7.3 for a microcontinuum of size 50 mm as previously defined for the present example. To avoid the influence of the distribution on this study, a fixed particle distribution for the aggregates was used for all meshes.

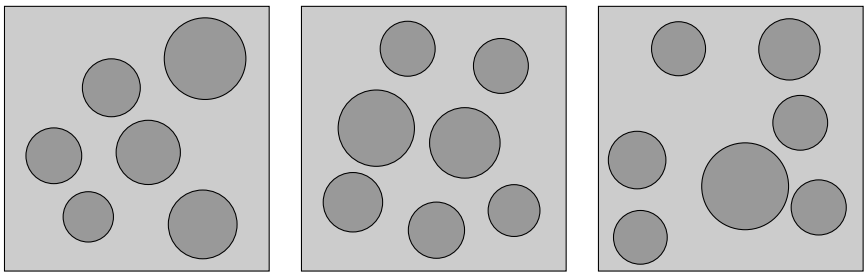

Figure 7.3: Mesh study: random generation of particles with same input parameters for a microcontinuum of size 50 mm

For each discretization, a heterogeneous microstructure was associated following the process illustrated in Figure 4.2 in order to obtain a heterogeneous microcontinuum. Subsequently, the homogenization process was carried out and the elastic constitutive operator for the micromorphic continuum obtained containing $\bar{A}_{klmn}$, $\bar{E}_{klmn}$, $\bar{E}_{mnkl}$, $\bar{B}_{klmn}$, and $\bar{C}_{lmknpq}$ (Eqs. 4.6, 4.7, and 4.8). For a plane model, this constitutive operator is organized in a matrix with 16 rows and 16 columns, as implemented for a FEM representation. This representation is presented in Figure 7.4 with the expected non-zero components of each constitutive tensor considering the uncoupling for isotropic linear elastic media [1] and the corresponding stress/strain components in Voigt notation. The values obtained for each component of the constitutive tensors versus the element size are presented in Figures 7.5 through 7.9.

[1] In this study, only expected non-zero components were considered. For a heterogeneous microcontinuum, values supposed to be zero for a plane analysis for a homogeneous microcontinuum presented non-zero values due to the heterogeneity. However, they were disregarded in this analysis and further analysis is needed to understand their behavior.

		1	2	3	4	5	6	7	8	9	10	11	12	13	14	15	16
		ε_{11}	ε_{22}	ε_{12}	ε_{21}	e_{11}	e_{22}	e_{12}	e_{21}	γ_{111}	γ_{221}	γ_{122}	γ_{212}	γ_{222}	γ_{112}	γ_{211}	γ_{121}
1	t_{11}	A_{1111}	A_{1122}	A_{1112}	A_{1121}	E_{1111}	E_{1122}	E_{1112}	E_{1121}								
2	t_{22}	A_{2211}	A_{2222}	A_{2212}	A_{2221}	E_{2211}	E_{2222}	E_{2212}	E_{2221}								
3	t_{12}	A_{1211}	A_{1222}	A_{1212}	A_{1221}	E_{1211}	E_{1222}	E_{1212}	E_{1221}								
4	t_{21}	A_{2111}	A_{2122}	A_{2112}	A_{2121}	E_{2111}	E_{2122}	E_{2112}	E_{2121}								
5	s_{11}	E_{1111}	E_{2211}	E_{1211}	E_{2111}	B_{1111}	B_{1122}	B_{1112}	B_{1121}								
6	s_{22}	E_{1122}	E_{2222}	E_{1222}	E_{2122}	B_{2211}	B_{2222}	B_{2212}	B_{2221}								
7	s_{12}	E_{1112}	E_{2212}	E_{1212}	E_{2112}	B_{1211}	B_{1222}	B_{1212}	B_{1221}								
8	s_{21}	E_{1121}	E_{2221}	E_{1221}	E_{2121}	B_{2111}	B_{2122}	B_{2112}	B_{2121}								
9	m_{111}									C_{111111}	C_{111221}	C_{111122}	C_{111212}				
10	m_{122}									C_{221111}	C_{221221}	C_{221122}	C_{221212}				
11	m_{212}									C_{122111}	C_{122221}	C_{122122}	C_{122212}				
12	m_{221}									C_{212111}	C_{212221}	C_{212122}	C_{212212}				
13	m_{222}													C_{222222}	C_{222112}	C_{222211}	C_{222121}
14	m_{211}													C_{112222}	C_{112112}	C_{112211}	C_{112121}
15	m_{121}													C_{211222}	C_{211112}	C_{211211}	C_{211121}
16	m_{112}													C_{121222}	C_{121112}	C_{121211}	C_{121121}

Figure 7.4: Grouped micromorphic constitutive matrix - plane state

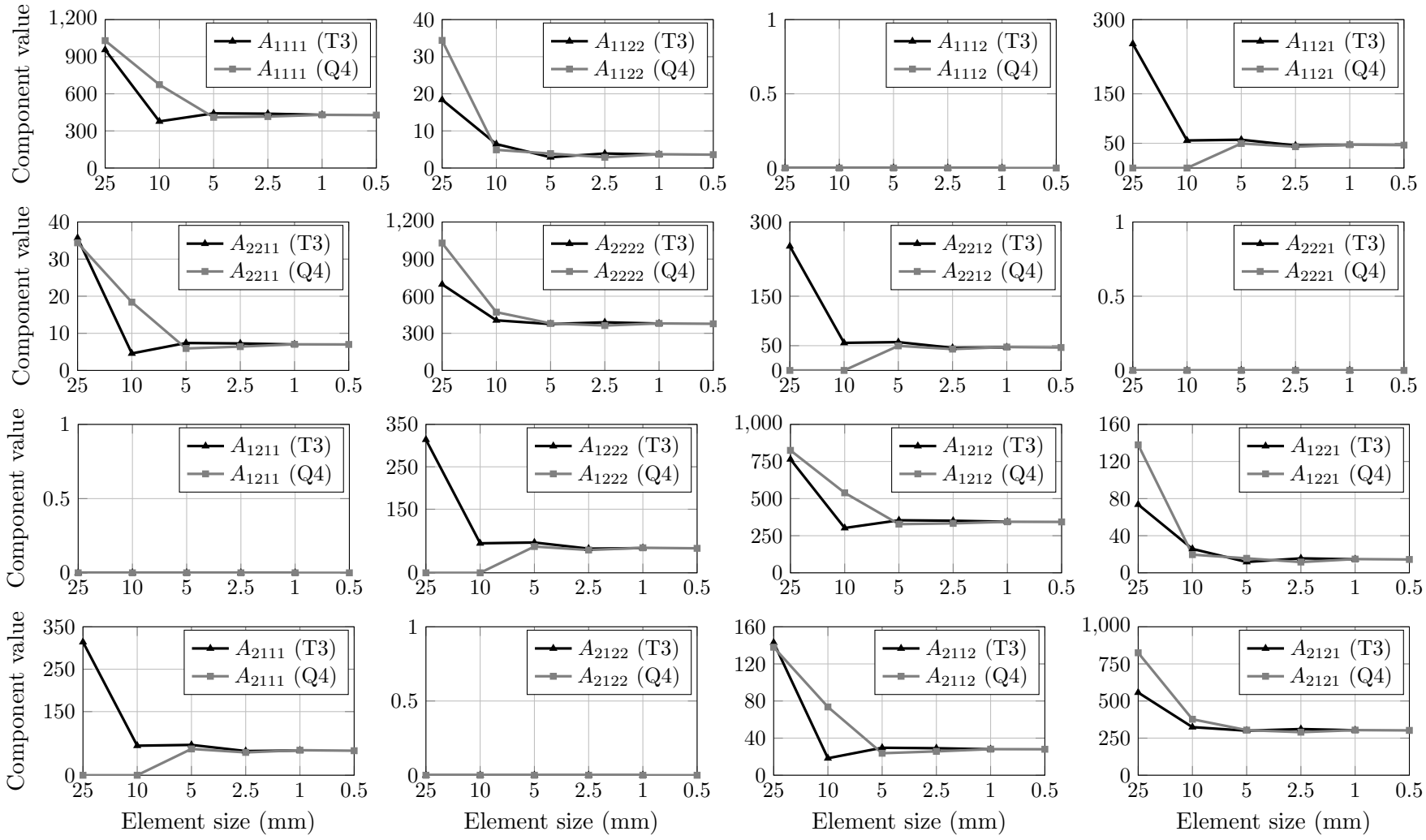

Figure 7.5: Mesh study: components of the constitutive operator A_{ijkl}

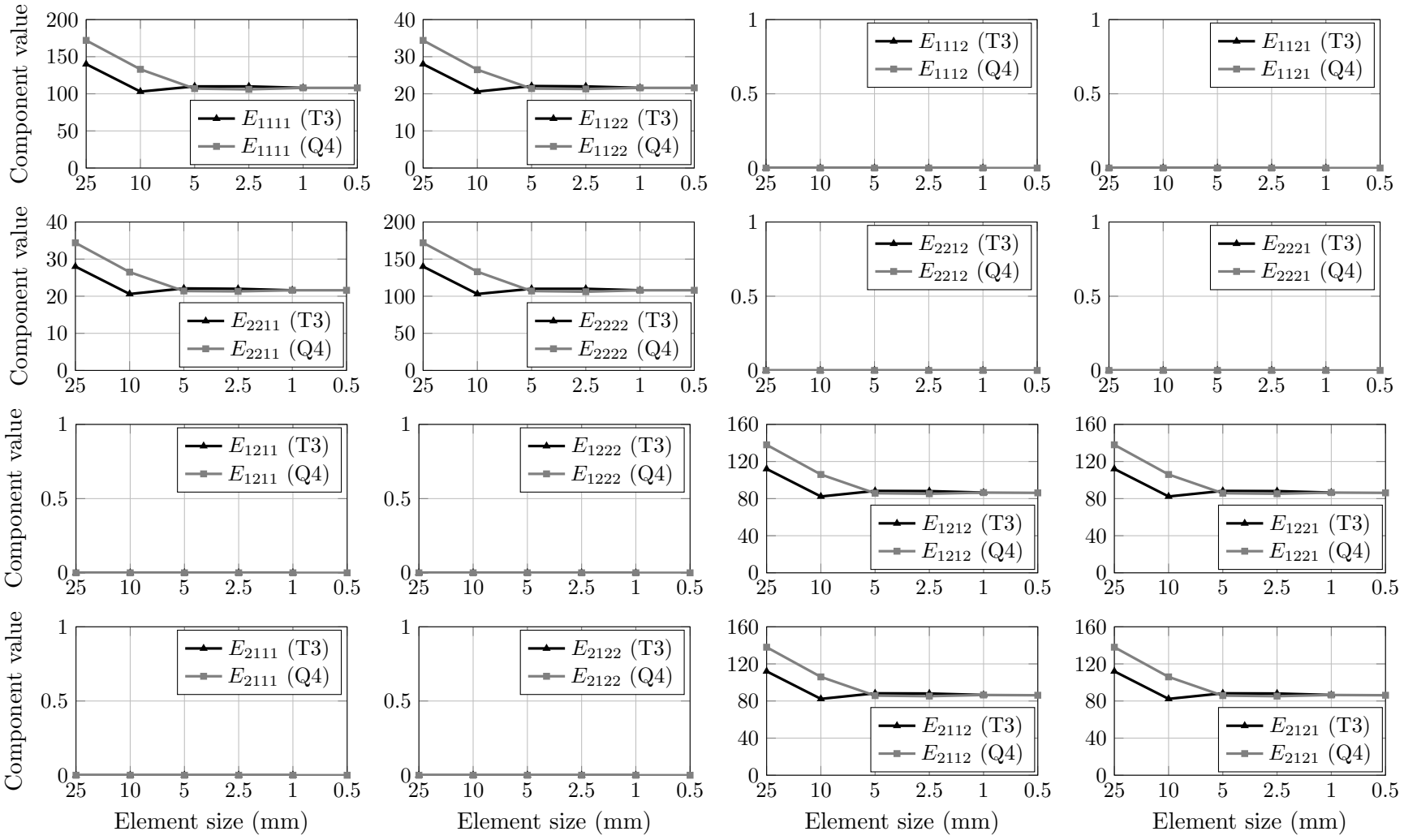

Figure 7.6: Mesh study: components of the constitutive operator E_{ijkl}

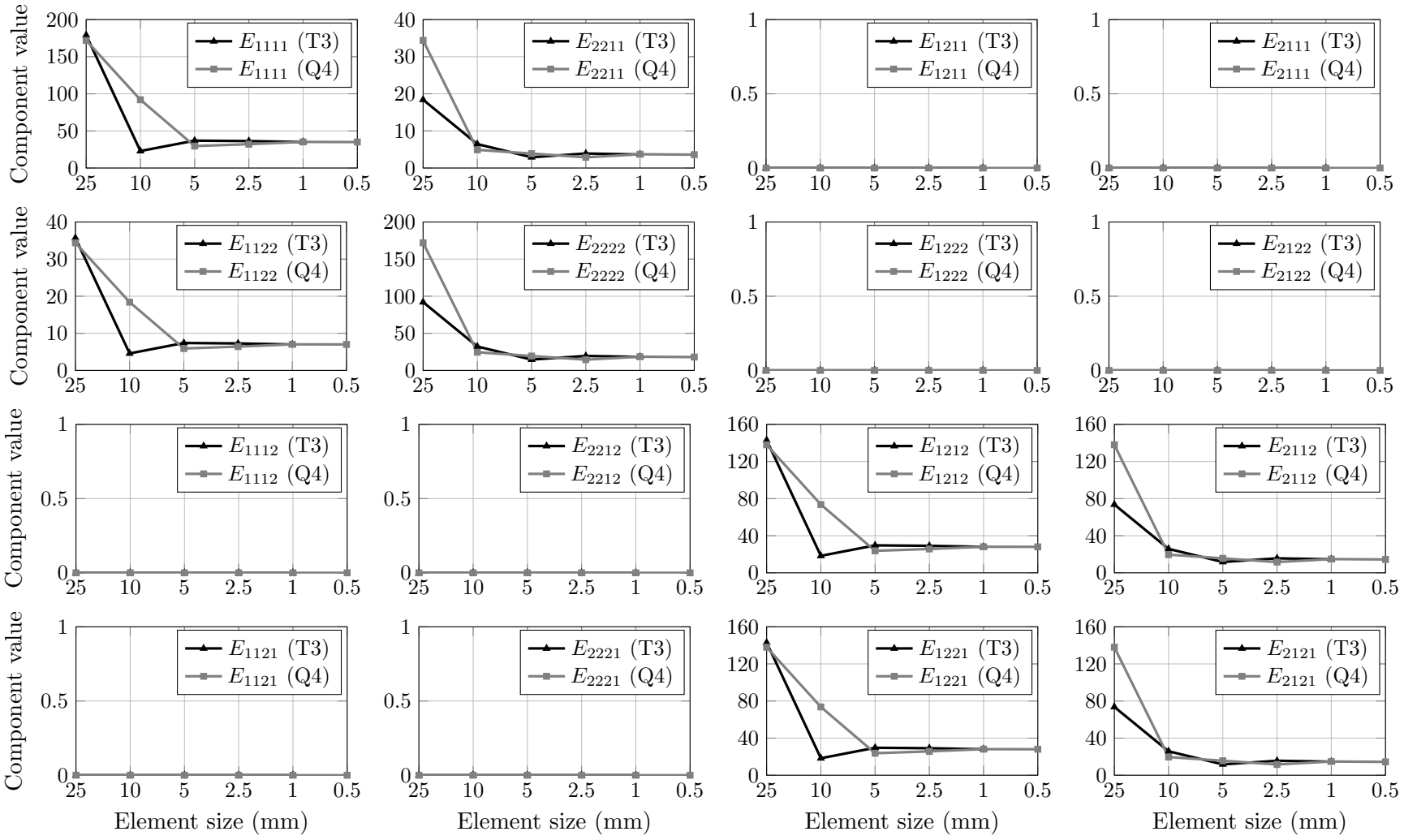

Figure 7.7: Mesh study: components of the constitutive operator E_{klij}

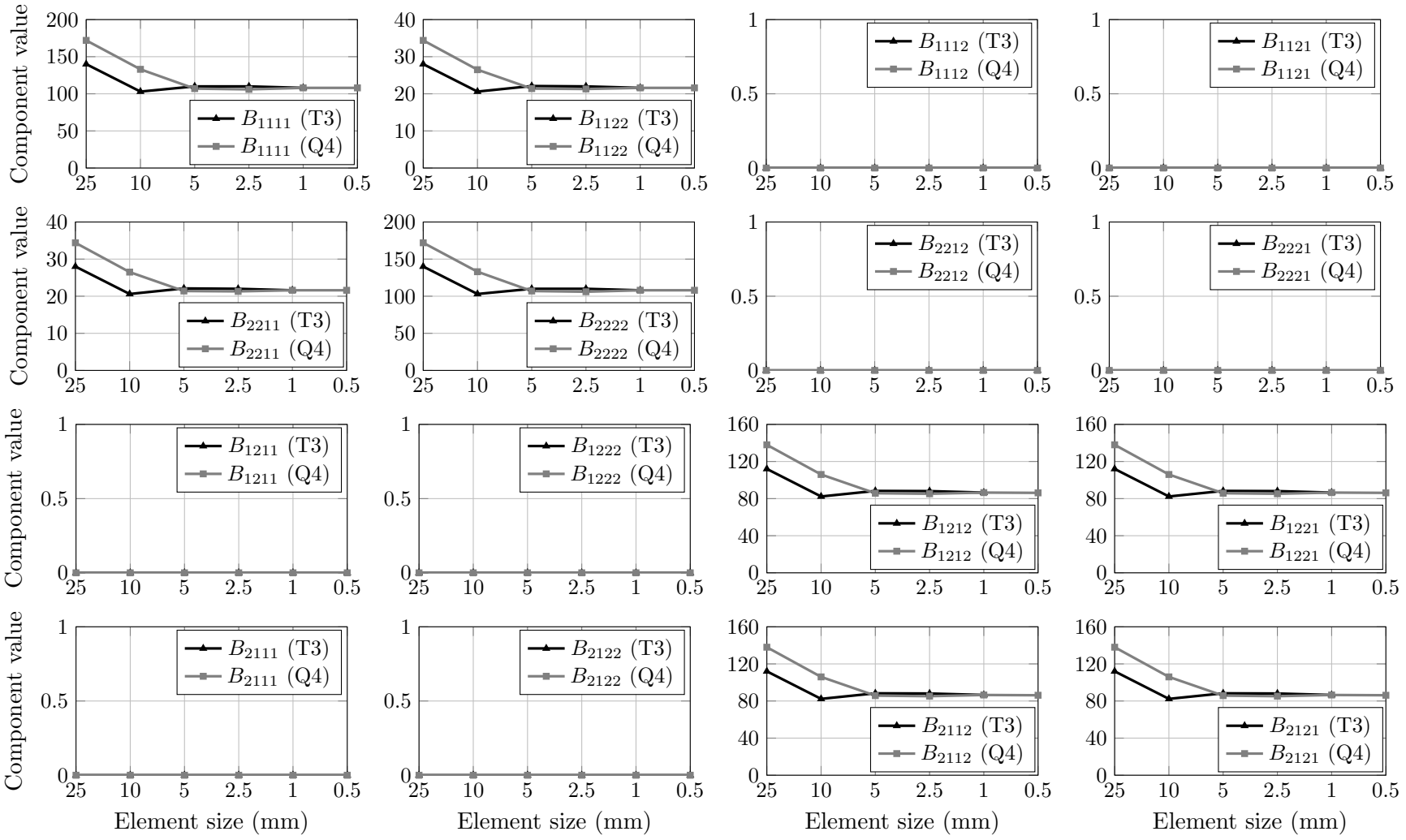

Figure 7.8: Mesh study: components of the constitutive operator B_{ijkl}

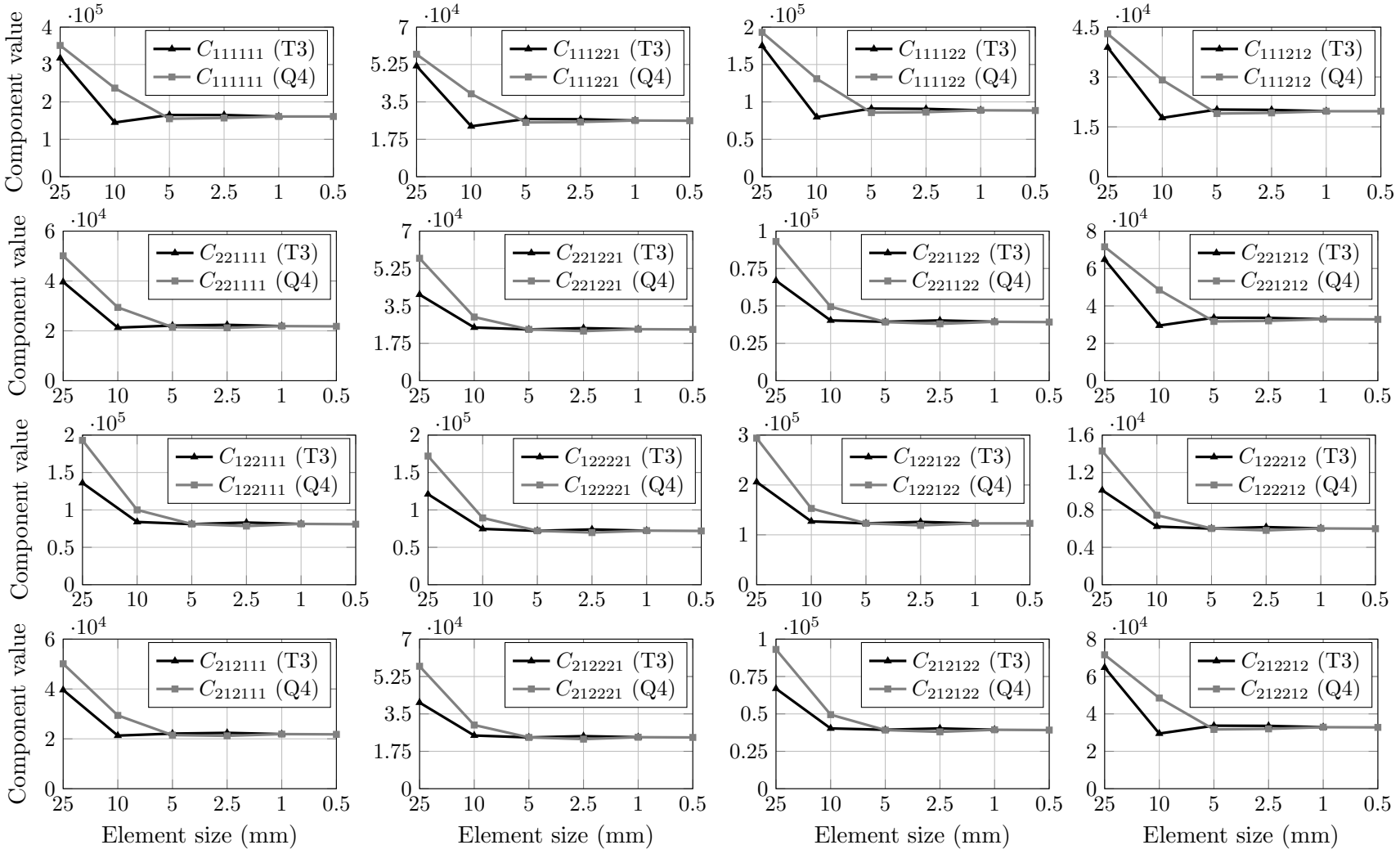

Figure 7.9: Mesh study: components of the constitutive operator C_{ijkl} - rows and columns 9 to 12 of the constitutive matrix

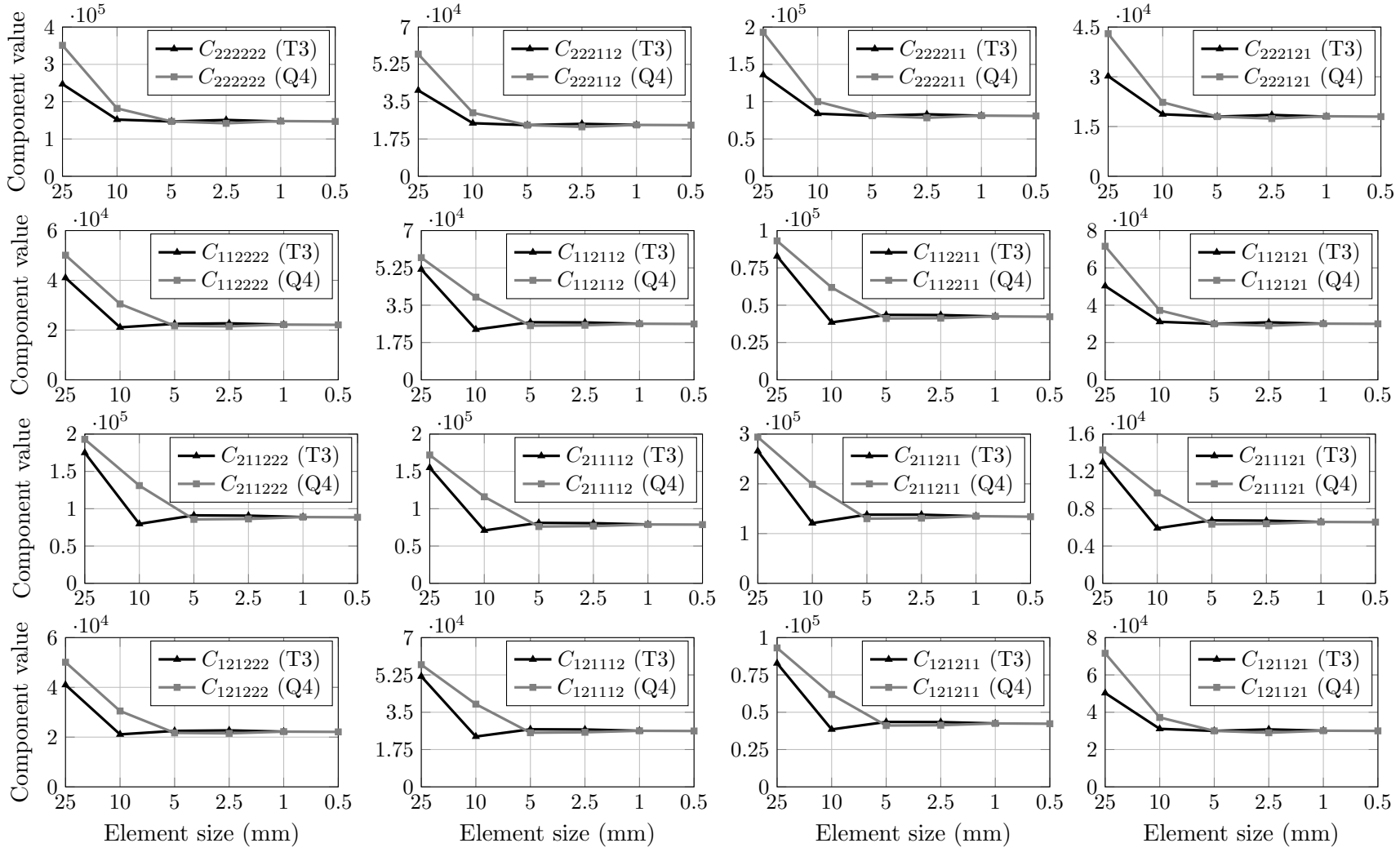

Figure 7.10: Mesh study: components of the constitutive operator C_{ijkl} - rows and columns 13 to 16 of the constitutive matrix

As the results obtained for each constitutive tensor shown, there is a convergence in the values for element sizes smaller than 5 mm for quadrilateral and triangular elements. In order to define the preferable element type, the processing time for each mesh in the study was taken into account. Figure 7.11 presents the time processing in milliseconds versus the element size. For more refined meshes the quadrilateral element presents a lower time for obtaining the constitutive tensor by the homogenization technique due to the presence of fewer elements in the mesh. Therefore, for the following examples that employs the homogenization strategy in heterogeneous particles, the microcontinuum is discretized with quadrilateral elements of size 5 mm.

It is important to note that the results for this study apply for a heterogeneous microstructure with the parameters previously specified, as particle fraction, distribution factor, and sieve sizes. For other distributions, another study should be conducted to determine the element type and size that yield better results with the lowest processing time.

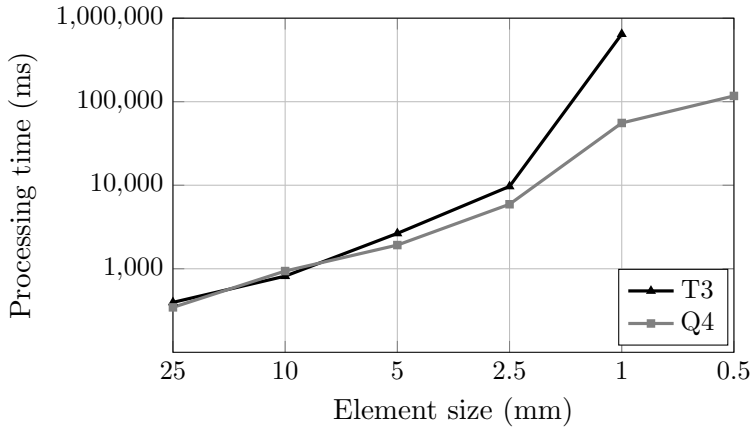

Figure 7.11: Mesh study: processing time versus element size

7.1.2 Microcontinuum size and distribution study

After the definition of the appropriate size and type of the element for the microstructure discretization, a study of the microcontinuum size associated with an analysis of the influence on the constitutive operator of the distribution randomness was conducted.

Adopting quadrilateral elements with dimension 5 mm, square RVE's with sizes varying from 20 mm up to 120 mm were studied. For each microcontinuum size, 200 particle distributions were generated to evaluate the variation of the components of

the constitutive operator due to the randomness of the take-and-place algorithm. Figure 7.12 shows some examples for the microstructure generated for the same input parameters considering a microcontinuum of size 100 mm, and Figures 7.13 through 7.18 illustrate the values for each component obtained for a microcontinuum of size 100 mm for the 200 distributions generated[2].

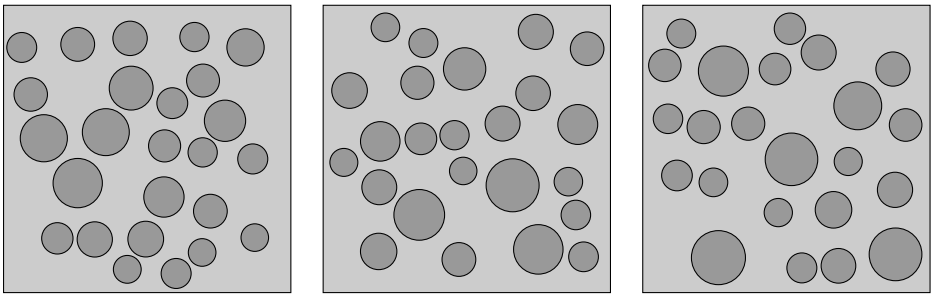

Figure 7.12: Distribution study: random generation of particles with same input parameters for microcontinuum of size 100 mm

The behavior of the tensors A_{ijkl}, E_{ijkl}, E_{klij}, and B_{ijkl} is similar, where components with indexes 1111, 1122, 2211, 2222, 1212, 1221, 2112, and 2121 tend to an average value and the remaining components oscillate around zero. This corresponds to the expected behavior of these tensors for a plane analysis due to the uncoupling of the corresponding stress-strain measures. The components of the tensor C_{ijkl} present a tendency to fluctuate around a average value, what also fits with the anticipated behavior for this type of analysis.

Considering all the microcontinuum sizes analyzed, the average value for each component for each RVE size was calculated. The results are presented in Figures 7.19 through 7.24 for the average values obtained versus the microcontinuum size[3]. The results for the tensors A_{ijkl}, E_{ijkl}, E_{klij}, and B_{ijkl} are similar, where non-zero components tend to a certain value with the increase in the microcontinuum size, probably due to the better representation of the microstructure and its particles. For tensors A_{ijkl} and E_{ijkl} components that were expected as null presented a negligible fluctuation around zero values. The average values obtained for the tensor C_{ijklmn} present an exponential growth as the microcontinuum increases, with no convergence to a value. These results may be correlated to the formulation of the micromorphic theory where the tensor C_{ijklmn} is more significant with the increase of the size of

[2]For a better text organization, the complete results obtained for all microcontinuum sizes are presented in Appendix A.

[3]The standard deviation for each component for each microcontinuum size was also determined and the results are shown in Appendix A, Figures A.61 through A.66.

the material particle, but further studies are necessary to attest this hypotheses. Another possible explanation is related to the integral solved in order to obtain the tensor C_{ijklmn} through the homogenization process, presented in (4.4). As it can be noted, the integer for defining the stress tensor $\bar{m}_{klm}$ used for constructing its corresponding constitutive tensor, presents the highest order among the integrals defined in the homogenization strategy ((4.3) and (4.5)), which may lead to a higher sensibility to the size of the material particle.

Based on these conclusions the shear band problem presented in Section 6.3 is modeled in the next section with a heterogeneous microstructure associated to a microcontinuum of size 100 mm in order to satisfactorily represent the aggregates with no large losses in computational efficiency, as, with larger RVE's, the homogenization process takes more time.

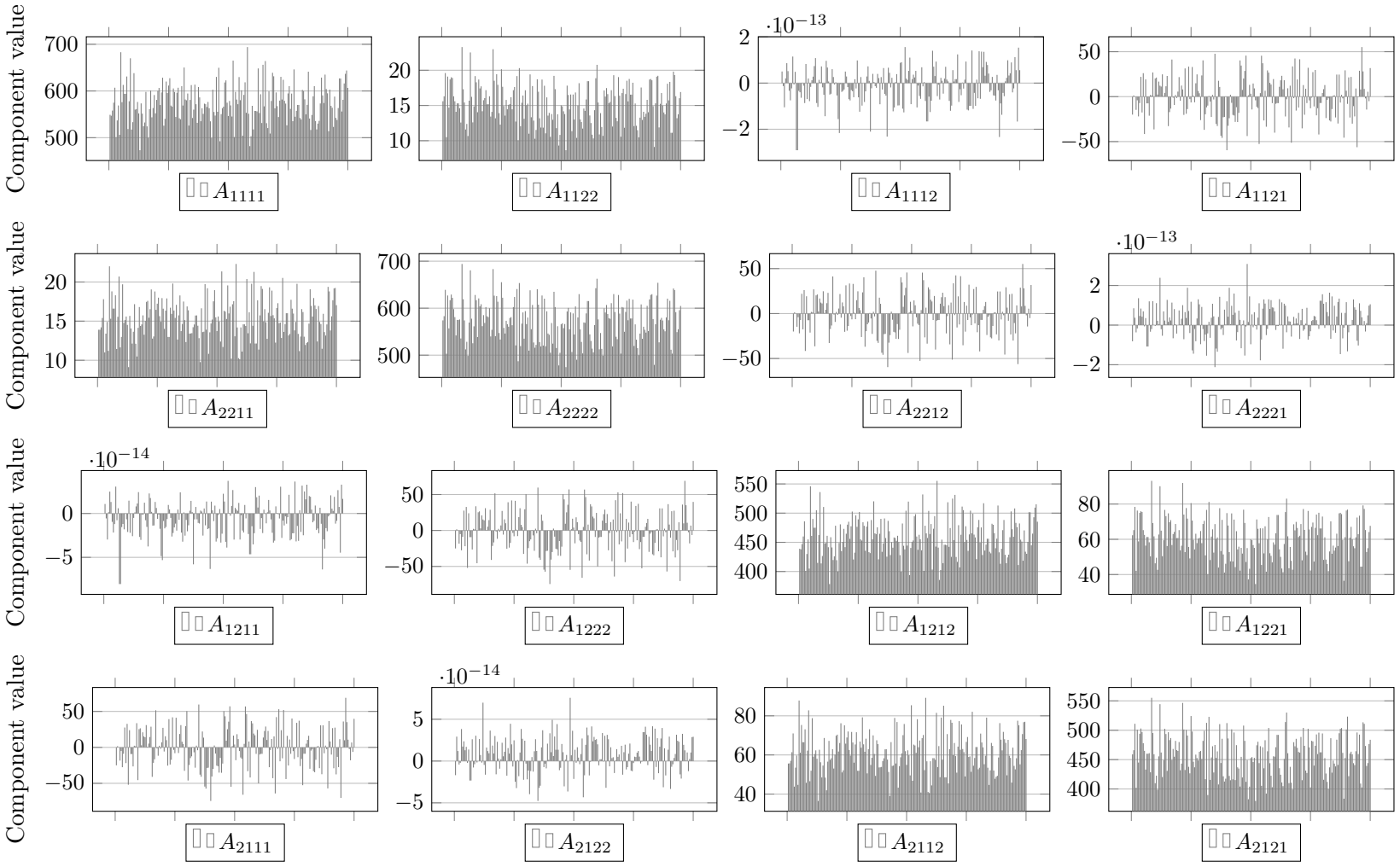

Figure 7.13: Distribution study: components of the constitutive operator A_{ijkl} (microcontinuum 100 mm)

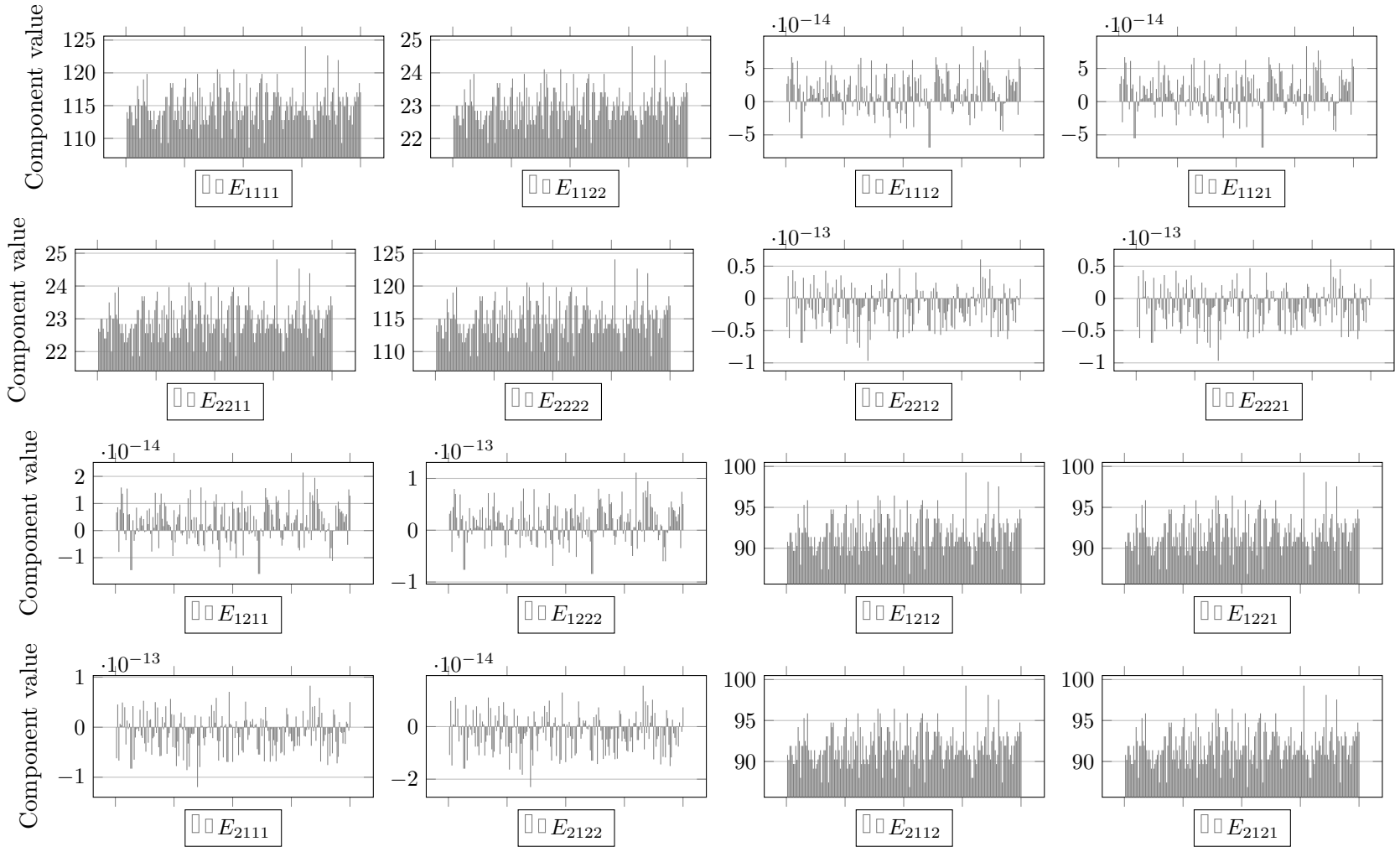

Figure 7.14: Distribution study: components of the constitutive operator E_{ijkl} (microcontinuum 100 mm)

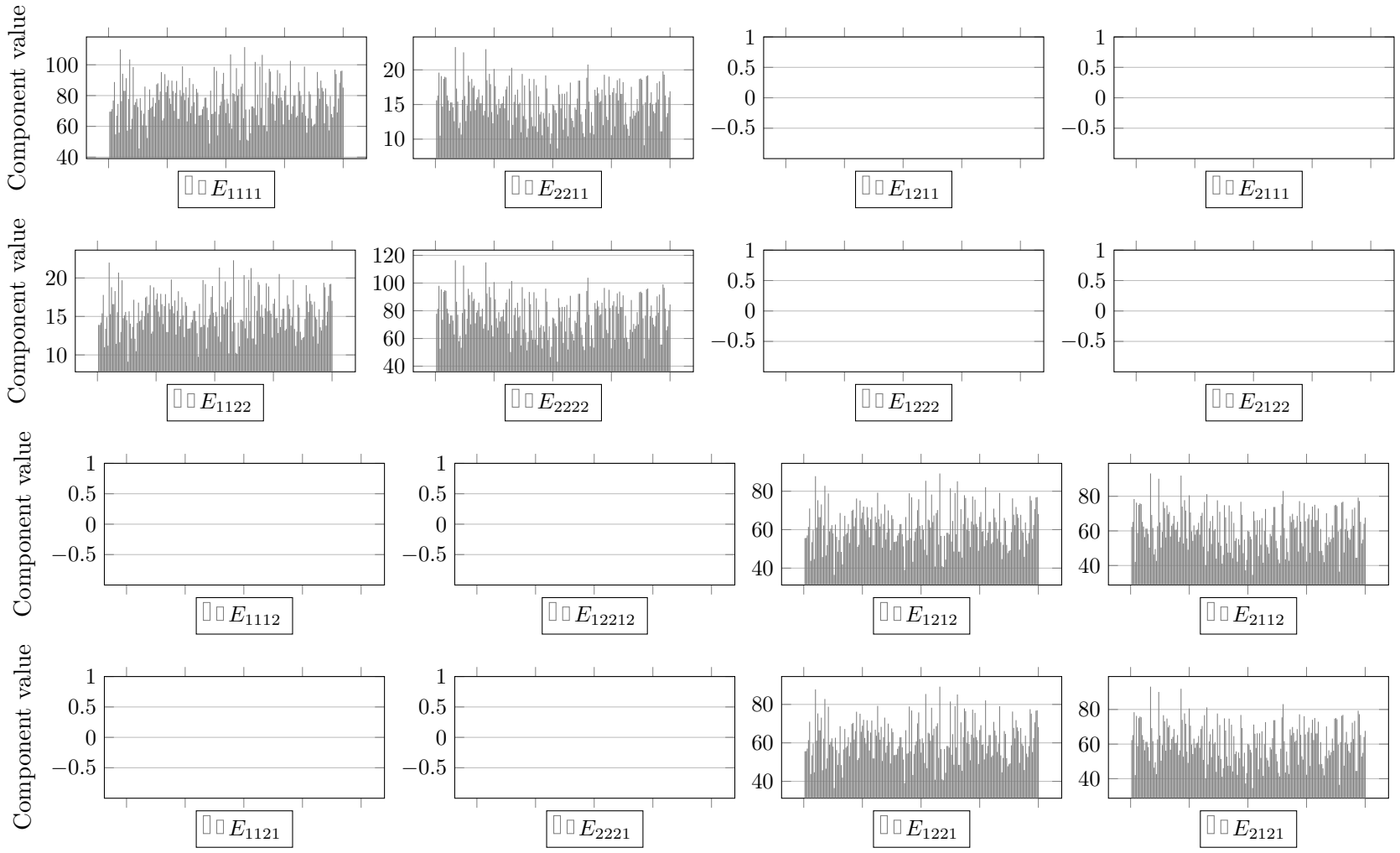

Figure 7.15: Distribution study: components of the constitutive operator E_{klij} (microcontinuum 100 mm)

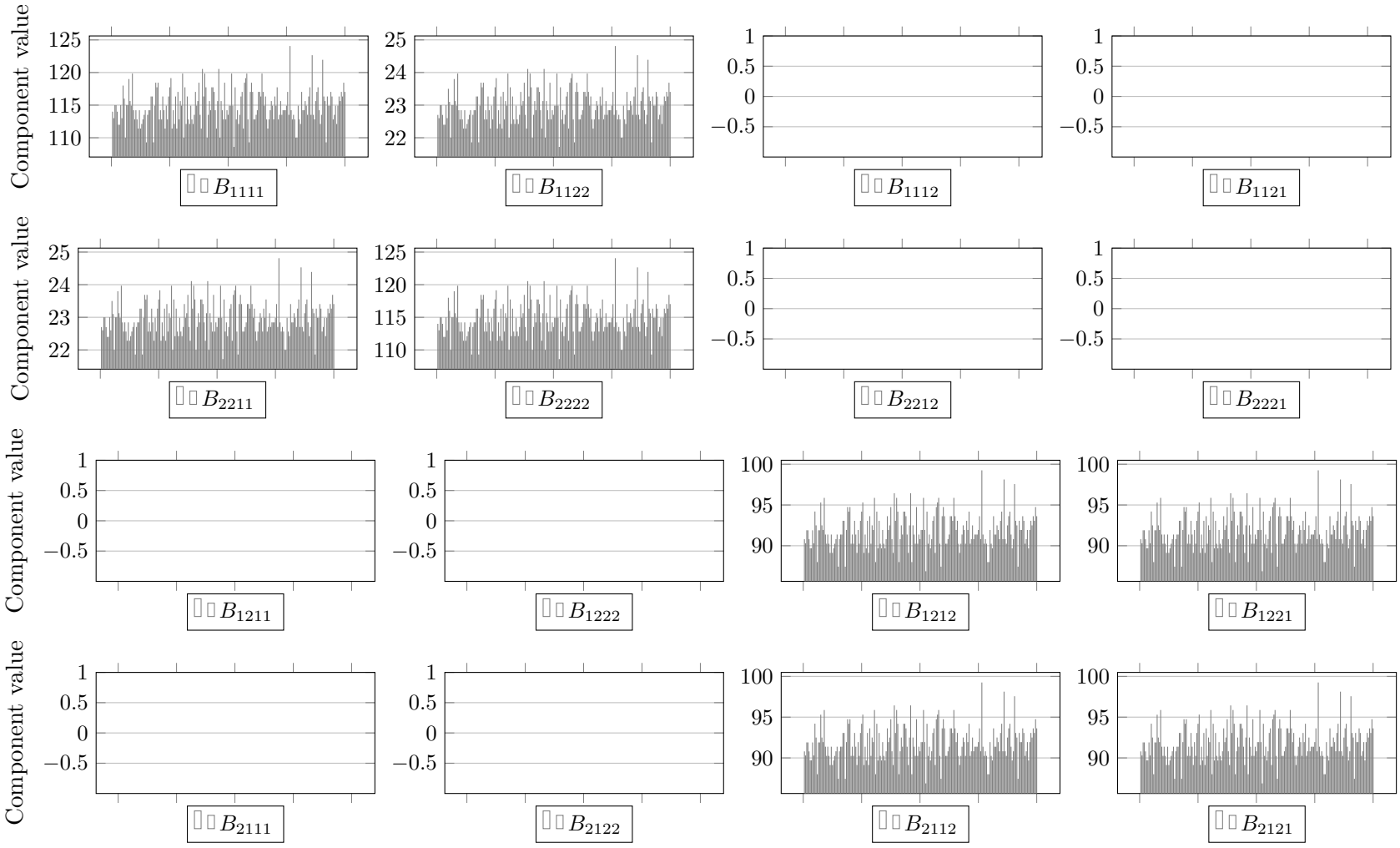

Figure 7.16: Distributionstudy: components of the constitutive operator B_{ijkl} (microcontinuum 100 mm)

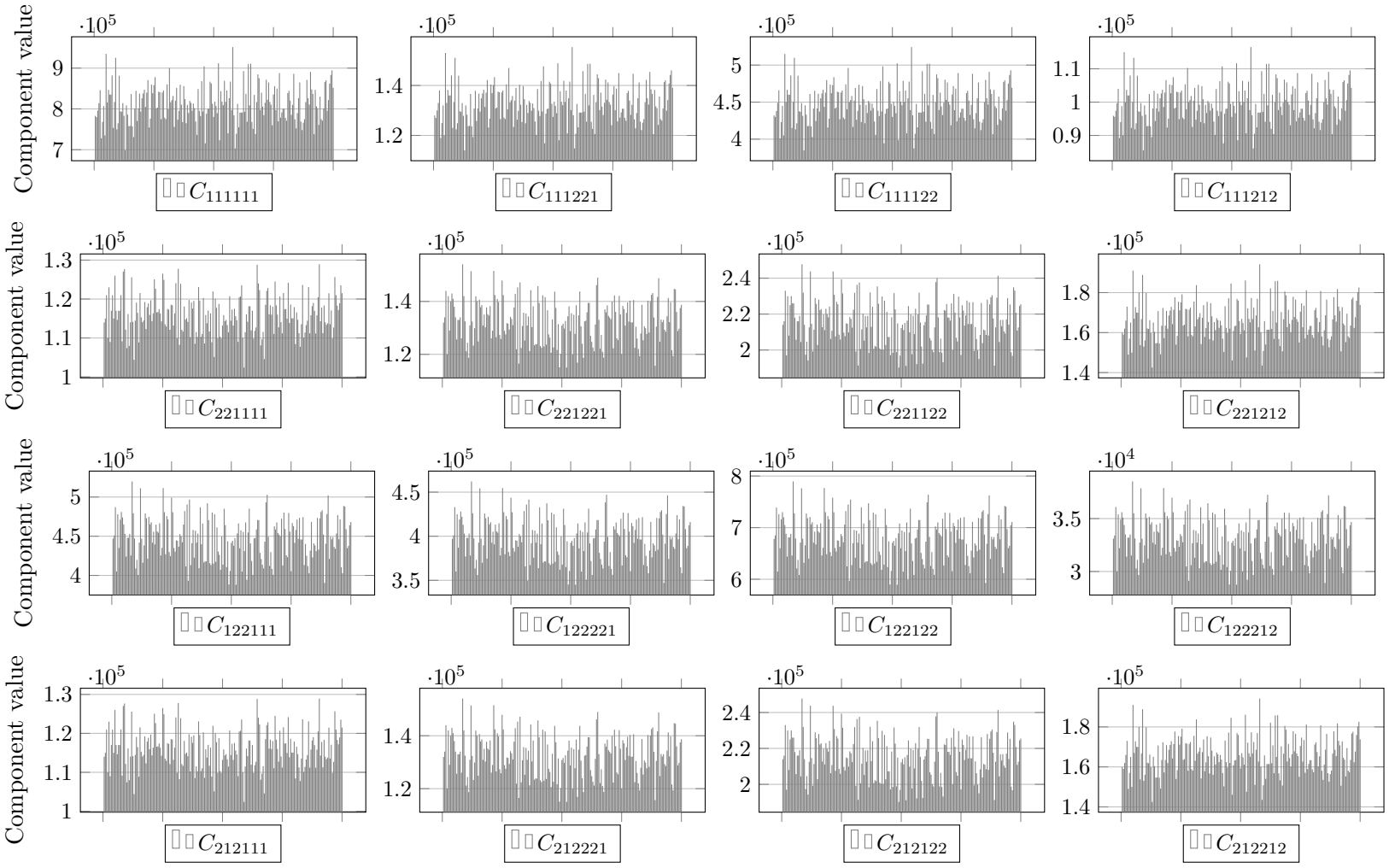

Figure 7.17: Distribution study: components of the constitutive operator C_{ijklmn} - rows and columns 9 to 12 of the constitutive matrix (microcontinuum 100 mm)

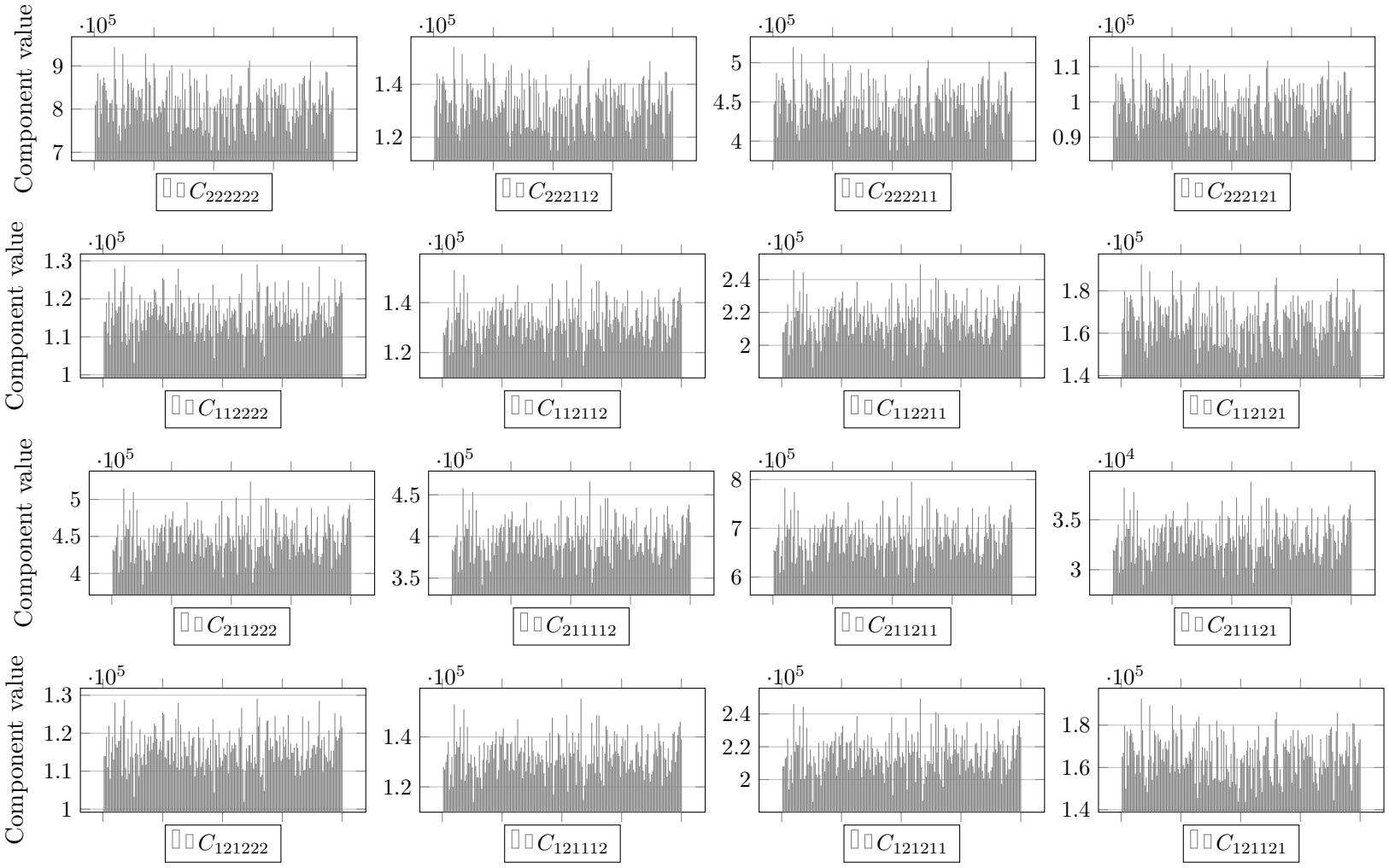

Figure 7.18: Distribution study: components of the constitutive operator C_{ijklmn} - rows and columns 13 to 16 of the constitutive matrix (microcontinuum 100 mm)

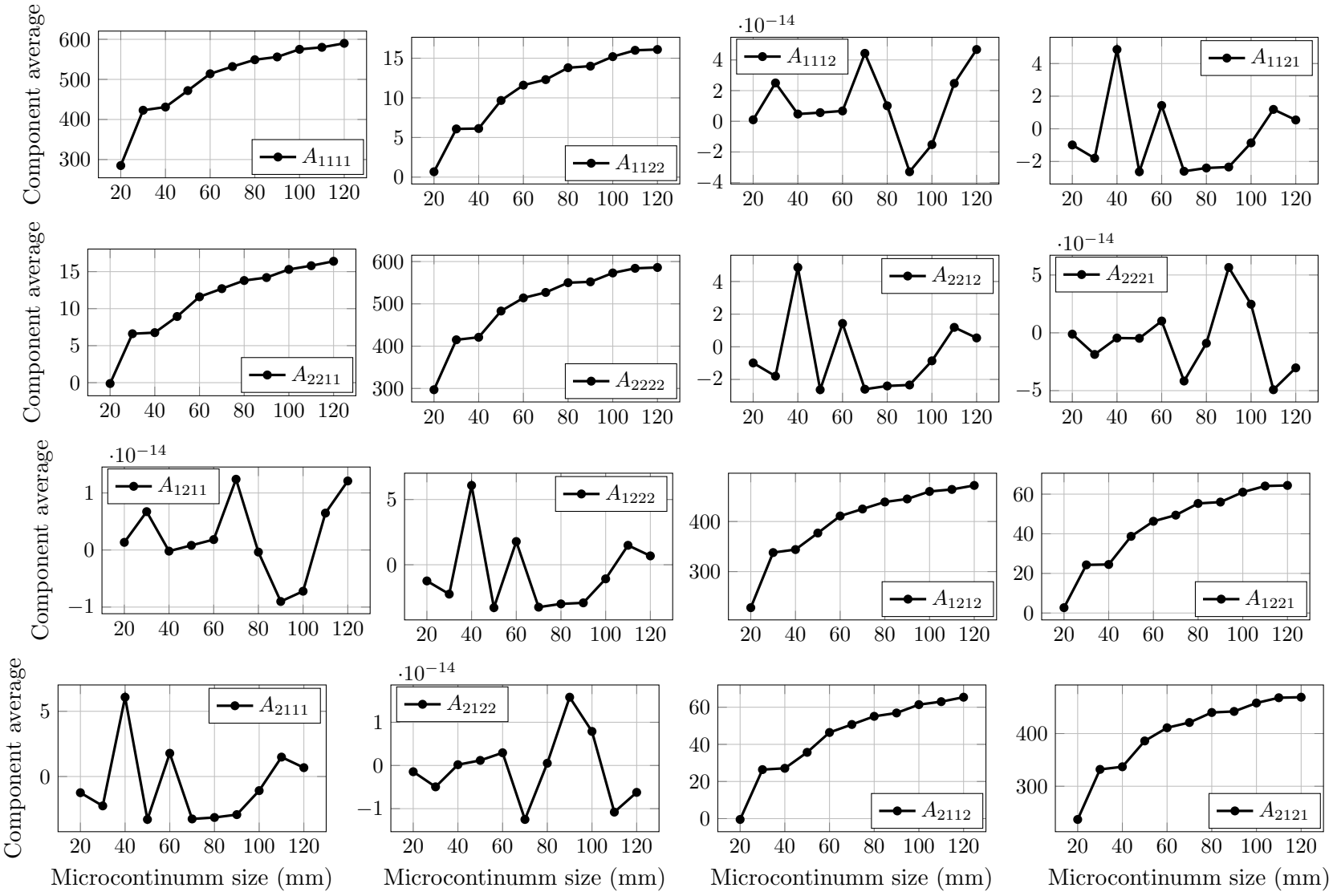

Figure 7.19: Distribution study: average of the components of the constitutive operator A_{ijkl} versus microcontinuum size

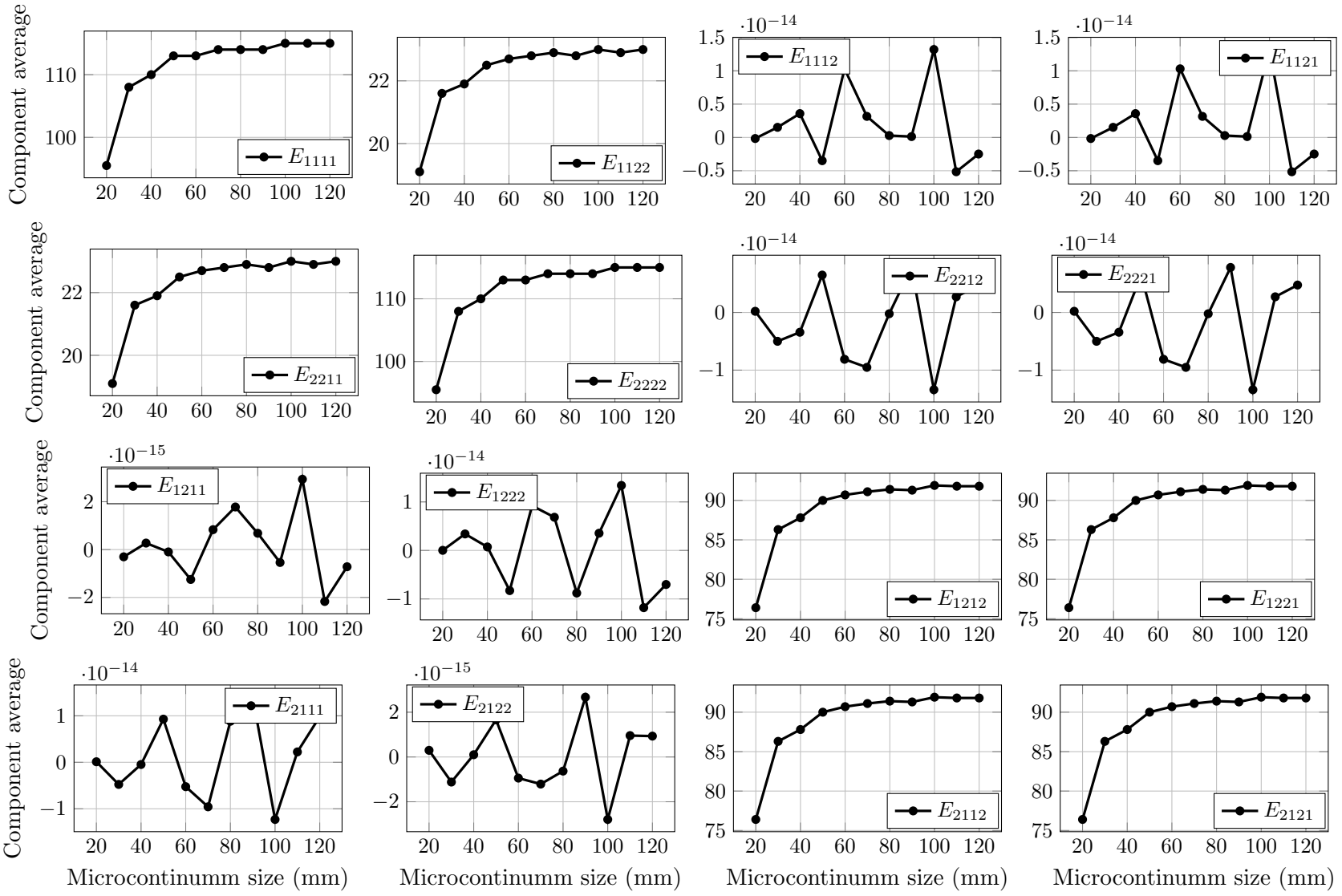

Figure 7.20: Distribution study: average of the components of the constitutive operator E_{ijkl} versus microcontinuum size

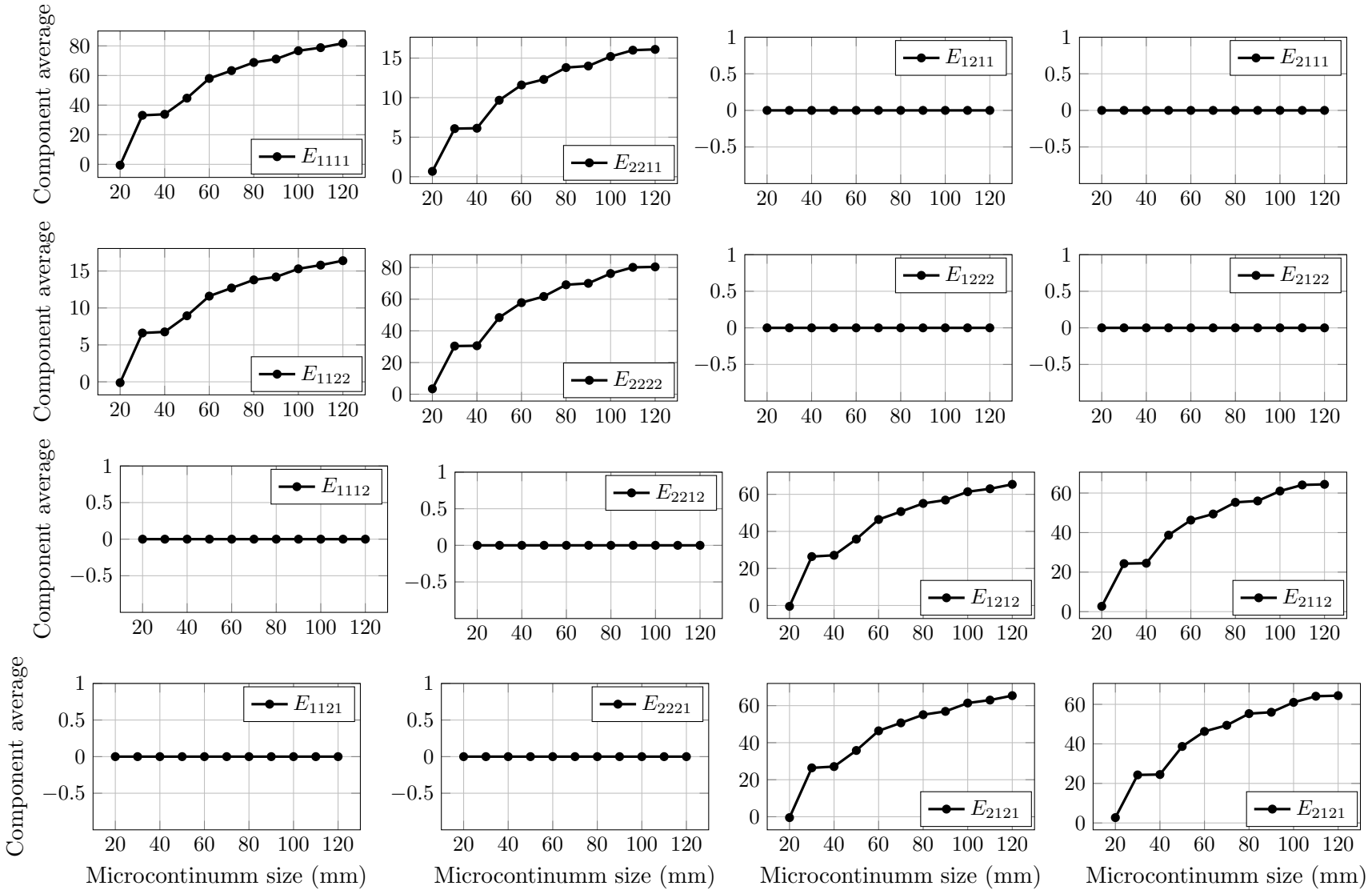

Figure 7.21: Distribution study: average of the components of the constitutive operator E_{klij} versus microcontinuum size

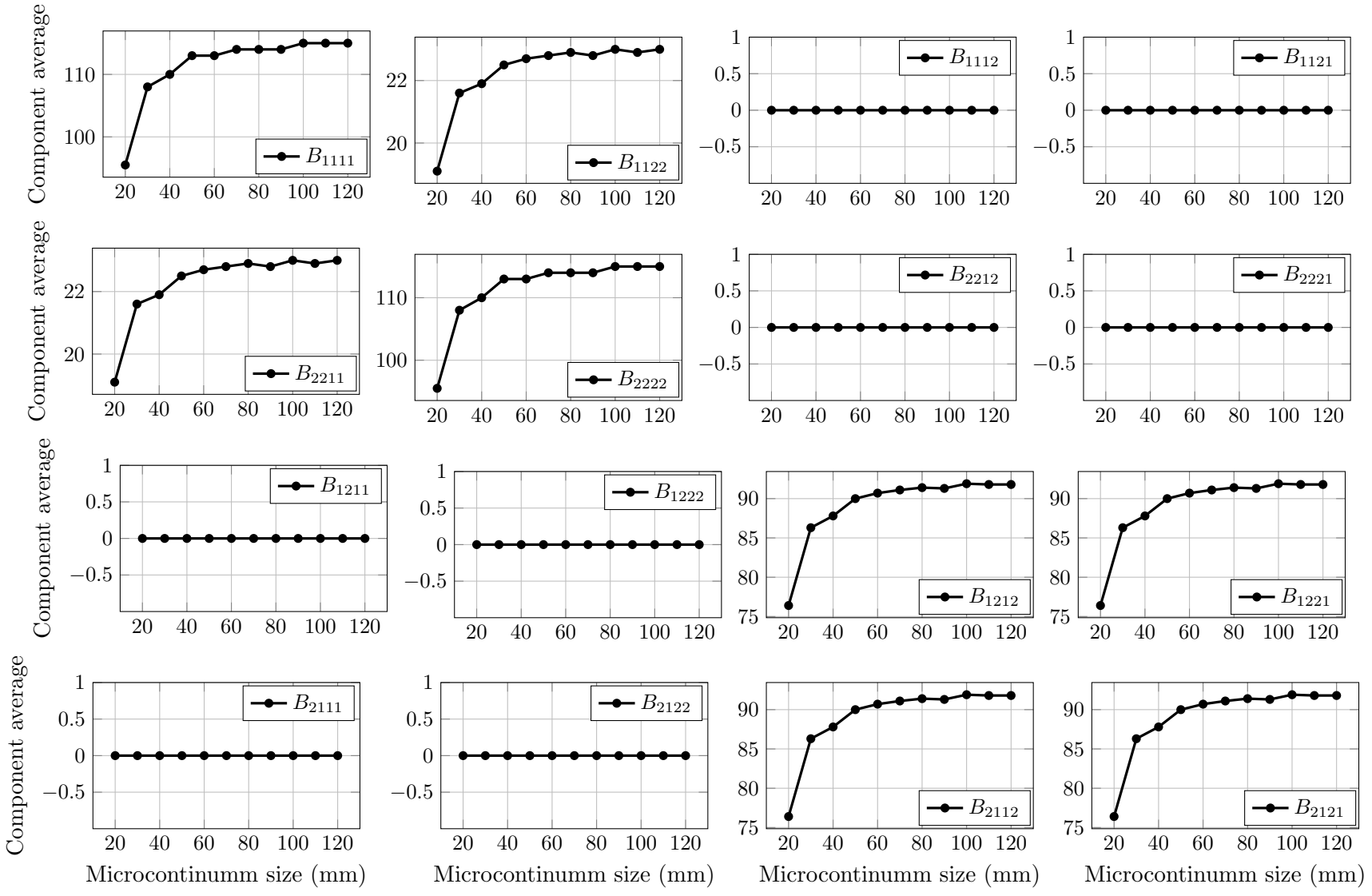

Figure 7.22: Distribution study: average of the components of the constitutive operator B_{ijkl} versus microcontinuum size

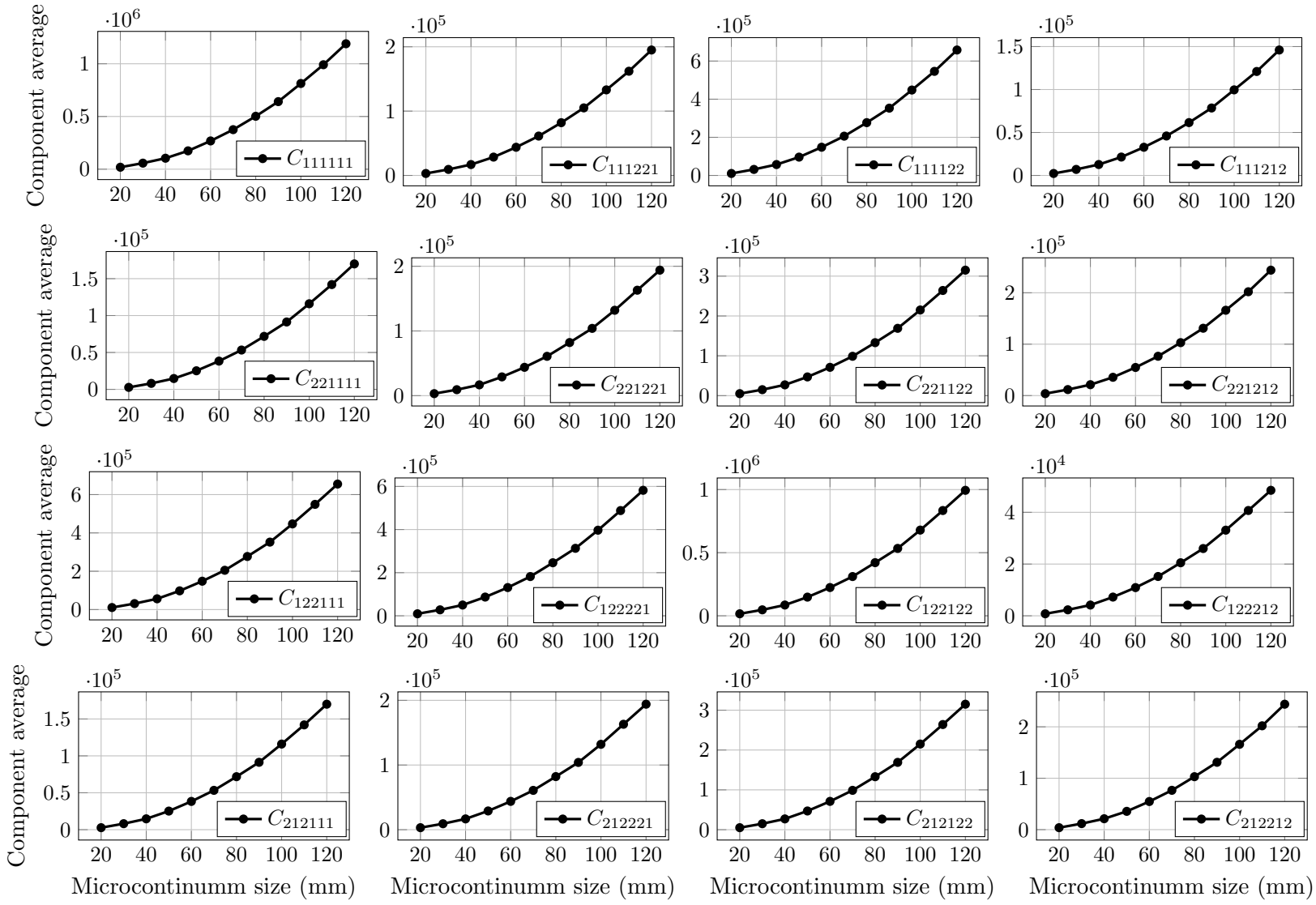

Figure 7.23: Distribution study: average of the components of the constitutive operator C_{ijklmn} versus microcontinuum size

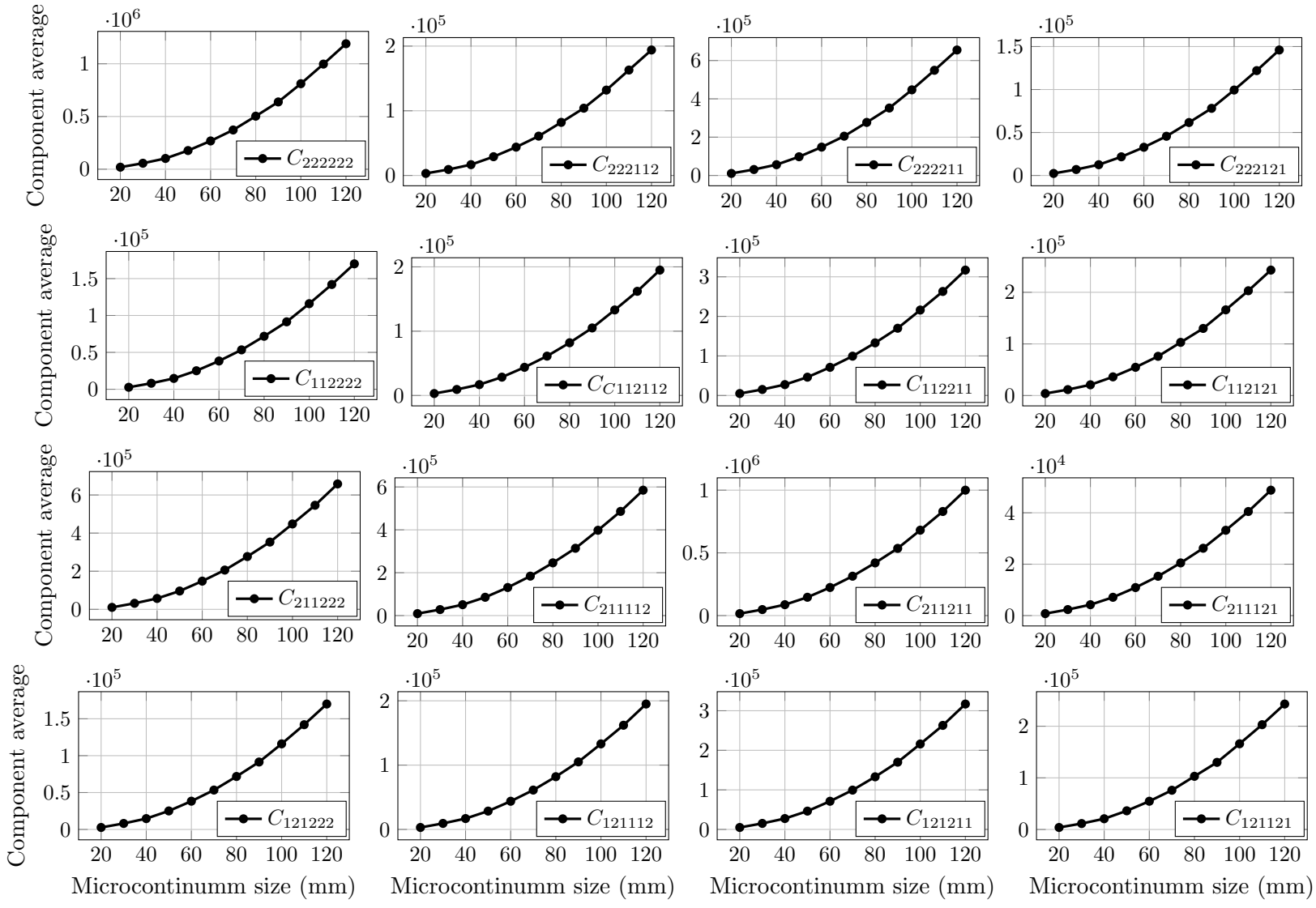

Figure 7.24: Distribution study: average of the components of the constitutive operator C_{ijklmn} versus microcontinuum size

7.2 Shear band with a heterogeneous media

For the study of the homogenization process applied to a non-linear analysis, the shear band problem presented in Section 6.3 with the geometry illustrated in Figure 6.18 and the meshes depicted in Figure 6.11 is modeled with a heterogeneous microstructure. The parameters for the construction of the microcontinuum are similar to the ones employed in the homogenization study presented in the previous section: maximum sieve size $d_{max} = 19$ mm; minimum sieve size $d_{min} = 9.5$ mm; continuous particle distribution; spherical particles; particle fraction PF = 30%; distribution factor DF = 0.2; $n = 0.5$ for the Fuller's distribution (Eq. 2.50); Young's modulus for the aggregates $E_{particle} = 9000$ MPa; Poisson's ratio for the aggregates $\nu_{particle} = 0.35$; Young's modulus for the matrix $E_{matrix} = 3000$ MPa; Poisson's ratio for the matrix $\nu_{matrix} = 0.35$.

The Mazars-Lemaitre micromorphic damage model (Eq. (3.47)) is employed with a linear damage law (Eq. (6.3)) and the following parameters: $K_0 = 0.0017$ and $K_f = 0.325$; $K_0 = 0.0016$ and $K_f = 0.325$ for the elements highlighted in Figure 6.11 in order to induce the localization phenomenon. The generalized displacement control method is used for the non-linear process with an initial load factor of 0.2 and tolerance for convergence of 10^{-4} in load.

To study the influence of the randomness of the take-and-place algorithm in the structural behavior, ten analysis were performed for each mesh in order to obtain an average result and, after, an analysis where the initial constitutive operator was obtained from the average of 200 different microstructures, following the idea of the previous study (Section 7.1.2). The results for the three meshes are presented in Figures 7.25, 7.26, and 7.27.

The behavior obtained for the three meshes is similar to the one observed for a homogeneous microcontinuum proving the proper functioning of the homogenization strategy proposed. The equilibrium path for the different tests present small variations due to the random generation of particles. The use of an average of different non-linear analysis is a possible solution for dealing with this variation, however time consuming as each non-linear analysis has high processing times specially for more refined meshes. An option that proved to be similar is the use of an average constitutive tensor constructed by a significant number of distributions, that, for this study, proved to be more computationally efficient[4].

[4]In this study, obtaining the average constitutive operator for 200 distributions required around 10% of the processing time of a complete non-linear analysis for the most refined mesh.

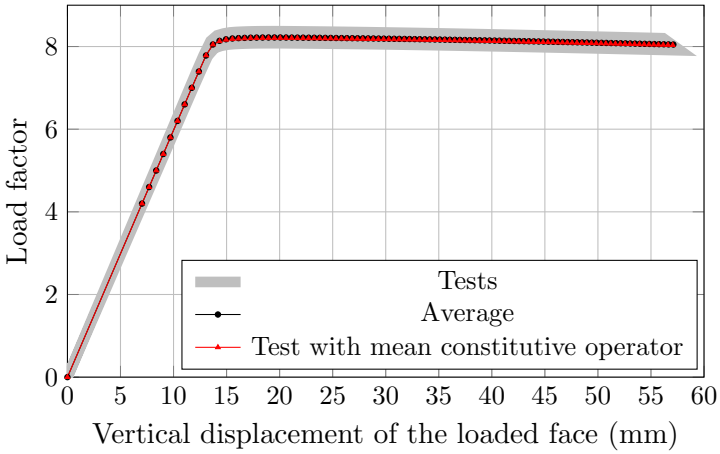

Figure 7.25: Heterogeneous shear band: load factor versus vertical displacement - mesh 1

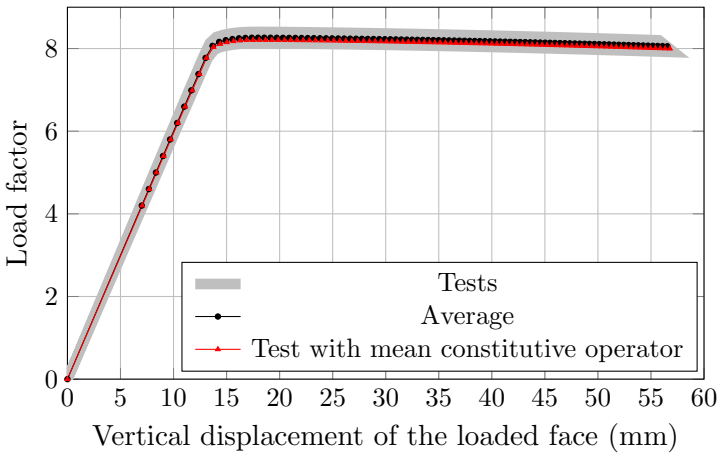

Figure 7.26: Heterogeneous shear band: load factor versus vertical displacement - mesh 2

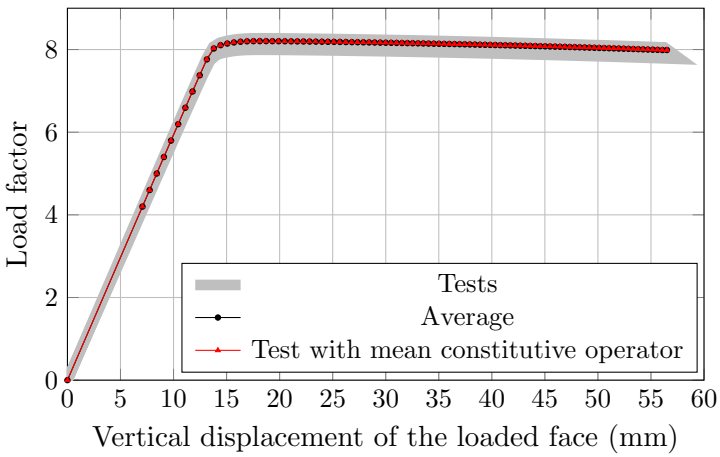

Figure 7.27: Heterogeneous shear band: load factor versus vertical displacement - mesh 3

Chapter 8

Conclusions

The main aim of the present work was to provide a basis for the modeling of heterogeneous quasi-brittle media by means of continuum damage models, more specifically scalar-isotropic models, with use of the micromorphic continuum theory in view of its ability to incorporate the microstructural behavior in the continuum formulation and, hence, address the strain localization phenomenon.

In order to incorporate the heterogeneity at the micro scale, the take-and-place algorithm for the particles generation associated to the homogenization technique proposed by Silva (2019) was used, allowing non-linear analysis of heterogeneous media with the micromorphic theory using only material parameters of the classical continuum.

The computational implementation was held in the INSANE system within a unified constitutive framework first proposed for classical media. To solve the compatibility problem, a compact tensorial formulation was proposed allowing the inclusion of damage models for the micromorphic theory with minimum intervention in the code.

The numerical simulations here presented attested the micromorphic continuum capacity to regularize problems where the numerical localization phenomenon occurs. In these analysis the homogenization strategy was employed for homogeneous and heterogeneous material particles associated to the damage models here proposed for the micromorphic continuum, verifying their proper functioning.

This work presents multiple possibilities for the study of the influence of the heterogeneous microstructure in the structural behavior with the use of the micromorphic theory.

8.1 Future research topics

Here some topics regarding the possible future research topics are presented, what could give continuity to this work, as some points were not well studied due to the time limit of this study:

1. Study the influence of the microcontinuum size in the formulation of the micromorphic theory and its constitutive tensors;
2. Adequate the microstructure generator to allow the inclusion of voids in the microcontinuum;
3. Perform mesh and distribution studies for other aggregate distributions;
4. Model other non-linear problems that present heterogeneous media applying the concepts here proposed.

Bibliography

ABNT NBR 7211, 2005, *Agregados para concreto - especificação*, Associação Brasileira de Normas Técnicas.

Armero, F. and Oller, S., 2000*a*. 'A general framework for continuum damage models. I. infinitesimal plastic damage models in stress space'. *International Journal of Solids and Structures*, vol. 37(48-50), pp. 7409–7436.

Armero, F. and Oller, S., 2000*b*. 'A general framework for continuum damage models. II. integration algorithms, with applications to numerical simulation of porous metals'. *International Journal of Solids and Structures*, vol. 37(48-50), pp. 7437–7464.

Bažant, Z. P., Tabbara, M. R., Kazemi, M. T. and Pijaudier-Cabot, G., 1990. 'Random particle model for fracture of aggregate or fiber composites'. *Journal of Engineering Mechanics*, vol. 116(8), pp. 1686–1705.

Carol, I., Rizzi, E. and Willam, K., 1994. 'A unified theory of elastic degradation and damage based on a loading surface'. *International Journal of Solids and Structures*, vol. 31(20), pp. 2835–2865.

Carol, I., Rizzi, E. and Willam, K., 2001*a*. 'On the formulation of anisotropic elastic degradation. I. theory based on a pseudo-logarithmic damage tensor rate'. *International Journal of Solids and Structures*, vol. 38(4), pp. 491–518.

Carol, I., Rizzi, E. and Willam, K., 2001*b*. 'On the formulation of anisotropic elastic degradation. II. generalized pseudo-rankine model for tensile damage'. *International Journal of Solids and Structures*, vol. 38(4), pp. 519–546.

Cauchy, A. L., 1828. 'Sur les équations qui expriment l'équilibre ou les lois du mouvement intérieur d'un corps solide élastique ou non élastique'. *Exercices de mathématiques*, vol. 2, pp. 160–187.

Cavalcante, M. A. A., Marques, S. P. C. and Pindera, M.-J., 2006*a*. 'Parametric Formulation of the Finite-Volume Theory for Functionally Graded Materials - Part I: Analysis'. *Journal of Applied Mechanics*, vol. 74(5), pp. 935–945.

Cavalcante, M. A. A., Marques, S. P. C. and Pindera, M.-J., 2006*b*. 'Parametric Formulation of the Finite-Volume Theory for Functionally Graded Materials - Part II: Numerical Results'. *Journal of Applied Mechanics*, vol. 74(5), pp. 946–957.

Christensen, R. M., 1990. 'A critical evaluation for a class of micro-mechanics models'. *Journal of the Mechanics and Physics of Solids*, vol. 38(3), pp. 379–404.

Cosserat, E. and Cosserat, F., 1909. *Théorie des corps déformables*. Librairie Scientifique A. Hermann et Fils, Paris.

Şuhubi, E. S. and Eringen, A. C., 1964. 'Nonlinear theory of simple micro-elastic solids – ii'. *International Journal of Engineering Science*, vol. 2(4), pp. 389–404.

de Borst, R., 1987. 'Smeared cracking, plasticity, creep, and thermal loading–a unified approach'. *Computer Methods in Applied Mechanics and Engineering*, vol. 62, pp. 89–110.

de Borst, R., (1990), Simulation of localisation using Cosserat theory, *in* N. Bicanic and H. A. Mang, eds, 'Computer Aided Analysis and Design of Concrete Structures', Proceedings of the 2nd International Conference, Pineridge Press, Swansea, pp. 931–944.

de Borst, R., 1991. 'Simulation of strain localization: A reappraisal of the Cosserat continuum'. *Engineering Computations*, vol. 8(4), pp. 317–332.

de Borst, R., 1993. 'A generalisation of J_2-flow theory for polar continua'. *Computer Methods in Applied Mechanics and Engineering*, vol. 103, pp. 347–362.

de Borst, R. and Gutiérrez, M. A., 1999. 'A unified framework for concrete damage and fracture models including size effects'. *International Journal of Fracture*, vol. 95, pp. 261–277.

de Borst, R. and Sluys, L. J., 1991. 'Localisation in a Cosserat continuum under static and dynamic loading conditions'. *Computer Methods in Applied Mechanics and Engineering*, vol. 90, pp. 805–827.

Eremeyev, V., 2005. 'Acceleration waves in micropolar elastic media'. *Doklady Physics*, vol. 50(4), pp. 204–206.

Eringen, A. C., 1966. 'Mechanics of micromorphic materials'. *Applied Mechanics*, vol. 8, pp. Pr4–39, Pr4–48.

Eringen, A. C., 1980. *Mechanics of Continua*. 2 edn, Robert E. Krieger Publishing Company, Huntington, New York.

Eringen, A. C., 1999. *Microcontinuum Field Theories: I. Foundations and solids*. Springer, New York.

Eringen, A. C. and Şuhubi, E. S., 1964. 'Nonlinear theory of simple micro-elastic solids – i'. *International Journal of Engineering Science*, vol. 2(2), pp. 189–203.

Forest, S., 1998. 'Mechanics of generalized continua: construction by homogenization'. *Journal de Physique IV*, vol. 8, pp. Pr4–39, Pr4–48.

Forest, S. and Sievert, R., 2006. 'Nonlinear microstrain theories'. *International Journal of Solids and Structures*, vol. 43(24), pp. 7224–7245. Size-dependent Mechanics of Materials.

Fuina, J. S., 2009. Formulações de Modelos Constitutivos de Microplanos para Contínuos Generalizados. Tese de Doutorado, Universidade Federal de Minas Gerais, Belo Horizonte, MG, Brasil.

Germain, P., 1973*a*. 'La méthode des puissances virtuelles en mécanique des millieux continus premiere partie: théorie du second gradient'. *Journal de Mécanique*, vol. 12(2), pp. 235–274.

Germain, P., 1973*b*. 'The method of virtual power in continuum mechanics. part 2: Microstructure'. *SIAM Journal of Applied Mathematics*, vol. 25(3), pp. 556–575.

Gori, L., 2018. Failure analysis of quasi-brittle media using the micropolar continuum theory, elastic-degrading constitutive models, and smoothed point interpolation methods. Tese de Doutorado, Universidade Federal de Minas Gerais, Belo Horizonte, MG, Brasil.

Gori, L., Penna, S. S. and Pitangueira, R. L., 2017*a*. 'A computational framework for constitutive modelling'. *Computer and Structures*, vol. 187, pp. 1–23.

Gori, L., Penna, S. S. and Pitangueira, R. L., 2017*b*. 'Discontinuous failure in micropolar elastic-degrading models'. *International Journal of Damage Mechanics*, vol. 27(10), pp. 1482–1515.

Gori, L., Penna, S. S. and Pitangueira, R. L., 2017*c*. 'An enhanced tensorial formulation for elastic degradation in micropolar continua'. *Applied Mathematical Modelling*, vol. 41, pp. 299–315.

Hashin, Z., 1983. 'Analysis of composite materials - a survey'. *Journal of Applied Mechanics*, vol. 50(3), pp. 481–505.

Hill, R., 1963. 'Elastics properties of reinforced solids: Some theoretical principles'. *J. Mech. Phys. Solids*, vol. 11, pp. 357–372.

Hill, R., 1967. 'The essential structure of constitutive laws for metal composites and polycrystals'. *J. Mech. Phys. Solids*, vol. 15, pp. 79–95.

Hirschberger, C. B., 2008. A Treatise on Micromorphic Continua. Theory, Homogenization, Computation. Tese de Doutorado, Technische Universität Kaiserslautern, Kaiserslautern, Germany.

Hult, J., 1987, *lntroduction and General Overview*, Springer-Verlag Wien, New York, pp. 1–36.

Hütter, G., 2017. 'Homogenization of a Cauchy continuum towards a micromorphic continuum'. *Journal of the Mechanics and Physics of Solids*, vol. 99, pp. 394–408.

Hütter, G., 2019. A theory for the homogenisation towards micromorphic media and its application to size effects and damage. Tese de Doutorado, Technische Universität Bergakademie Freiberg.

Ju, J., 1989. 'On energy-based coupled elastoplastic damage theories: Constitutive modeling and computational aspects'. *International Journal of Solids and Structures*, vol. 25(7), pp. 803–833.

Kachanov, L., 1958. 'On time to rupture in creep conditions'. *Izvestia Akademii Nauk SSSR, Otdelenie Tekhnicheskikh Nauk*, (8), pp. 26–31. in russian.

Krajcinovic, D., 1996. *Damage Mechanics*. Vol. 41 of *North-Holland Series in Applied Mathematics and Mechanics*, Elsevier Science, Amsterdam, The Netherlands.

Krajcinovic, D. and Lemaitre, J., eds, 1987. *Continuum damage mechanics - Theory and applications*. Number 295 *in* 'CISM courses and lectures - International centre for mechanical sciences', SPRINGER-VERLAG WIEN GMBH.

Krajcinovic, D. and Sumarac, D., 1987, *Micromechanics of the Damage Processes*, Springer-Verlag Wien, New York, pp. 135–194.

Kröner, E., 1977. 'Bounds for effective elastic moduli of disordered materials'. *Journal of the Mechanics and Physics of Solids*, vol. 25(2), pp. 137–155.

Lages, E. N., 1997. Modelagem de Localização de Deformações com Teorias de Contínuo Generalizado. Tese de Doutorado, Pontifícia Universidade Católica do Rio de Janeiro, Rio de Janeiro, Brasil.

Lages, E. N. and Cavalcanti Marques, S. P., 2022. 'Prediction of effective thermal conductivity of multiphase composites with periodic microstructures using an expanded micromechanical model'. *International Journal of Thermal Sciences*, vol. 171, pp. 107226.

Lemaitre, J., 1987, *Formulation and Identification of Damage Kinetic Constitutive Equations*, Springer-Verlag Wien, New York, pp. 37–90.

Lemaitre, J. and Desmorat, R., 2005. *Engineering Damage Mechanics: Ductile, Creep, Fatigue and Brittle Failures*. Springer.

Mal, A. K. and Singh, S. J., 1991. *Deformation of elastic solids*. Prentice Hall, Inc., Englewood Cliffs, NJ, USA.

Marigo, J., 1985. 'Modelling of brittle and fatigue damage for elastic material by growth of microvoids'. *Engineering Fracture Mechanics*, vol. 21(4), pp. 861 – 874.

Maugin, G. A., 2014, *Continuum Mechanics Through the Eighteenth and Nineteenth Centuries*, Springer International Publishing, Switzerland.

Maugin, G. A., 2017, *What Is Classical Continuum Mechanics?*, Springer Nature Singapore Pte Ltd.

Mazars, J. and Lemaitre, J., 1985, *Application of Continuous Damage Mechanics to Strain and Fracture Behavior of Concrete*, Springer Netherlands, Dordrecht, pp. 507–520.

Mindlin, R., 1965. 'Second gradient of strain and surface-tension in linear elasticity'. *International Journal of Solids and Structures*, vol. 1(4), pp. 417 – 438.

Mindlin, R. D., 1964. 'Micro-structure in linear elasticity'. *Archive for Rational Mechanics and Analysis*, vol. 16, pp. 51–78. Communicated by R. A. Toupin.

Monteiro, H. A. S., Pitangueira, R. L. S. and Barros, F. B., (2017), Multiscale strategy for the analysis of softening media using the generalized finite element method, *in* L. M. R.H. Lopez and P. Farias, eds, 'Proceedings of the XXXVIII Iberian Latin-American Congress on Computational Methods in Engineering', Florianópolis, SC, Brazil.

Mühlhaus, H.-B. and Vardoulakis, I., 1987. 'The thickness of shear bands in granular materials'. *Géotechnique*, vol. 37(3), pp. 271–283.

Nemat-Nasser, S. and Hori, M., 1993, *Micromechanics: Overall Properties of Heterogeneous Materials*, Elsevier Science Publishers.

Penna, S. S., 2011. Formulação Multipotencial para Modelos de Degradação Elástica - Unificação Teórica, Proposta de Novo Modelo, Implementação Computacional e Modelagem de Estruturas de Concreto. Tese de Doutorado, Universidade Federal de Minas Gerais, Belo Horizonte, MG, Brasil.

Ristinmaa, M. and Vecchi, M., 1996. 'Use of couple-stress theory in elasto-plasticity'. *Computer Methods in Applied Mechanics and Engineering*, vol. 136, pp. 205–224.

Roelfstra, P., Sadouki, H. and Wittmann, F., 1985. 'Le béton numérique'. *Materials and Structures*, vol. 18, pp. 327–335.

Schlangen, E. and van Mier, J., 1992. 'Simple lattice model for numerical simulation of fracture of concrete materials and structures'. *Materials and Structures*, vol. 25, pp. 534–542.

Schorn, H. and Rode, U., 1991. 'Numerical simulation of crack propagation from microcracking to fracture'. *Cement and Concrete Composites*, vol. 13(2), pp. 87–94.

Shah, S. and Slate, F. O., (1965), Internal microcracking, mortar-aggregate bond and the stress-strain curve of concrete, *in* A. E. Brooks and K. Newman, eds, 'The Structure of Concrete', Proceedings of an International Conference, London, pp. 82–92.

Silva, L. L., 2019. Estratégia Multiescala para Descrição Micromórfica do Contínuo a partir do Contínuo Clássico. Tese de Doutorado, Universidade Federal de Minas Gerais, Belo Horizonte, MG, Brasil.

Simo, J. and Ju, J., 1987. 'Strain- and stress-based continuum damage models–i. formulation'. *International Journal of Solids and Structures*, vol. 23(7), pp. 821 – 840.

Sluys, L. J., 1992. Wave propagation, localisation and dispersion in softening solids. Dissertação de Mestrado, Delft University of Technology, Delft.

Steinmann, P., 1994. 'An improved FE expansion for micropolar localization analysis'. *Communications in Numerical Methods in Engineering*, vol. 10, pp. 1005–1012.

Steinmann, P., 1995. 'Theory and numerics of ductile micropolar elastoplastic damage'. *International Journal for Numerical Methods in Engineering*, vol. 38, pp. 583–606.

Van Mier, J., 1995. 'Fracture mechanics of concrete: Will applications start to emerge?'. *HERON*, vol. 40(2), pp. 147–162.

Voigt, W., 1887. 'Theoretische studien über die elasticitätsverhältnisse der krystalle'. *Abhandlungen der Königlichen Gesellschaft der Wissenschaften*, vol. 34, pp. 3–52.

Wang, Z., Kwan, A. and Chan, H., 1999. 'Mesoscopic study of concrete i: generation of random aggregate structure and finite element mesh'. *Computers & Structures*, vol. 70(5), pp. 533–544.

Willis, J. R., 1981. 'Variational and related methods for the overall properties of composites'. *Advances in Applied Mechanics*, vol. 21, pp. 1–78.

Wittmann, F., Roelfstra, P. and Sadouki, H., 1985. 'Simulation and analysis of composite structures'. *Materials Science and Engineering*, vol. 68(2), pp. 239–248.

Wong, H. S., Zobel, M., Buenfeld, N. R. and Zimmerman, R. W., 2009. 'Influence of the interfacial transition zone and microcracking on the diffusivity, permeability and sorptivity of cement-based materials after drying'. *Magazine of Concrete Research*, vol. 61(8), pp. 571–589.

Wriggers, P. and Moftah, S., 2006. 'Mesoscale models for concrete: Homogenisation and damage behaviour'. *Finite Elements in Analysis and Design*, vol. 42(7), pp. 623–636. The Seventeenth Annual Robert J. Melosh Competition.

Appendix A

Microcontinuum size and distribution study: complete results

Chapter 7 discusses some of the results obtained for the study in which the microcontinuum size and the randomness of the particle distribution were considered to verify their influence in the micromorphic constitutive tensor obtained by the homogenization strategy exposed in Chapter 4. As presented in Section 7.1.2, square RVE's with sizes varying from 20 mm up to 120 mm were studied adopting quadrilateral elements with dimension 5 mm for the microstructure discretization. To evaluate the impact of the random generation of aggregates, 200 particle distributions were considered for each microcontinuum size and the respective components of the initial constitutive tensor computed. Furthermore, besides evaluating the average for the studied cases, the standard deviation was also calculated.

In this appendix, the results for the remaining simulations are presented, as only the variation obtained for a microcontinuum of size 100 mm was illustrated in Section 7.1.2. The standard deviation computed for each component is also here presented (for the average values see Figures 7.19 through 7.24).

The observed behavior for the components values of each distribution is similar to the one previously discussed for a microcontinuum of size 100 mm. Observing the results obtained for the standard deviation, it may be perceived that, with the increase in the size of the microcontinuum, there is a reduction in the standard deviation except for the tensor C_{ijklm} that experiences an increase in the values. The same conclusion as presented in Section 7.1.2 can be drawn, but further studies should be conducted to verify the hypotheses.

A.1 Microcontinuum of size 20 mm

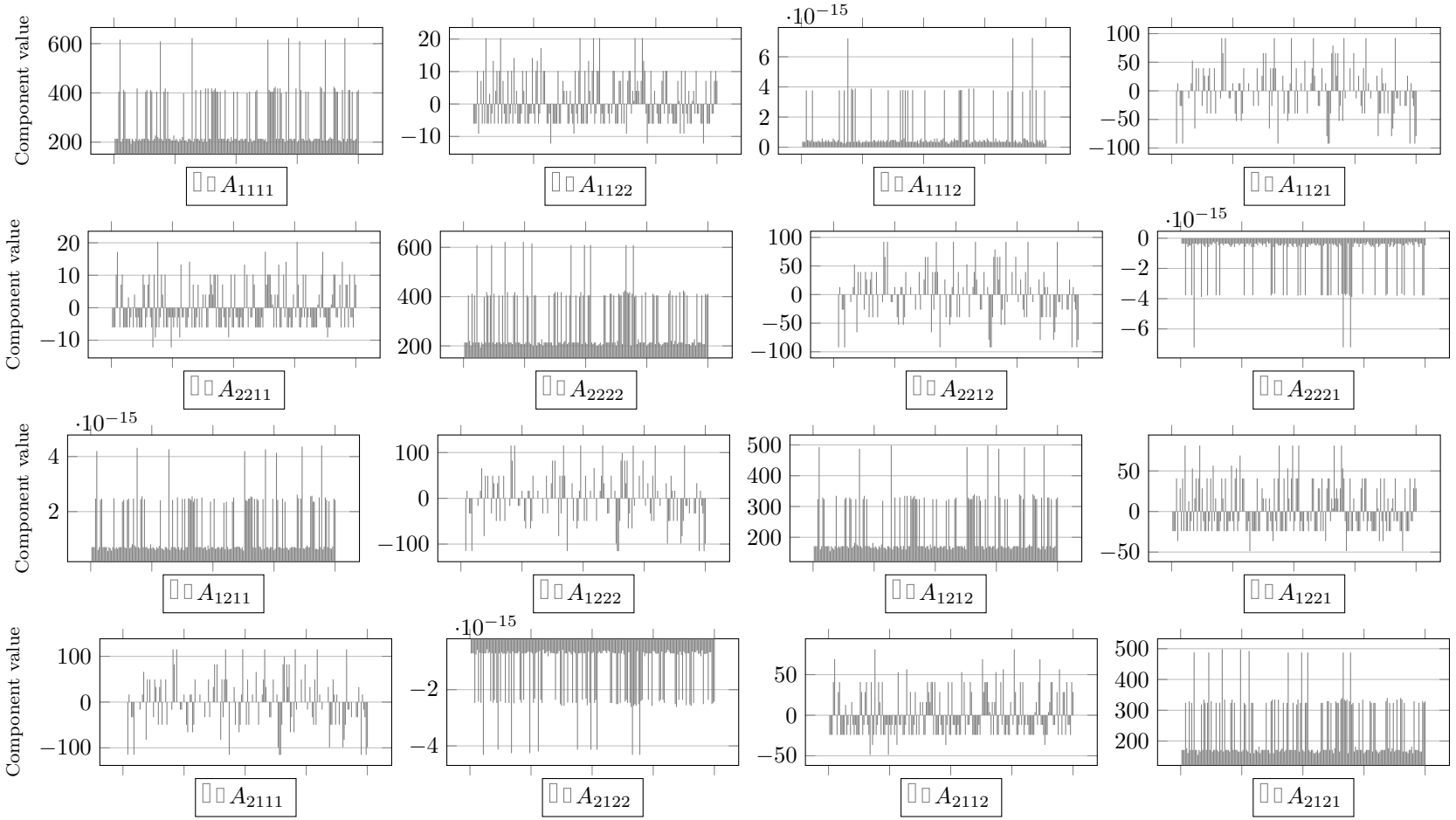

Figure A.1: Distribution study: components of the constitutive operator A_{ijkl} (microcontinuum 20 mm)

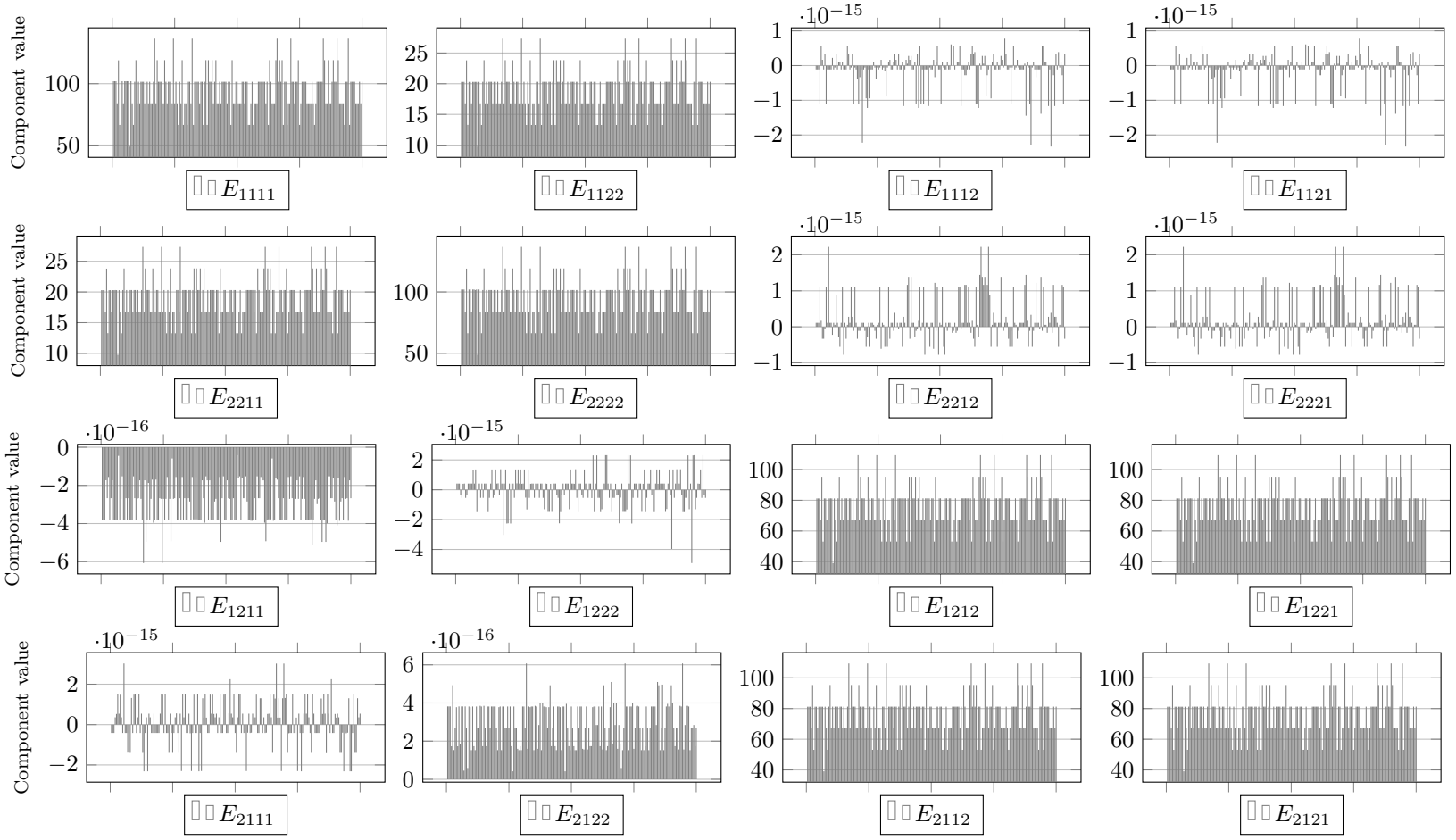

Figure A.2: Distribution study: components of the constitutive operator E_{ijkl} (microcontinuum 20 mm)

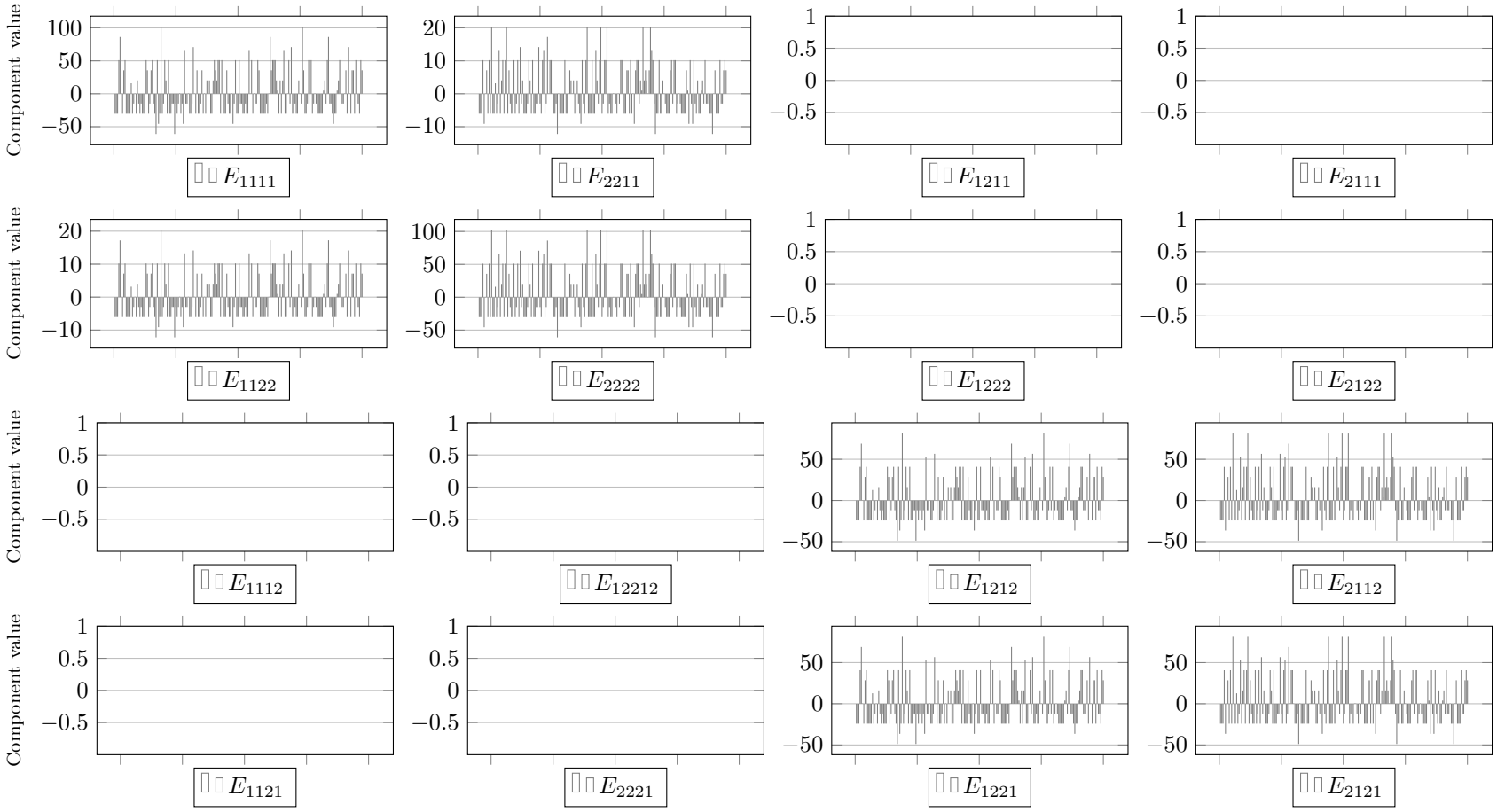

Figure A.3: Distribution study: components of the constitutive operator E_{klij} (microcontinuum 20 mm)

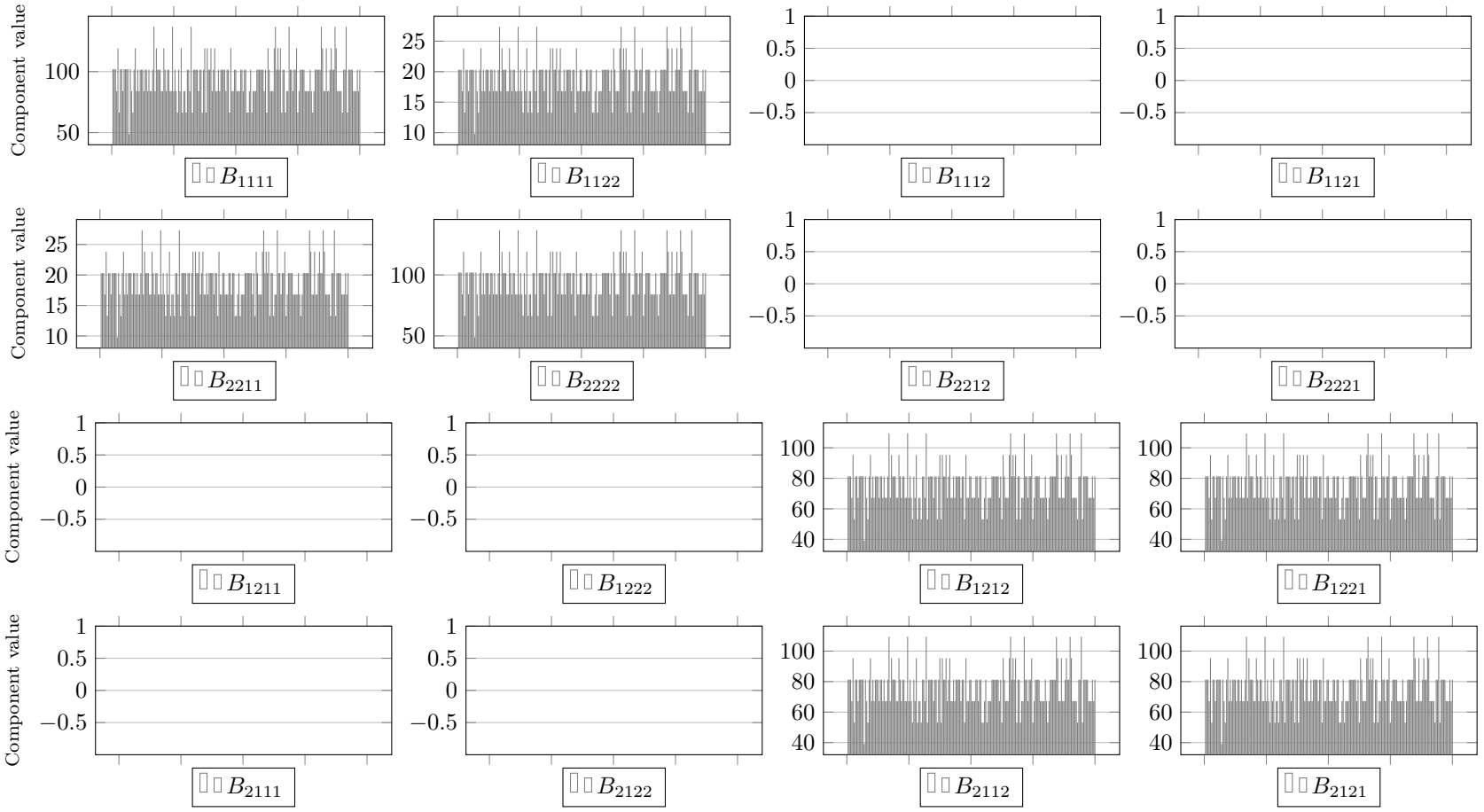

Figure A.4: Distribution study: components of the constitutive operator B_{ijkl} (microcontinuum 20 mm)

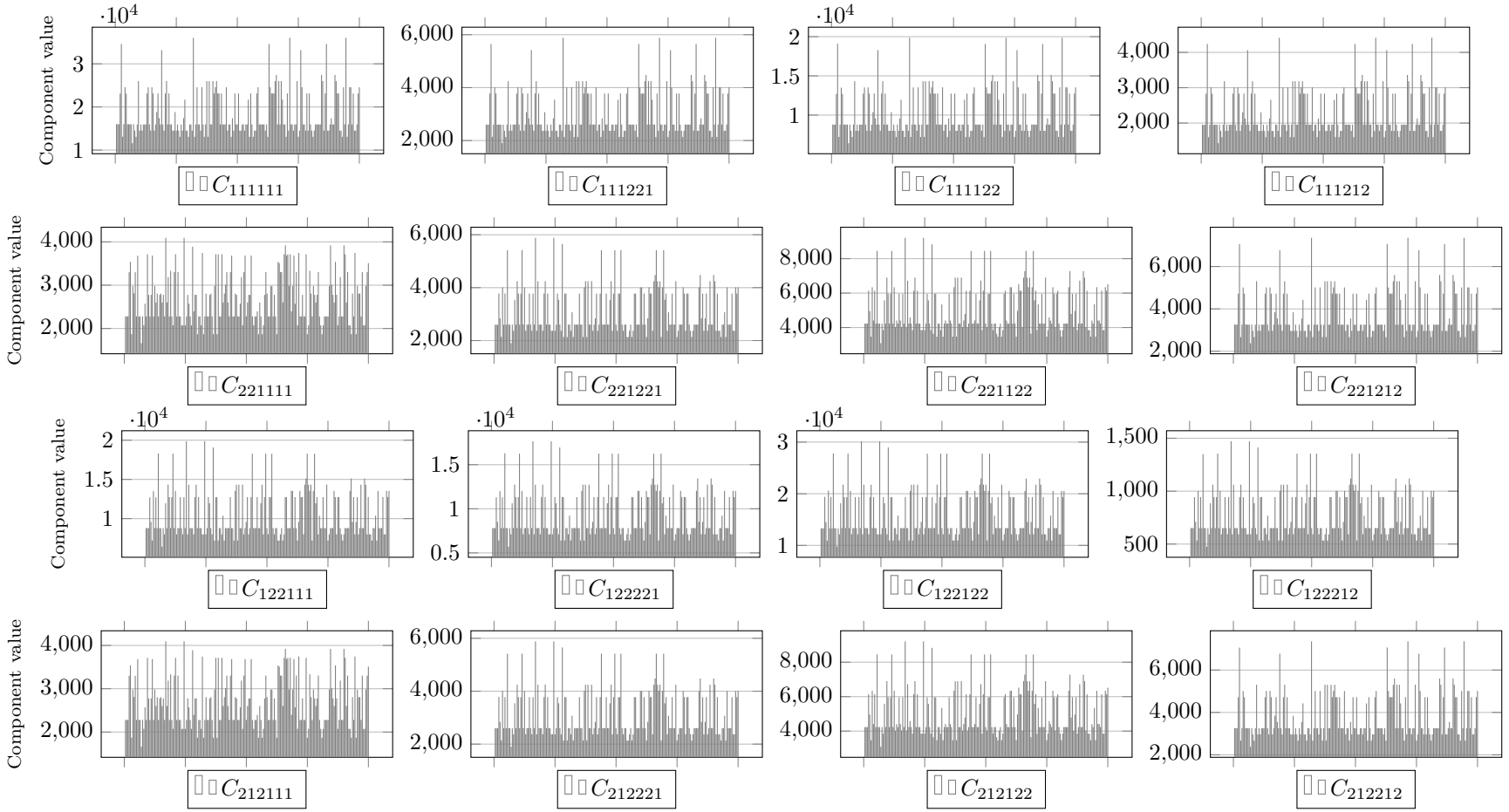

Figure A.5: Distribution study: components of the constitutive operator C_{ijklmn} - rows and columns 9 to 12 of the constitutive matrix (microcontinuum 20 mm)

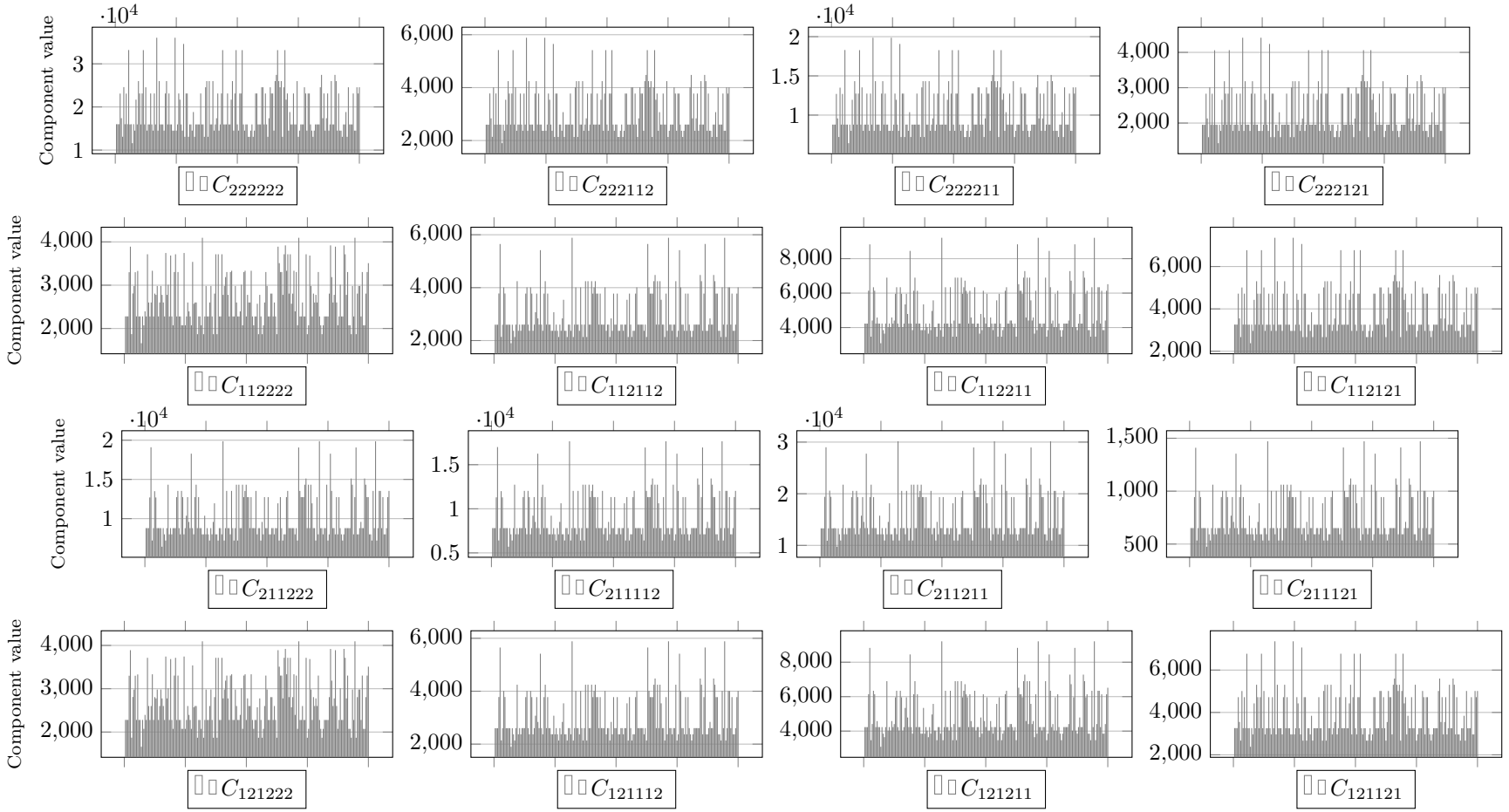

Figure A.6: Distribution study: components of the constitutive operator C_{ijklmn} - rows and columns 13 to 16 of the constitutive matrix (microcontinuum 20 mm)

A.2 Microcontinuum of size 30 mm

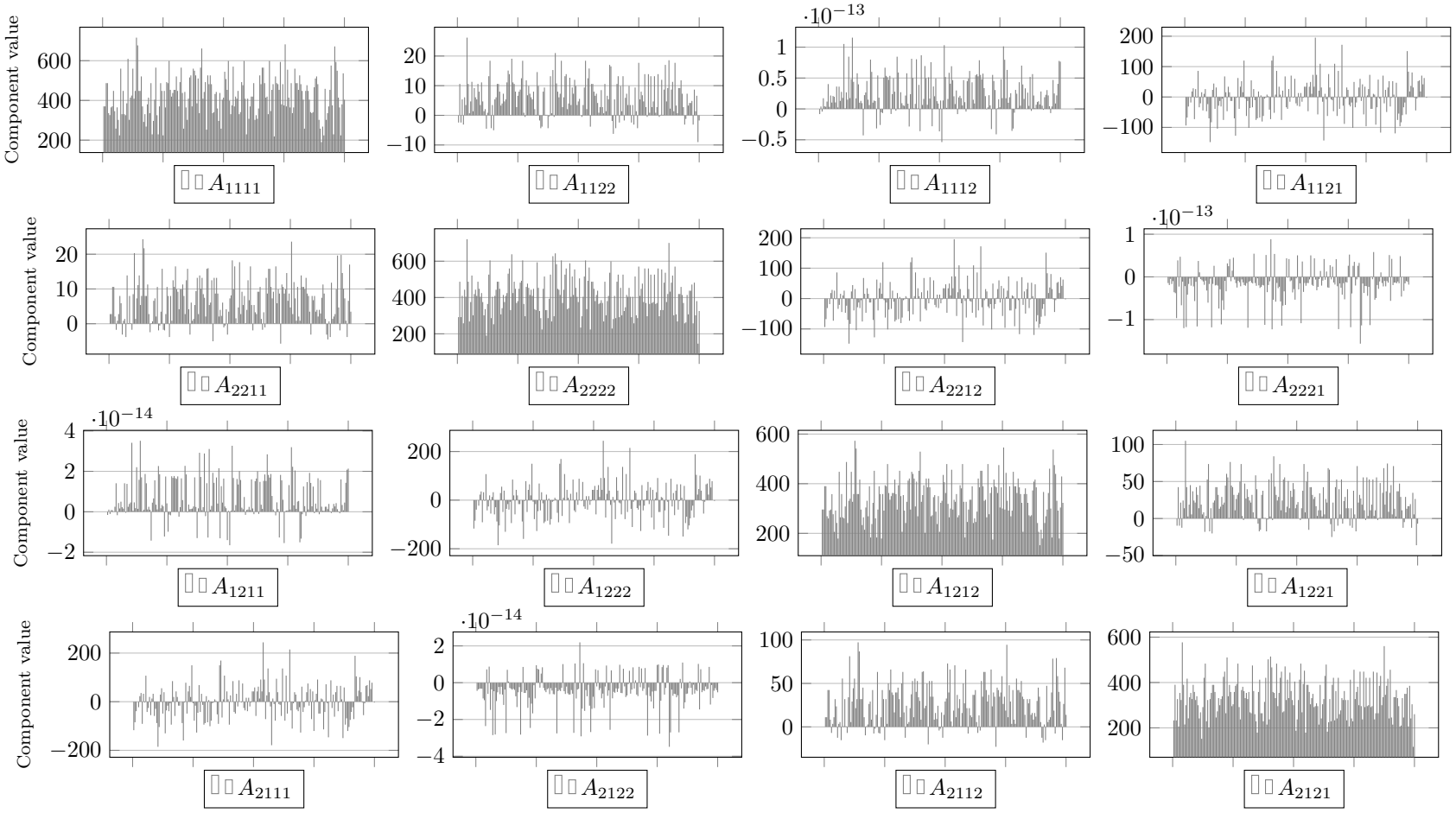

Figure A.7: Distribution study: components of the constitutive operator A_{ijkl} (microcontinuum 30 mm)

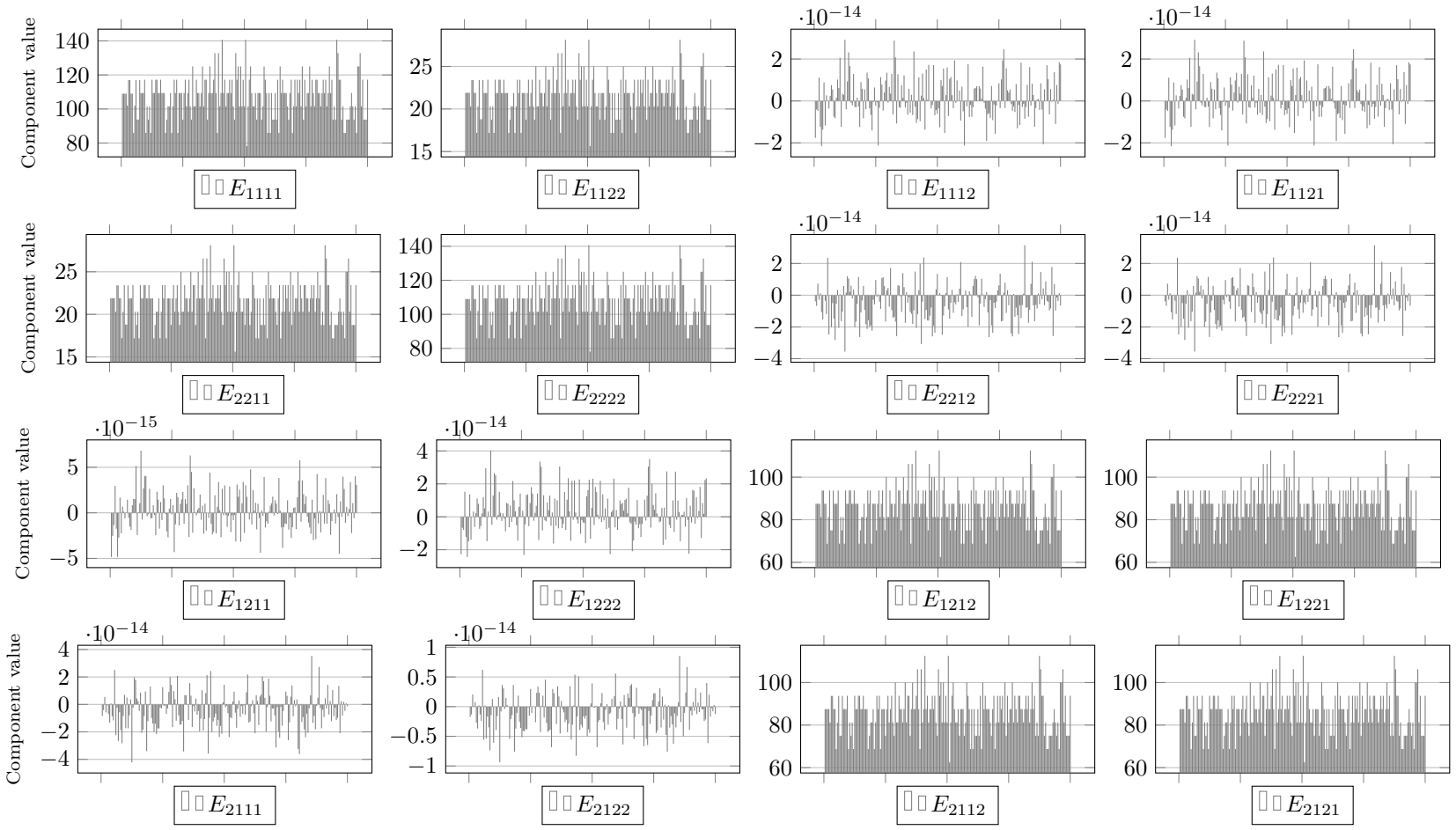

Figure A.8: Distribution study: components of the constitutive operator E_{ijkl} (microcontinuum 30 mm)

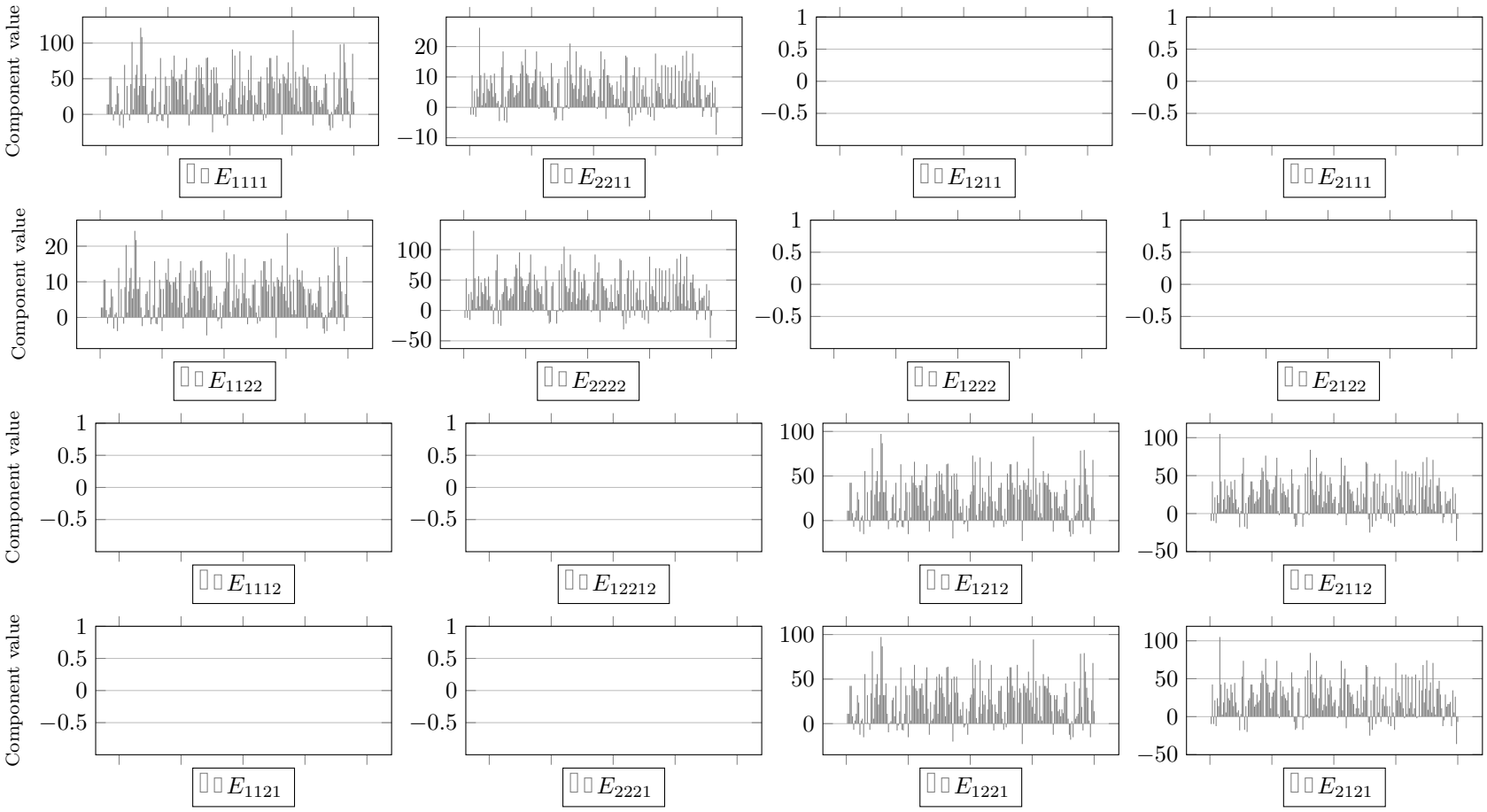

Figure A.9: Distribution study: components of the constitutive operator E_{klij} (microcontinuum 30 mm)

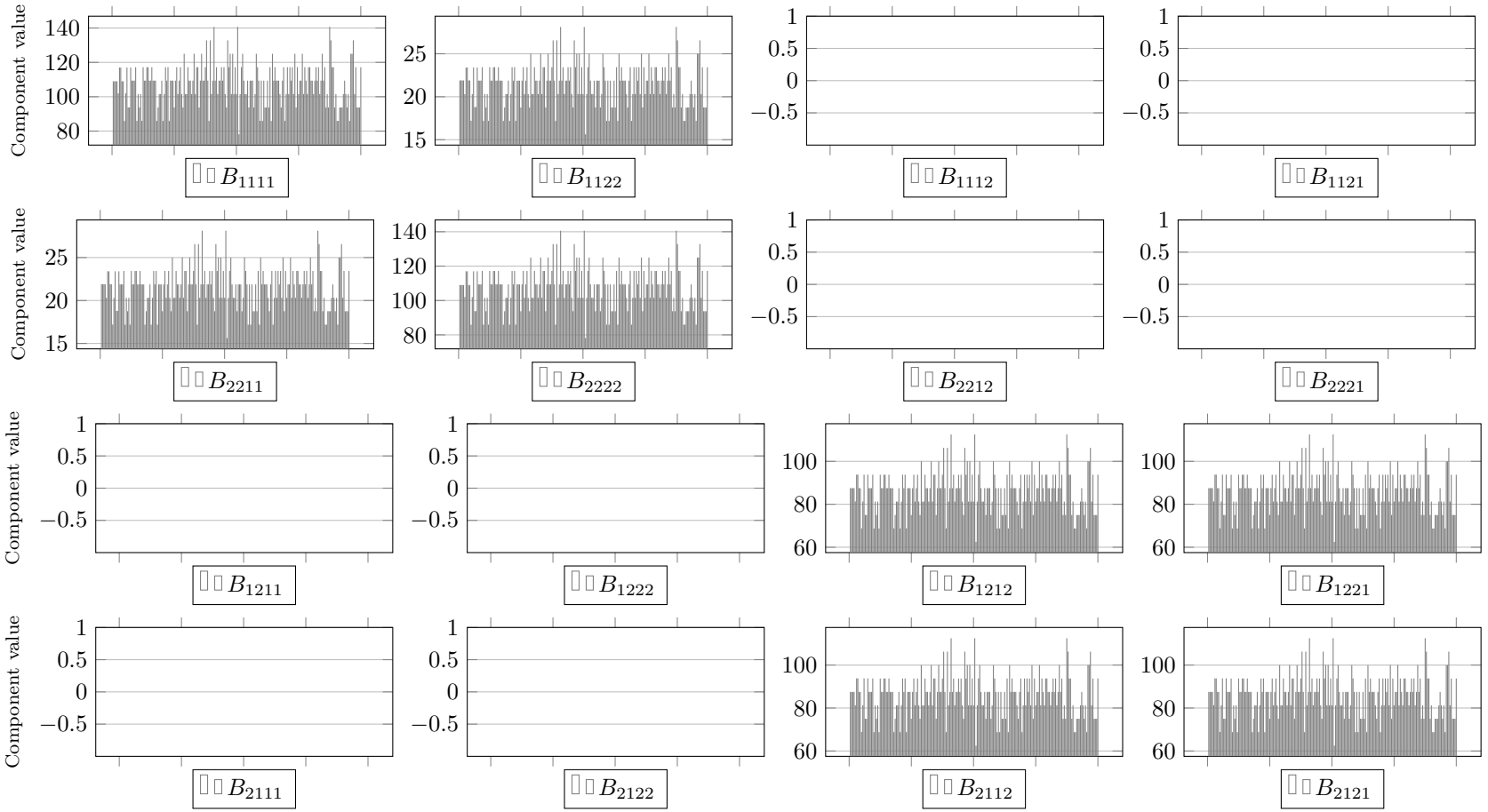

Figure A.10: Distribution study: components of the constitutive operator B_{ijkl} (microcontinuum 30 mm)

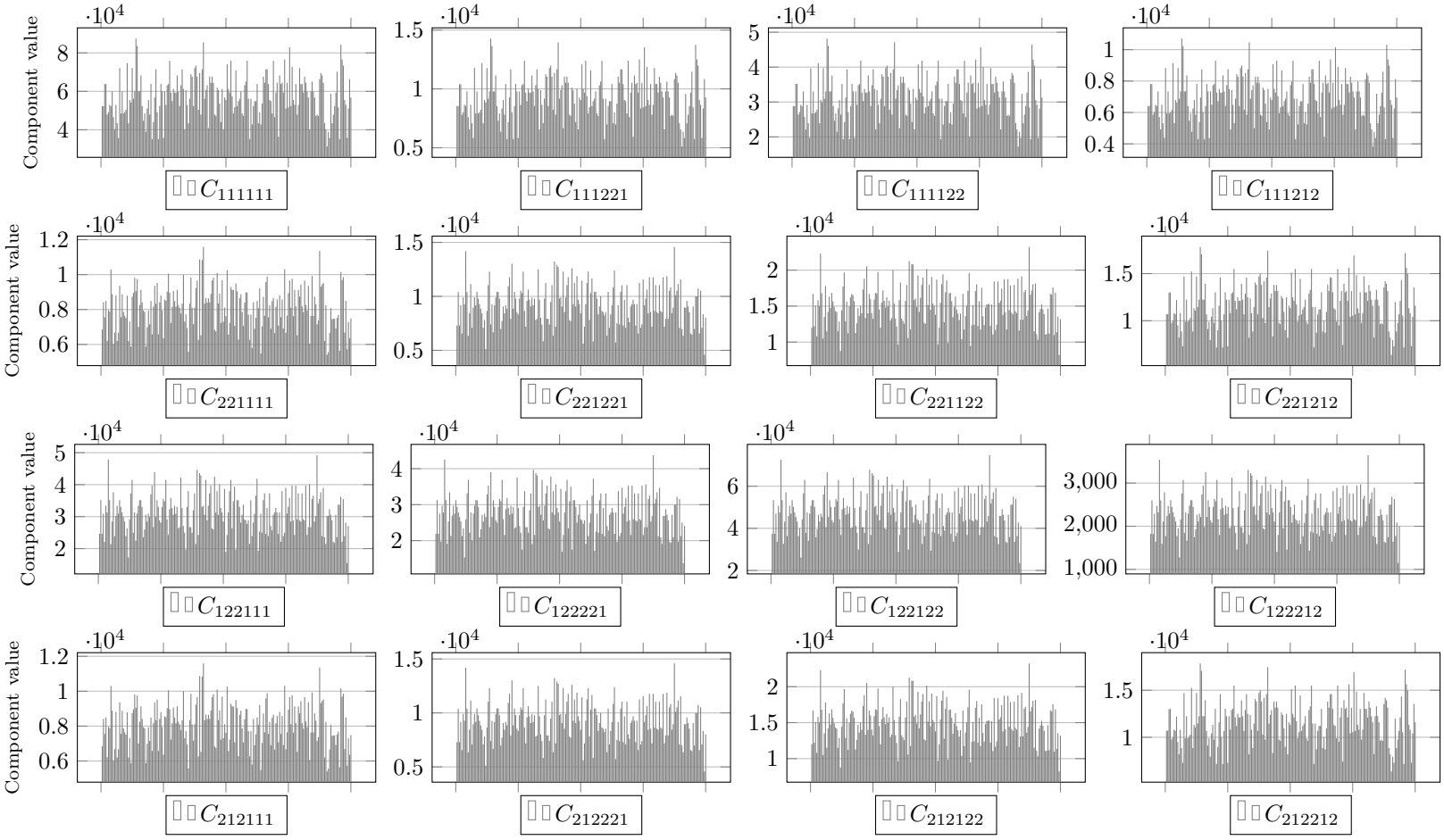

Figure A.11: Distribution study: components of the constitutive operator C_{ijklmn} - rows and columns 9 to 12 of the constitutive matrix (microcontinuum 30 mm)

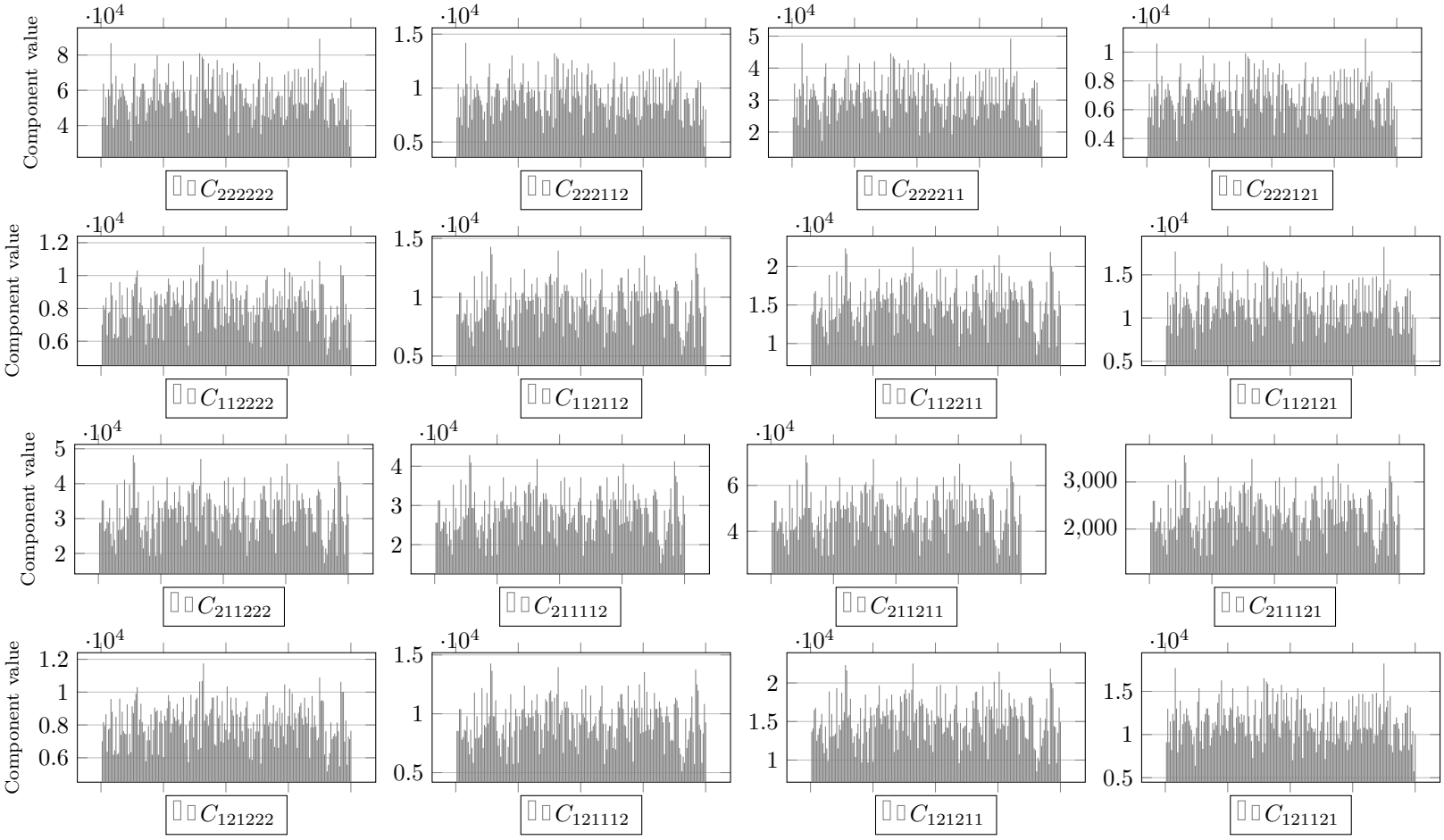

Figure A.12: Distribution study: components of the constitutive operator C_{ijklmn} - rows and columns 13 to 16 of the constitutive matrix (microcontinuum 30 mm)

A.3 Microcontinuum of size 40 mm

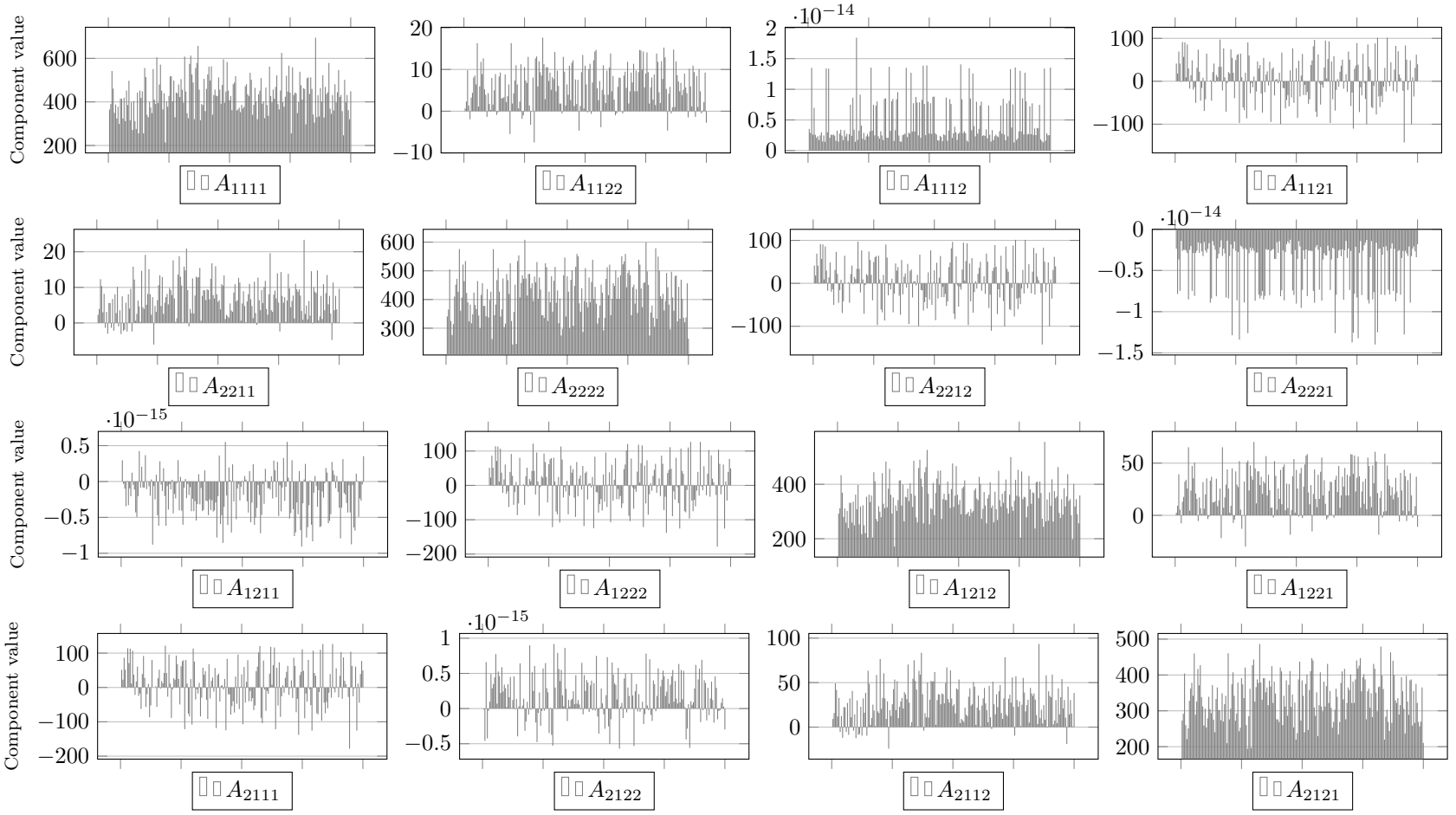

Figure A.13: Distribution study: components of the constitutive operator A_{ijkl} (microcontinuum 40 mm)

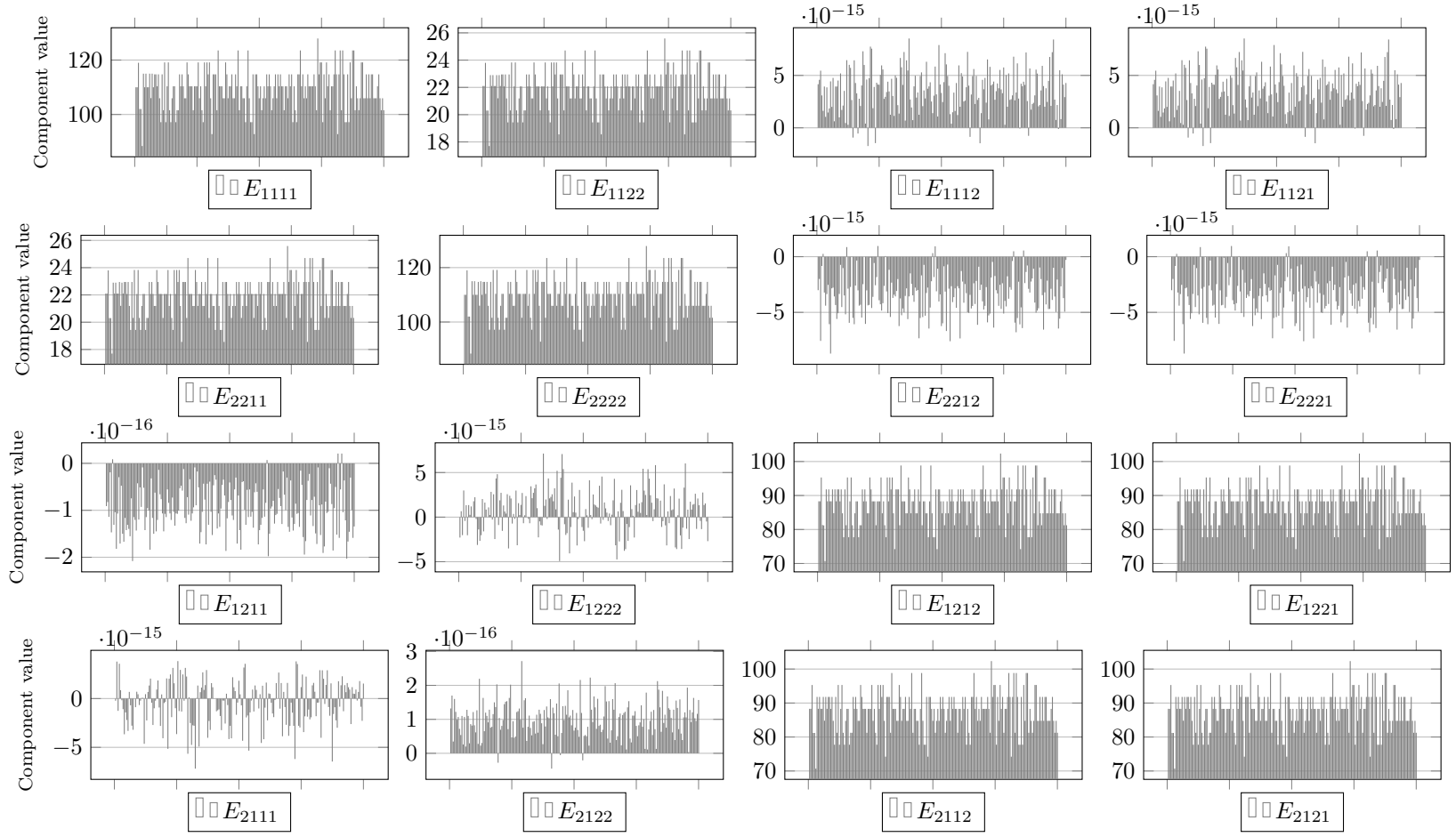

Figure A.14: Distribution study: components of the constitutive operator E_{ijkl} (microcontinuum 40 mm)

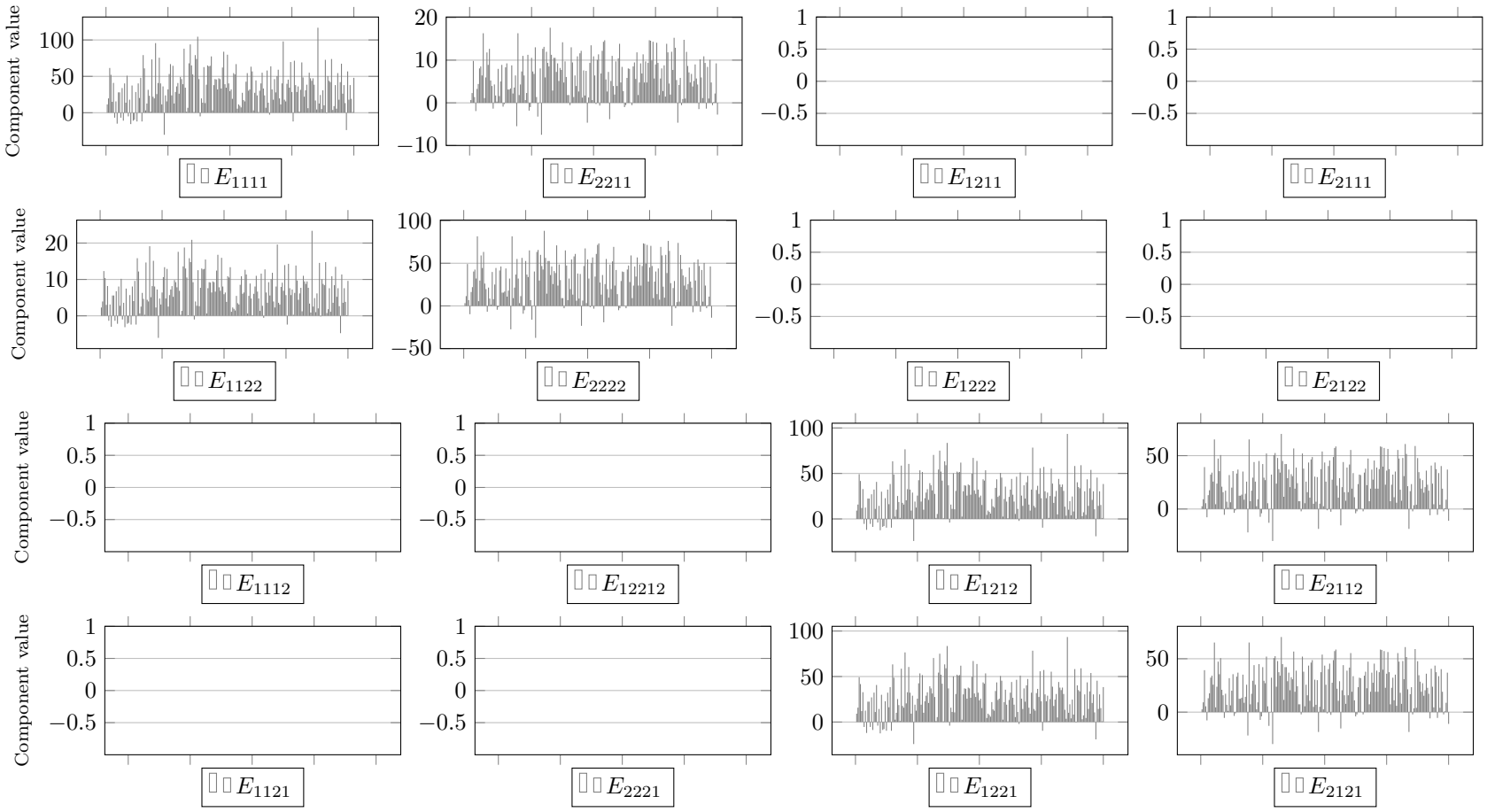

Figure A.15: Distribution study: components of the constitutive operator E_{klij} (microcontinuum 40 mm)

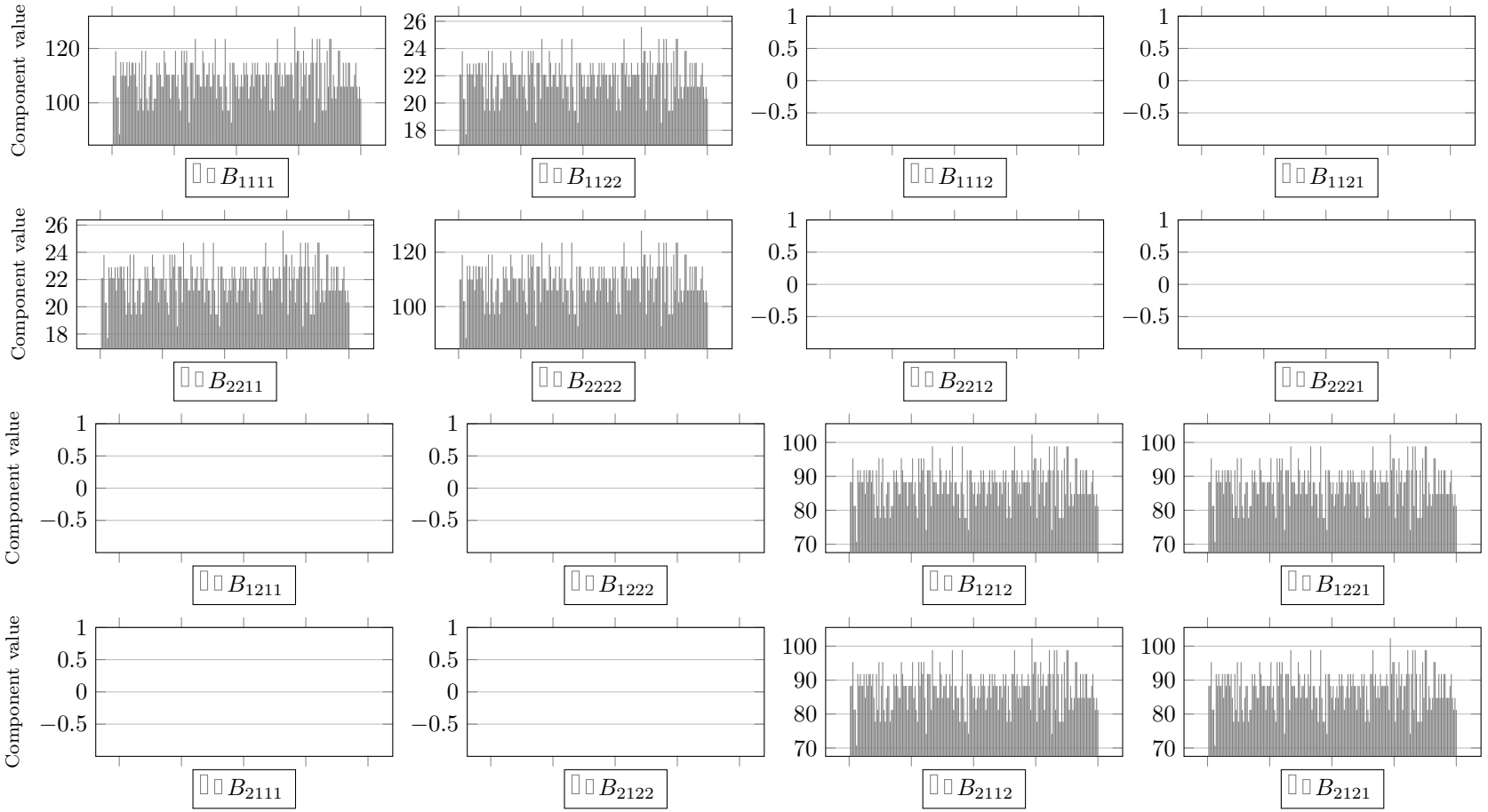

Figure A.16: Distribution study: components of the constitutive operator B_{ijkl} (microcontinuum 40 mm)

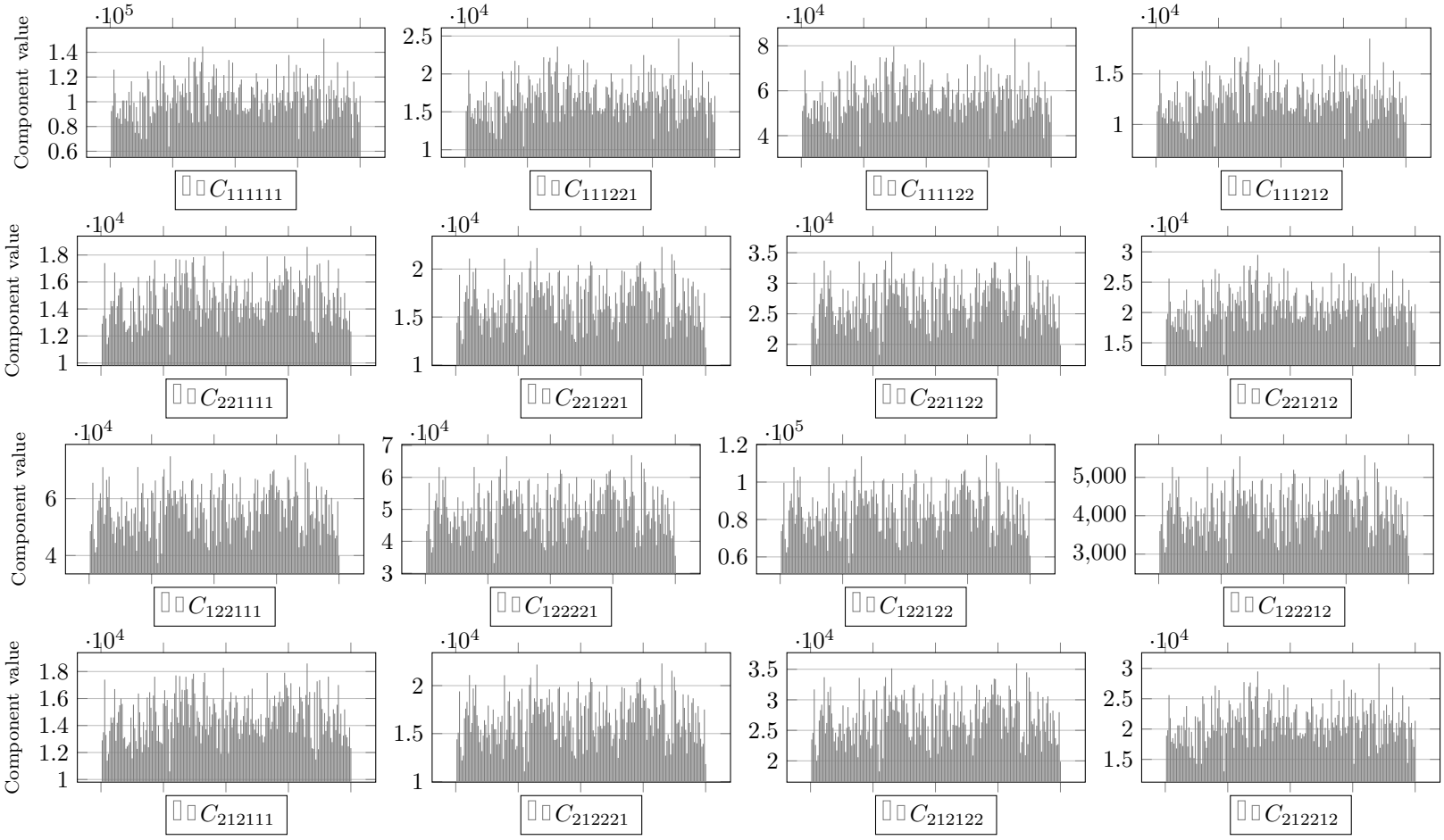

Figure A.17: Distribution study: components of the constitutive operator C_{ijklmn} - rows and columns 9 to 12 of the constitutive matrix (microcontinuum 40 mm)

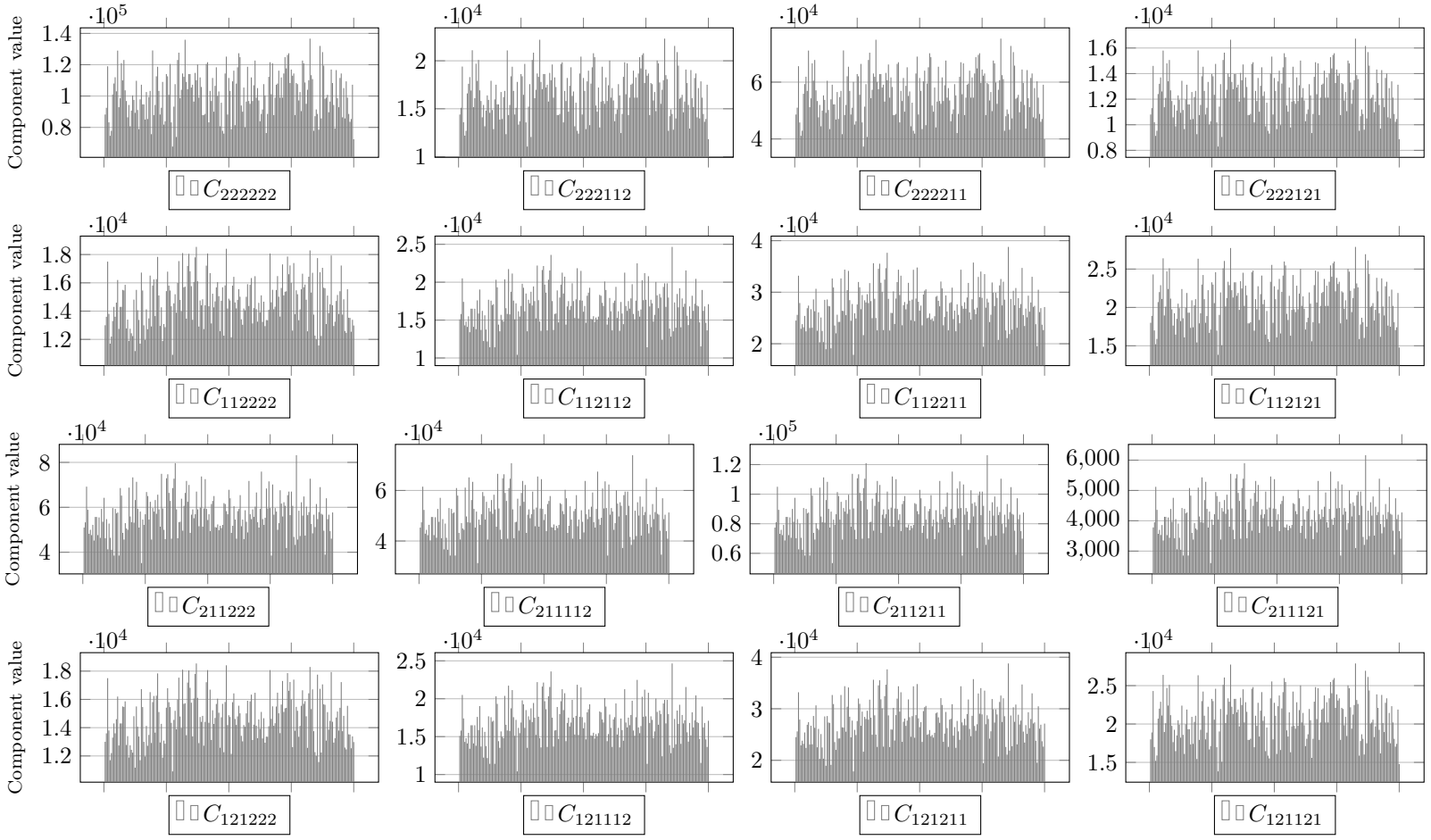

Figure A.18: Distribution study: components of the constitutive operator C_{ijklmn} - rows and columns 13 to 16 of the constitutive matrix (microcontinuum 40 mm)

A.4 Microcontinuum of size 50 mm

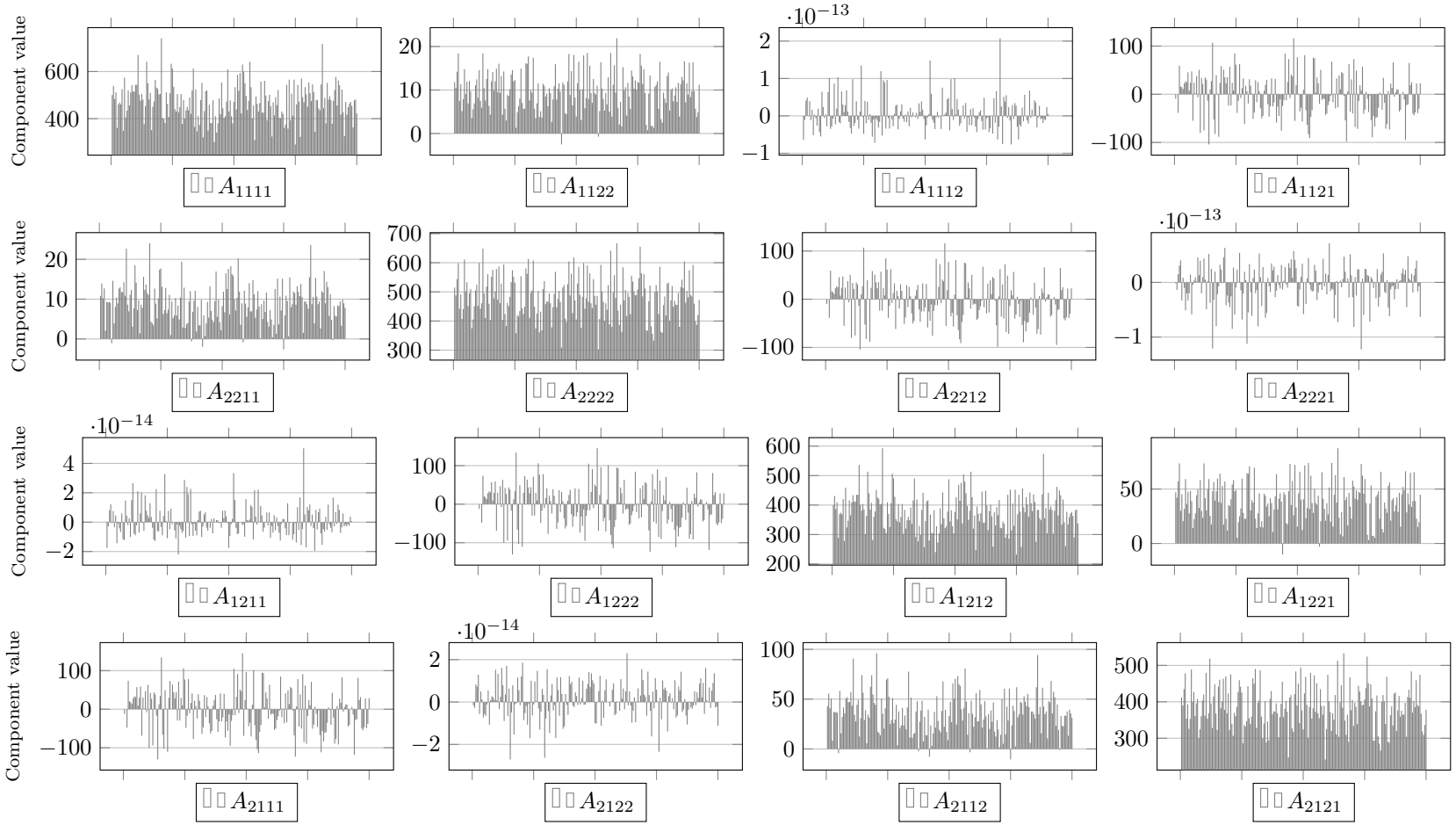

Figure A.19: Distribution study: components of the constitutive operator A_{ijkl} (microcontinuum 50 mm)

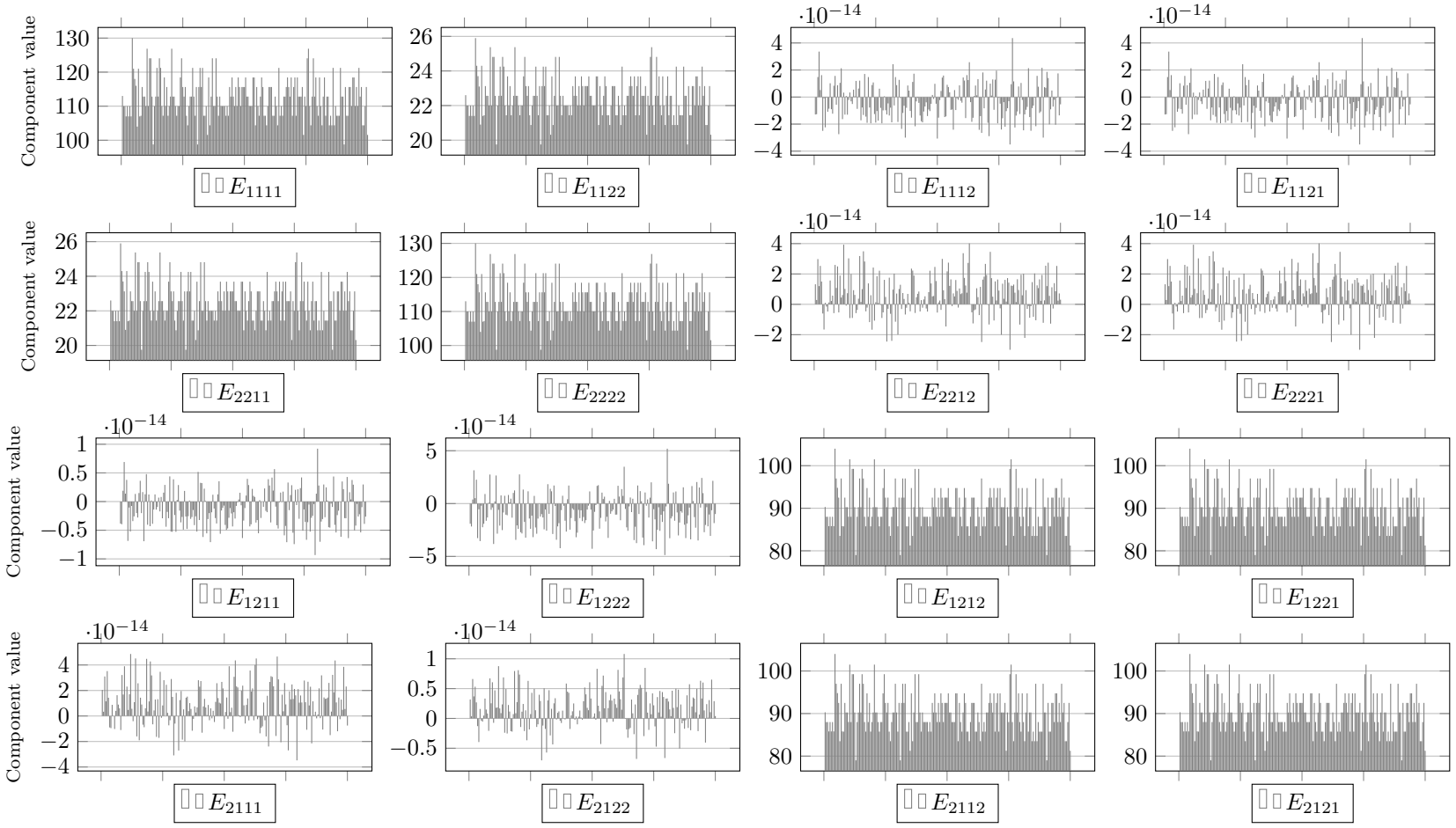

Figure A.20: Distribution study: components of the constitutive operator E_{ijkl} (microcontinuum 50 mm)

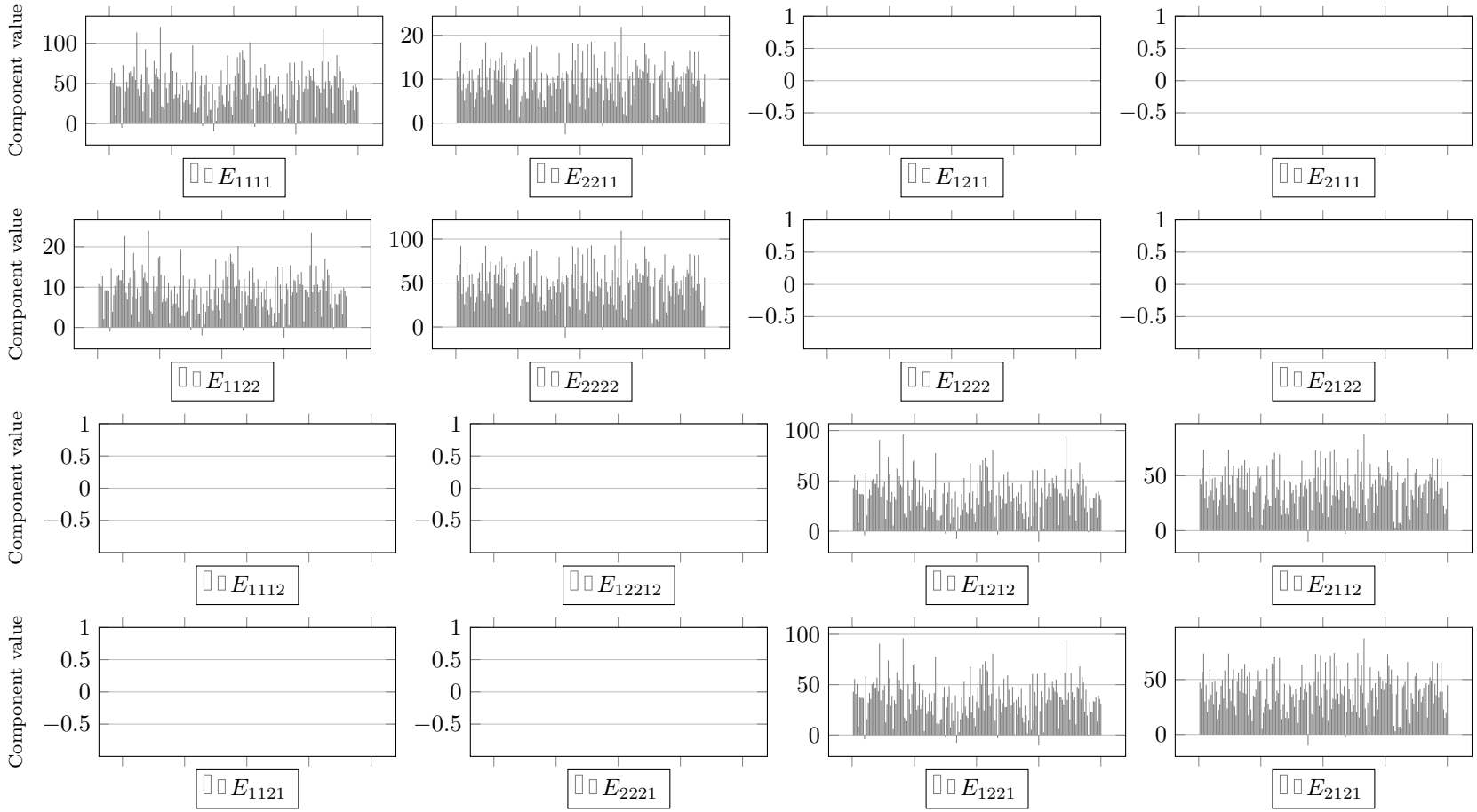

Figure A.21: Distribution study: components of the constitutive operator E_{klij} (microcontinuum 50 mm)

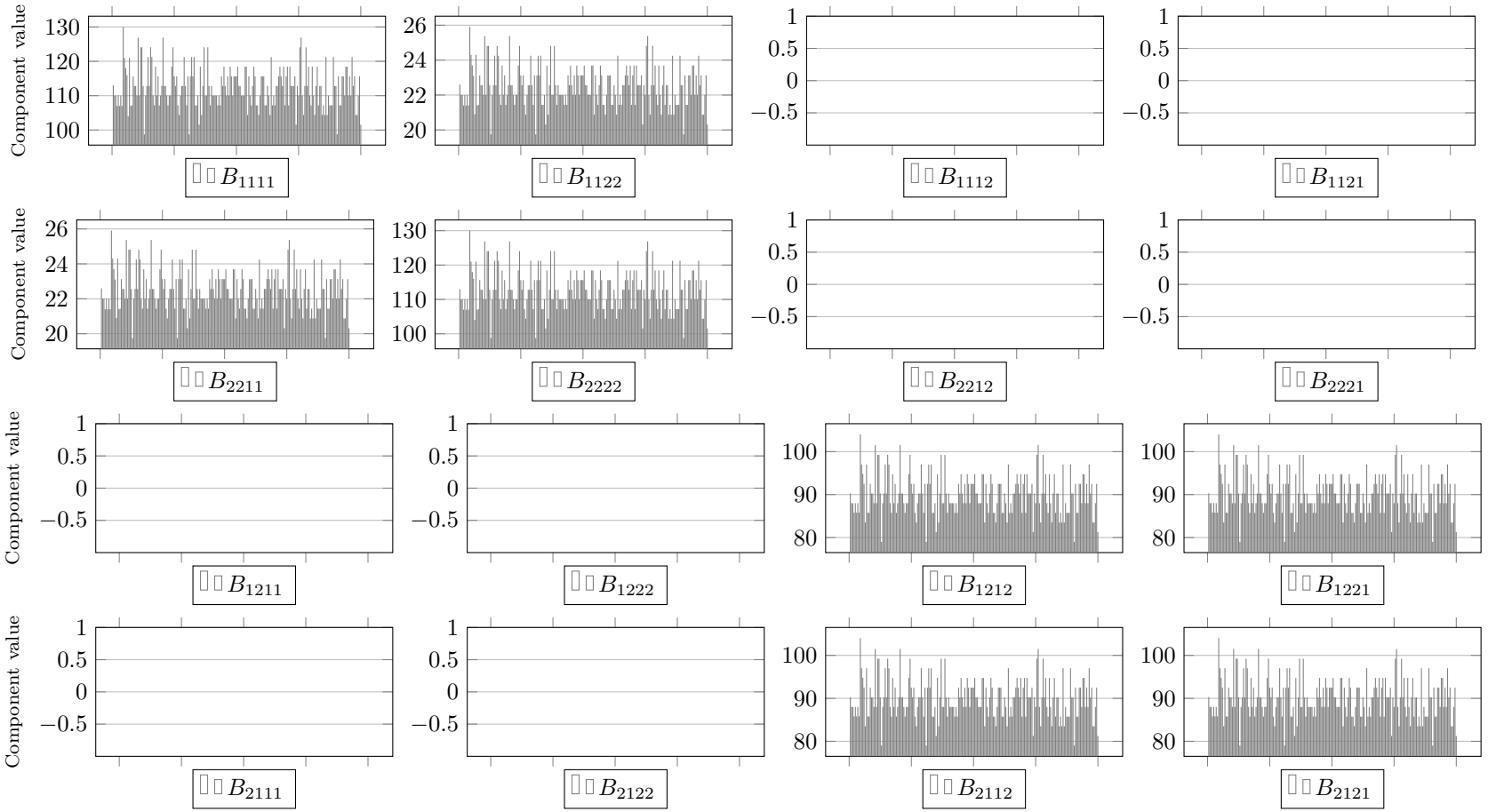

Figure A.22: Distribution study: components of the constitutive operator B_{ijkl} (microcontinuum 50 mm)

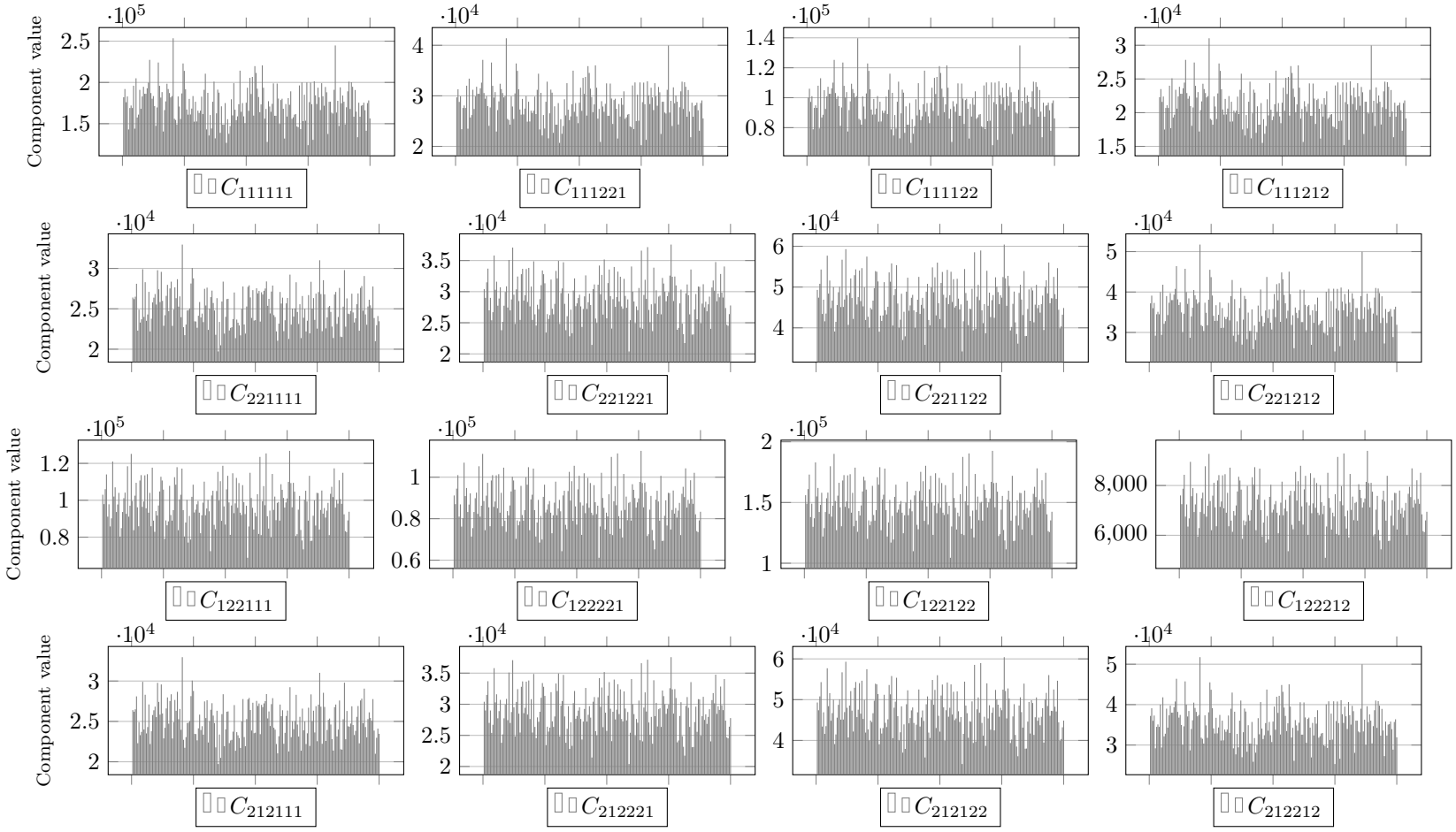

Figure A.23: Distribution study: components of the constitutive operator C_{ijklmn} - rows and columns 9 to 12 of the constitutive matrix (microcontinuum 50 mm)

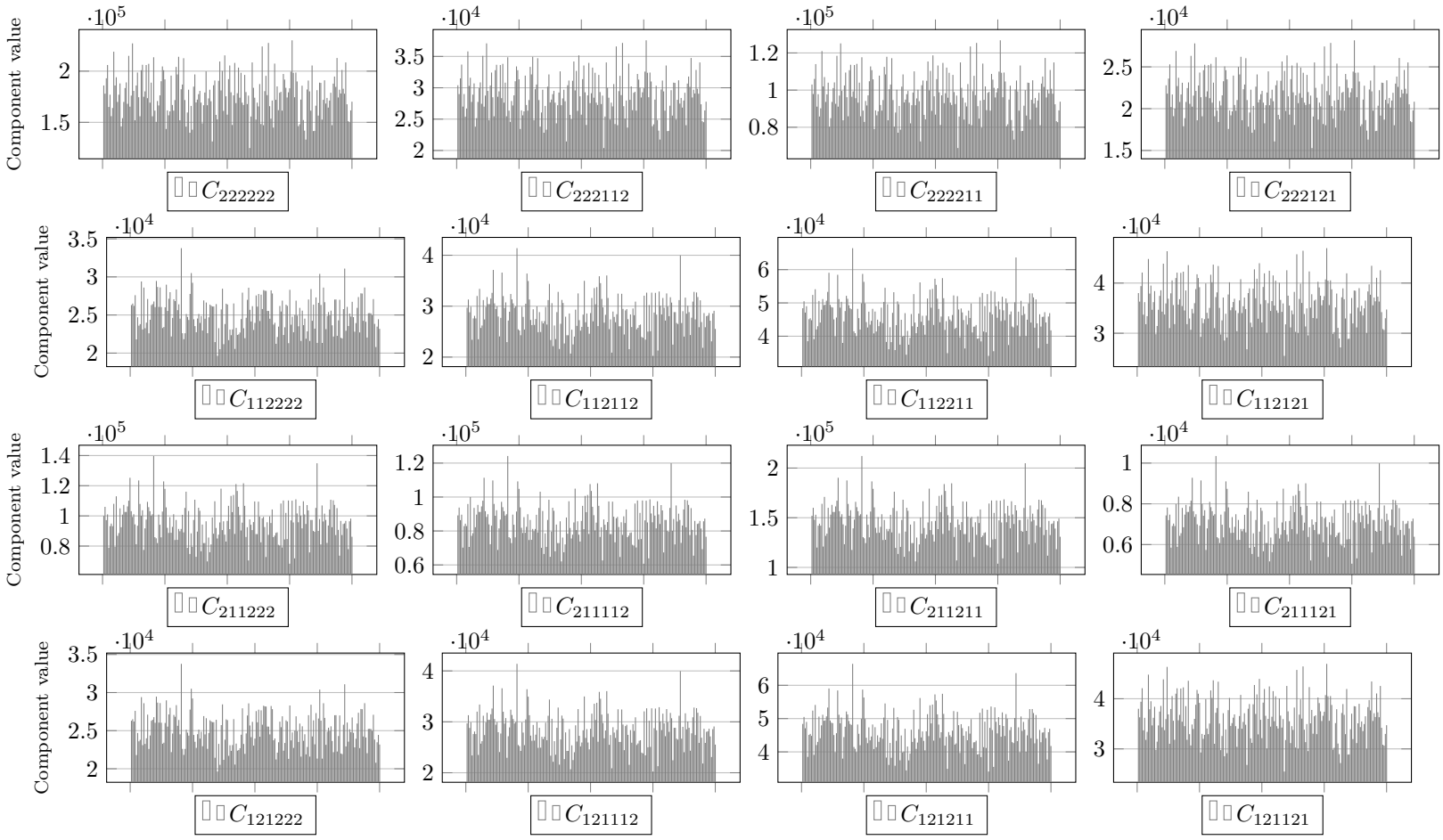

Figure A.24: Distribution study: components of the constitutive operator C_{ijklmn} - rows and columns 13 to 16 of the constitutive matrix (microcontinuum 50 mm)

A.5 Microcontinuum of size 60 mm

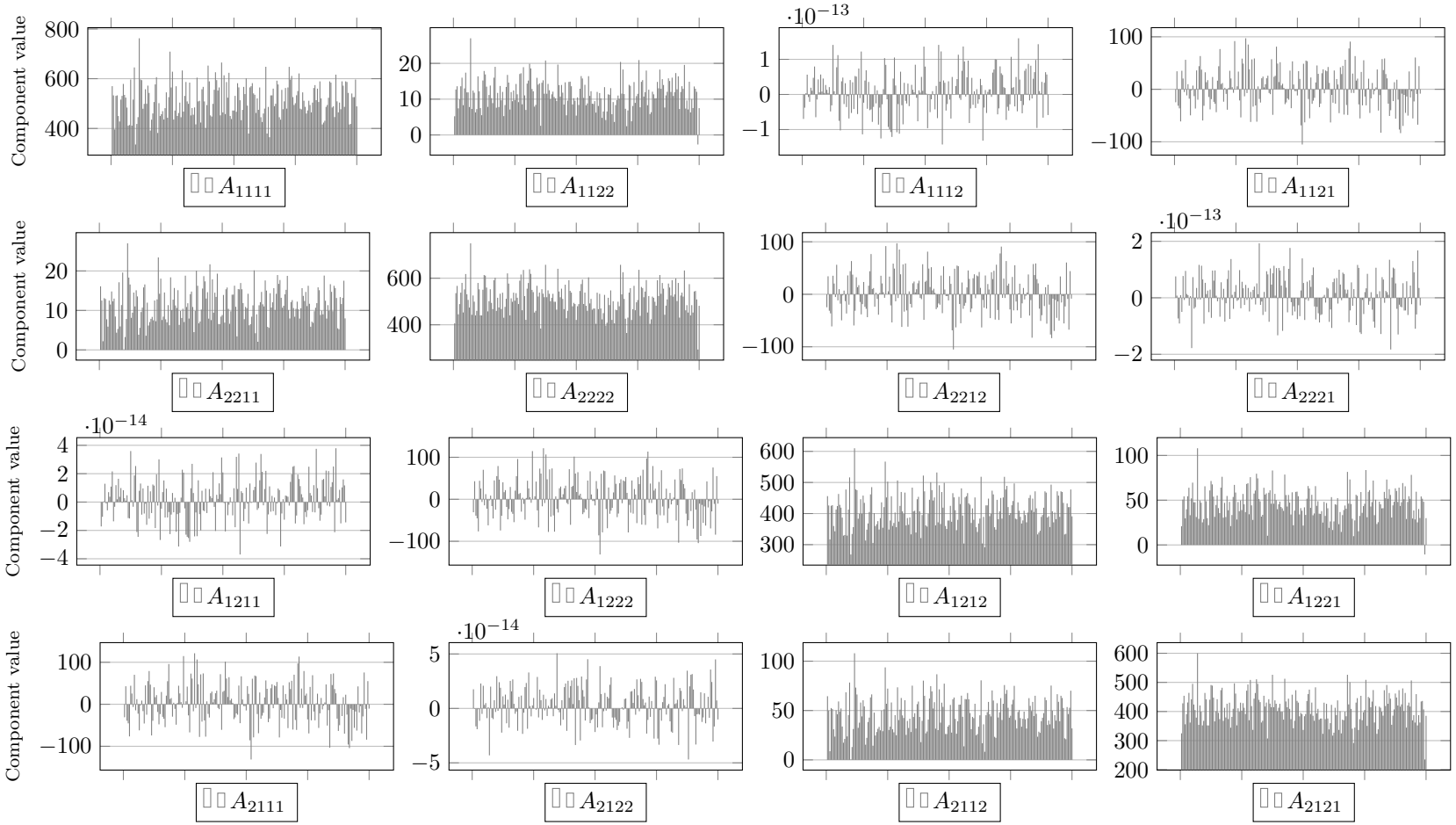

Figure A.25: Distribution study: components of the constitutive operator A_{ijkl} (microcontinuum 60 mm)

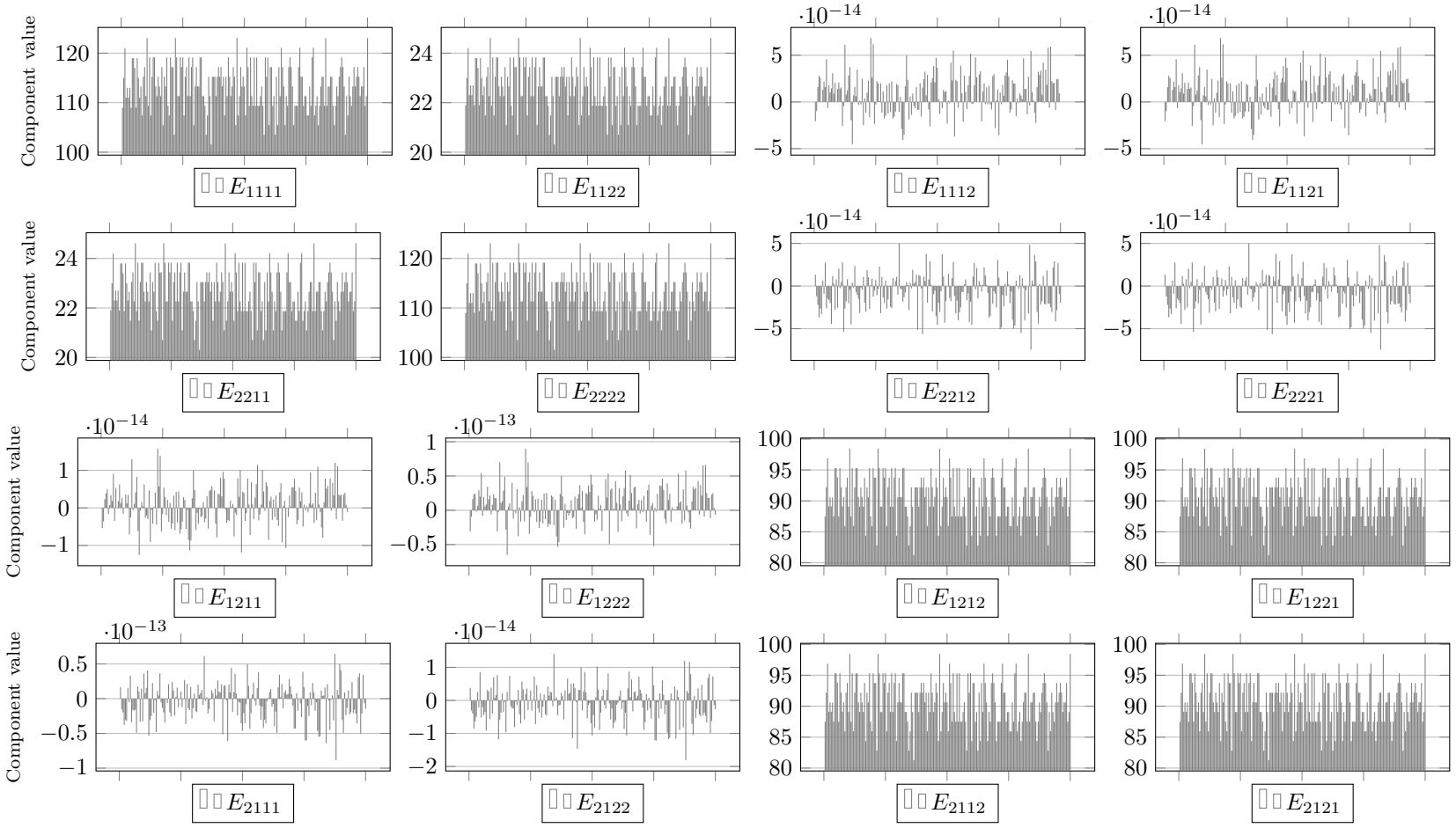

Figure A.26: Distribution study: components of the constitutive operator E_{ijkl} (microcontinuum 60 mm)

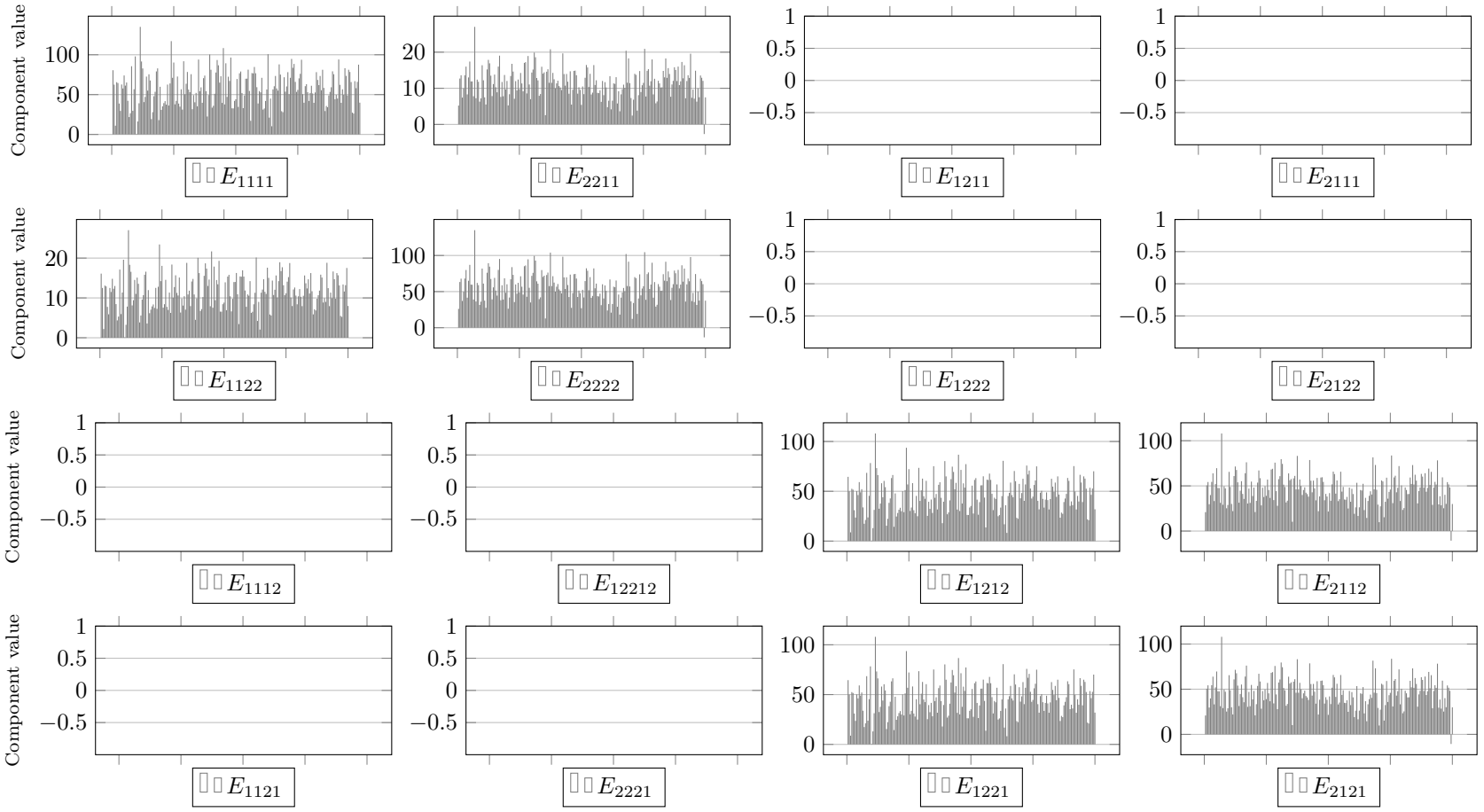

Figure A.27: Distribution study: components of the constitutive operator E_{klij} (microcontinuum 60 mm)

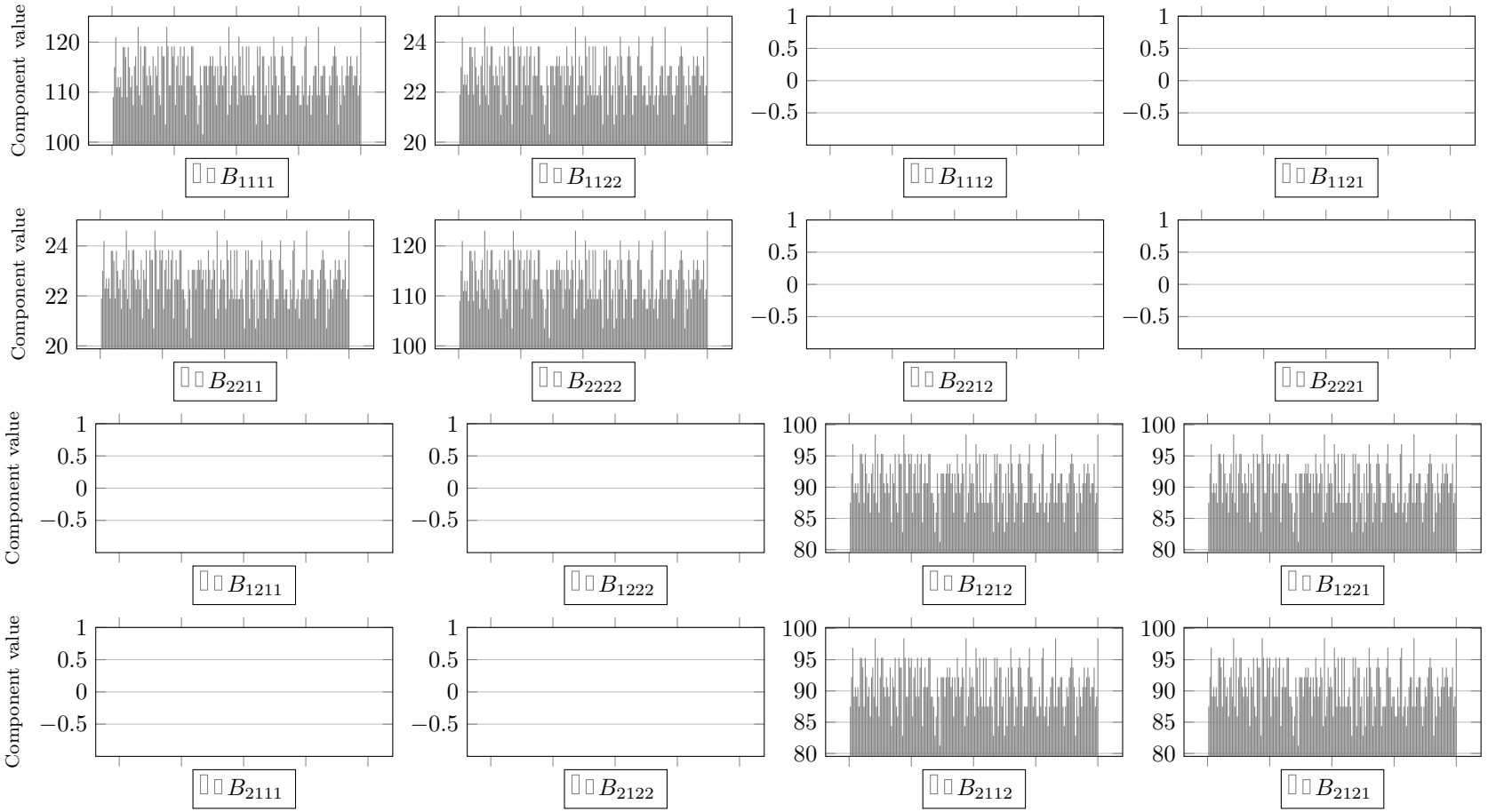

Figure A.28: Distribution study: components of the constitutive operator B_{ijkl} (microcontinuum 60 mm)

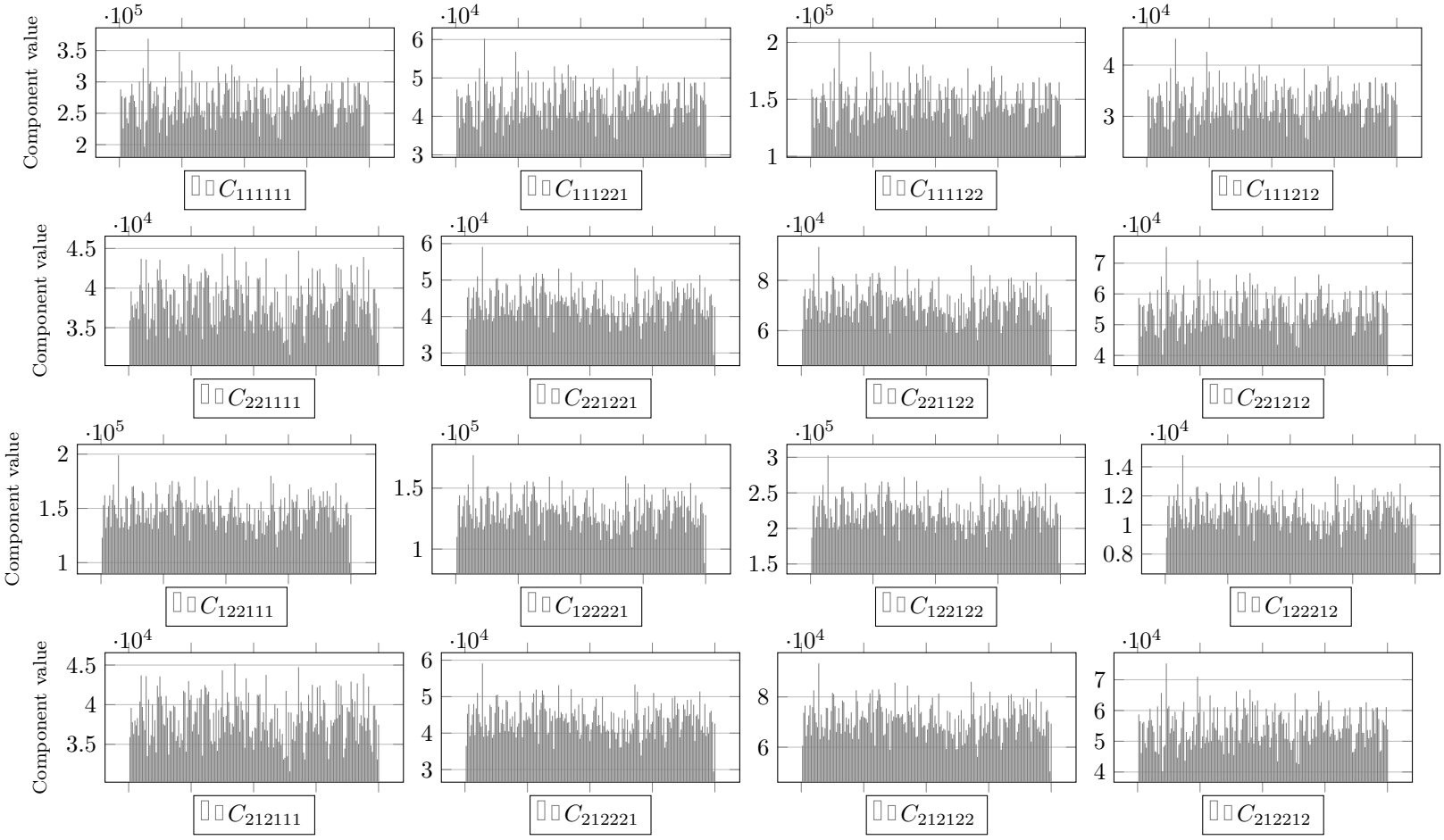

Figure A.29: Distribution study: components of the constitutive operator C_{ijklmn} - rows and columns 9 to 12 of the constitutive matrix (microcontinuum 60 mm)

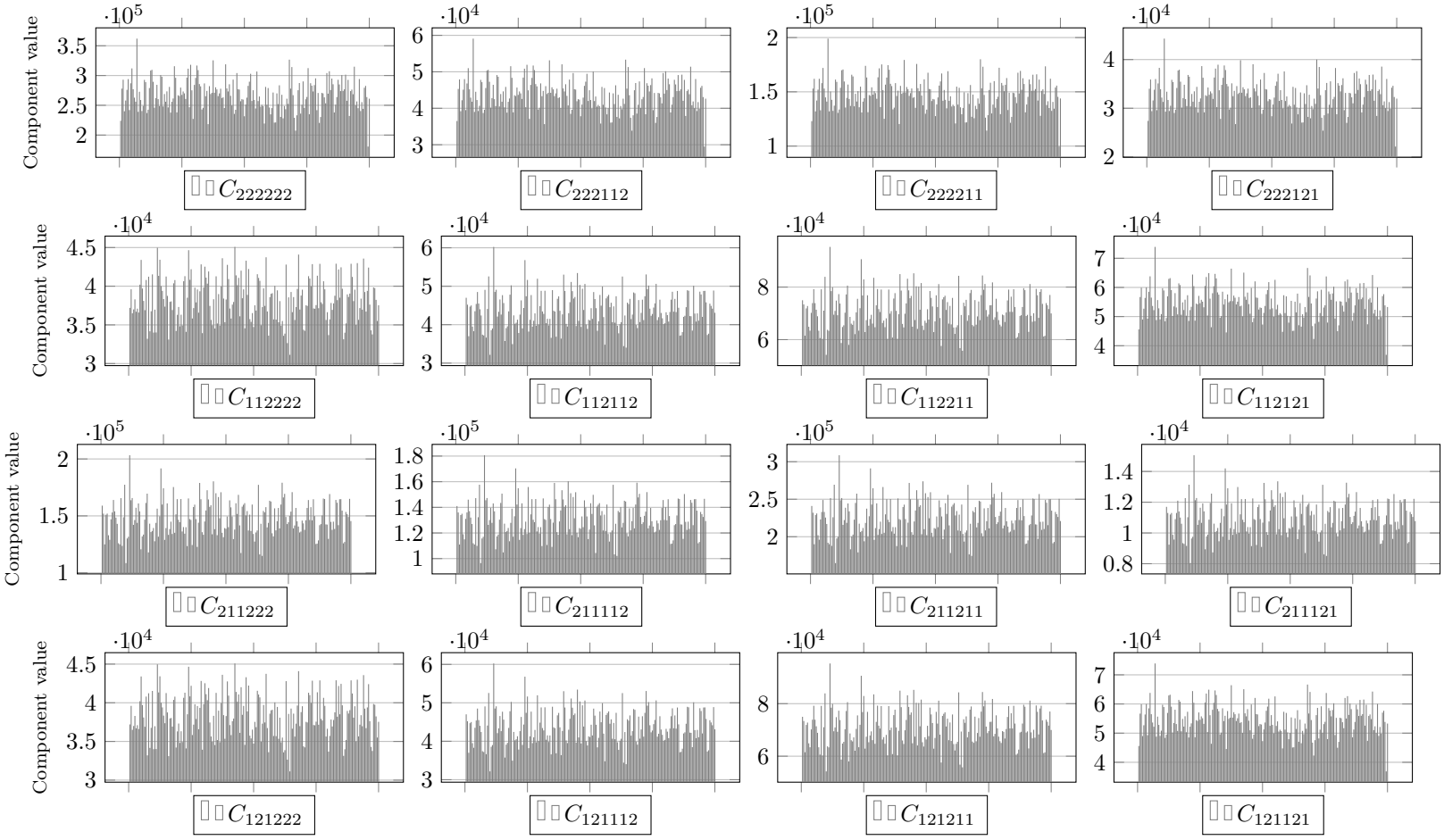

Figure A.30: Distribution study: components of the constitutive operator C_{ijklmn} - rows and columns 13 to 16 of the constitutive matrix (microcontinuum 60 mm)

A.6 Microcontinuum of size 70 mm

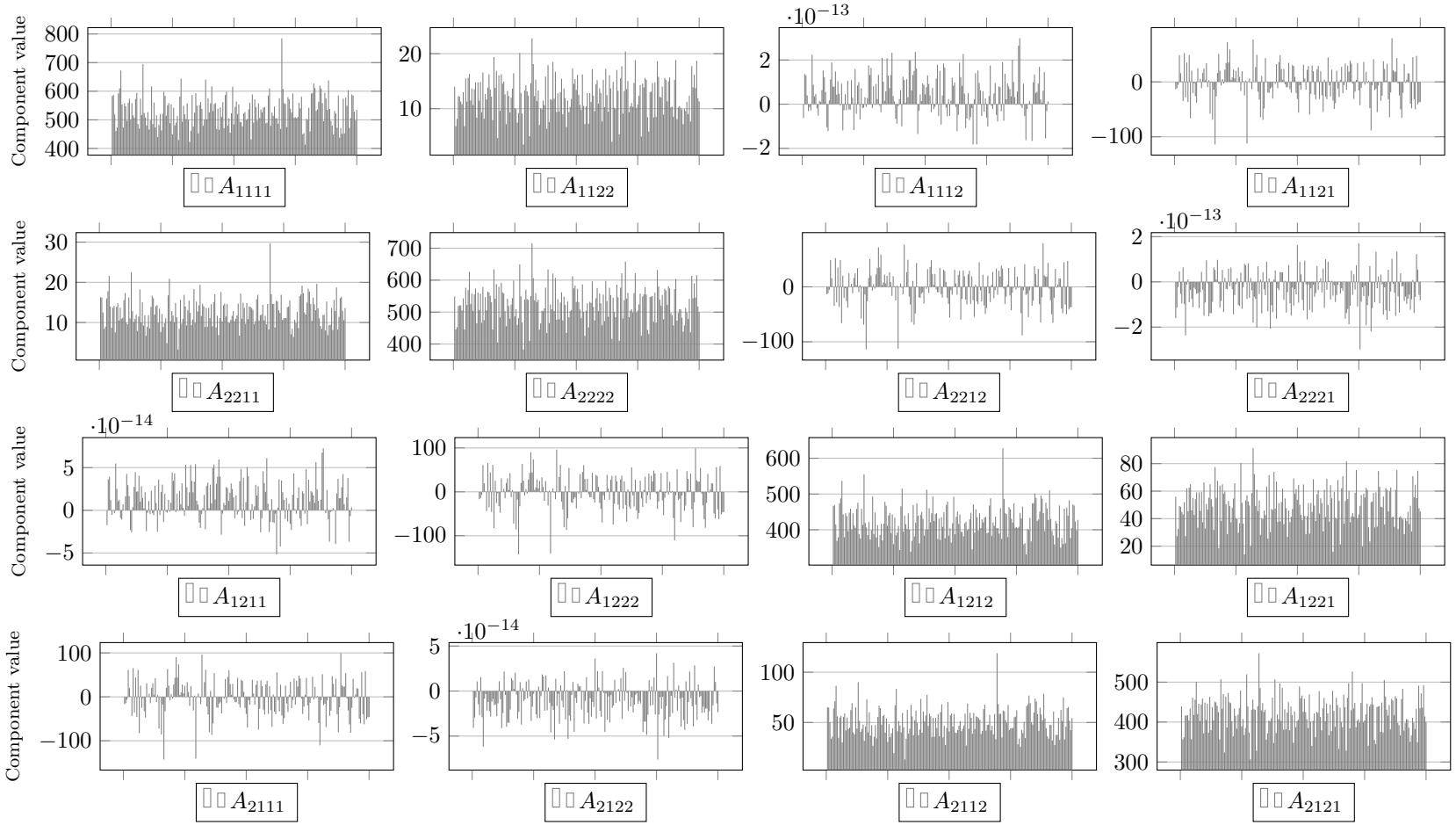

Figure A.31: Distribution study: components of the constitutive operator A_{ijkl} (microcontinuum 70 mm)

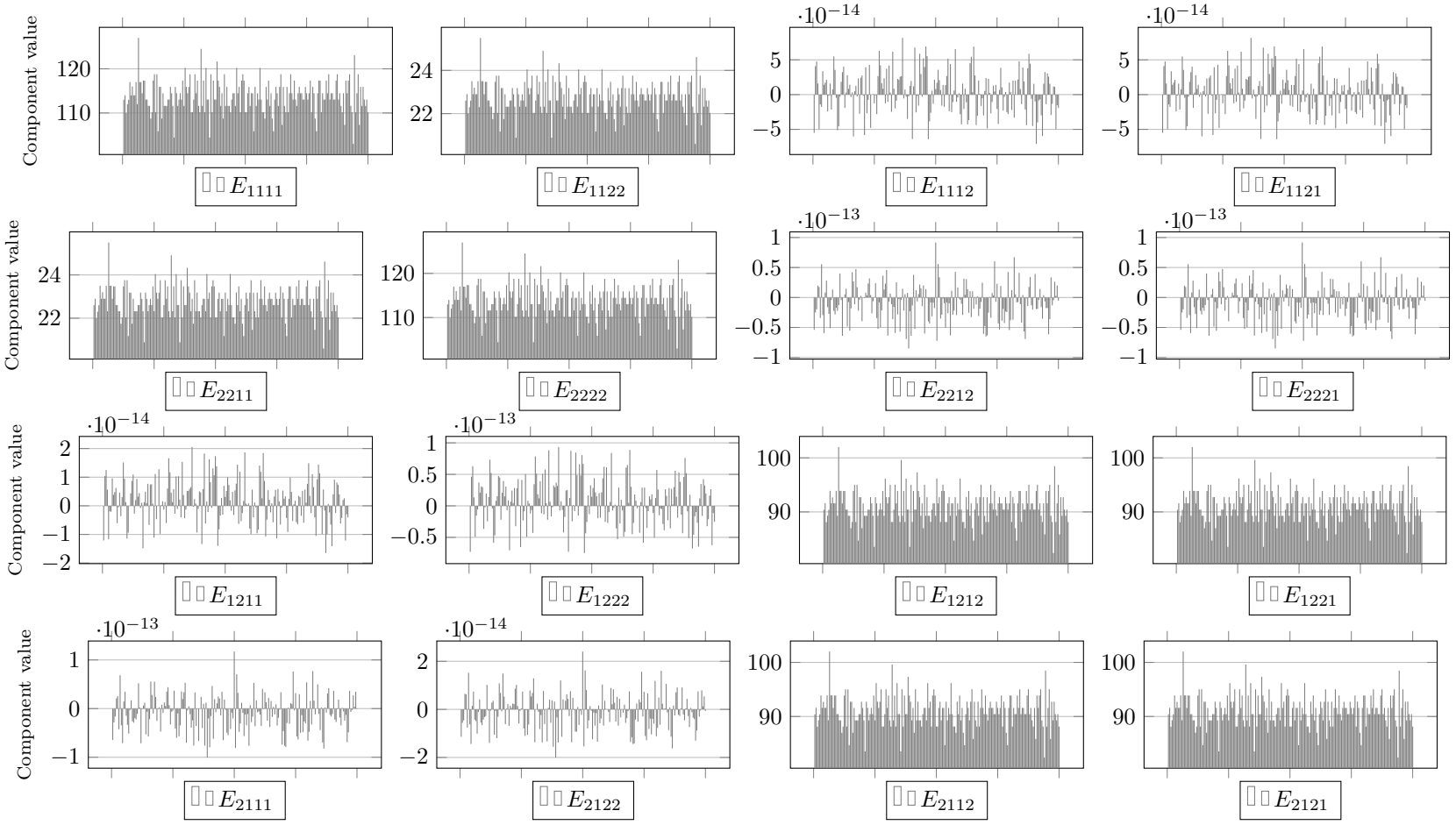

Figure A.32: Distribution study: components of the constitutive operator E_{ijkl} (microcontinuum 70 mm)

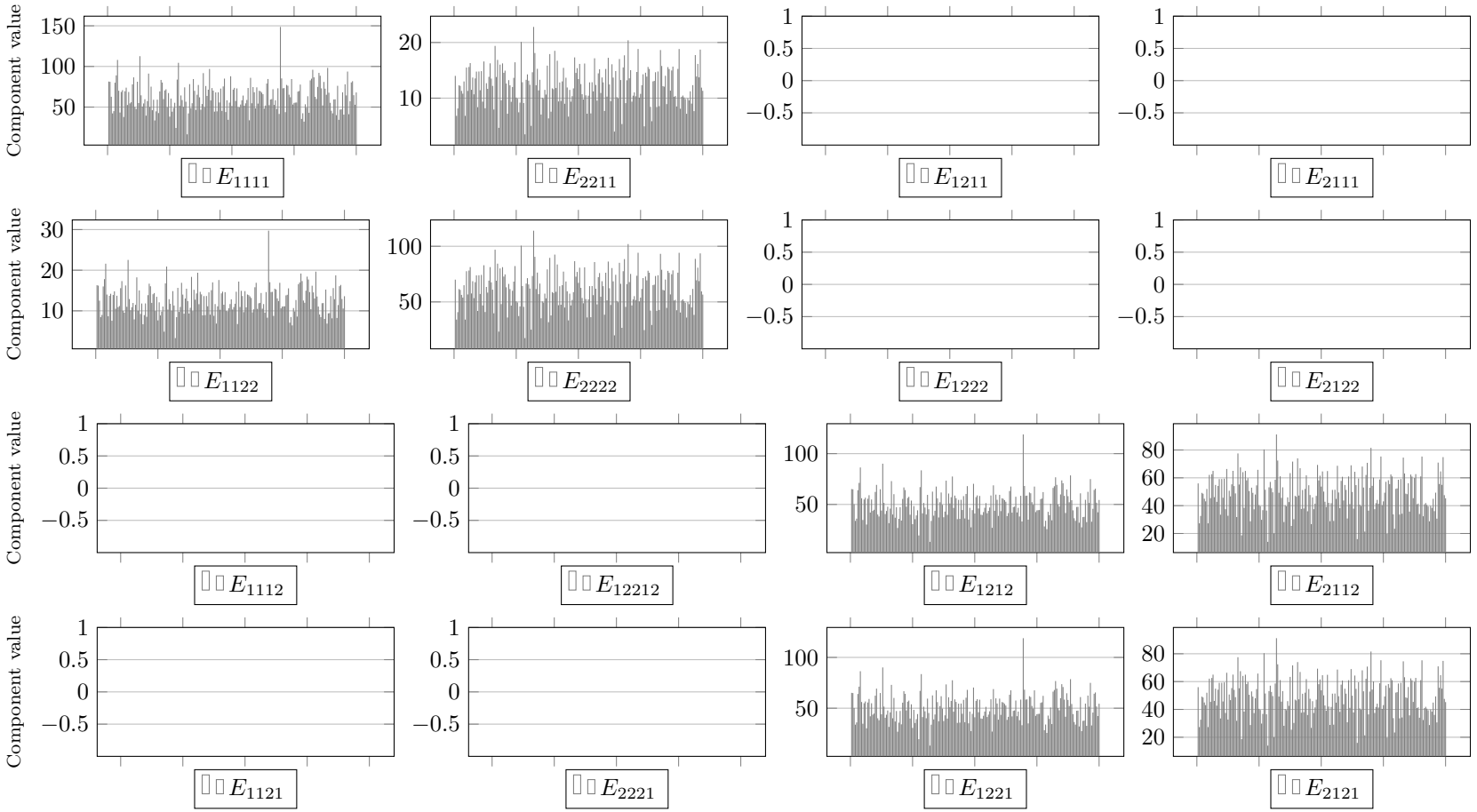

Figure A.33: Distribution study: components of the constitutive operator E_{klij} (microcontinuum 70 mm)

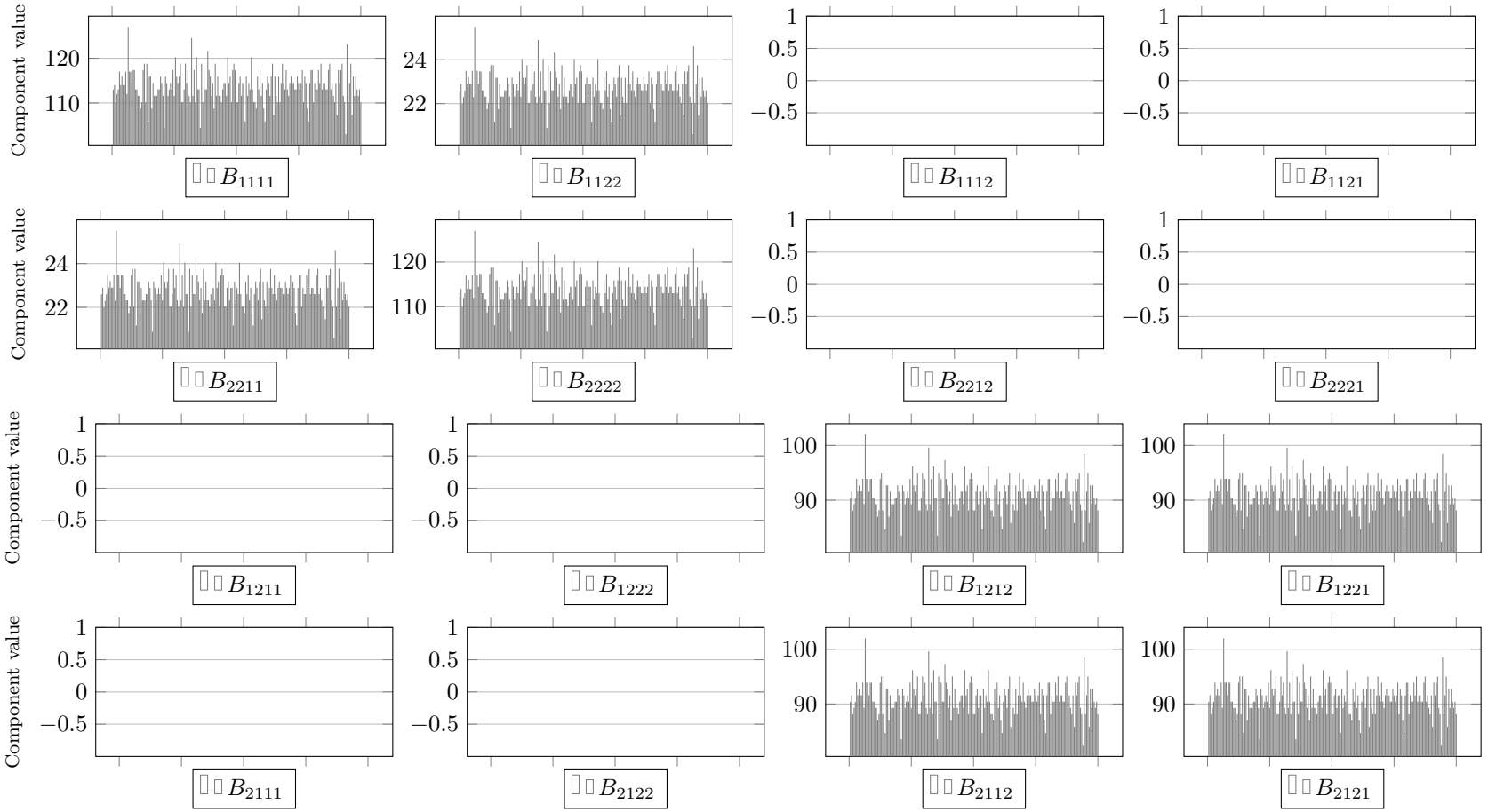

Figure A.34: Distribution study: components of the constitutive operator B_{ijkl} (microcontinuum 70 mm)

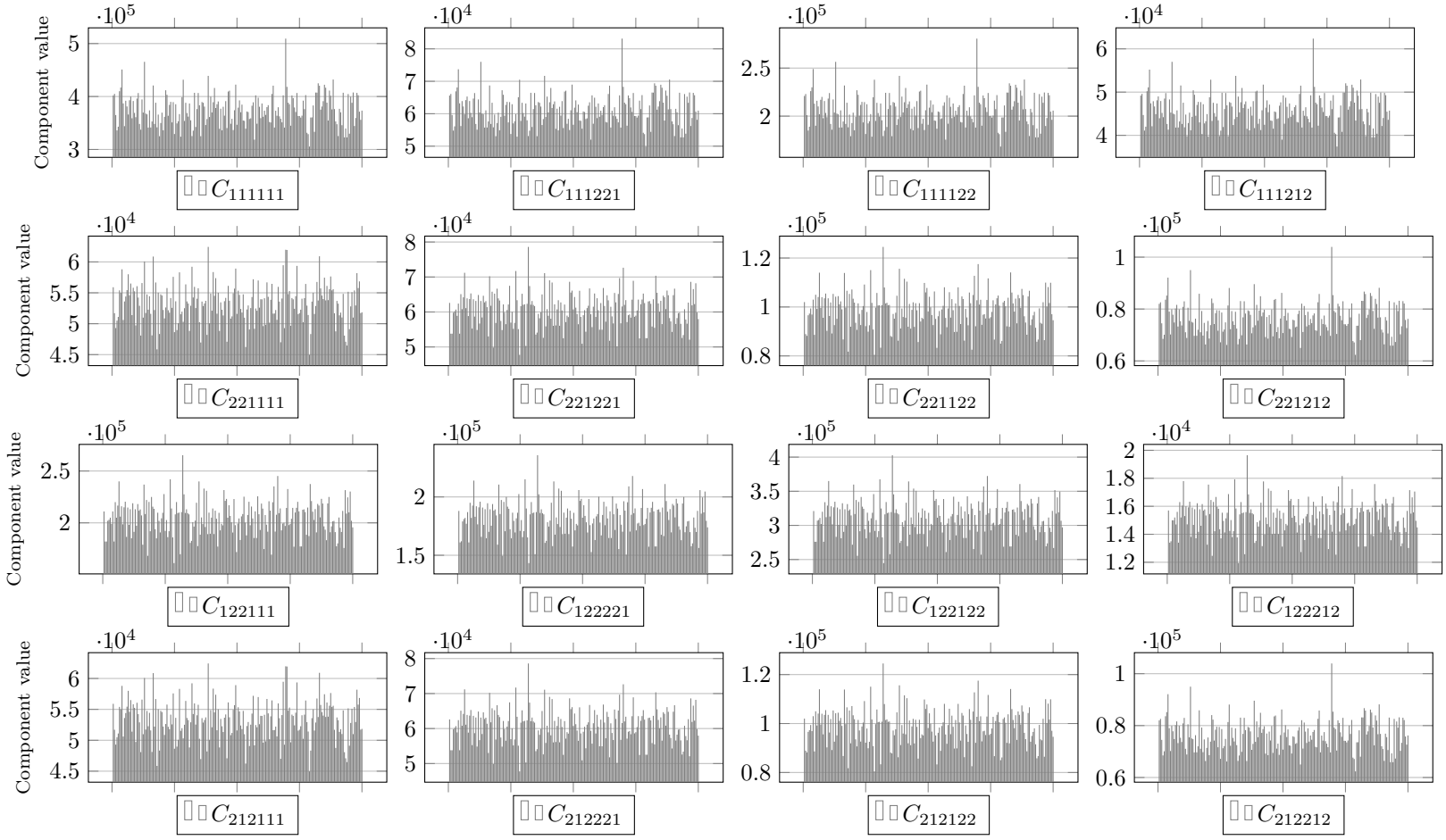

Figure A.35: Distribution study: components of the constitutive operator C_{ijklmn} - rows and columns 9 to 12 of the constitutive matrix (microcontinuum 70 mm)

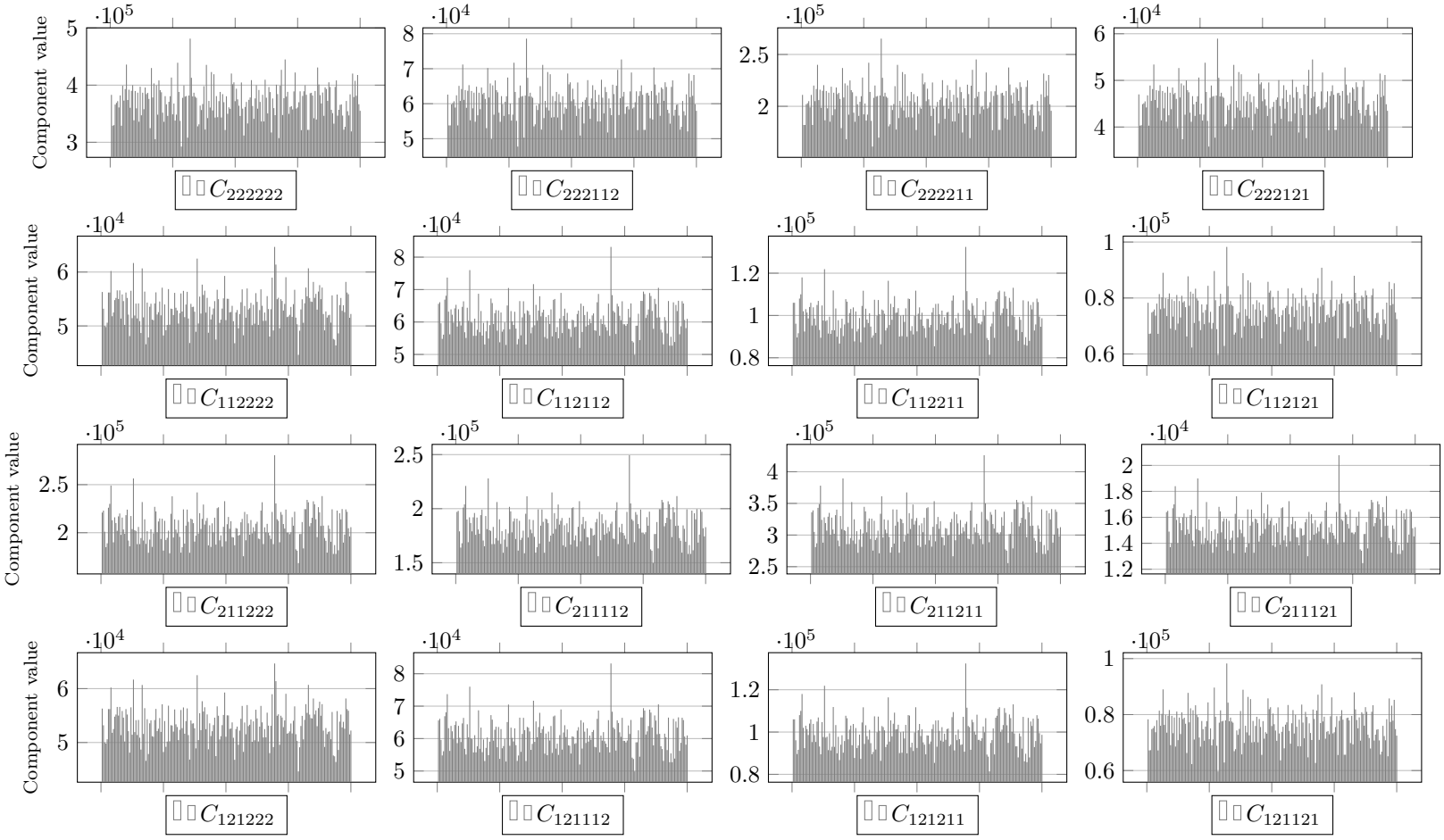

Figure A.36: Distribution study: components of the constitutive operator C_{ijklmn} - rows and columns 13 to 16 of the constitutive matrix (microcontinuum 70 mm)

A.7 Microcontinuum of size 80 mm

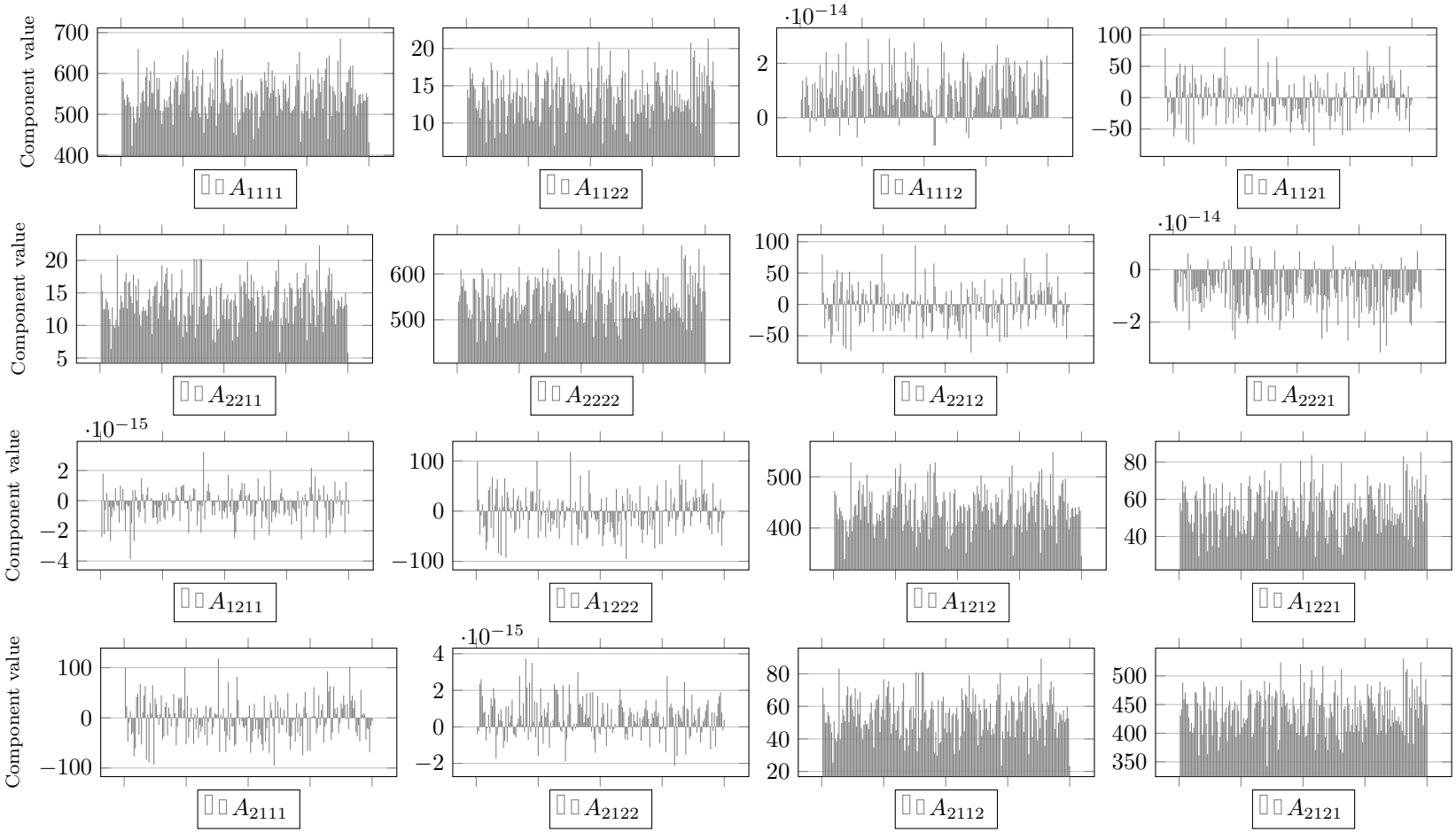

Figure A.37: Distribution study: components of the constitutive operator A_{ijkl} (microcontinuum 80 mm)

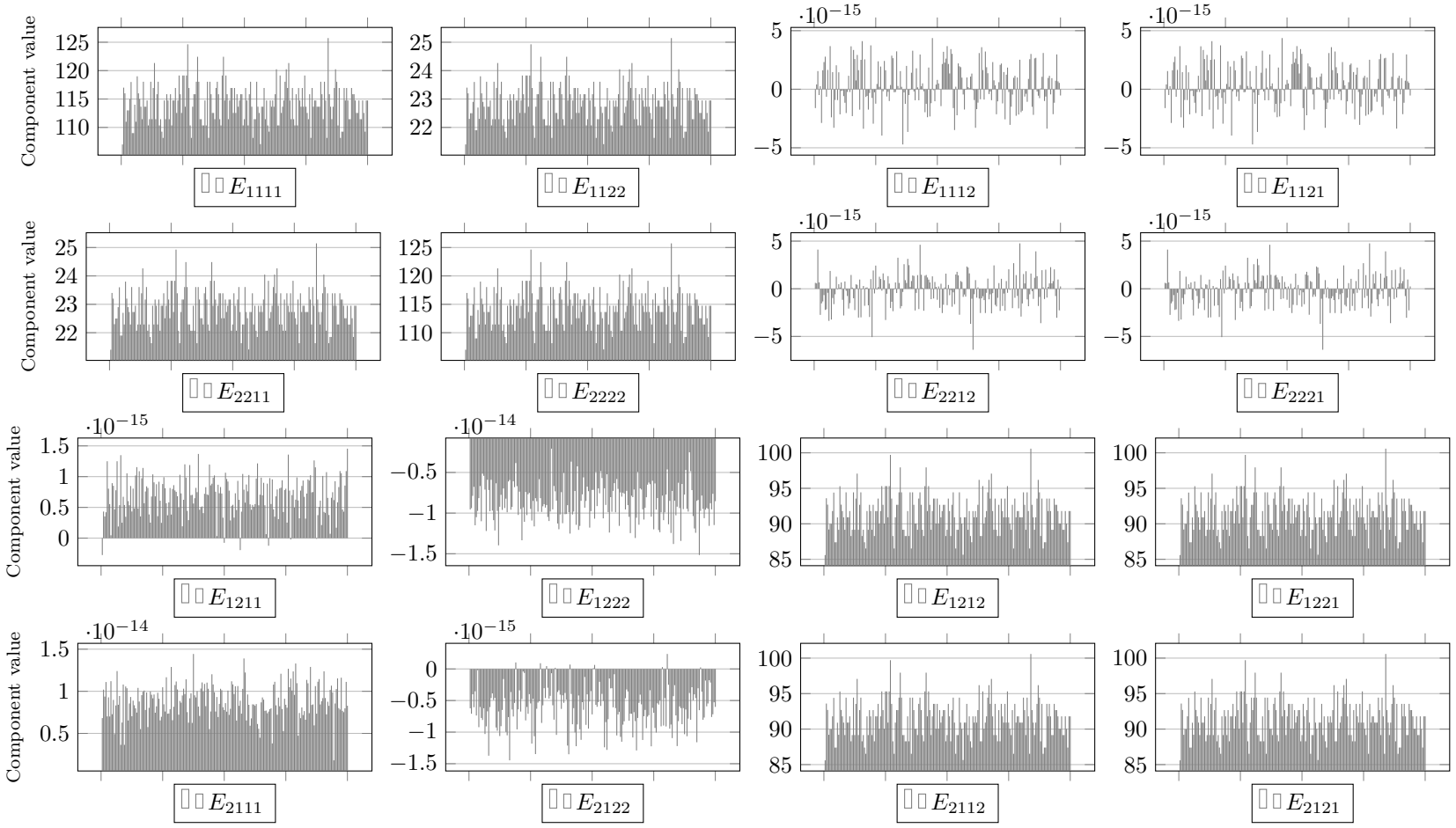

Figure A.38: Distribution study: components of the constitutive operator E_{ijkl} (microcontinuum 80 mm)

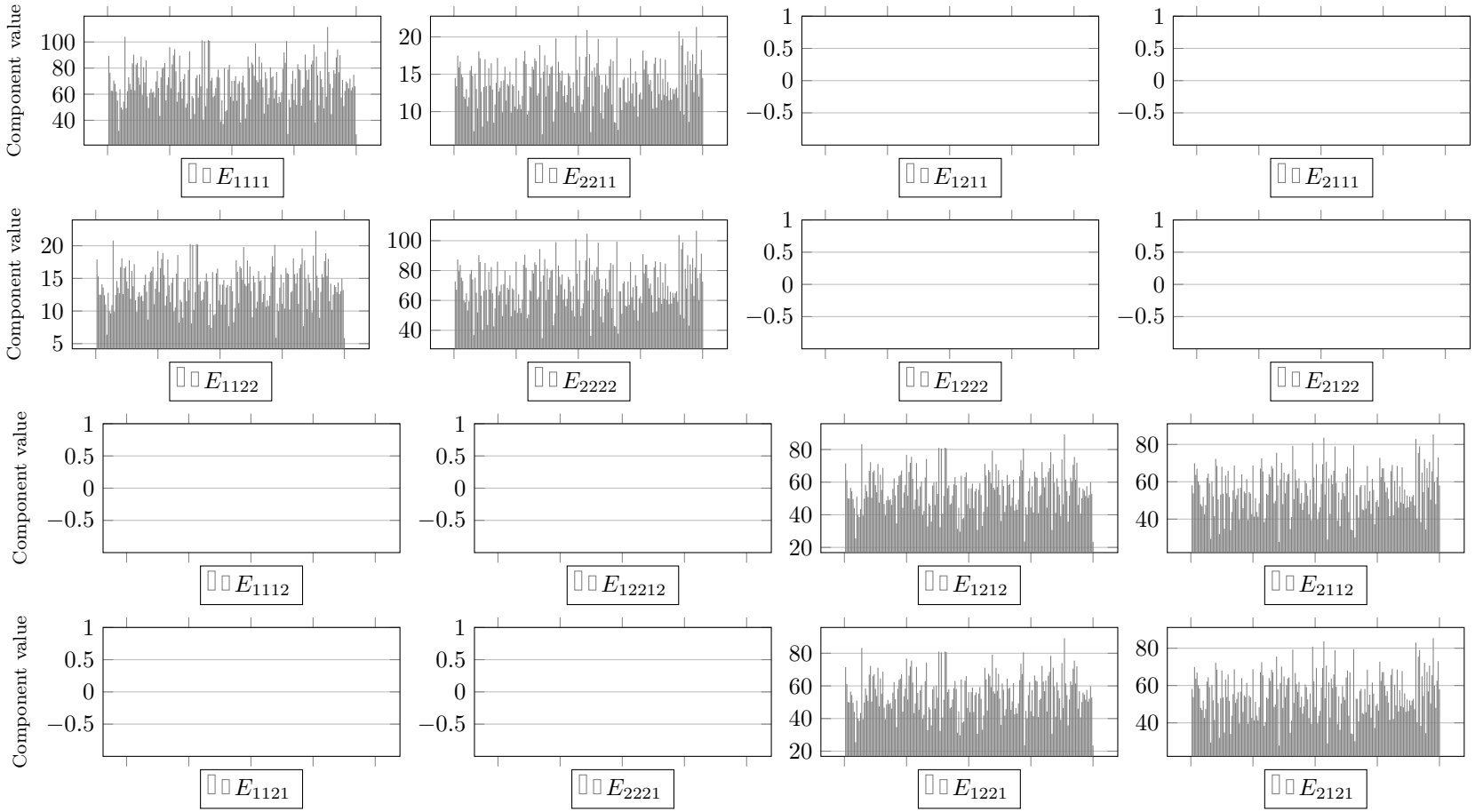

Figure A.39: Distribution study: components of the constitutive operator E_{klij} (microcontinuum 80 mm)

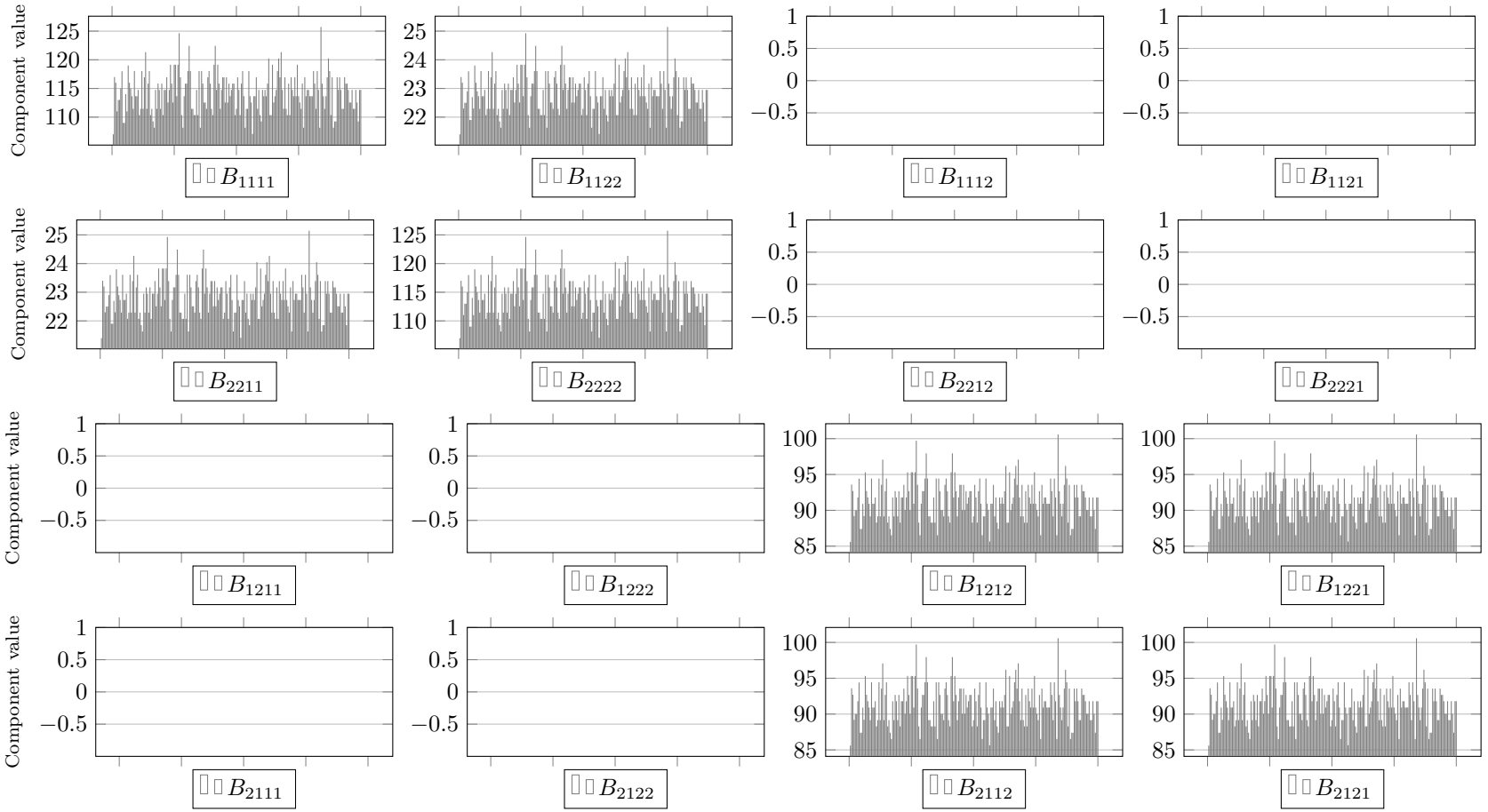

Figure A.40: Distribution study: components of the constitutive operator B_{ijkl} (microcontinuum 80 mm)

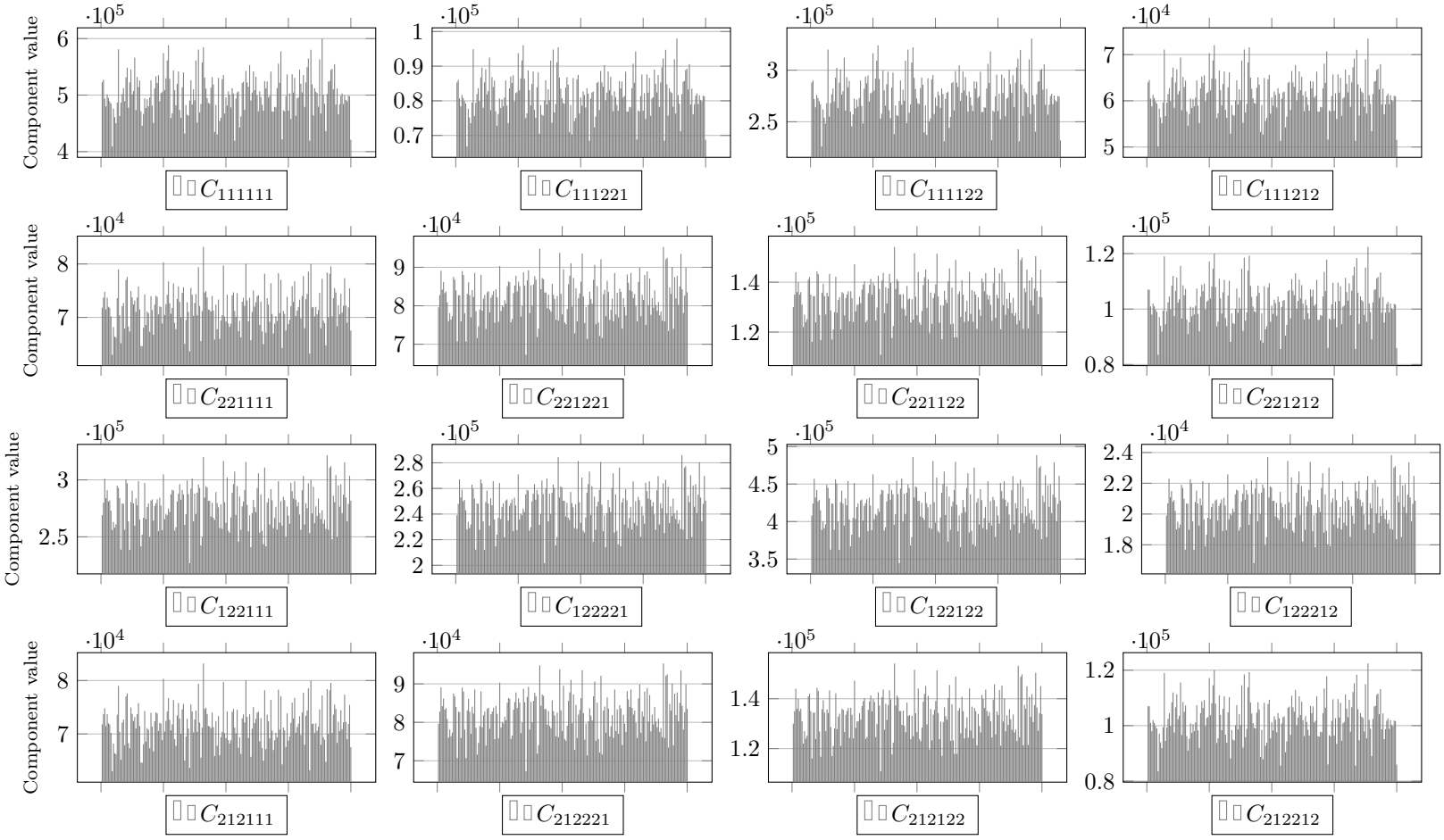

Figure A.41: Distribution study: components of the constitutive operator C_{ijklmn} - rows and columns 9 to 12 of the constitutive matrix (microcontinuum 80 mm)

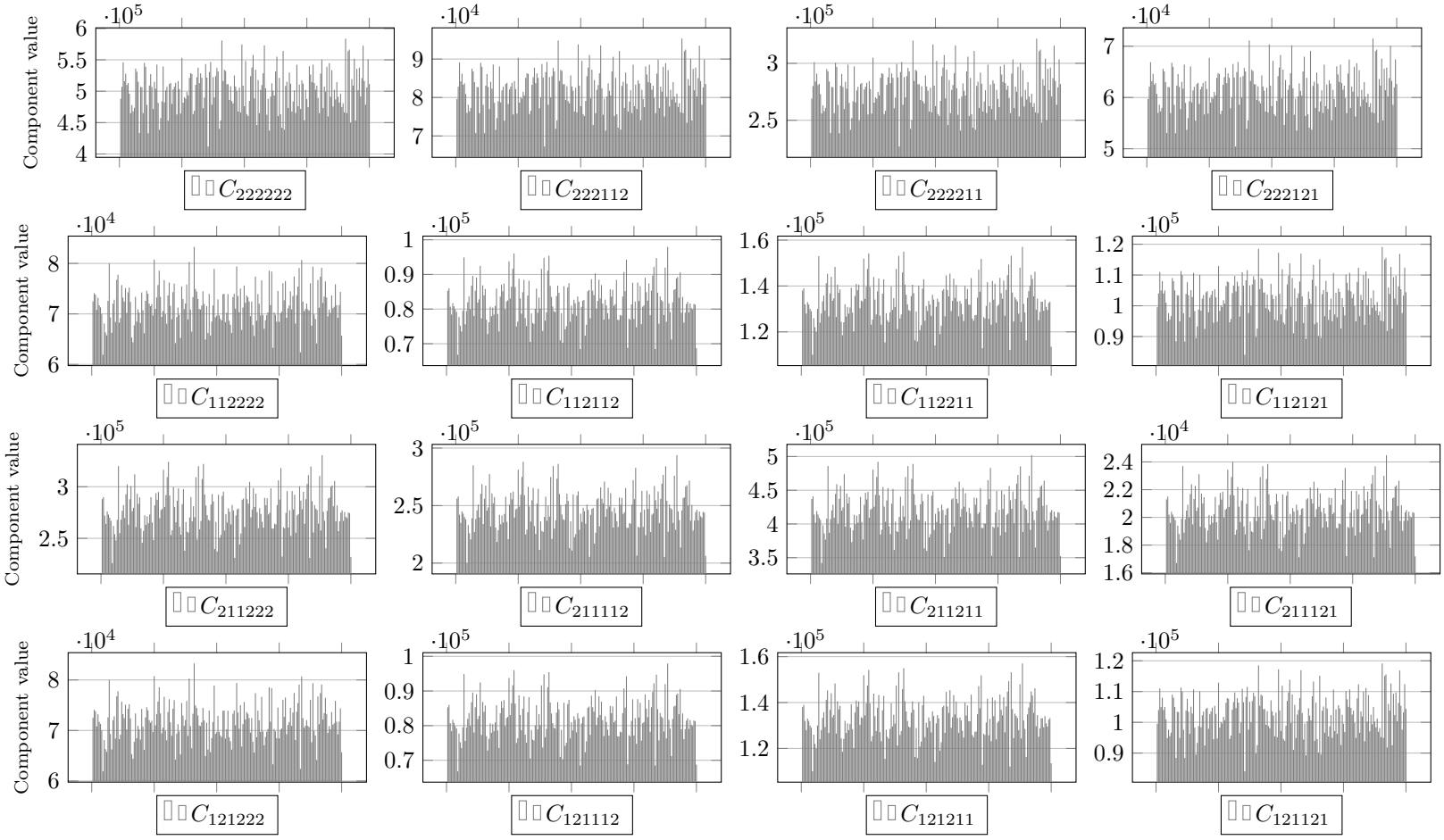

Figure A.42: Distribution study: components of the constitutive operator C_{ijklmn} - rows and columns 13 to 16 of the constitutive matrix (microcontinuum 80 mm)

A.8 Microcontinuum of size 90 mm

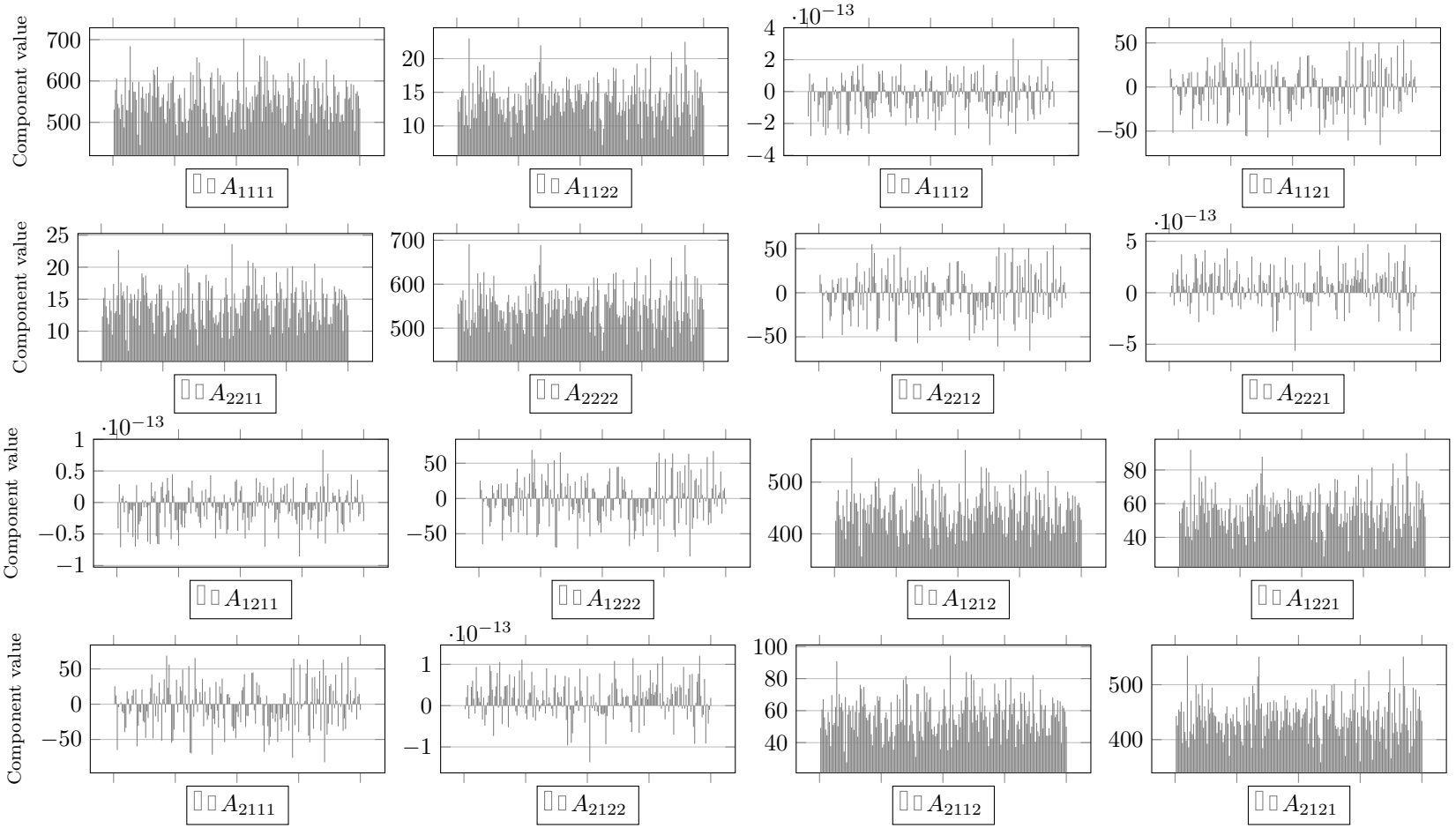

Figure A.43: Distribution study: components of the constitutive operator A_{ijkl} (microcontinuum 90 mm)

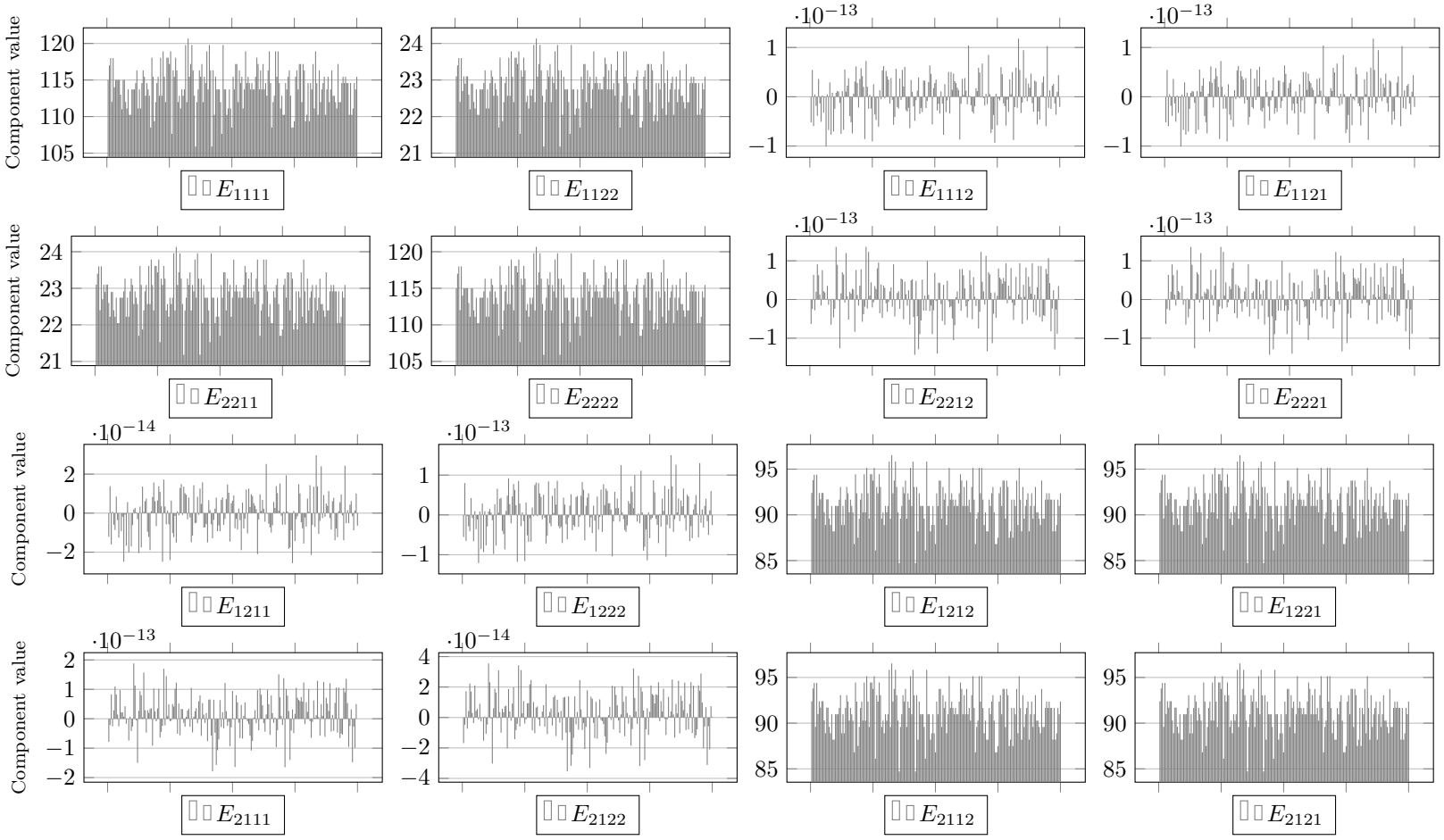

Figure A.44: Distribution study: components of the constitutive operator E_{ijkl} (microcontinuum 90 mm)

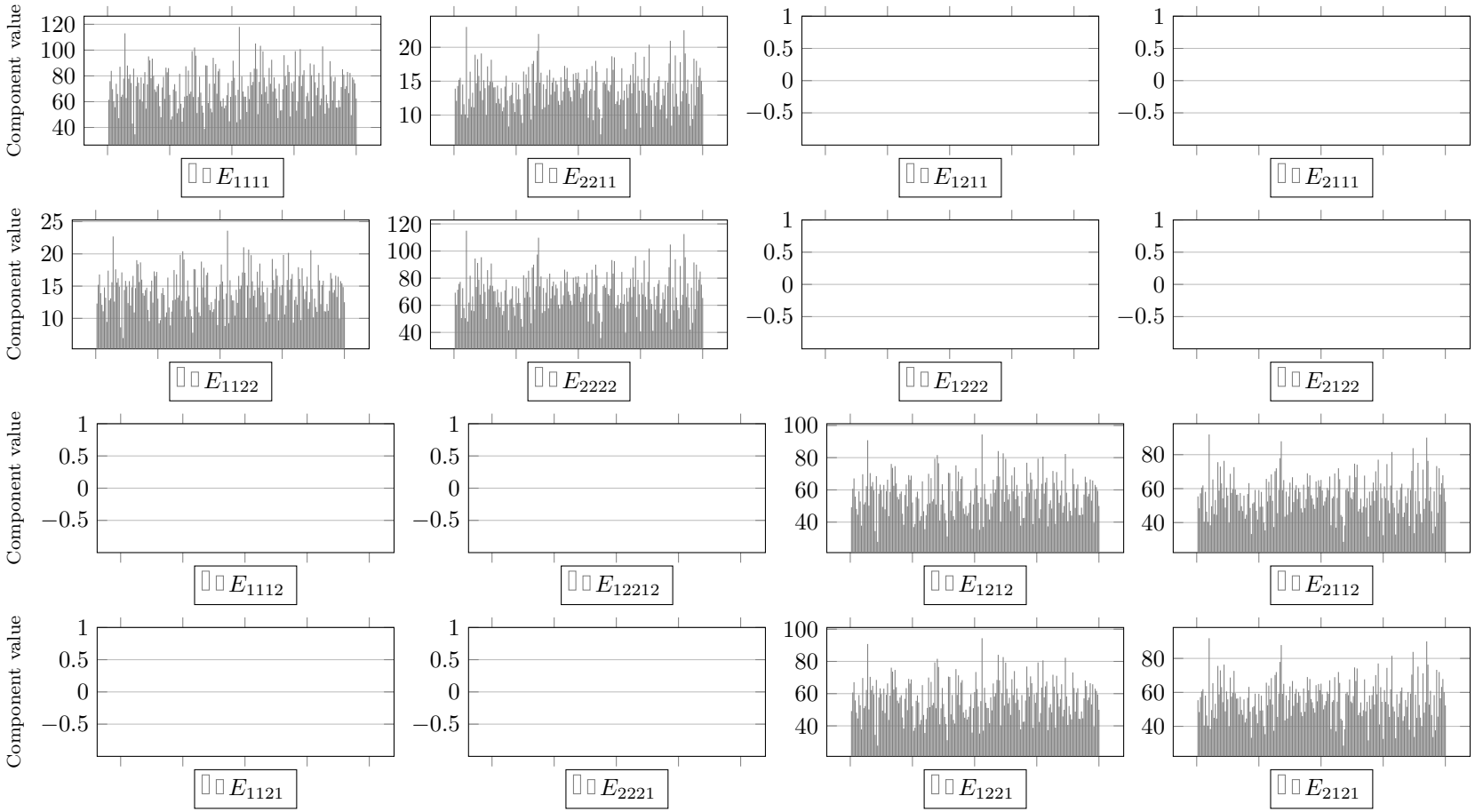

Figure A.45: Distribution study: components of the constitutive operator E_{klij} (microcontinuum 90 mm)

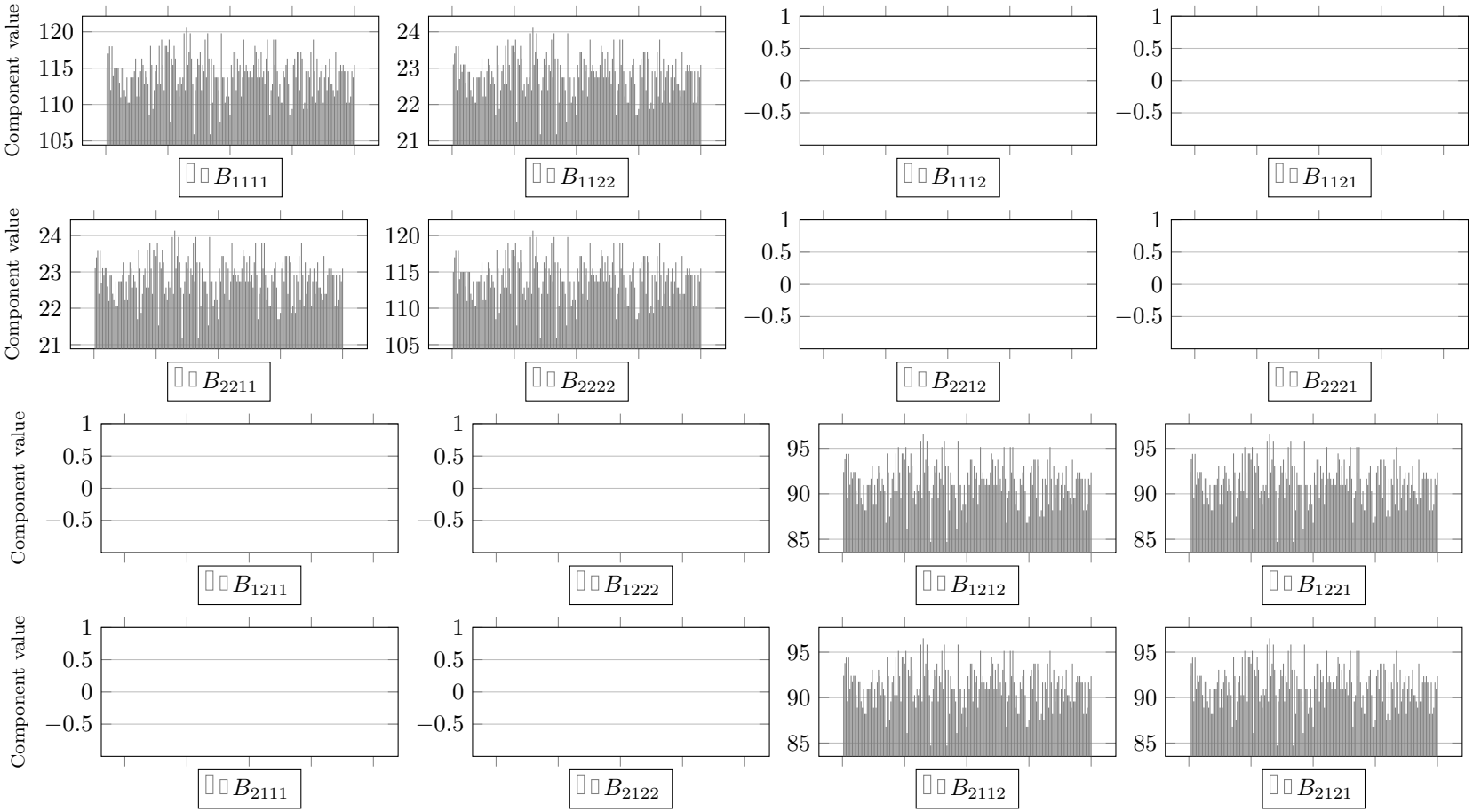

Figure A.46: Distribution study: components of the constitutive operator B_{ijkl} (microcontinuum 90 mm)

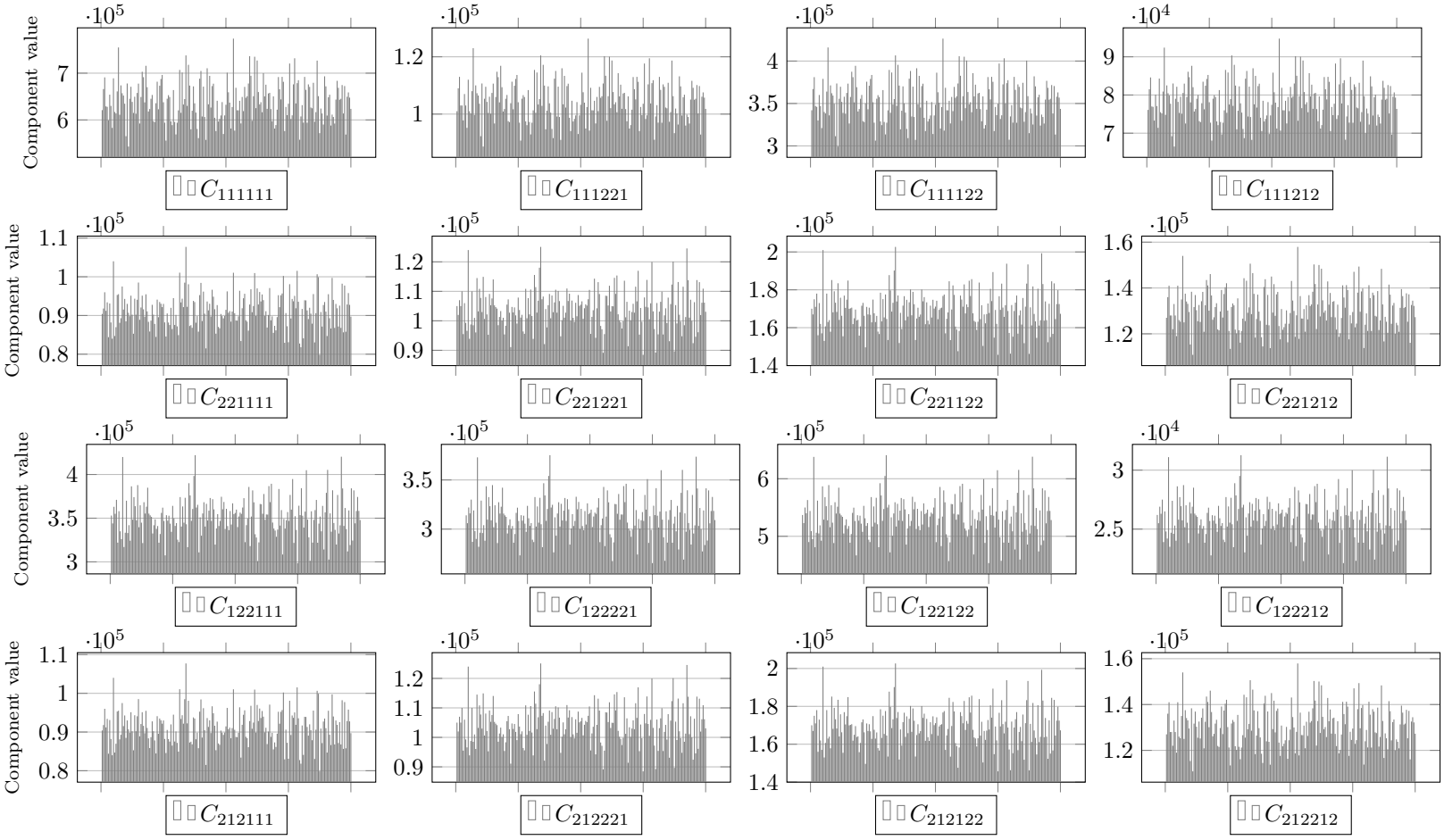

Figure A.47: Distribution study: components of the constitutive operator C_{ijklmn} - rows and columns 9 to 12 of the constitutive matrix (microcontinuum 90 mm)

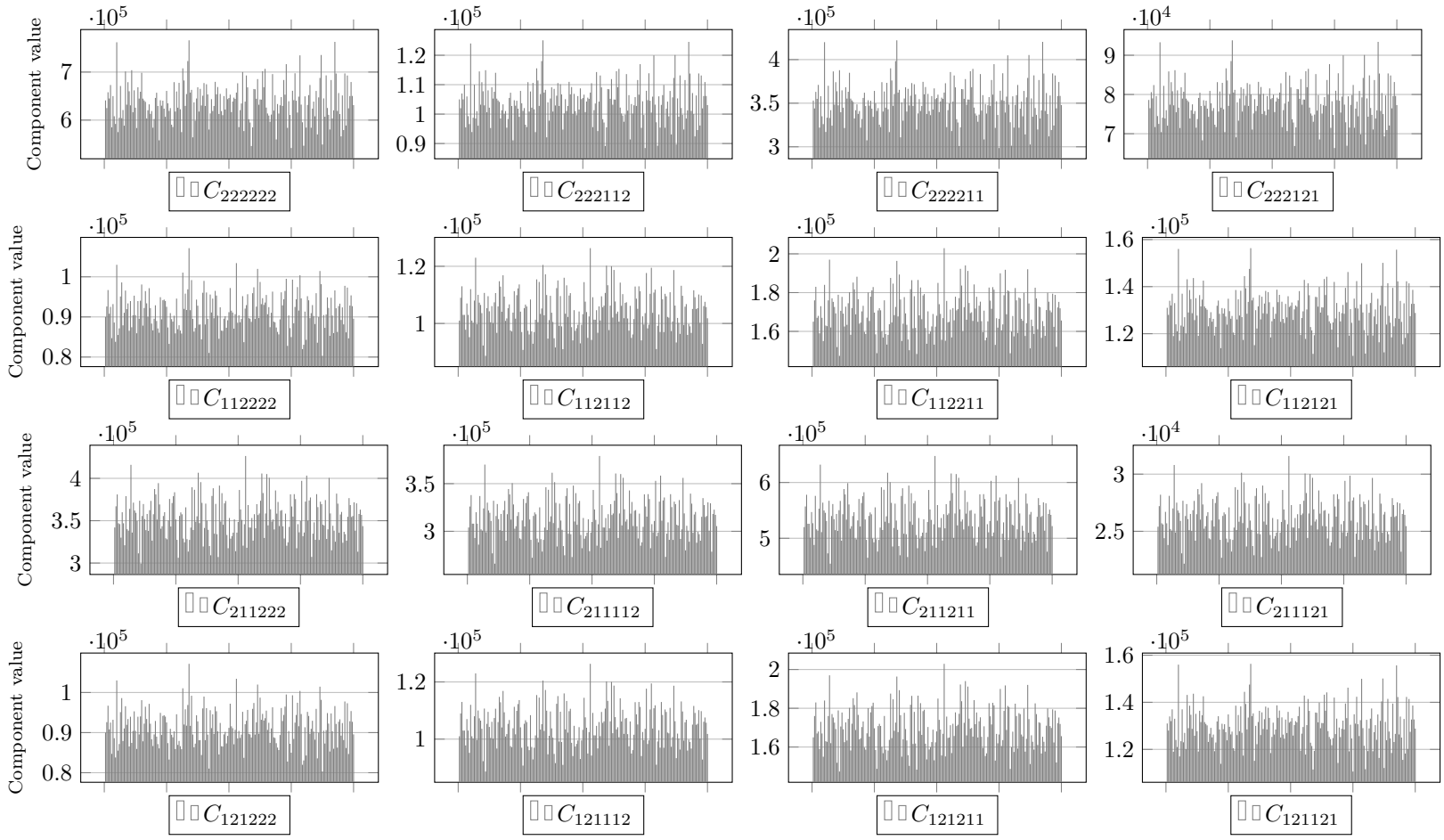

Figure A.48: Distribution study: components of the constitutive operator C_{ijklmn} - rows and columns 13 to 16 of the constitutive matrix (microcontinuum 90 mm)

A.9 Microcontinuum of size 110 mm

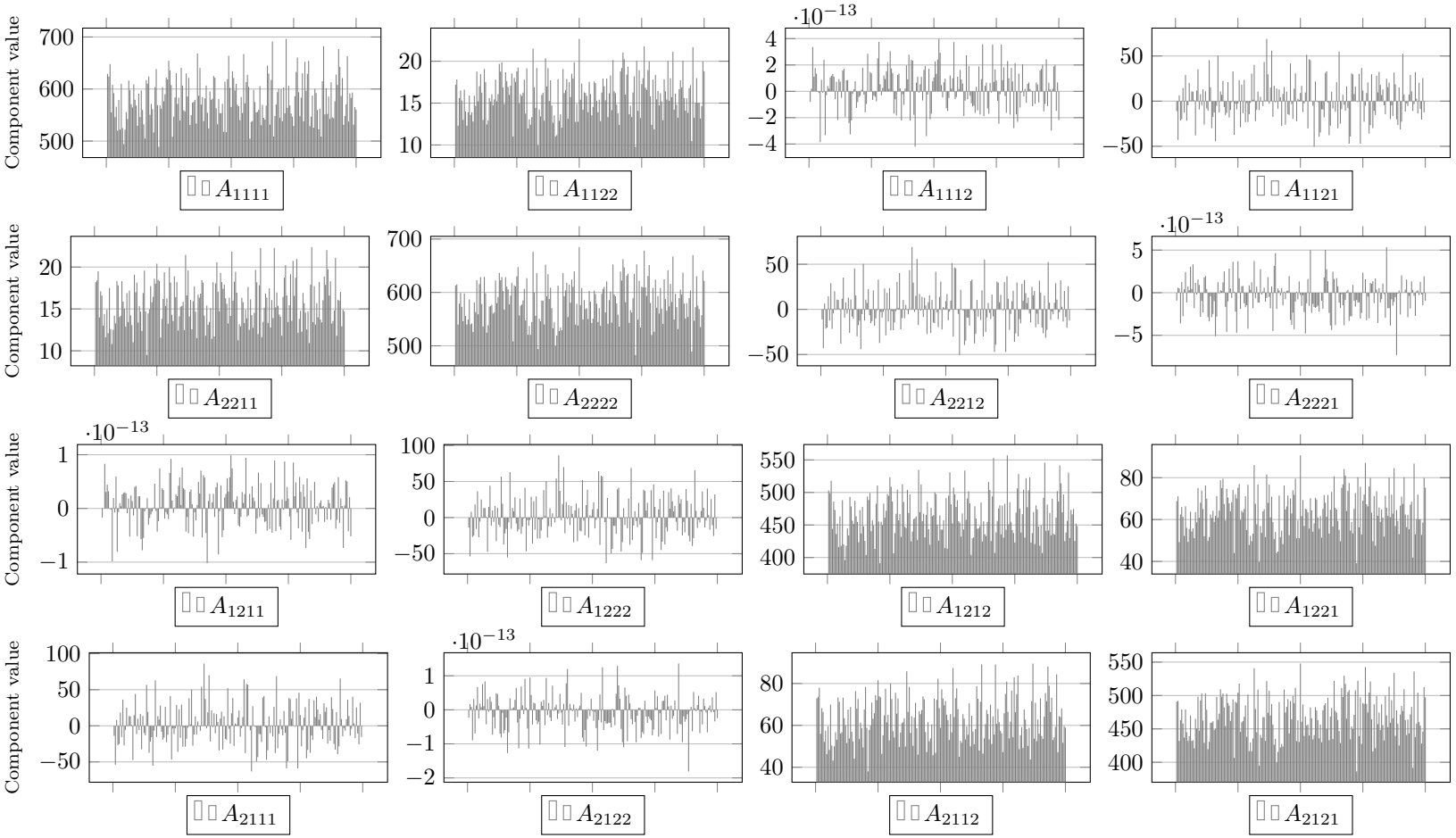

Figure A.49: Distribution study: components of the constitutive operator A_{ijkl} (microcontinuum 110 mm)

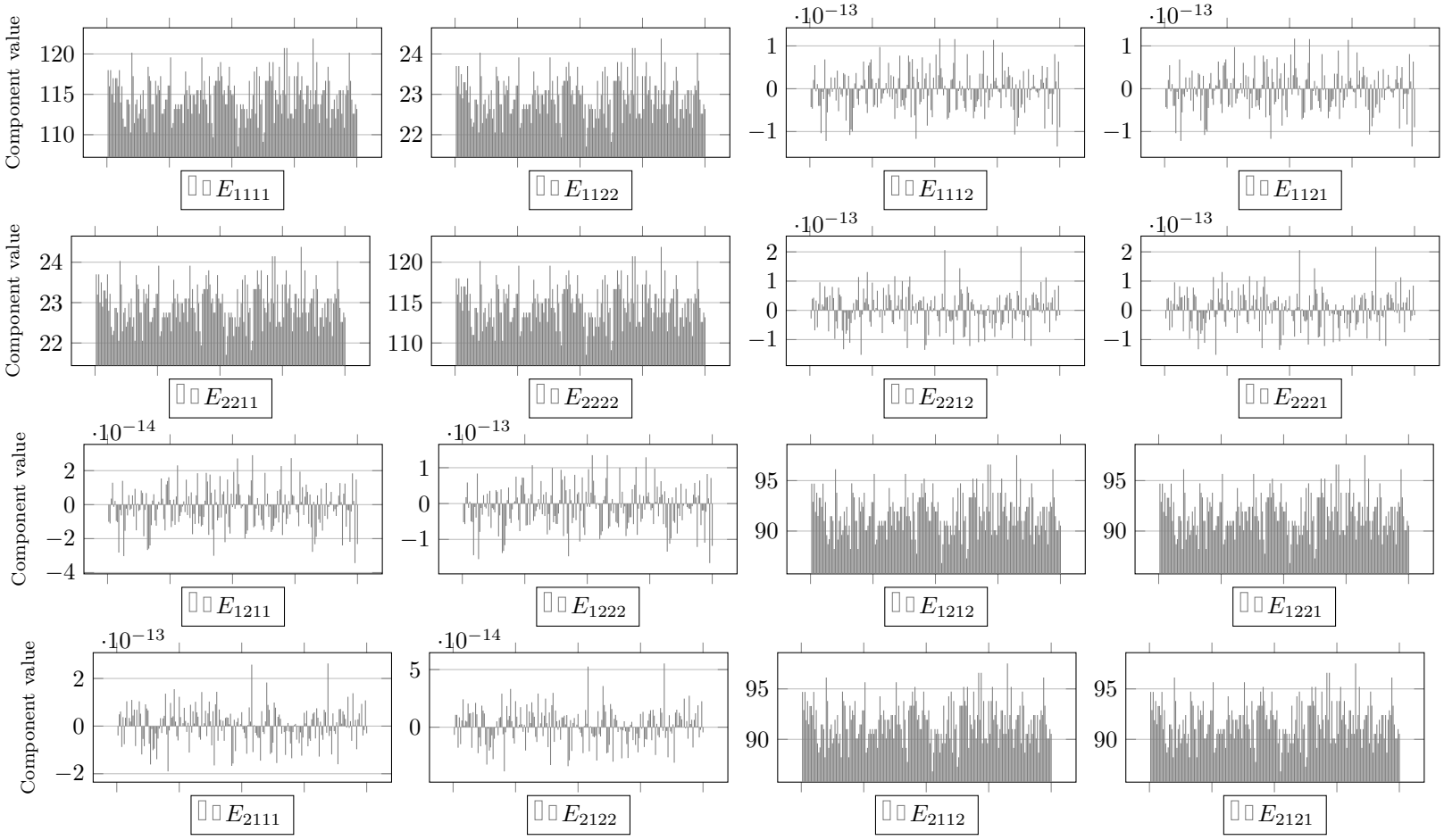

Figure A.50: Distribution study: components of the constitutive operator E_{ijkl} (microcontinuum 110 mm)

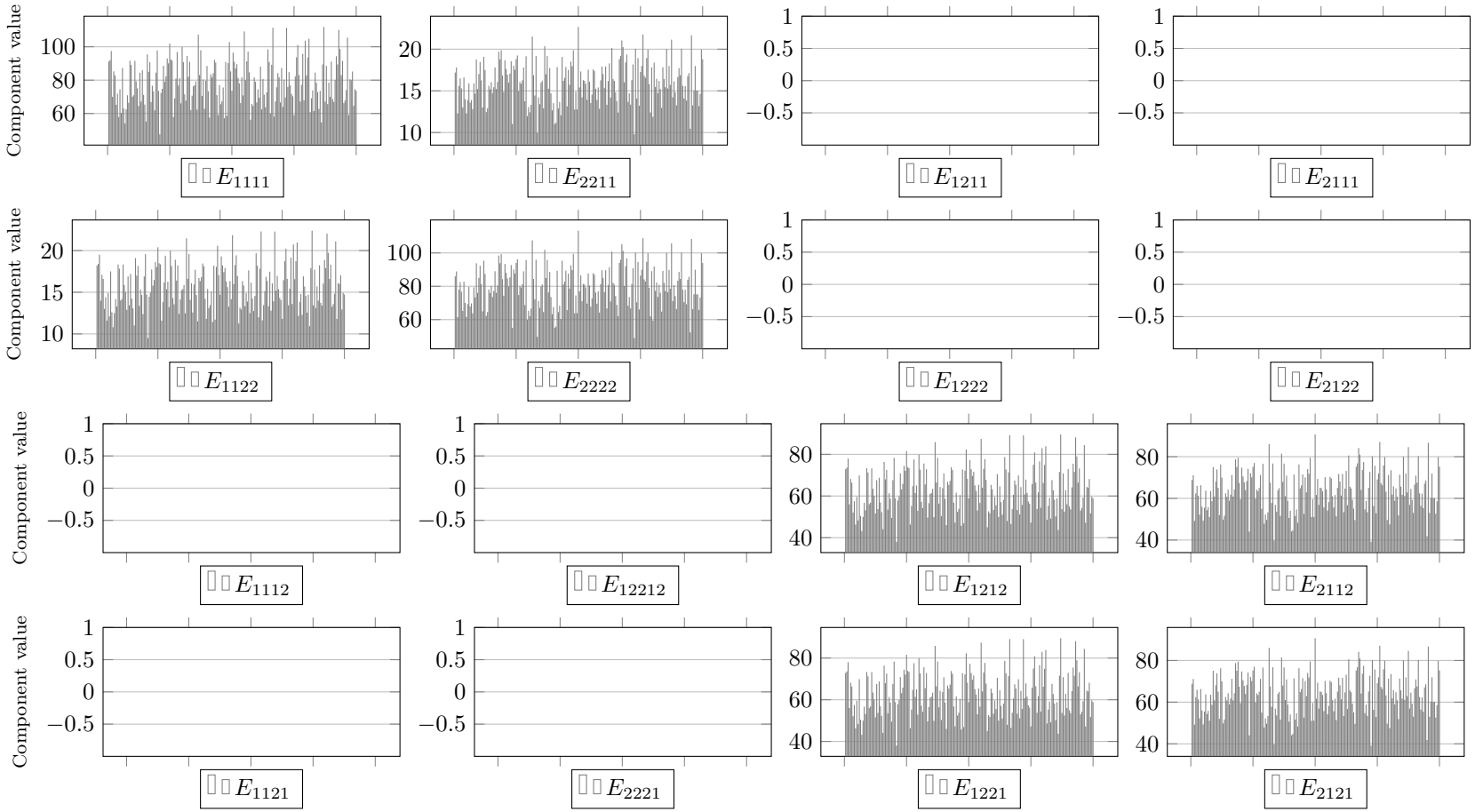

Figure A.51: Distribution study: components of the constitutive operator E_{klij} (microcontinuum 110 mm)

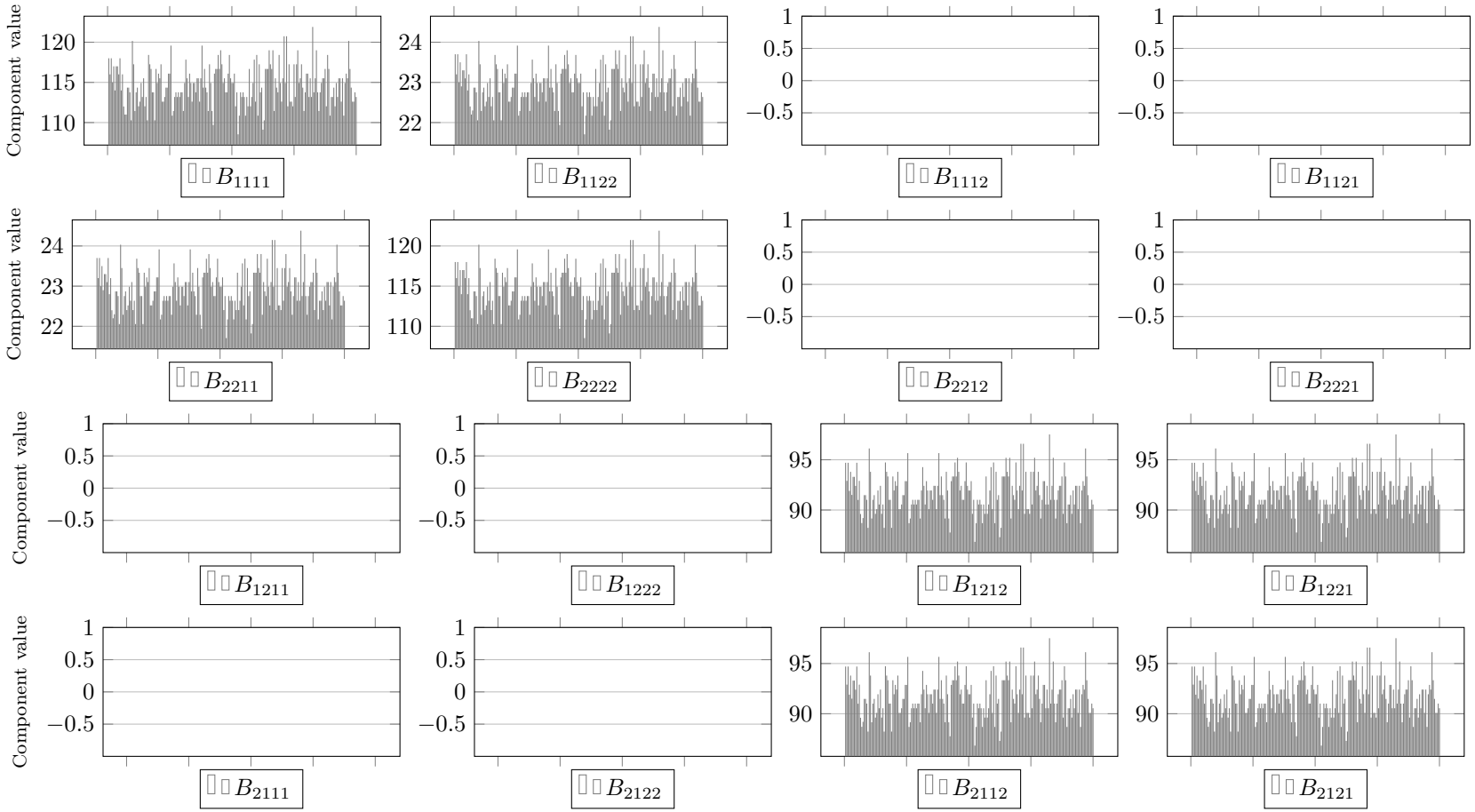

Figure A.52: Distribution study: components of the constitutive operator B_{ijkl} (microcontinuum 110 mm)

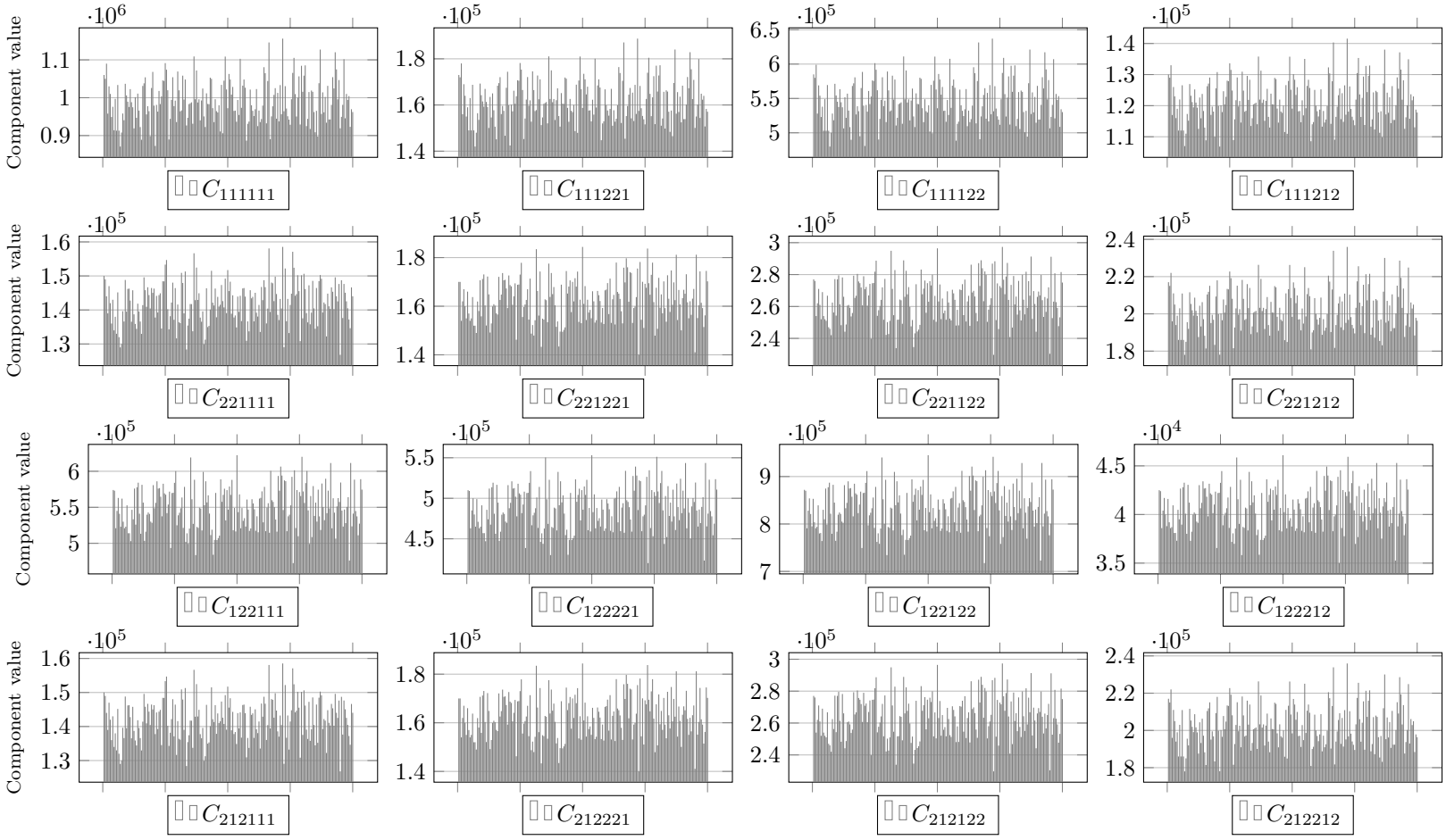

Figure A.53: Distribution study: components of the constitutive operator C_{ijklmn} - rows and columns 9 to 12 of the constitutive matrix (microcontinuum 110 mm)

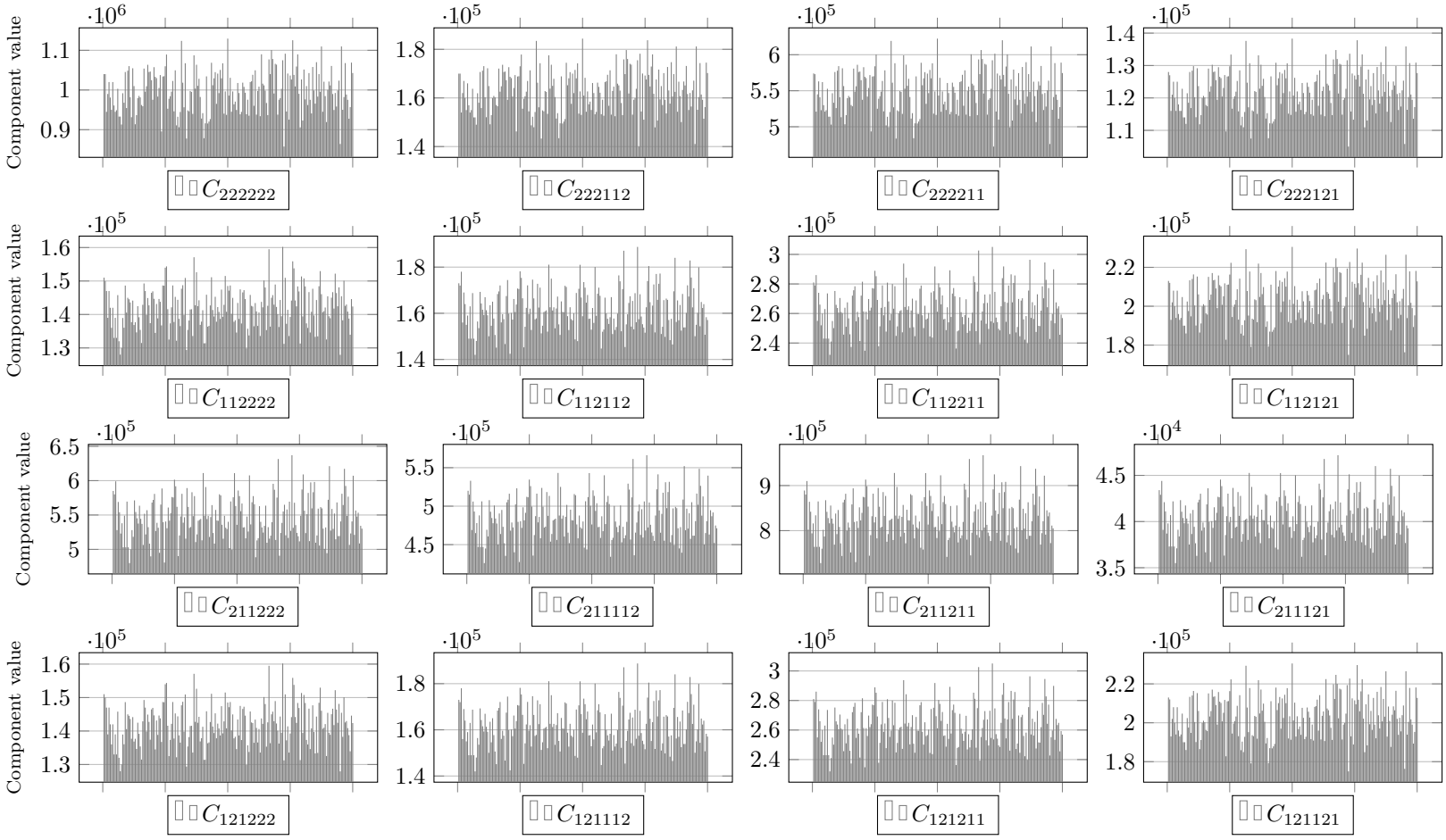

Figure A.54: Distribution study: components of the constitutive operator C_{ijklmn} - rows and columns 13 to 16 of the constitutive matrix (microcontinuum 110 mm)

A.10 Microcontinuum of size 120 mm

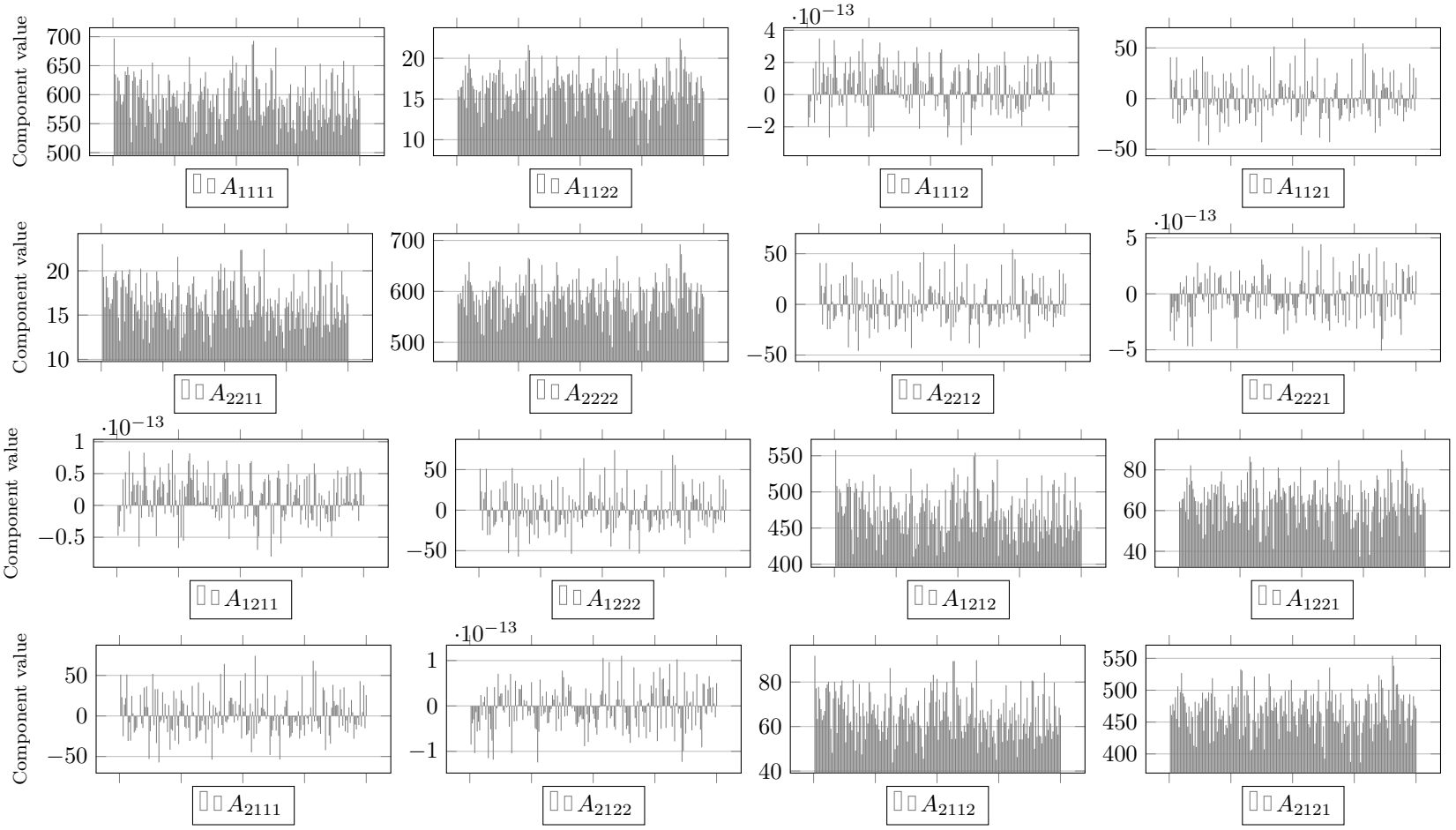

Figure A.55: Distribution study: components of the constitutive operator A_{ijkl} (microcontinuum 120 mm)

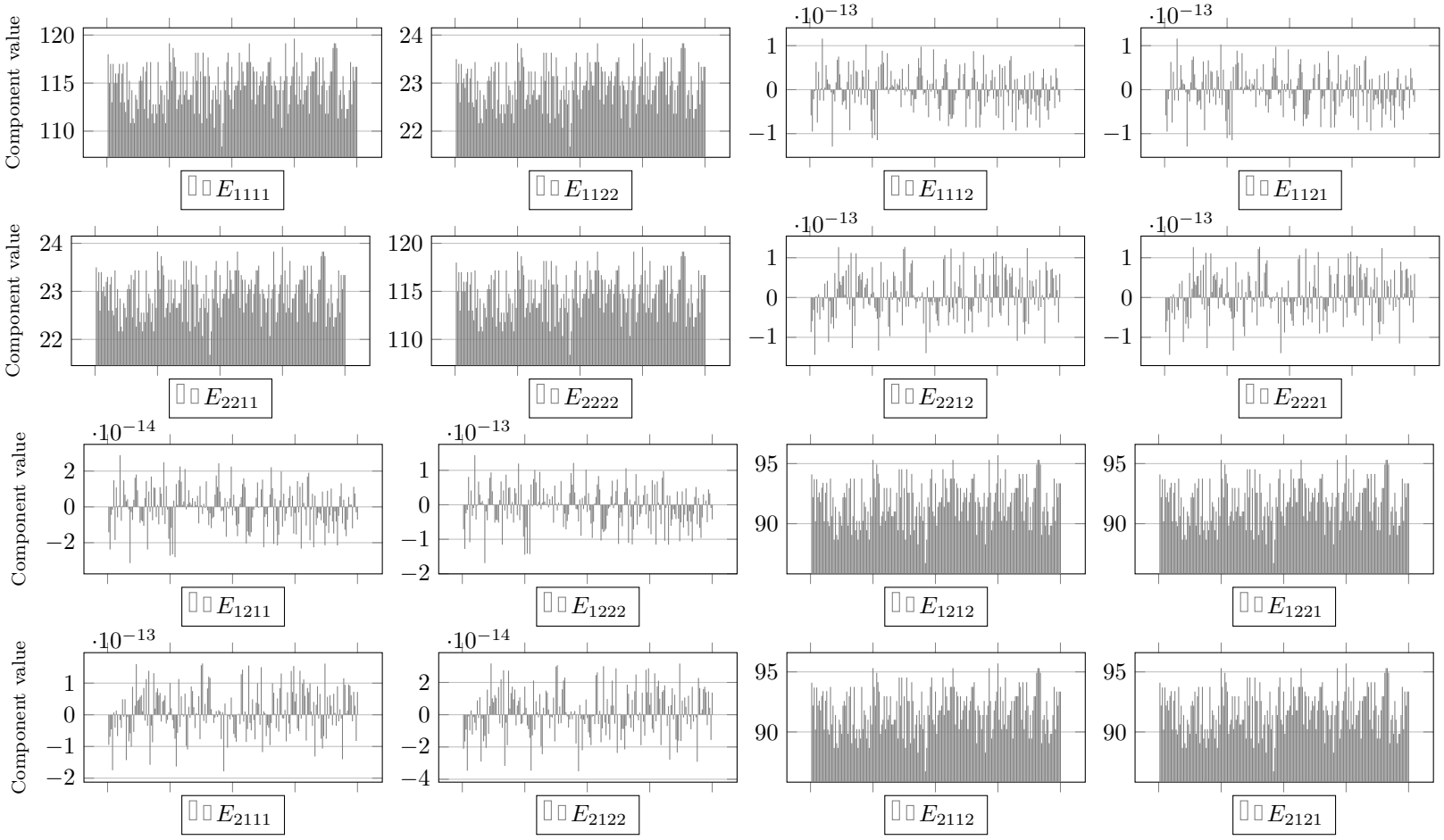

Figure A.56: Distribution study: components of the constitutive operator E_{ijkl} (microcontinuum 120 mm)

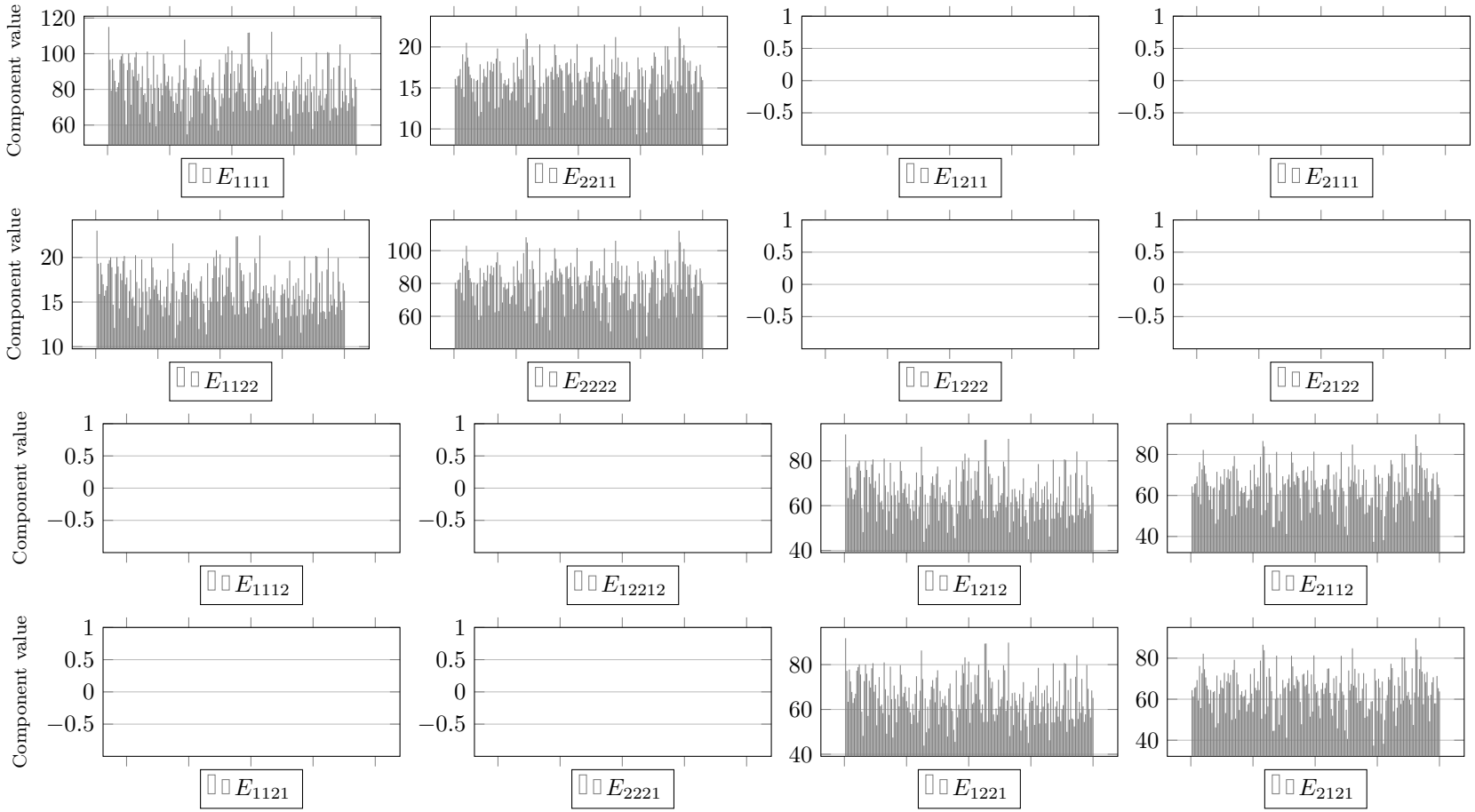

Figure A.57: Distribution study: components of the constitutive operator E_{klij} (microcontinuum 120 mm)

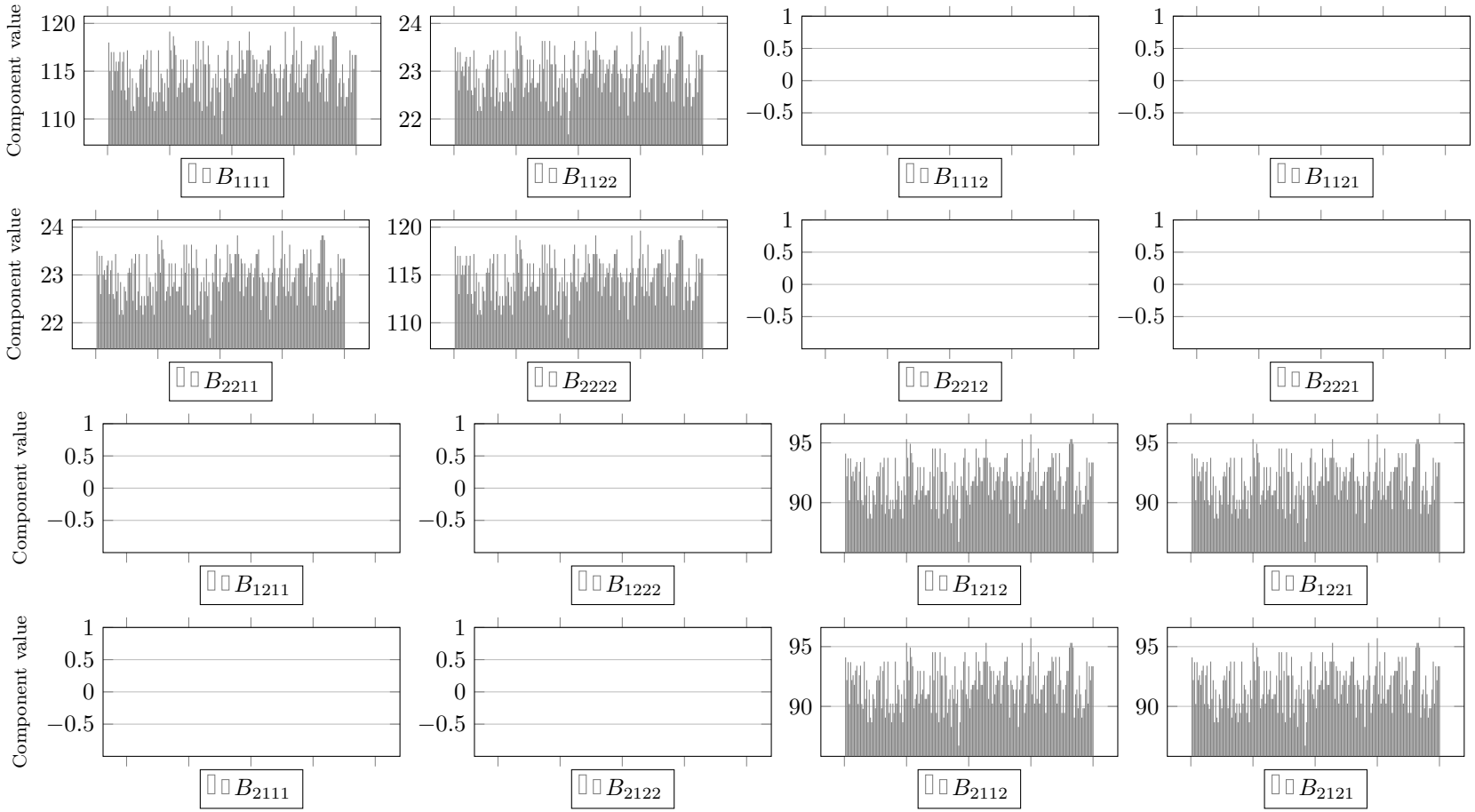

Figure A.58: Distribution study: components of the constitutive operator B_{ijkl} (microcontinuum 120 mm)

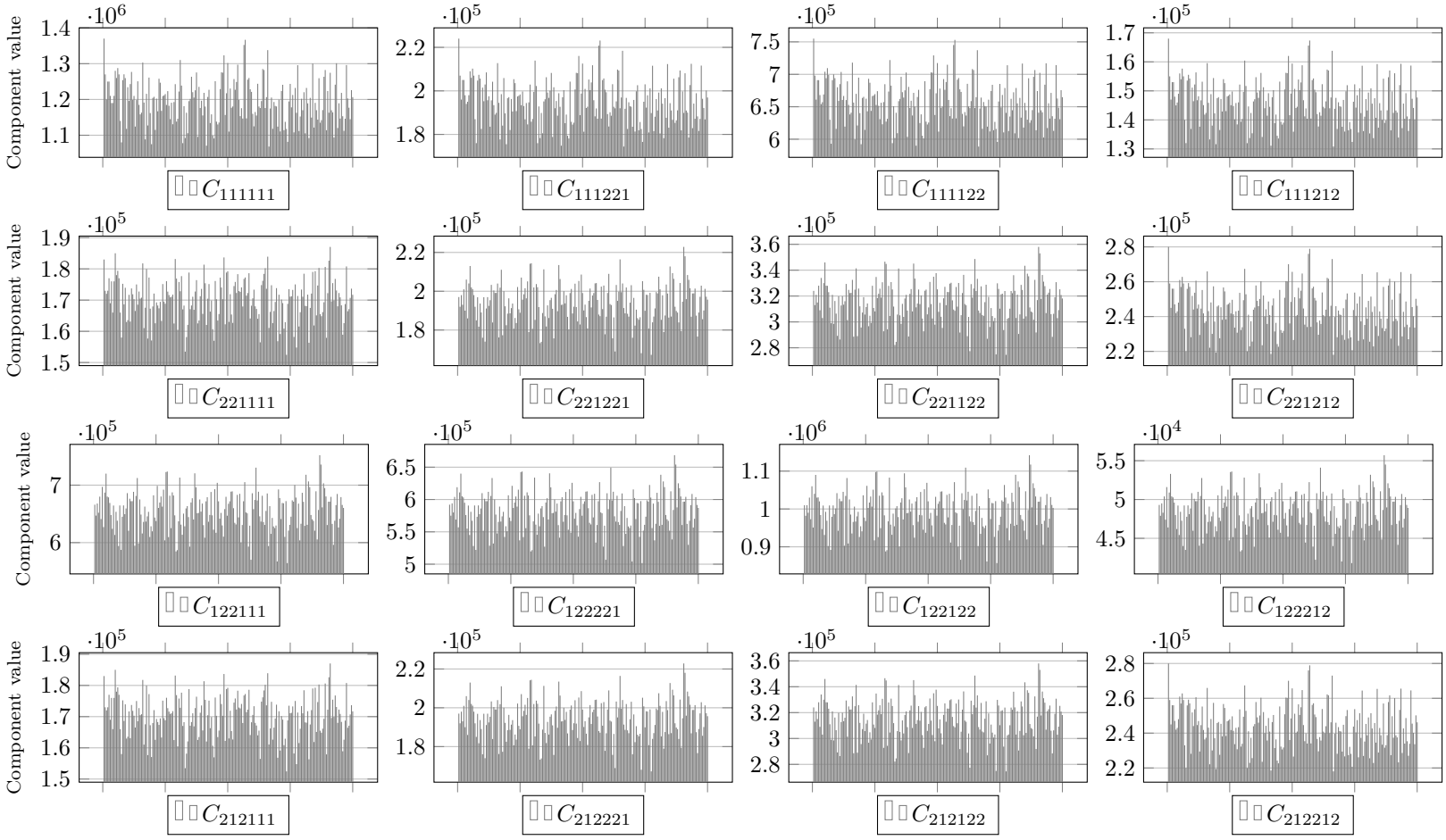

Figure A.59: Distribution study: components of the constitutive operator C_{ijklmn} - rows and columns 9 to 12 of the constitutive matrix (microcontinuum 120 mm)

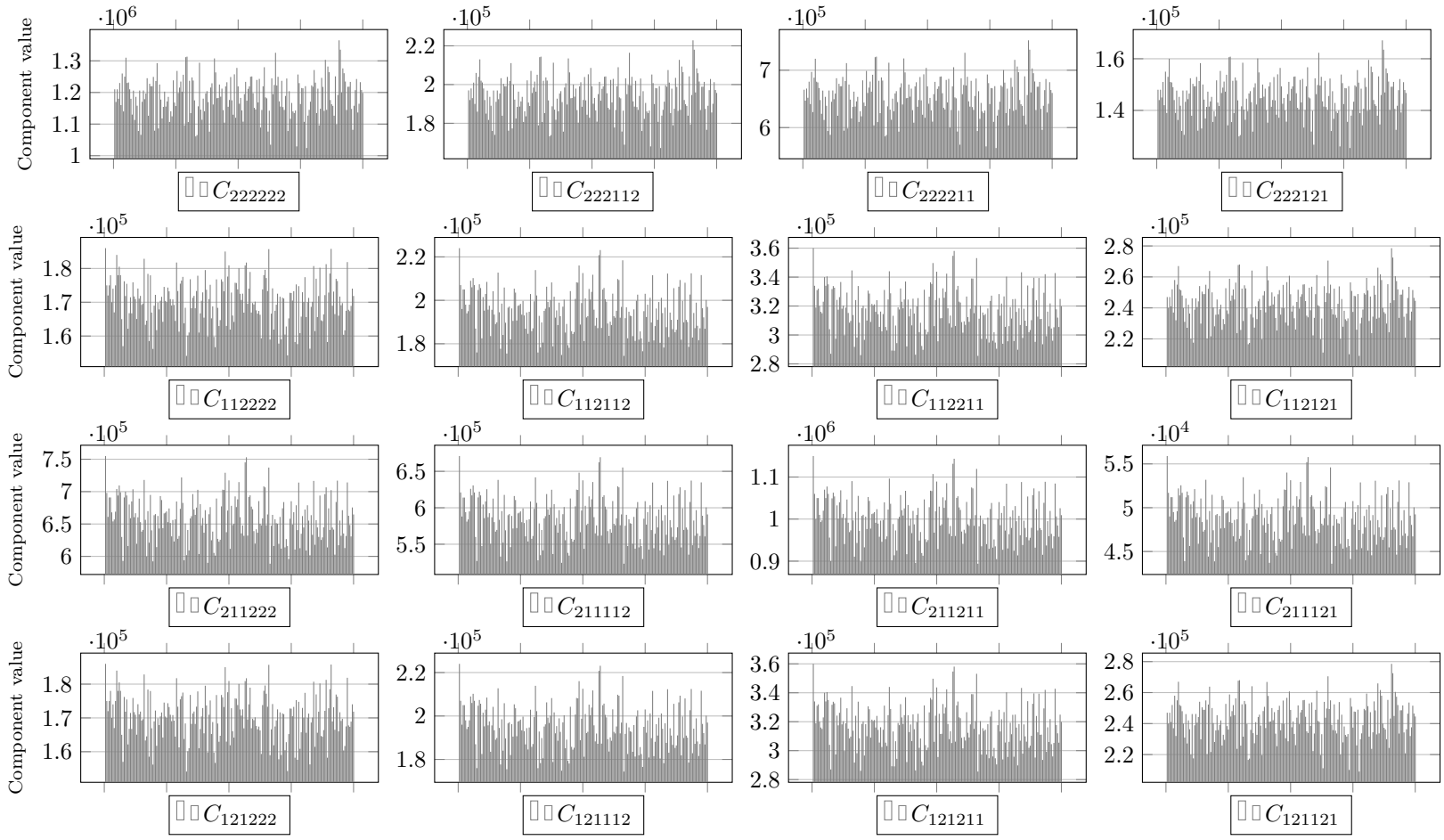

Figure A.60: Distribution study: components of the constitutive operator C_{ijklmn} - rows and columns 13 to 16 of the constitutive matrix (microcontinuum 120 mm)

A.11 Standard deviation results

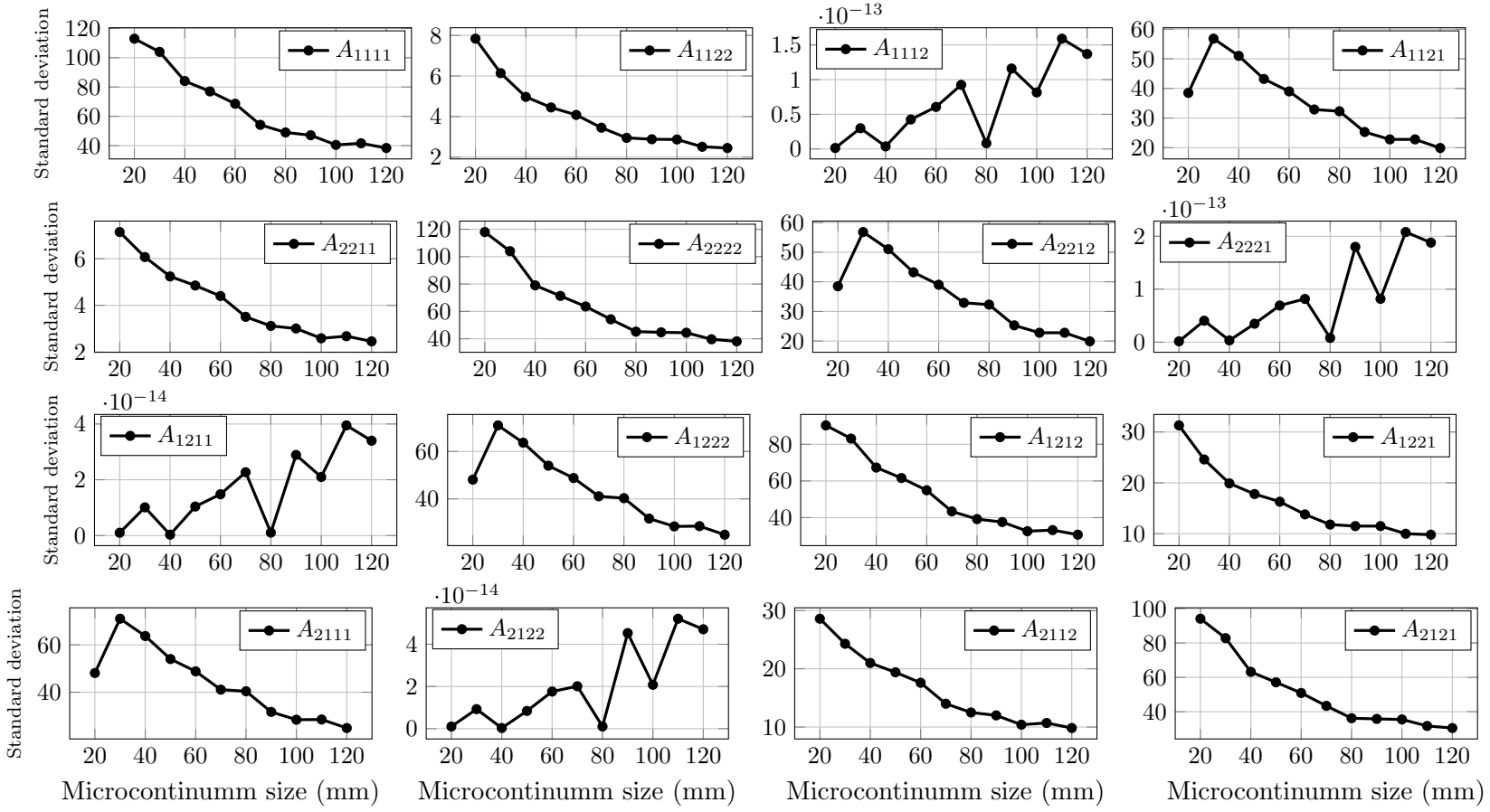

Figure A.61: Distribution study: standard deviation of the components of the constitutive operator A_{ijkl} versus microcontinuum size

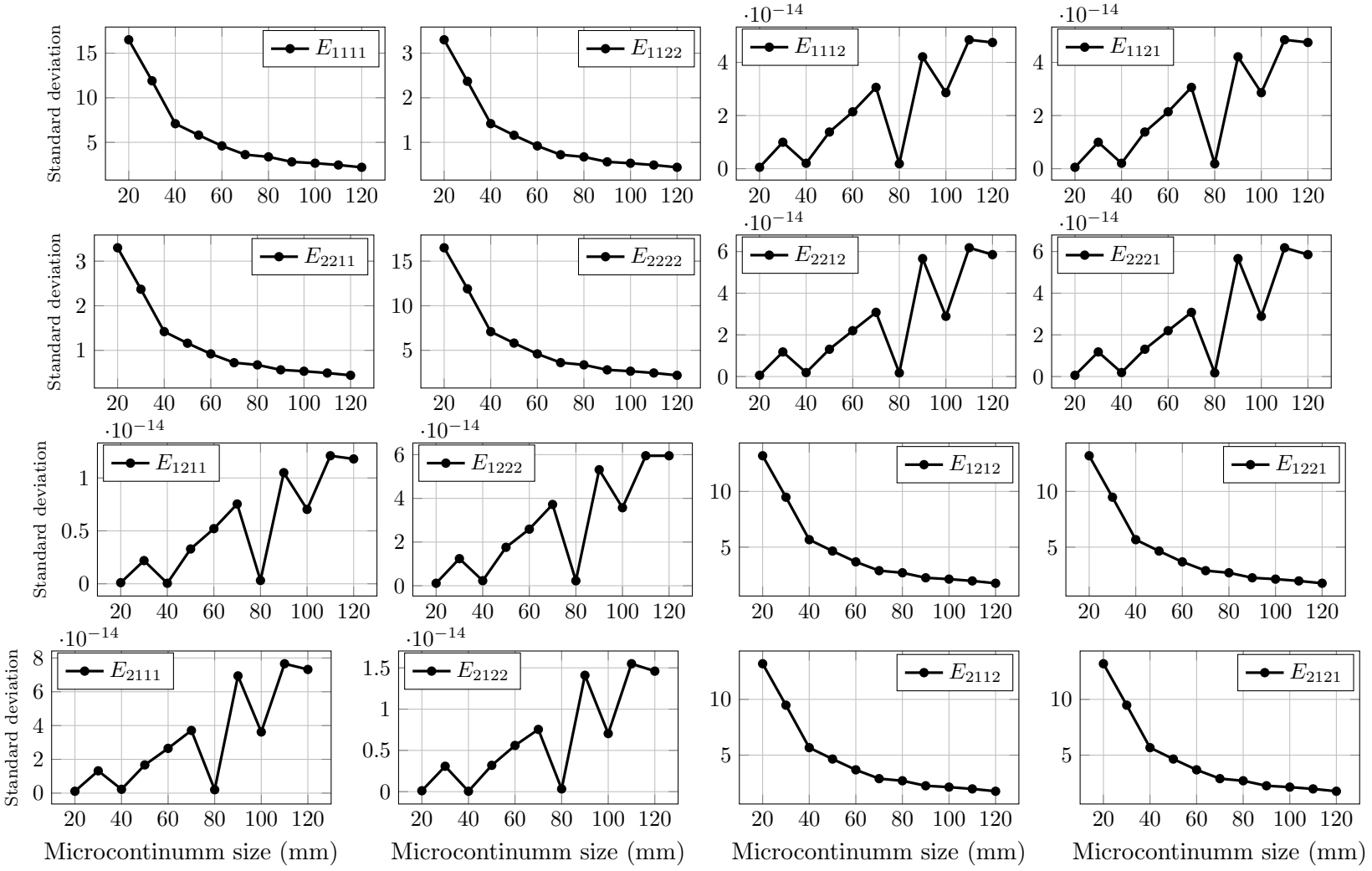

Figure A.62: Distribution study: standard deviation of the components of the constitutive operator E_{ijkl} versus microcontinuum size

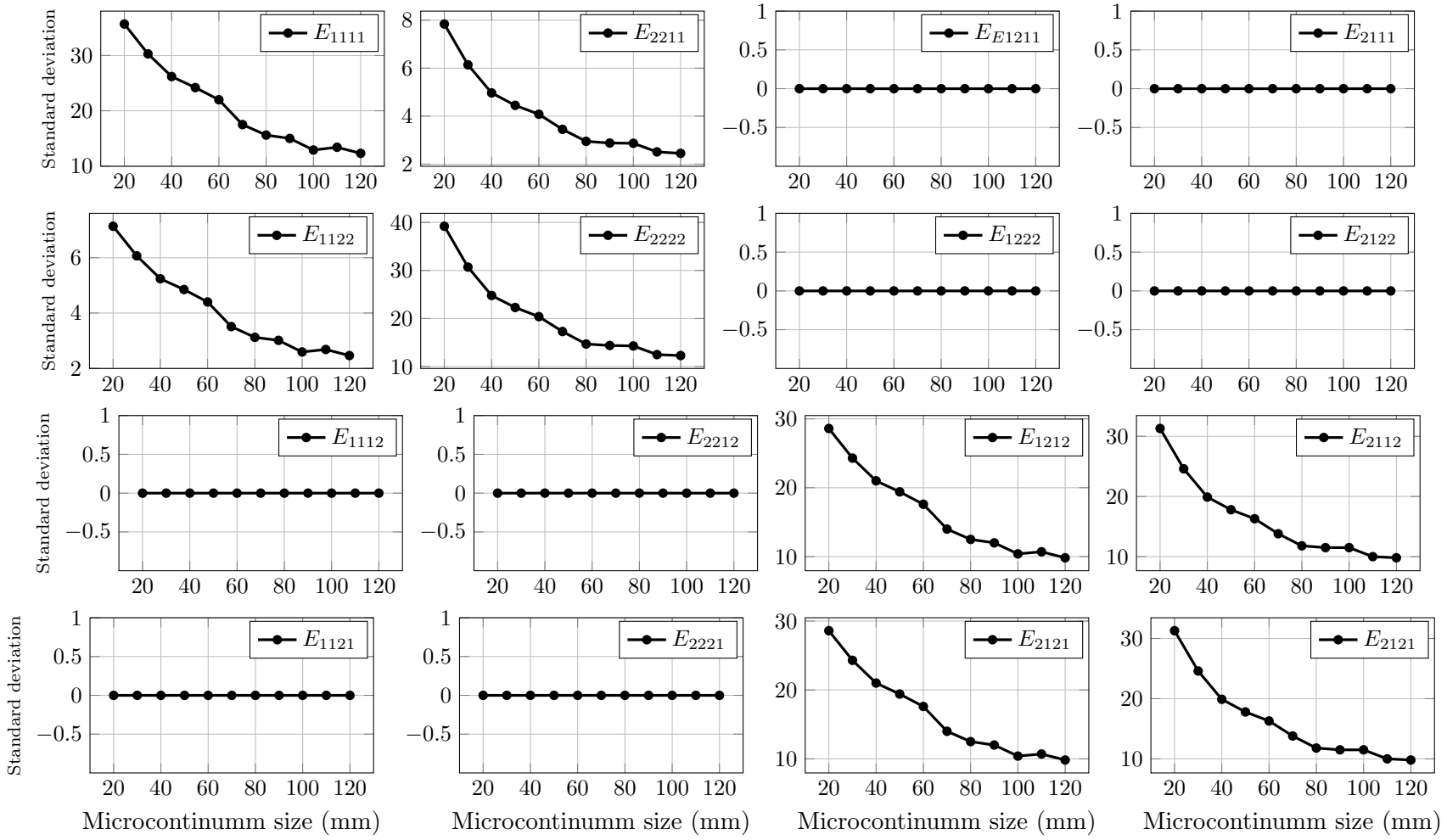

Figure A.63: Distribution study: standard deviation of the components of the constitutive operator E_{klij} versus microcontinuum size

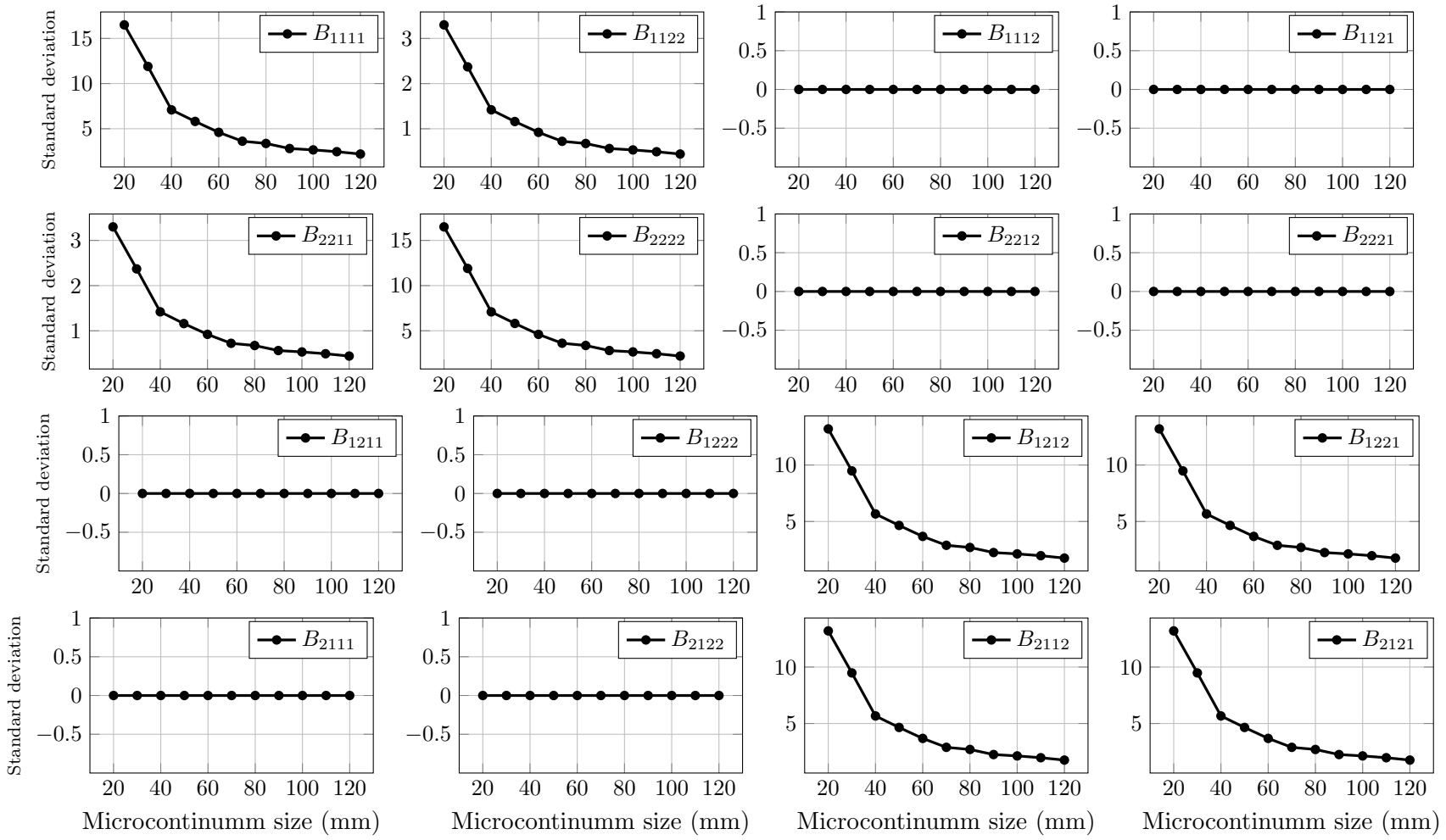

Figure A.64: Distribution study: standard deviation of the components of the constitutive operator B_{ijkl} versus microcontinuum size

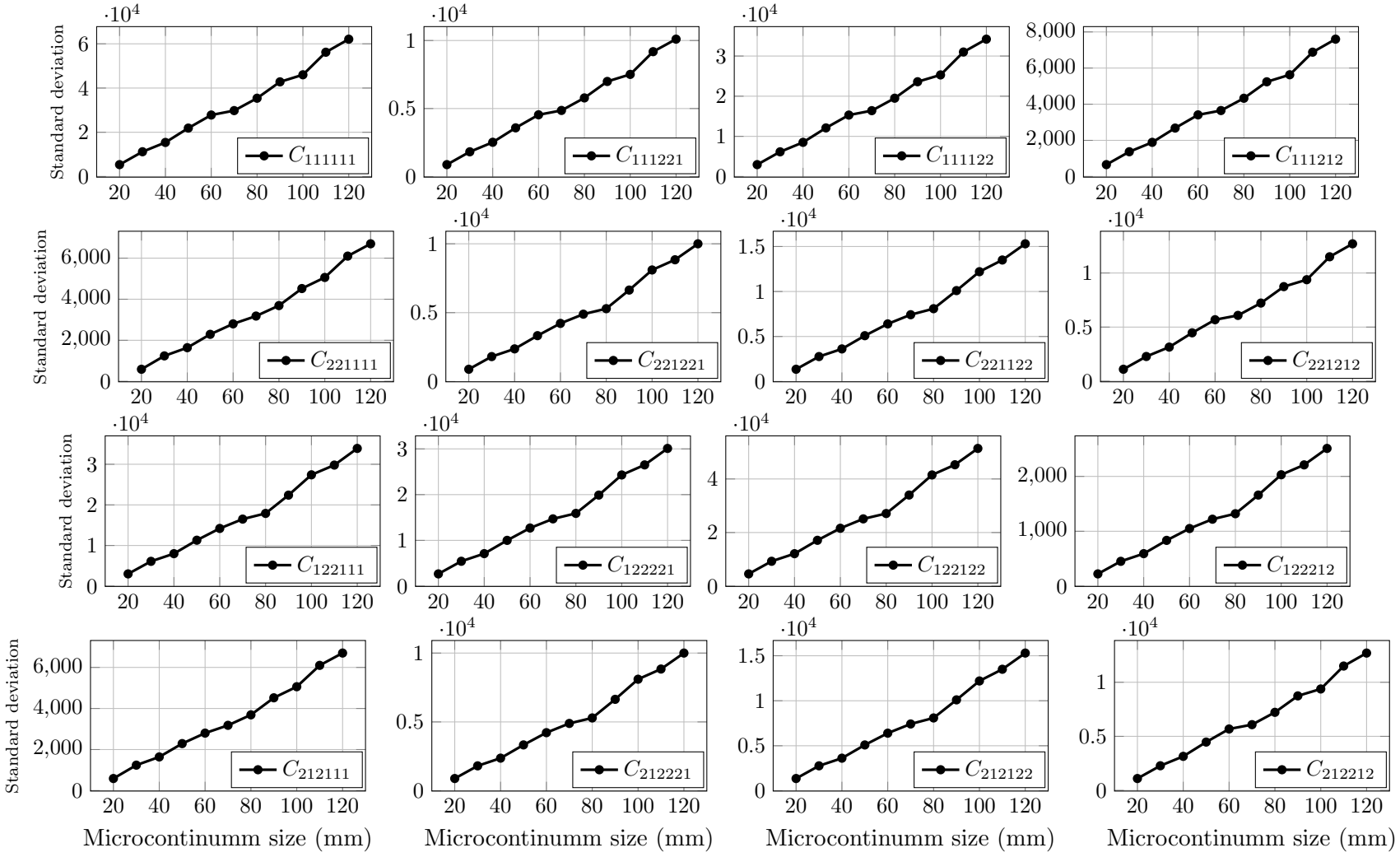

Figure A.65: Distribution study: Standard deviation of the components of the constitutive operator C_{ijklmn} versus microcontinuum size

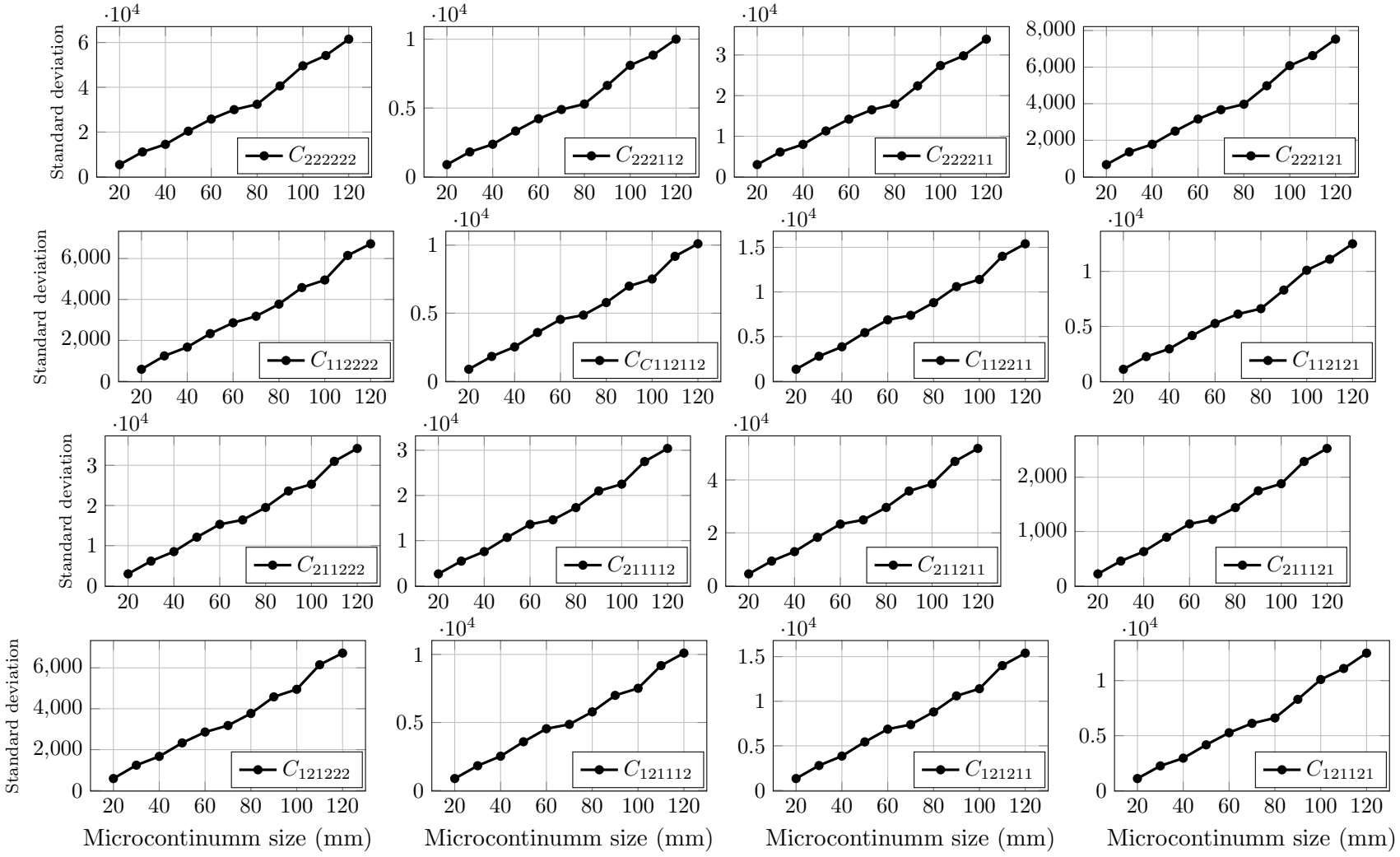

Figure A.66: Distribution study: standard deviation of the components of the constitutive operator C_{ijklmn} versus microcontinuum size